Some quite obvious observational constraints on cosmological models

Standard Cosmology at the threshold of change?

Aristotle University of Thessaloniki

02-06 June 2023

Pavel Kroupa

Helmholtz-Institut für Strahlungs- und Kernphysik (HISKP)

University of Bonn

Astronomisches Institut,

Karls Universität in Prag

c/o Argelander-Institut für Astronomie

University of Bonn

The SMoC
(Standard Model of Cosmology)

2 fundamental assumptions / axioms :

The Standard Modell of Cosmology (SMoC)

2 fundamental assumptions / axioms :

1. The Einstein/Newton formulation of gravitation is valid everywhere.
2. All matter is created at the Big Bang.

The Standard Modell of Cosmology (SMoC)

2 fundamental assumptions / axioms :

1. The Einstein/Newton formulation of gravitation is valid everywhere.
2. All matter is created at the Big Bang.

observations

The Standard Modell of Cosmology (SMoC)

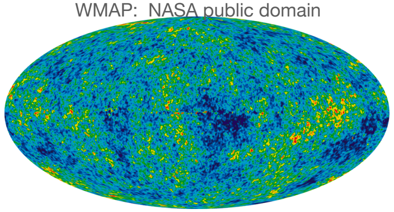

galaxy
rotation
curves

for e.g.

observations

2 fundamental assumptions / axioms :

1. The Einstein/Newton formulation of gravitation is valid everywhere.
2. All matter is created at the Big Bang.

The Standard Modell of Cosmology (SMoC)

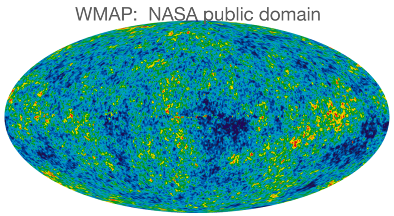

galaxy
rotation
curves

for e.g.

observations

2 fundamental assumptions / axioms :

1. The Einstein/Newton formulation of gravitation is valid everywhere.
2. All matter is created at the Big Bang.

auxiliary assumptions

inflation
+
dark matter
+
dark energy

needed

The Standard Modell of Cosmology (SMoC)

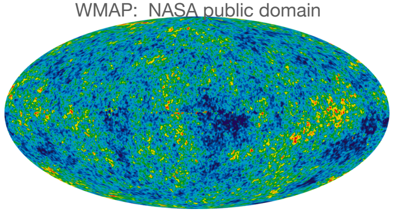

galaxy rotation curves

for e.g.

observations

2 fundamental assumptions / axioms :

1. The Einstein/Newton formulation of gravitation is valid everywhere.
2. All matter is created at the Big Bang.

auxiliary assumptions

inflation
+
dark matter
+
dark energy

needed

Note: "dark matter" = cold, warm, fuzzy, axion
(results for structure formation and properties of galaxies similar)

(eg. May & Springel 2021 arXiv)

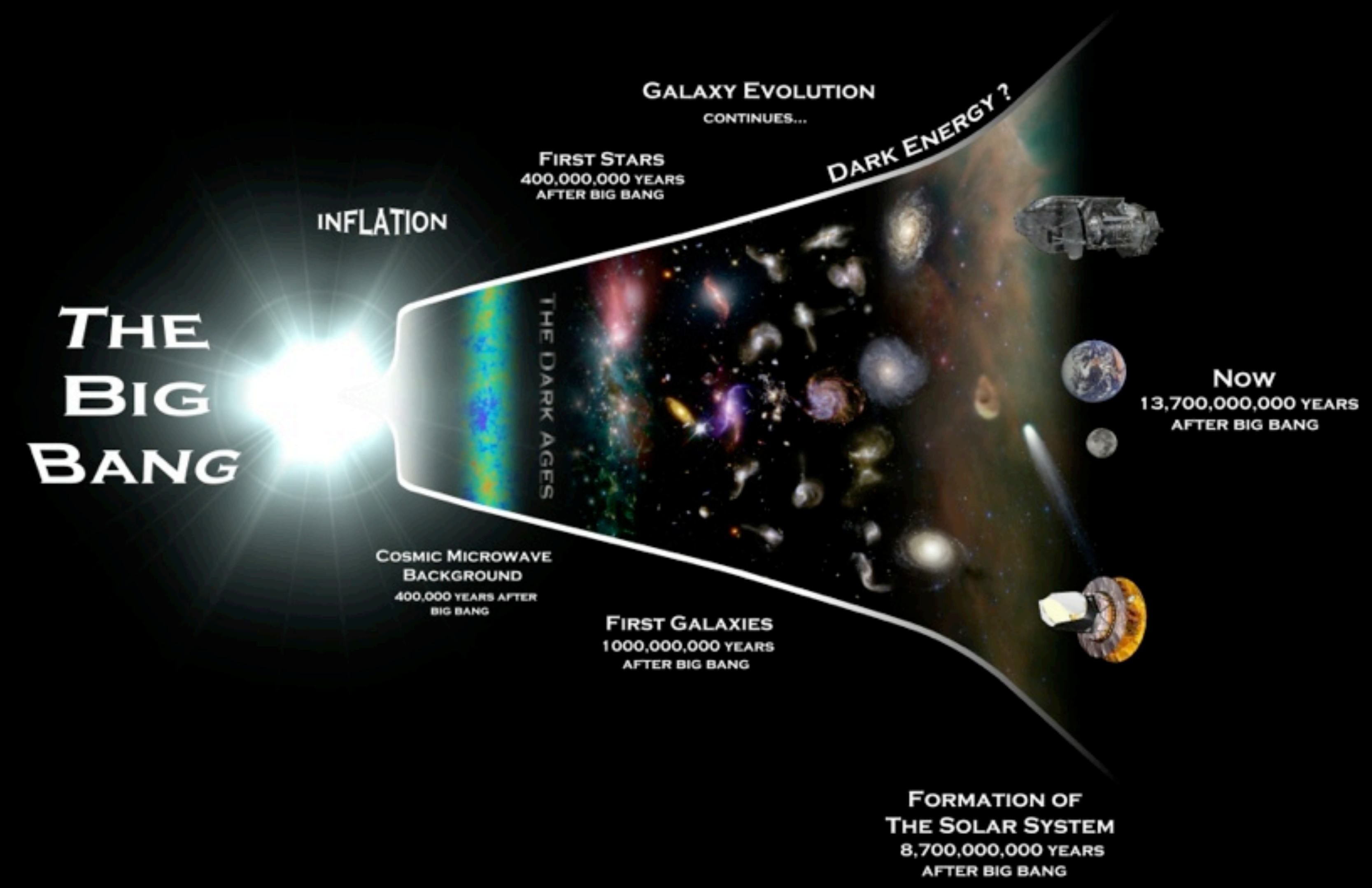

The expanding Universe. Image credit: Rhys Taylor

https://blogs.cardiff.ac.uk/physicsoutreach/2019/04/02/pythagorean-astronomy-flying-space-shrapnel-and-a-misbehaving-universe/

In the SMoC
galaxies grow mostly through
mergers

https://www.physics.uci.edu/~stewartk/research.html

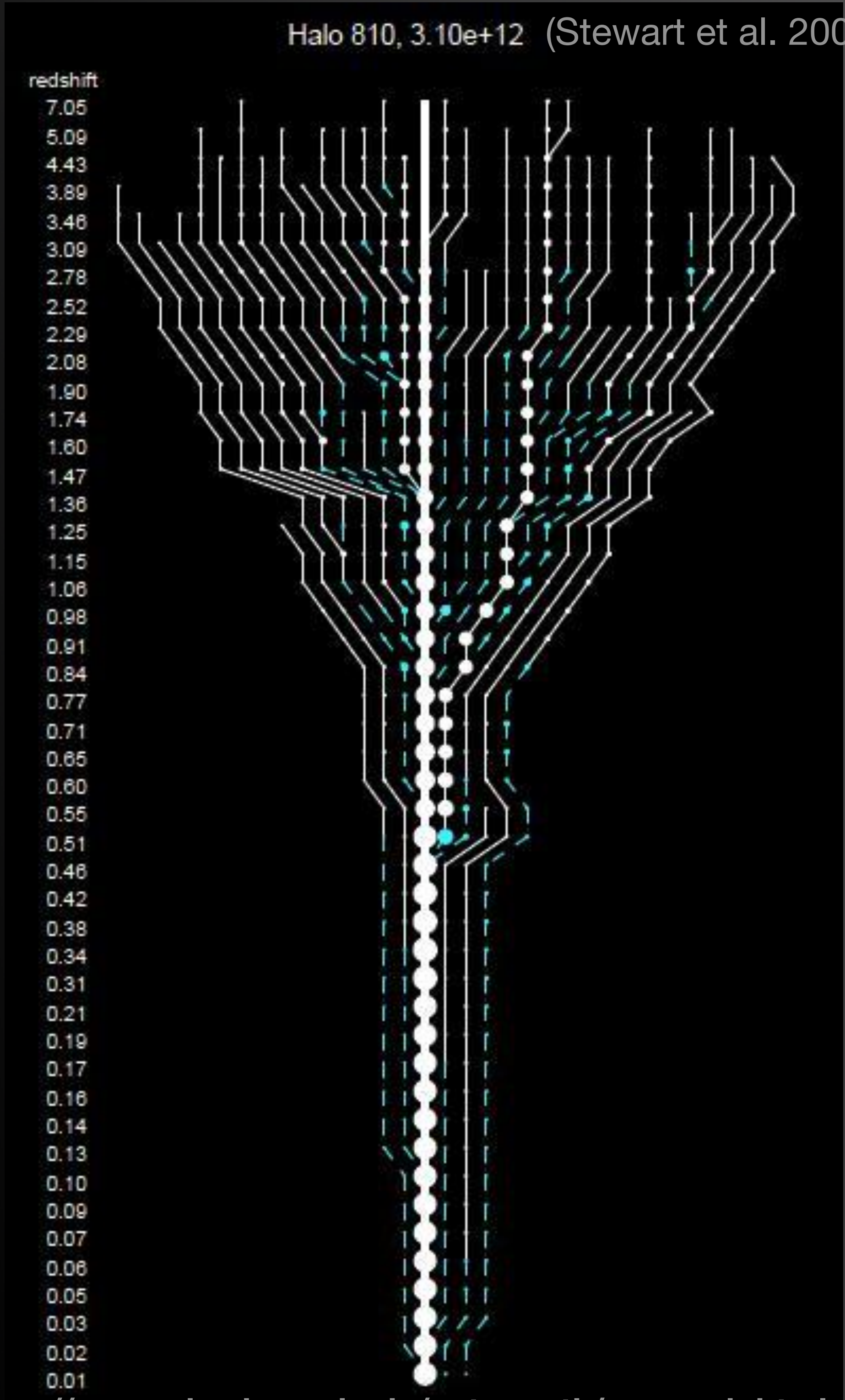

(Stewart et al. 2008)

In the SMoC galaxies grow mostly through mergers

https://www.physics.uci.edu/~stewartk/research.html

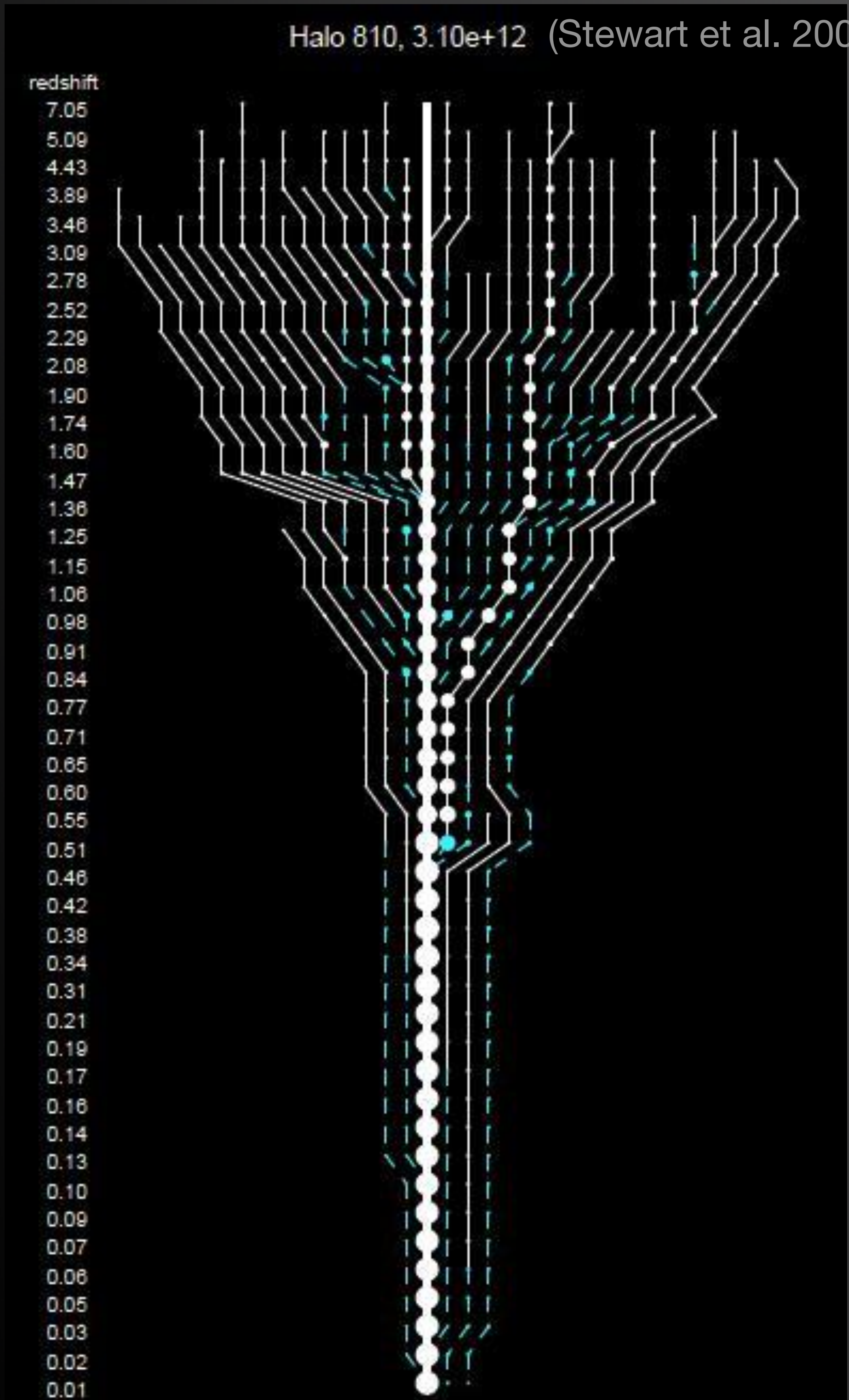

(Stewart et al. 2008)

https://www.physics.uci.edu/~stewartk/research.html

In the SMoC
galaxies grow mostly through
mergers

. . . why ?

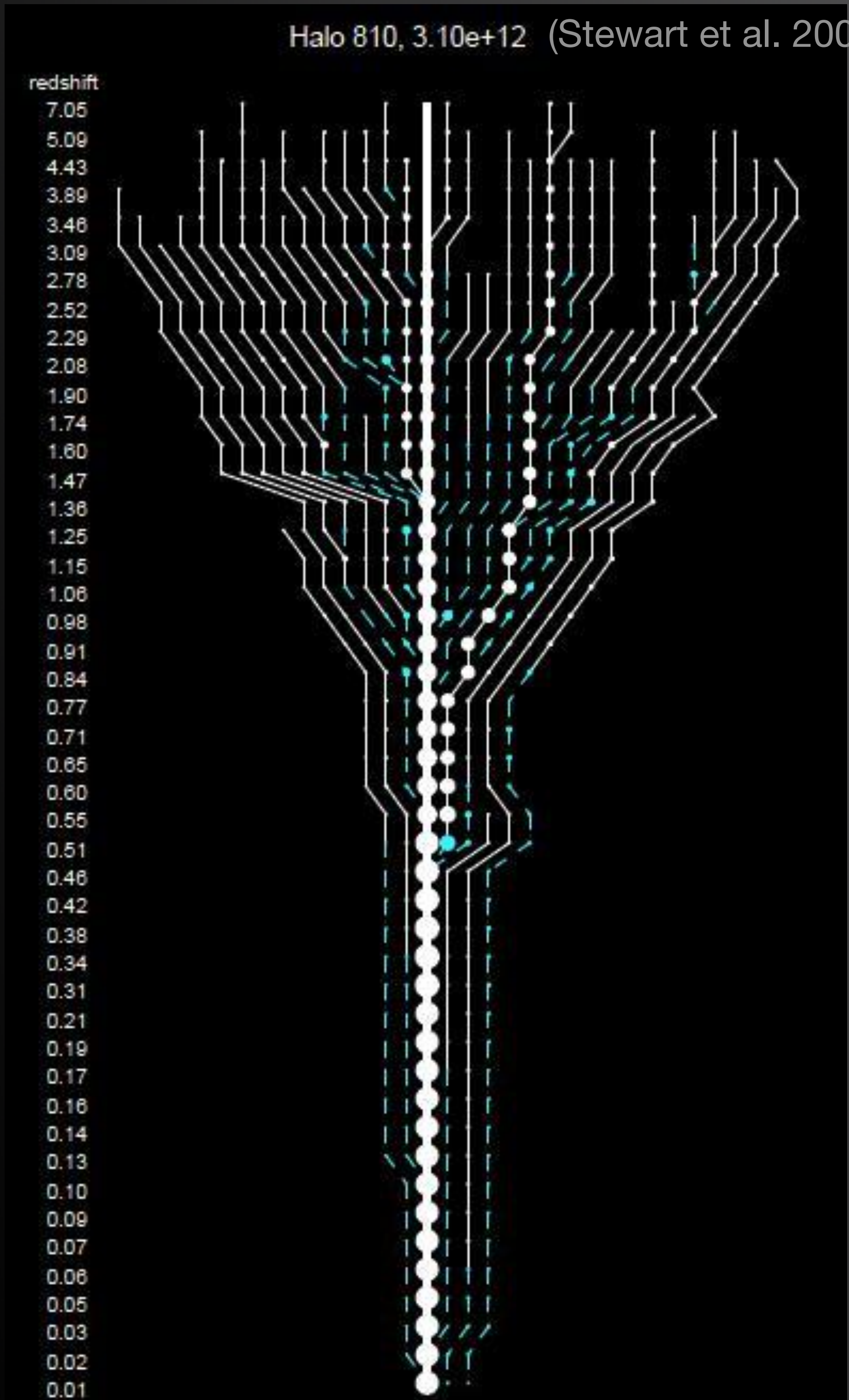

(Stewart et al. 2008)

https://www.physics.uci.edu/~stewartk/research.html

In the SMoC
galaxies grow mostly through
mergers

. . . why ?

Why don't two passing stars merge ?

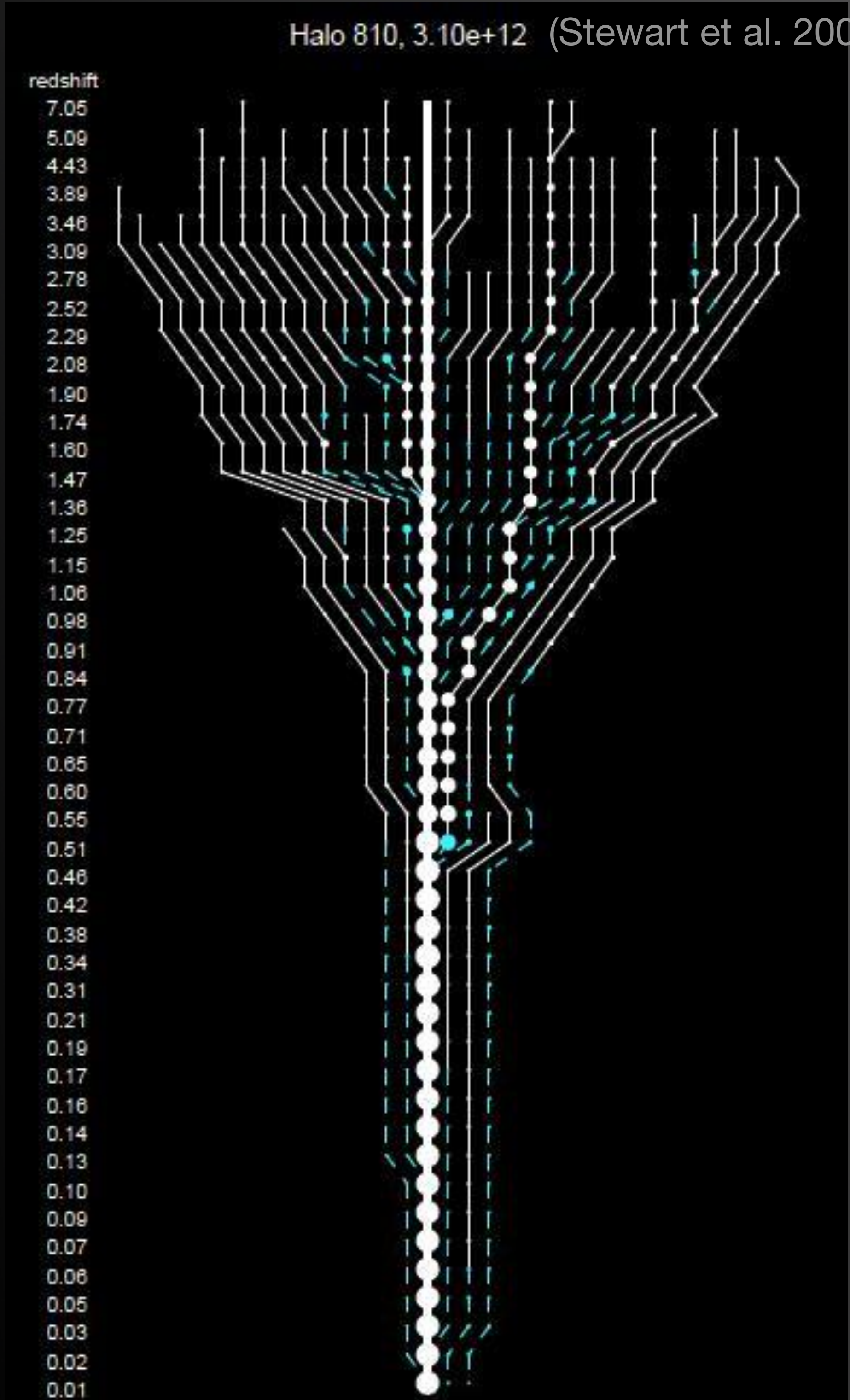

(Stewart et al. 2008)

https://www.physics.uci.edu/~stewartk/research.html

In the SMoC
galaxies grow mostly through
mergers

. . . why ?
Why don't two passing stars merge ?

. . . and why then are most
real galaxies
ancient thin disk galaxies ?

---> Haslbauer, Banik et al. 2022

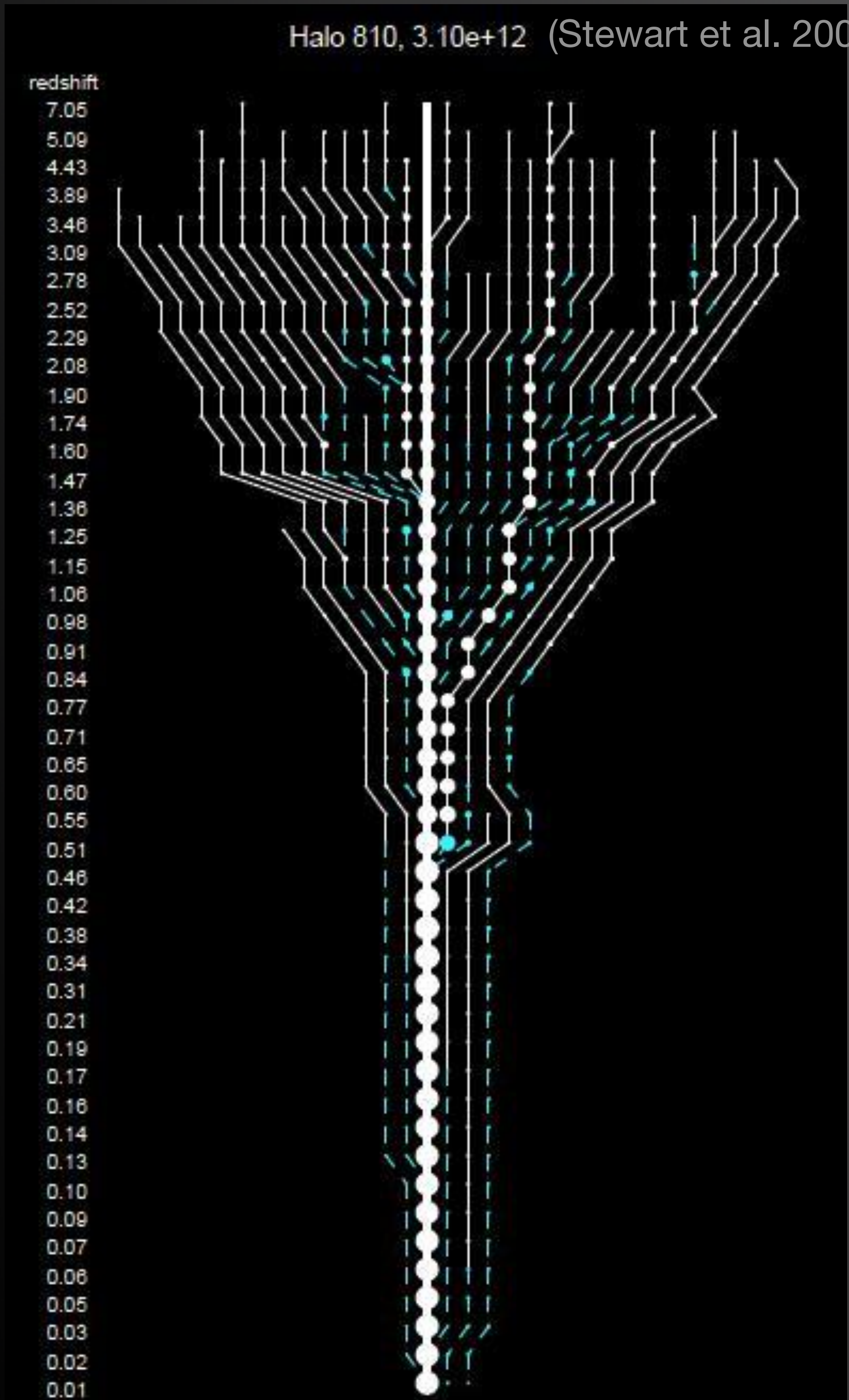

(Stewart et al. 2008)

https://www.physics.uci.edu/~stewartk/research.html

In the SMoC
galaxies grow mostly through
mergers

. . . why ?
Why don't two passing stars merge ?

. . . and why then are most
real galaxies
ancient thin disk galaxies ?
---> Haslbauer, Banik et al. 2022

. . . and why then do
real elliptical galaxies
form in <1Gyr and extremely early ?
---> Yan, Jerabkova+21; Eappen+2022, 2024

For Einsteinian gravitation to be valid, dark matter particles absolutely must exist.

For Einsteinian gravitation to be valid, dark matter particles absolutely must exist.

But does dark matter even exist?

For Einsteinian gravitation to be valid, dark matter particles absolutely must exist.

But does dark matter even exist ?

How can
we test for
dark matter ?

How can one test for the existence of dark matter?

How can one test for the existence of dark matter?

We do know some of the properties dark matter particles must have:

How can one test for the existence of dark matter?

We do know some of the properties dark matter particles must have:

By construction of the standard cold- or warm-dark matter models, the dark matter particle interacts only gravitationally with ordinary matter.

How can one test for the existence of dark matter?

We do know some of the properties dark matter particles must have :

By construction of the standard cold- or warm-dark matter models,
the dark matter particle interacts only gravitationally with ordinary matter.

Any finite interaction cross section
with dark-matter particles
and particles from the Standard Model of Particle Physics
must be negligible :

How can one test for the existence of dark matter ?

We do know some of the properties dark matter particles must have :

By construction of the standard cold- or warm-dark matter models,
the dark matter particle interacts only gravitationally with ordinary matter.

Any finite interaction cross section
with dark-matter particles
and particles from the Standard Model of Particle Physics
must be negligible :

Otherwise :
- galaxies would look different (e.g. E galaxies in galaxy clusters), e.g. Gnedin & Ostriker 2001
- pre-CMB structure formation would be incompatible with the CMB, and
- no trace of a dark matter particle has been found in any experiment despite a very large world-wide 40-yr-long effort under, on, and above the ground.

How can one test for the existence of dark matter ?

We do know some of the properties dark matter particles must have :

By construction of the standard cold- or warm-dark matter models,
the dark matter particle interacts only gravitationally with ordinary matter.

Any finite interaction cross section
with dark-matter particles
and particles from the Standard Model of Particle Physics
must be negligible :

Otherwise :

- galaxies would look different (e.g. E galaxies in galaxy clusters), e.g. Gnedin & Ostriker 2001
- pre-CMB structure formation would be incompatible with the CMB, and
- no trace of a dark matter particle has been found in any experiment despite a very large world-wide 40-yr-long effort under, on, and above the ground.

How can one test for the existence of such a dark matter particle ?

How can one test for the existence of dark matter ?

We do know some of the properties dark matter particles must have :

By construction of the standard cold- or warm-dark matter models,
the dark matter particle interacts only gravitationally with ordinary matter.

Any finite interaction cross section
with dark-matter particles
and particles from the Standard Model of Particle Physics
must be negligible :

Otherwise :
- galaxies would look different (e.g. E galaxies in galaxy clusters), e.g. Gnedin & Ostriker 2001
- pre-CMB structure formation would be incompatible with the CMB, and
- no trace of a dark matter particle has been found in any experiment despite a very large world-wide 40-yr-long effort under, on, and above the ground.

How can one test for the existence of such a dark matter particle ?

By applying Chandrasekhar dynamical friction !

Kroupa 2015
Oehm & Kroupa 2024

How can one test for the existence of dark matter ?

We do know some of the properties dark matter particles must have :

By construction of the standard cold- or warm-dark matter models,
the dark matter particle interacts only gravitationally with ordinary matter.

Any finite interaction cross section
with dark-matter particles
and particles from the Standard Model of Particle Physics
must be negligible :

Otherwise :

- galaxies would look different (e.g. E galaxies in galaxy clusters), e.g. Gnedin & Ostriker 2001
- pre-CMB structure formation would be incompatible with the CMB, and
- no trace of a dark matter particle has been found in any experiment despite a very large world-wide 40-yr-long effort under, on, and above the ground.

How can one test for the existence of such a dark matter particle ?

By applying Chandrasekhar dynamical friction !

Kroupa 2015
Oehm & Kroupa 2024
decisive test !

The SMoC predicts
each galaxy to be in a massive very extended
dark matter halo.

The SMoC predicts
each galaxy to be in a massive very extended
dark matter halo.

This is due to each galaxy growing
through many mergers.

≈ 250 kpc

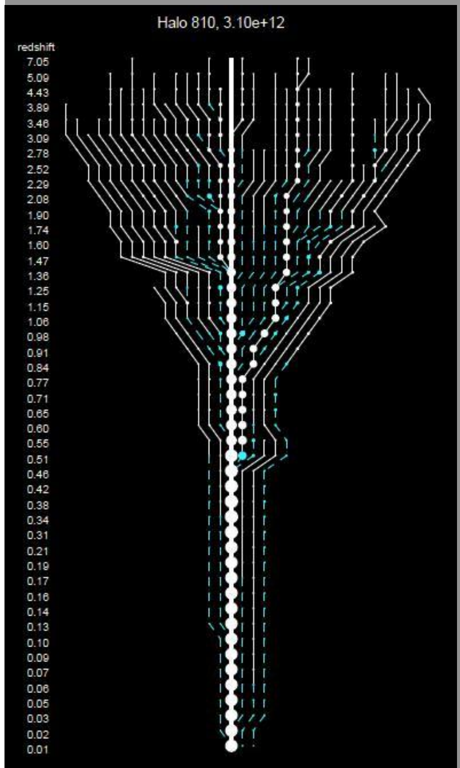

(Diemand et al. 2008)

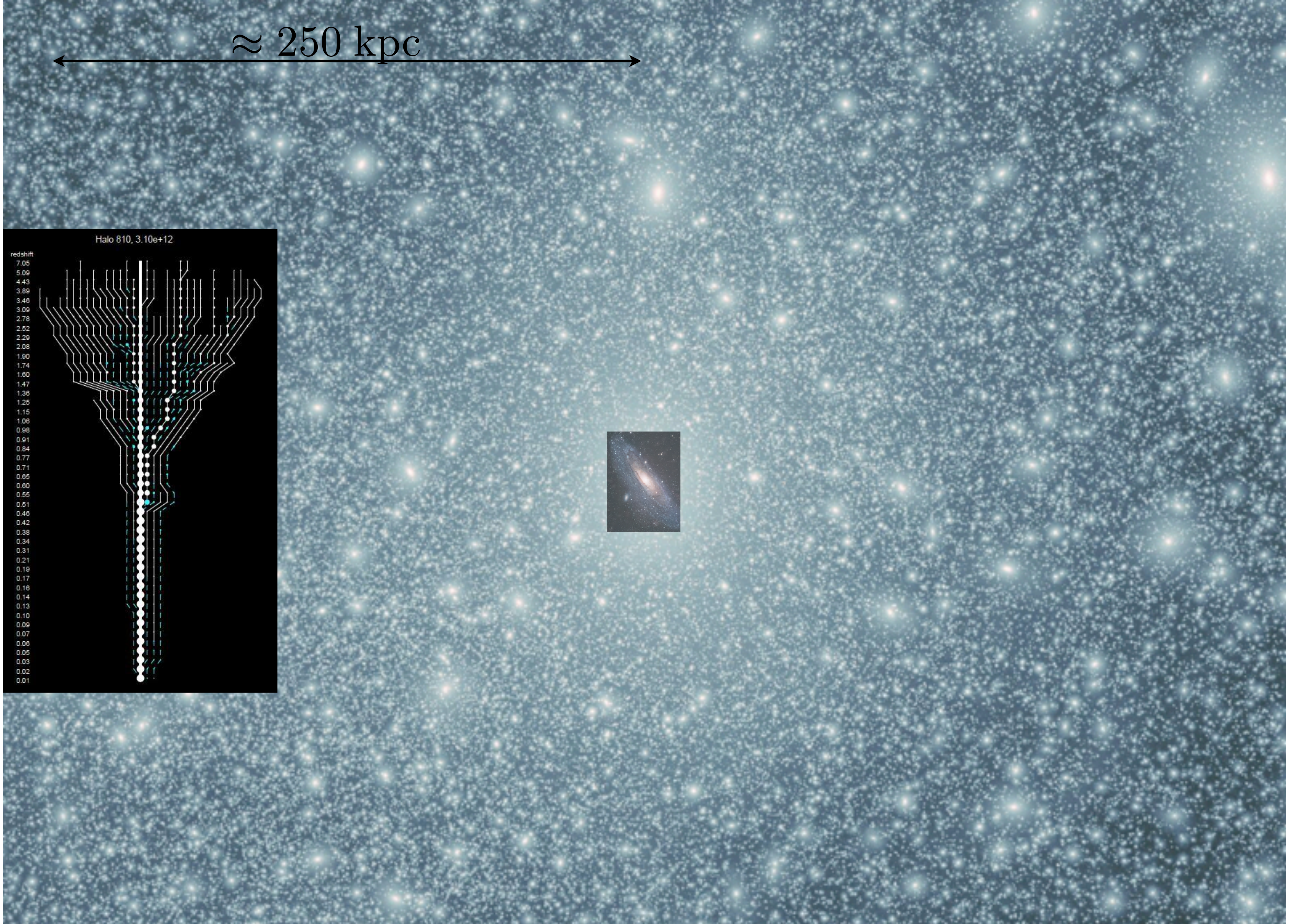

(Diemand et al. 2008)

The SMoC predicts
each galaxy to be in a massive very extended dark matter halo.

This is due to each galaxy growing through many mergers.

The SMoC predicts
each galaxy to be in a massive very extended
dark matter halo.

This is due to each galaxy growing
through many mergers.

For a galaxy with
a mass M_{bar} in
stars + gas,
the SMoC
predicts the
properties
of its dark
matter halo.

The SMoC predicts
each galaxy to be in a massive very extended
dark matter halo.

This is due to each galaxy growing
through many mergers.

Sales, Navarro et al. 2017, MNRAS, "The low-mass end of the baryonic Tully–Fisher relation" (EAGLE simulation)

For a galaxy with a mass M_{bar} in stars + gas, the SMoC predicts the properties of its dark matter halo.

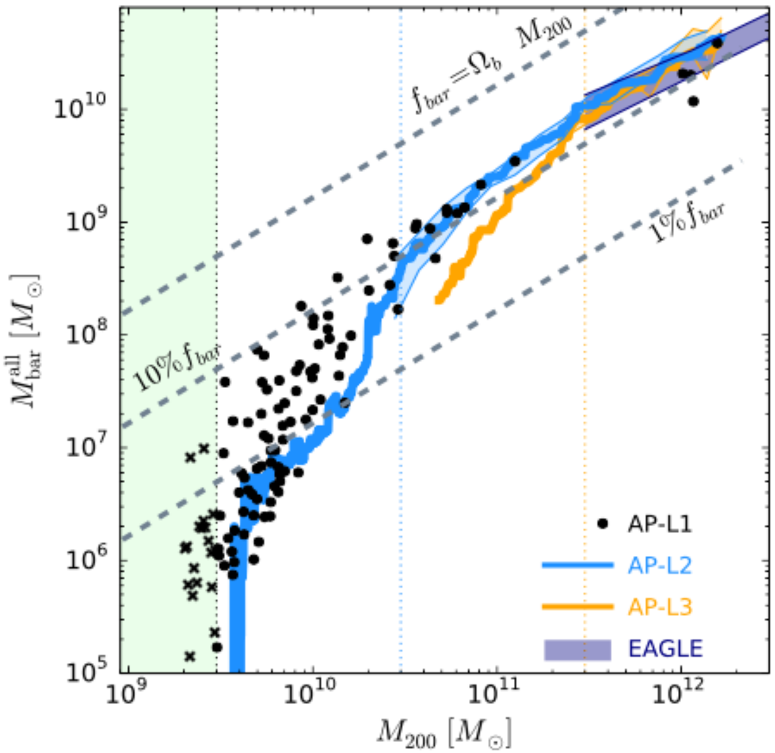

The SMoC predicts
each galaxy to be in a massive very extended
dark matter halo.

This is due to each galaxy growing
through many mergers.

Sales, Navarro et al. 2017, MNRAS, "The low-mass end of the baryonic Tully–Fisher relation" (EAGLE simulation)

For a galaxy with a mass M_{bar} in stars + gas, the SMoC predicts the properties of its dark matter halo.

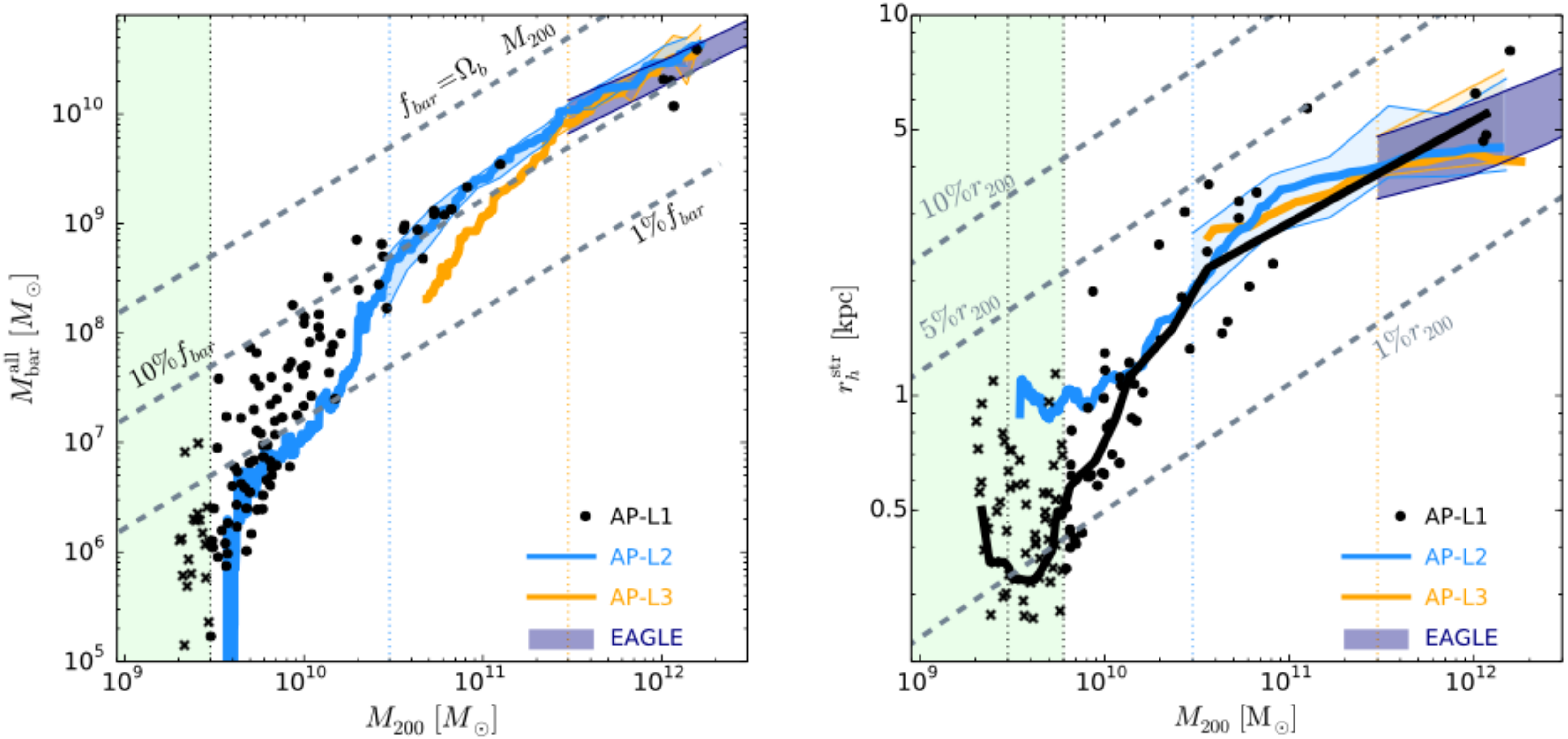

The SMoC predicts
each galaxy to be in a massive very extended
dark matter halo.

This is due to each galaxy growing
through many mergers.

Sales, Navarro et al. 2017, MNRAS, "The low-mass end of the baryonic Tully–Fisher relation" (EAGLE simulation)

For a galaxy with a mass M_{bar} in stars + gas, the SMoC predicts the properties of its dark matter halo.

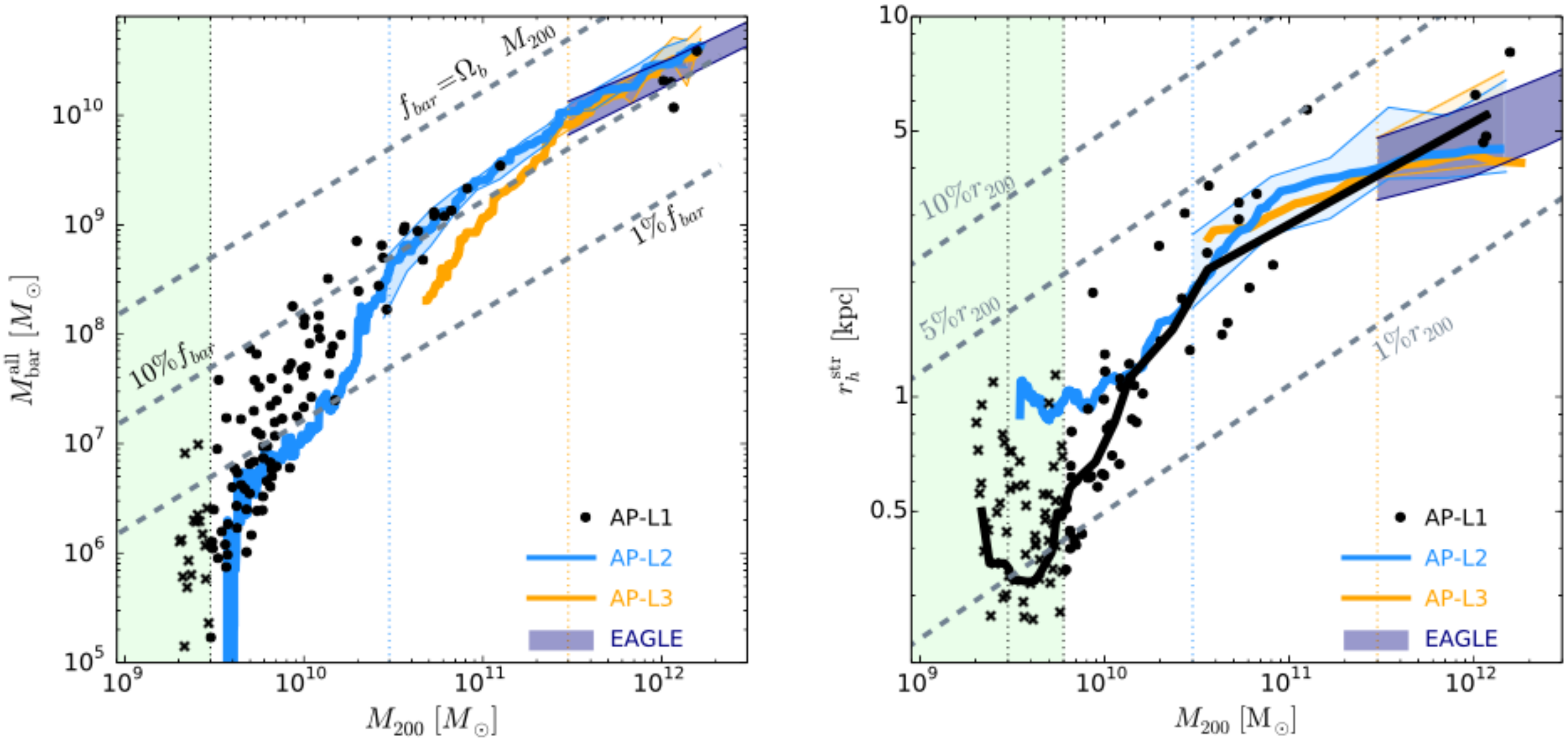

For a given galaxy,
its dark-matter halo is thus known
(within a well specified range of properties)

Testing for the existence
of

Dark Matter

via

Chandrasekhar
dynamical friction

Testing for the existence
of

Dark Matter

via

Chandrasekhar
dynamical friction

The SMoC predicts a new phenomenon :

If there is dark matter, then there must be *Chandrasekhar dynamical friction*.

The SMoC predicts a new phenomenon :

If there is dark matter, then there must be *Chandrasekhar dynamical friction*.

The situation :

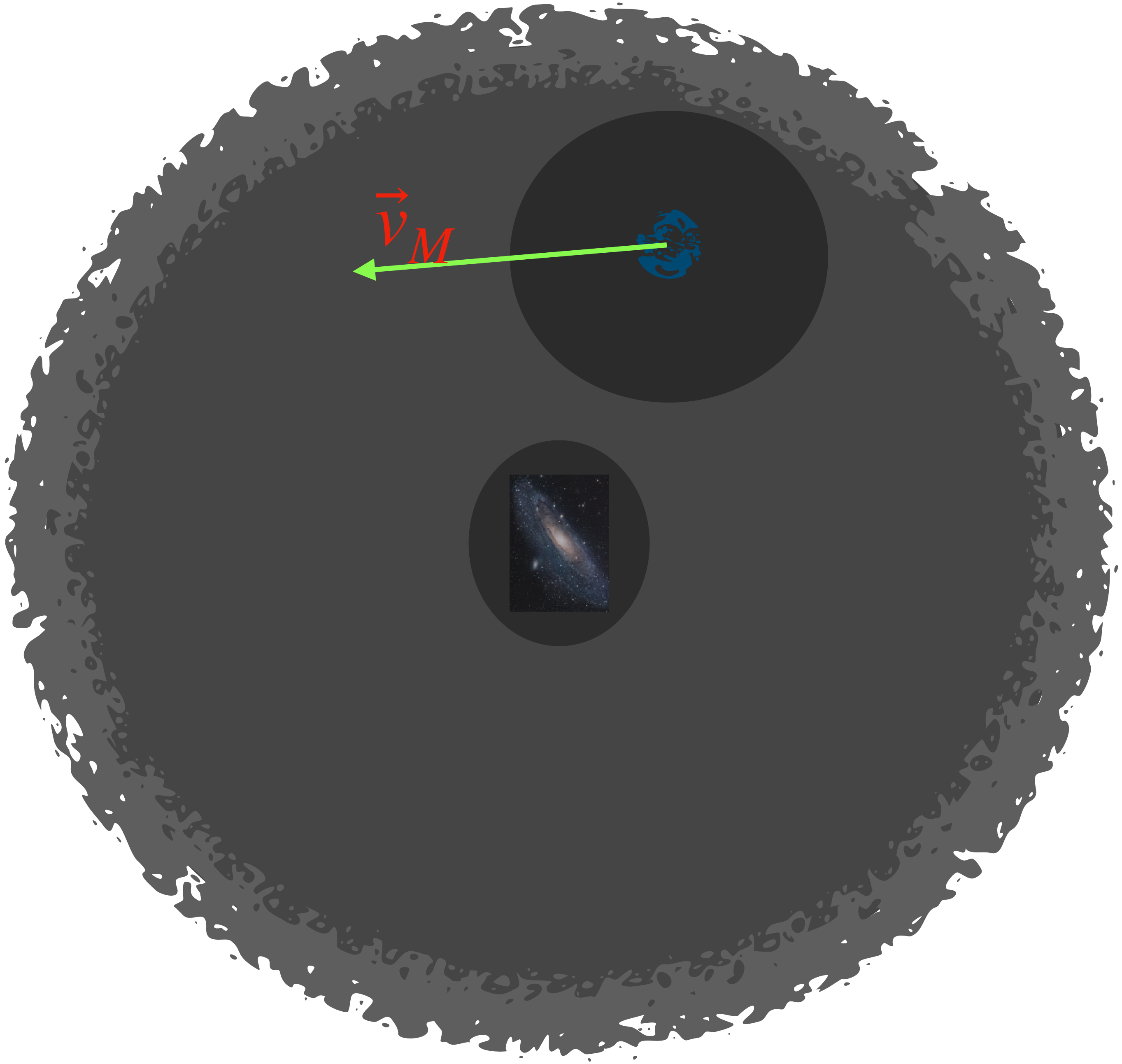

The SMoC predicts a new phenomenon :

If there is dark matter, then there must be *Chandrasekhar dynamical friction*.

Visualisation (integrate over all satellite--DM-particle encounters)

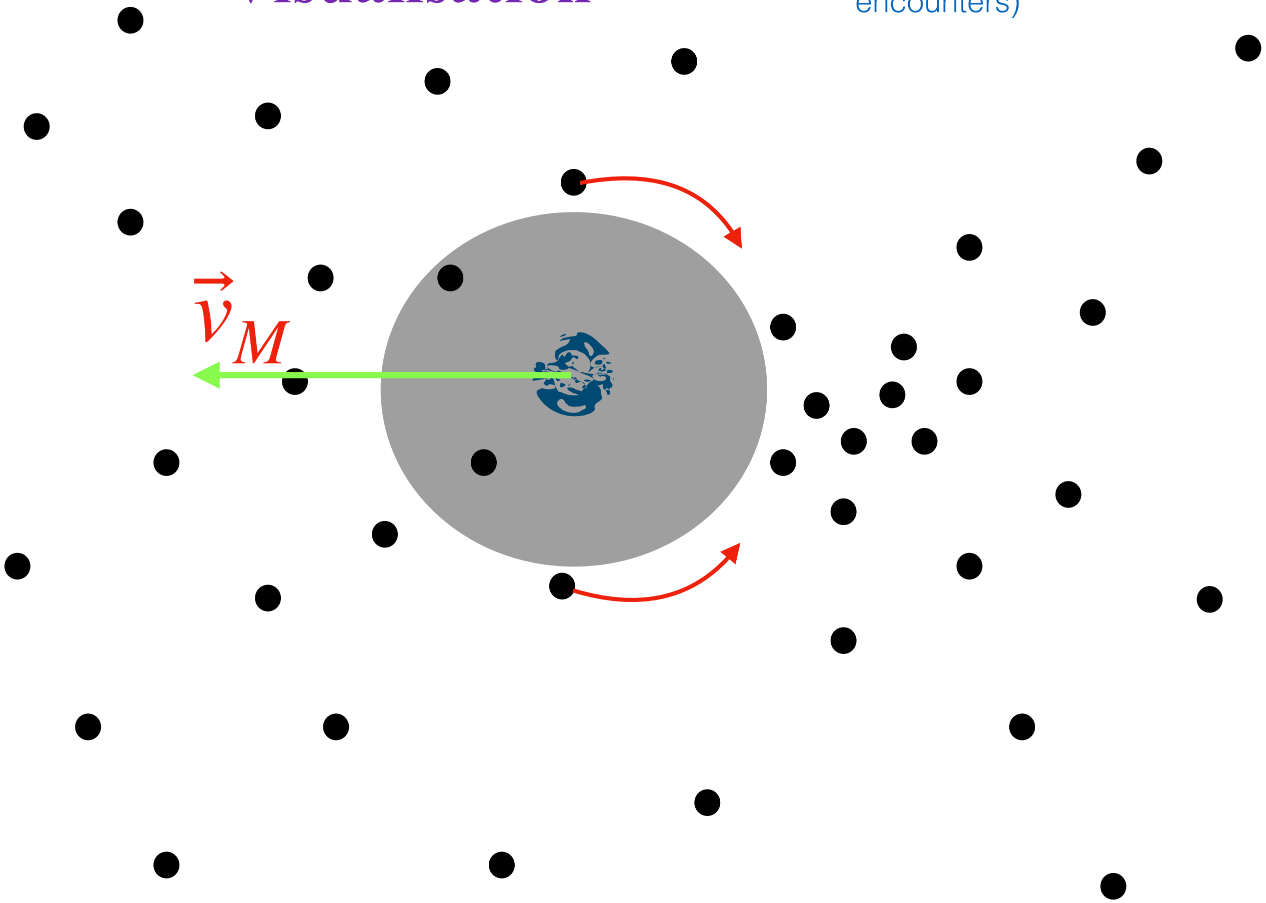

The SMoC predicts a new phenomenon :

If there is dark matter, then there must be *Chandrasekhar dynamical friction*.

Visualisation

(integrate over all satellite--DM-particle encounters)

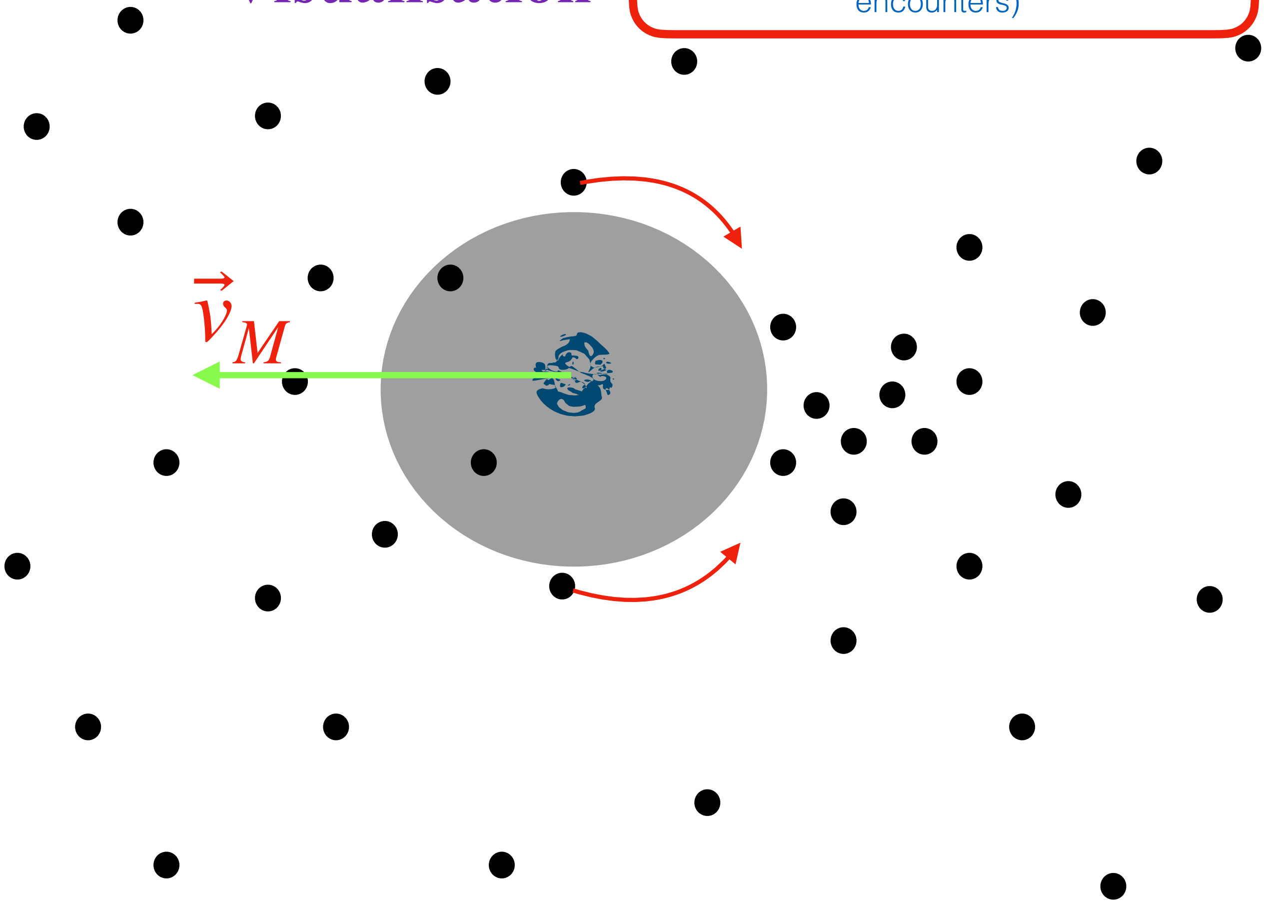

The SMoC predicts a new phenomenon :

If there is dark matter, then there must be *Chandrasekhar dynamical friction*.

Visualisation

(integrate over all satellite--DM-particle encounters)

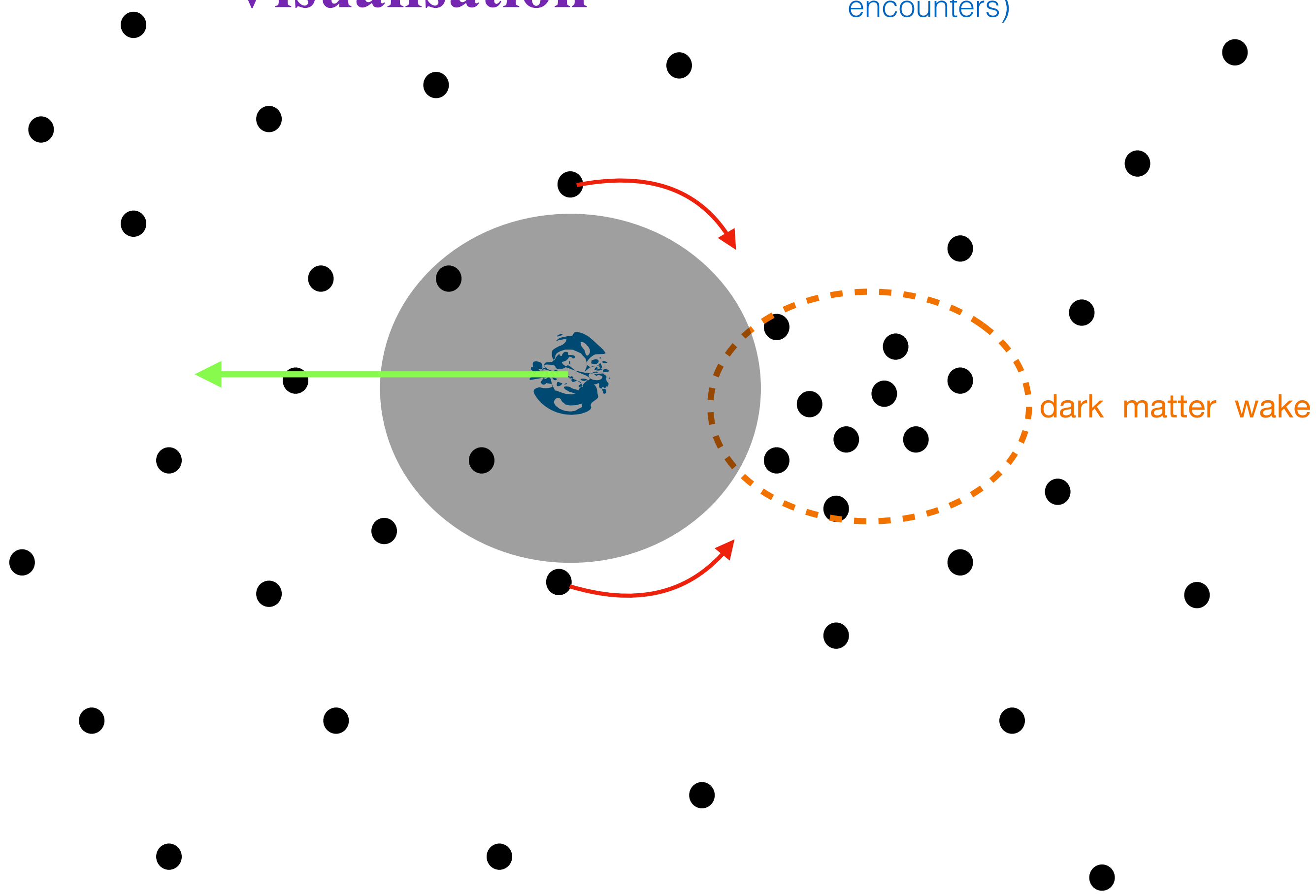

The SMoC predicts a new phenomenon :

If there is dark matter, then there must be *Chandrasekhar dynamical friction*.

Visualisation

(integrate over all satellite--DM-particle encounters)

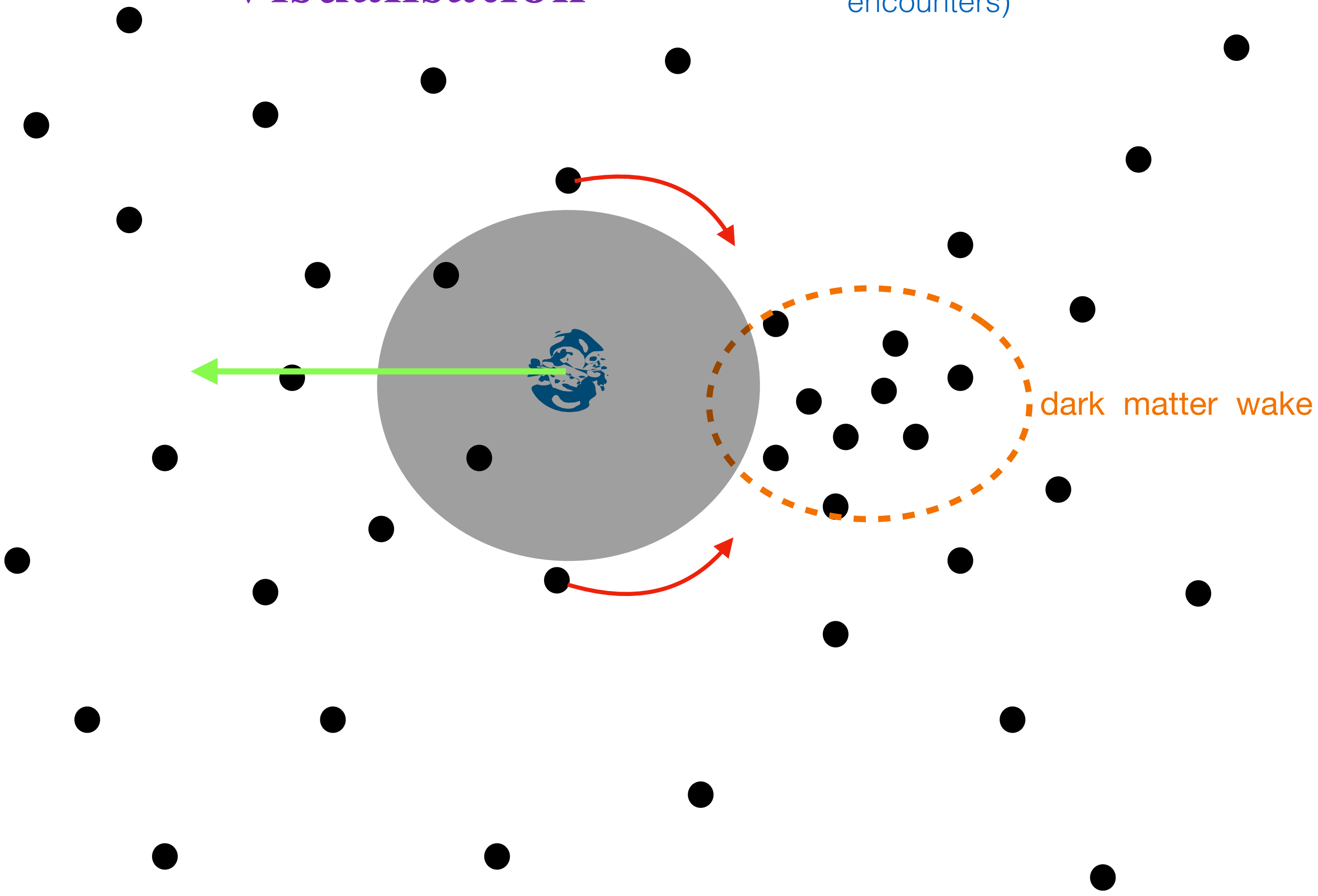

$$\frac{d\vec{v}_M}{dt} = -\frac{4\,\pi \ln\Lambda\, G^2\,(M+m)\,\rho_0\, m}{v_M^3}\left[\mathrm{erf}(X) - \frac{2\,X}{\sqrt{\pi}}\,e^{-X^2}\right]\,\vec{v}_M$$

eg. Binney & Tremaine (1987): "Galactic Dynamics"

The SMoC predicts a new phenomenon :

If there is dark matter, then there must be *Chandrasekhar dynamical friction*.

Visualisation (integrate over all satellite--DM-particle encounters)

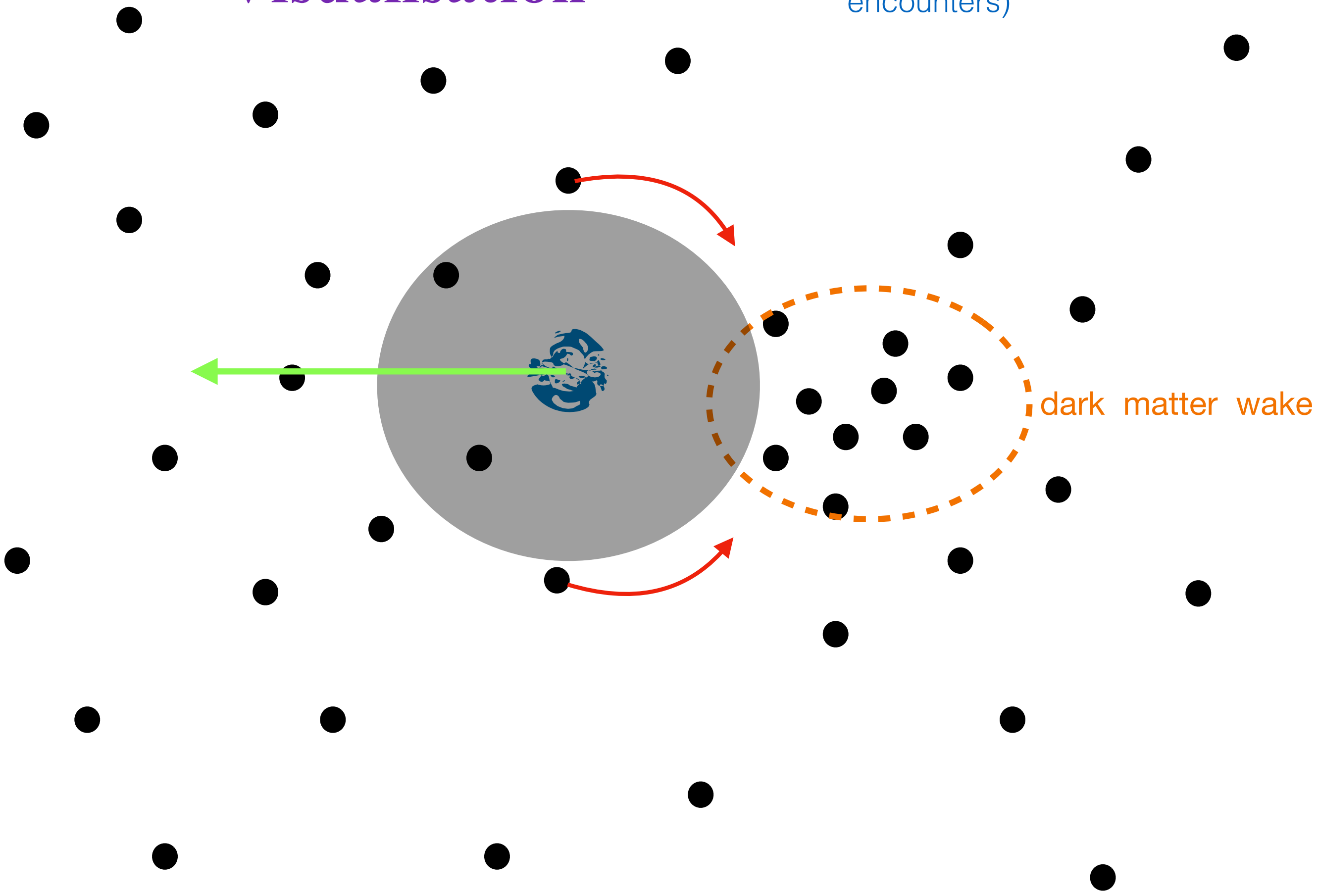

$$\frac{d\vec{v}_M}{dt} = -\frac{4\,\pi \ln\Lambda\, G^2\,(M+m)\,\rho_0\, m}{v_M^3}\left[\mathrm{erf}(X) - \frac{2\,X}{\sqrt{\pi}}\, e^{-X^2}\right]\,\vec{v}_M$$

eg. Binney & Tremaine (1987): "Galactic Dynamics"

fixed by the CMB / SMoC (cannot be adjusted)

The SMoC predicts a new phenomenon :

If there is dark matter, then there must be *Chandrasekhar dynamical friction*.

Visualisation (integrate over all satellite--DM-particle encounters)

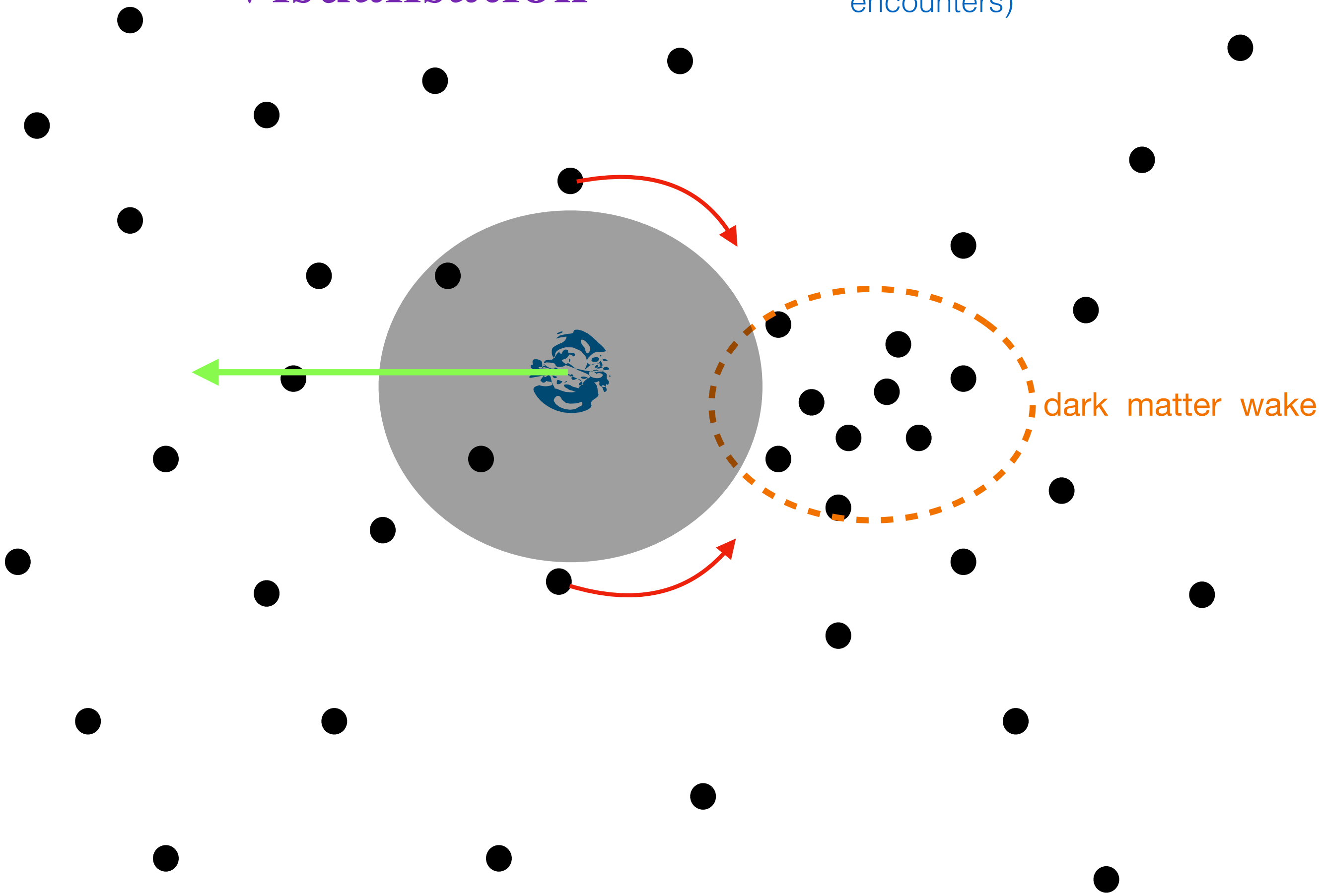

This test *insensitive* to mass, *m*, of dark matter particle

$$\frac{d\vec{v}_M}{dt} = -\frac{4\,\pi \ln\Lambda\, G^2\,(M+m)\,\rho_0\, m}{v_M^3}\left[\mathrm{erf}(X) - \frac{2\,X}{\sqrt{\pi}}\, e^{-X^2}\right]\vec{v}_M$$

eg. Binney & Tremaine (1987): "Galactic Dynamics"

fixed by the CMB / SMoC (cannot be adjusted)

Thus, if there is dark matter, then there must be *Chandrasekhar dynamical friction*.

The situation :

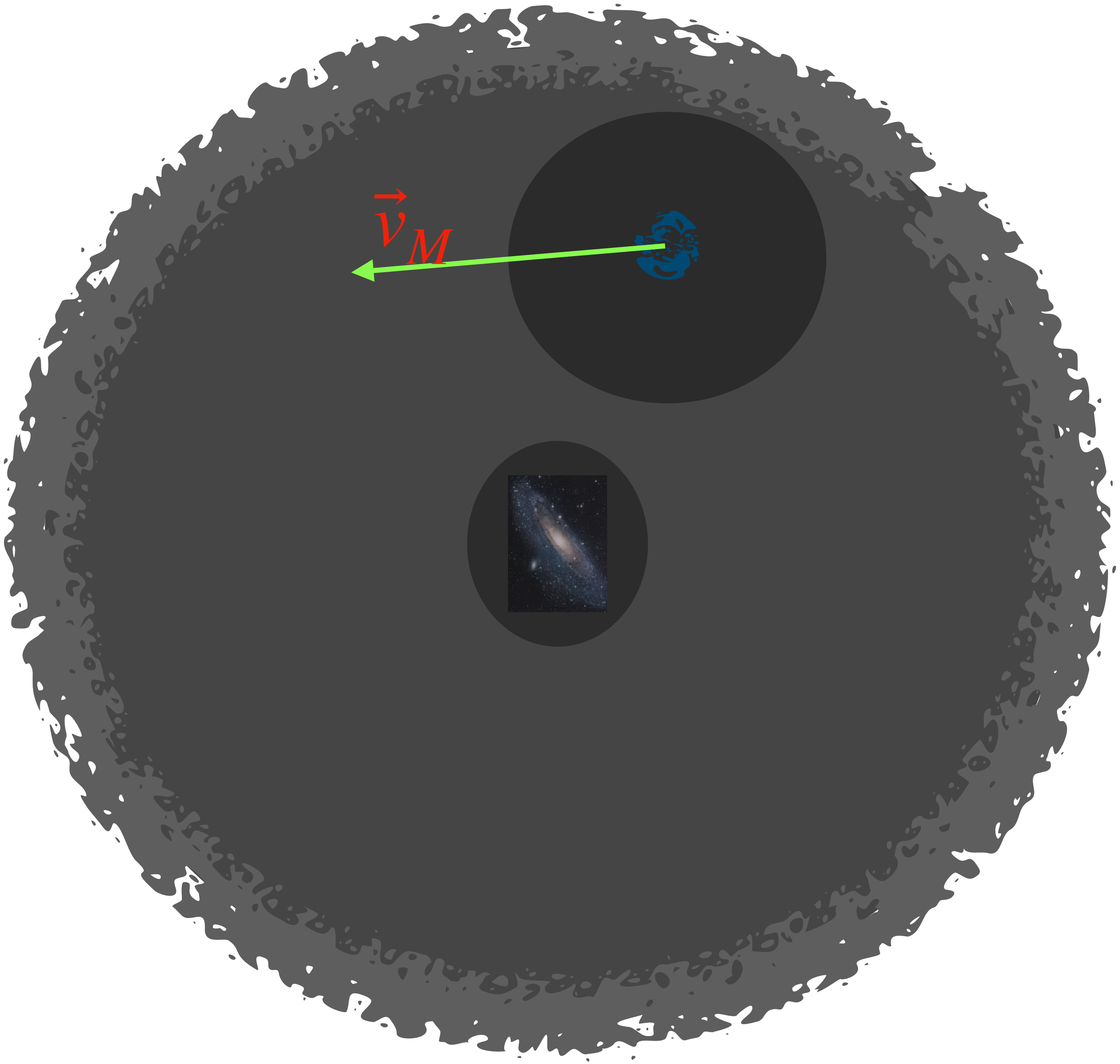

Prediction of new phenomenon :

Thus, essentially **:**

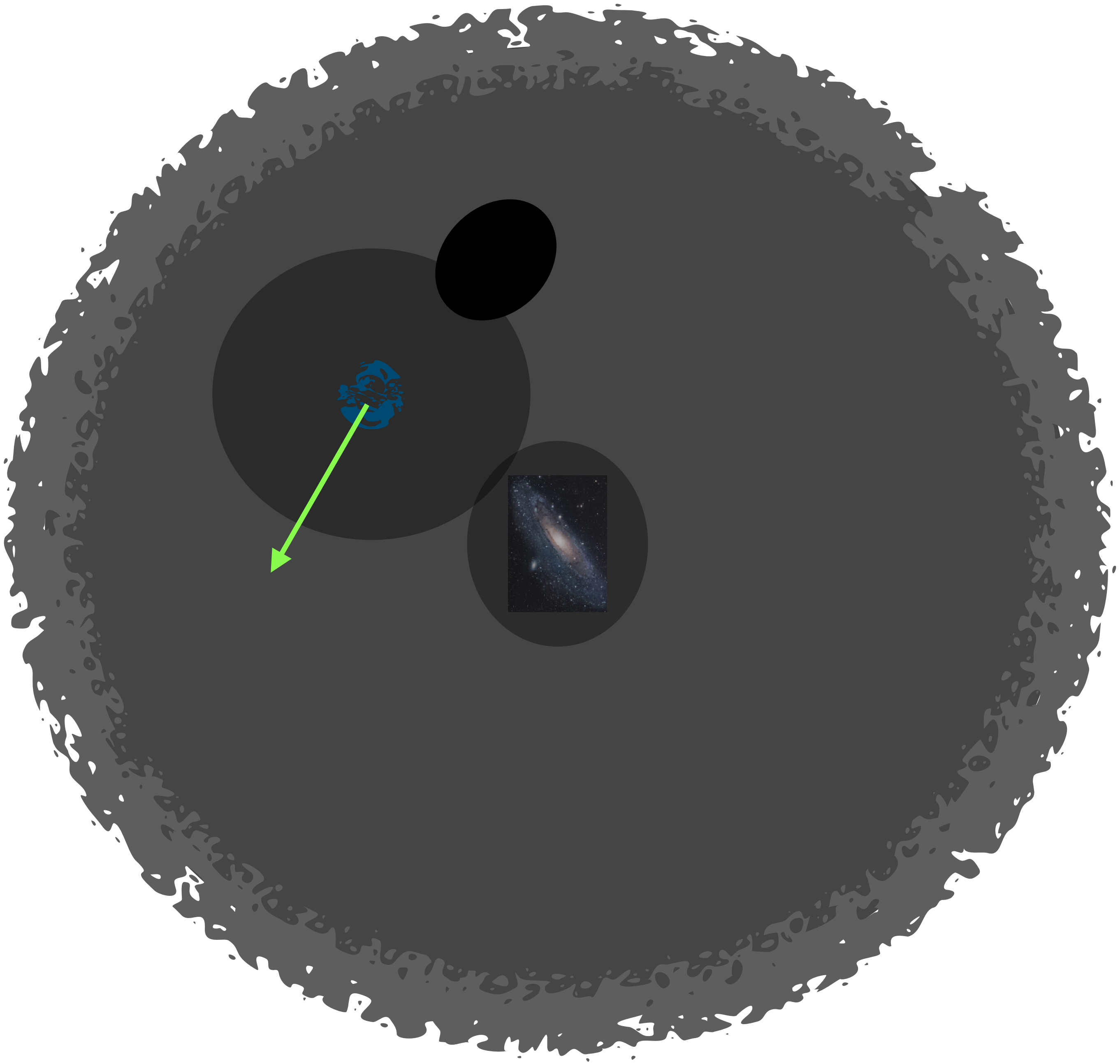

Prediction of new phenomenon :

Thus, essentially **:**

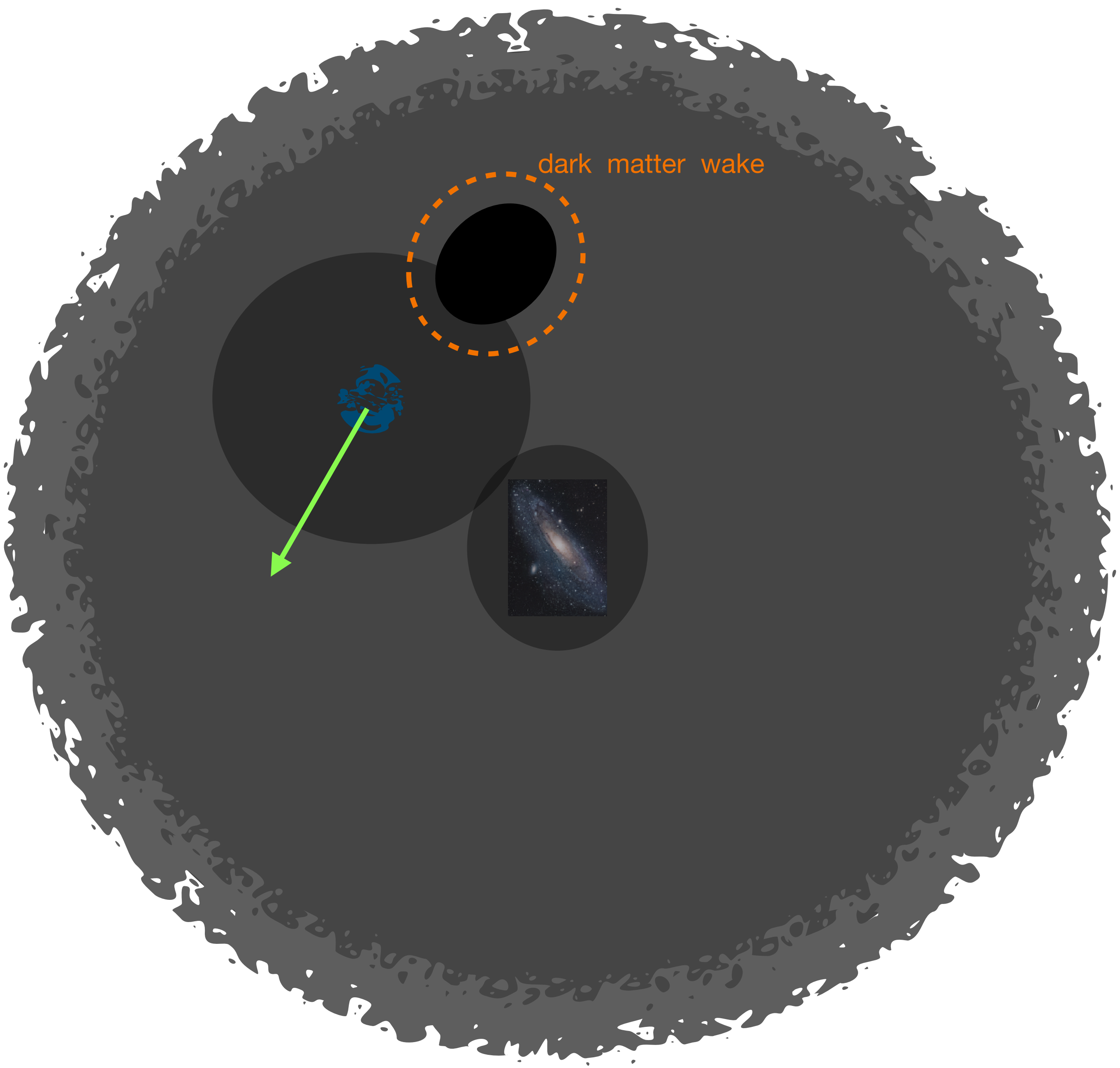

Prediction of new phenomenon :

Thus, essentially :

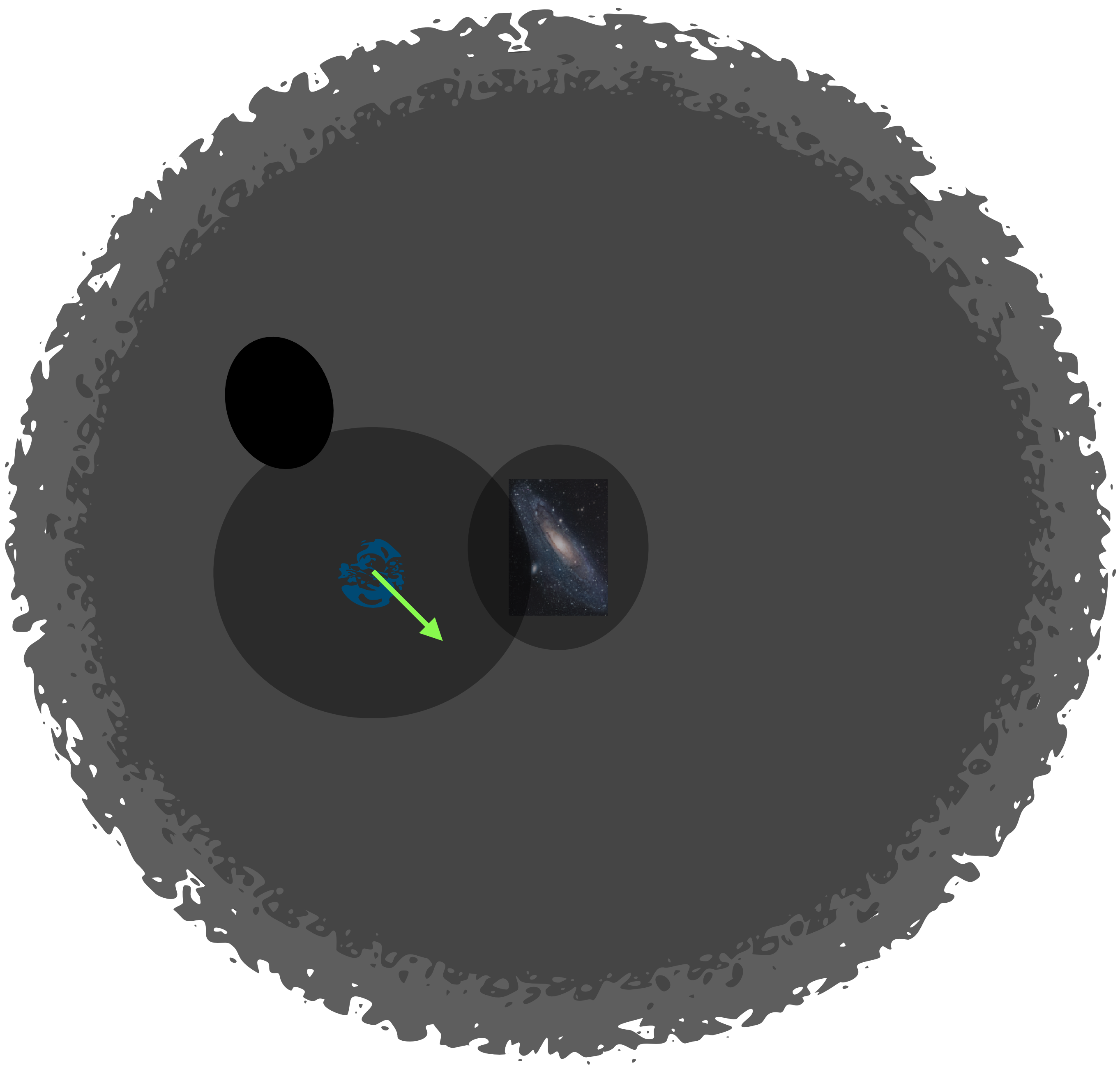

Prediction of new phenomenon :

Thus, essentially **:**

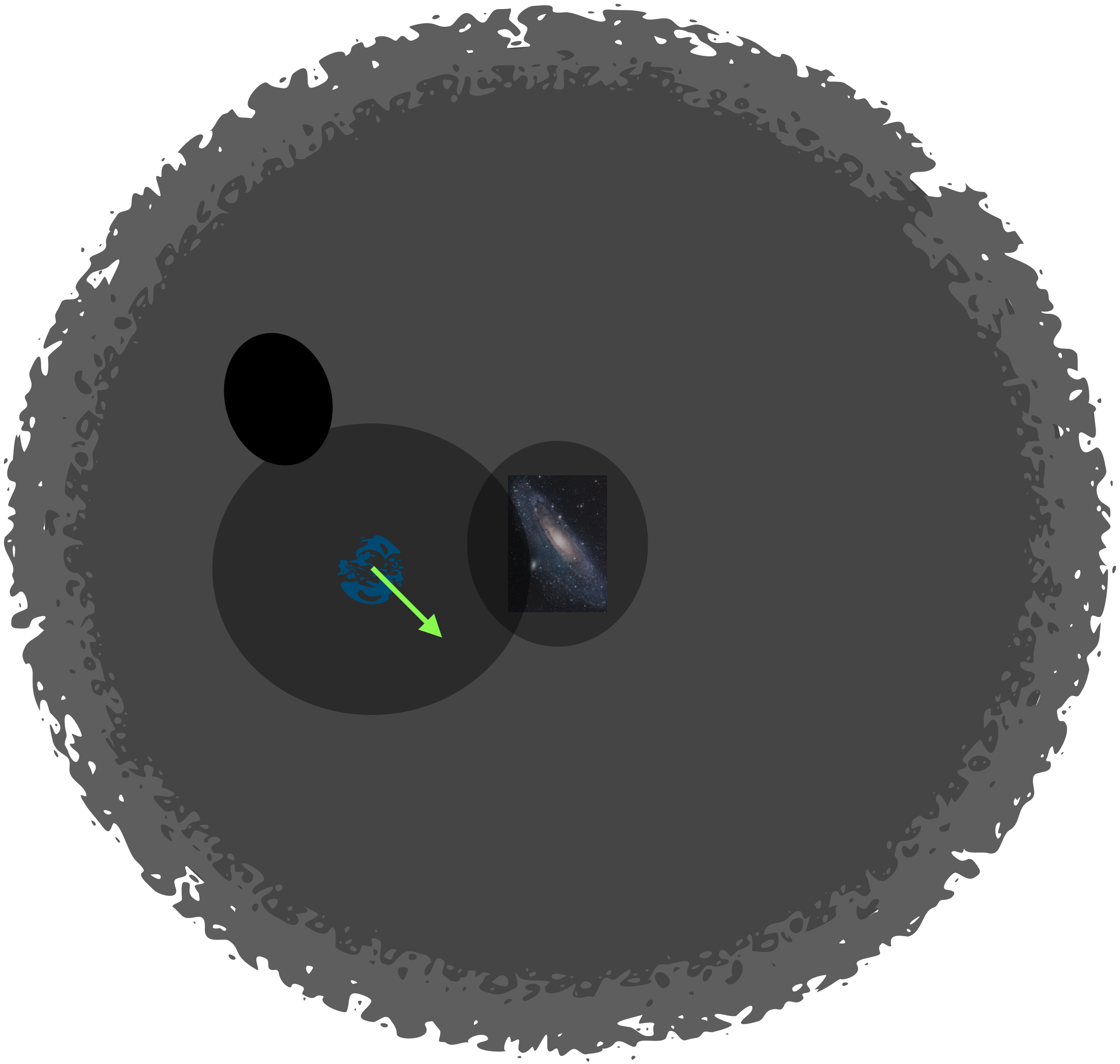

And this is
why galaxies
merge**,**

Prediction of new phenomenon :

Thus, essentially **:**

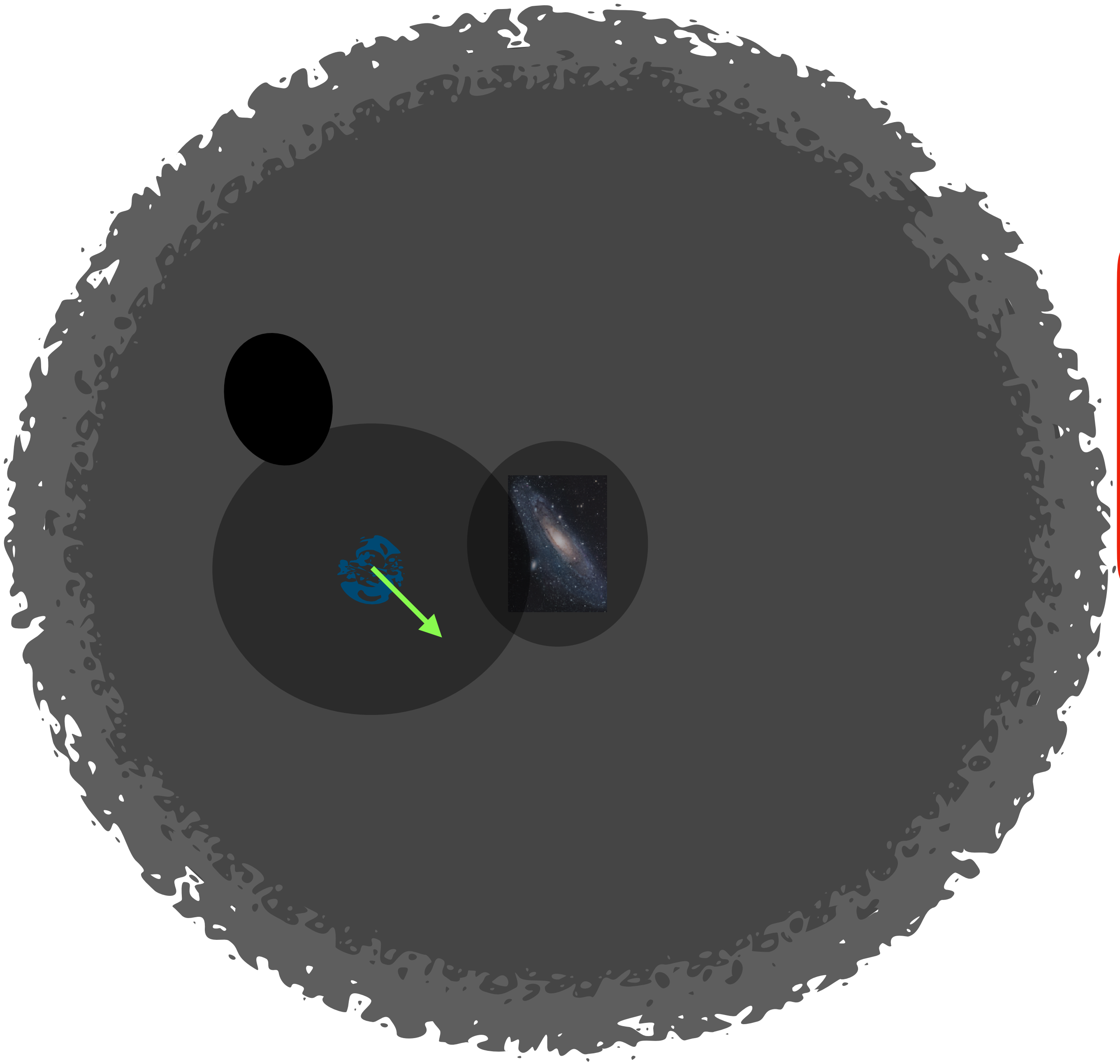

And this is why galaxies merge**,**

but only in the dark matter theory

Newtonian plus dark matter calculations of the encounter of two disk galaxies

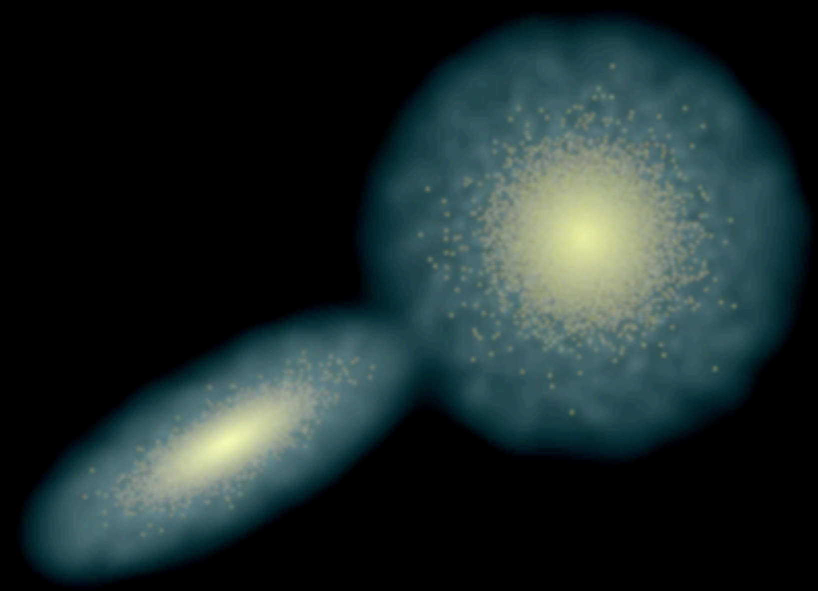

Wetzstein, Naab & Burkert 2007

Newtonian plus dark matter calculations of the encounter of two disk galaxies

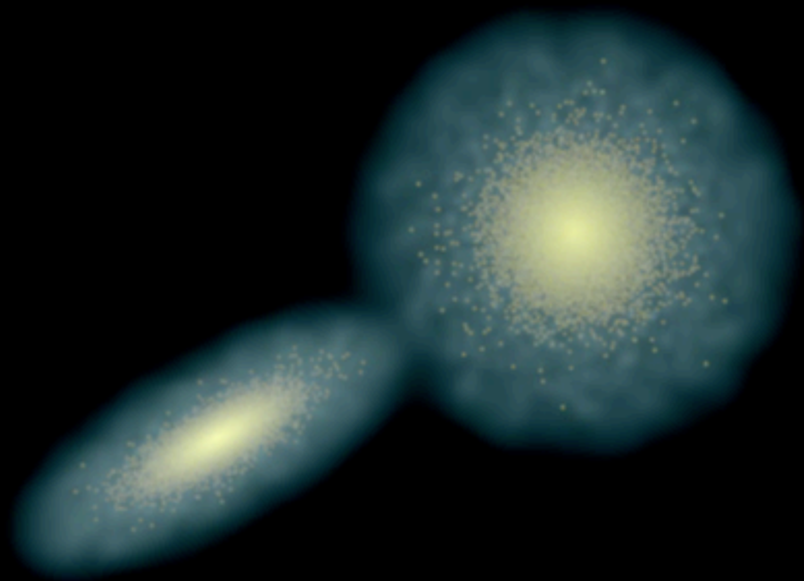

Wetzstein, Naab & Burkert 2007

Chandrasekhar dynamical friction

is very well understood.

e.g. Binney & Tremaine 1987 - textbook

For a given galaxy,
its dark-matter halo is thus known
(within a well specified range of properties)

For a given galaxy,
its dark-matter halo is thus known
(within a well specified range of properties)

Given these properties,
we can test if the observed
satellite galaxies
(e.g. around our Milky Way)
comply with these
in terms of their
ages, *stellar masses*, *position and velocity vectors*.

For a given galaxy,
its dark-matter halo is thus known
(within a well specified range of properties)

Given these properties,
we can test if the observed
satellite galaxies
(e.g. around our Milky Way)
comply with these
in terms of their
ages, *stellar masses, position and velocity vectors*.

As the satellite galaxy obits,
it induces a wake of dark matter particles behind itself,
and this leads to
Chandrasekhar dynamical friction,
the strength of which depends on the
total mass of the satellite galaxy.

For a given galaxy,
its dark-matter halo is thus known
(within a well specified range of properties)

Given these properties,
we can test if the observed
satellite galaxies
(e.g. around our Milky Way)
comply with these
in terms of their
ages, *stellar masses*, *position and velocity vectors*.

As the satellite galaxy obits,
it induces a wake of dark matter particles behind itself,
and this leads to
Chandrasekhar dynamical friction,
the strength of which depends on the
total mass of the satellite galaxy.

They must have fallen-in -- so, are there infall solutions **?**

Chandrasekhar dynamical friction :

Orbits of satellite galaxies

Sales, Navarro et al. 2017, MNRAS, "The low-mass end of the baryonic Tully–Fisher relation" (EAGLE simulation)

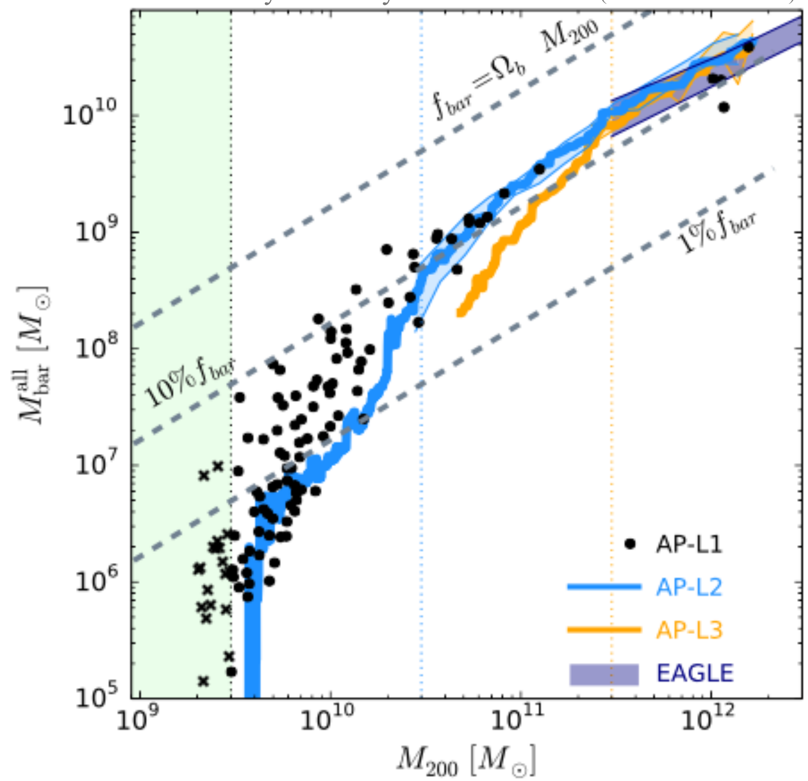

Chandrasekhar dynamical friction :

Orbits of satellite galaxies

Angus et al. 2011

Table 2. Galactocentric distances and velocities of the dSphs. For Fornax, Sculptor and Ursa Minor, our V_{x_0} corresponds to Piatek et al. (2003, 2005, 2006, 2007a) V_r and our V_{y_0} to their V_t. For Carina, the proper motion comes directly from Pasetto et al. (2011). Distances come from Mateo (1998).

dSph	r_0 (kpc)	V_{x_0} (km s^{-1})	V_{y_0} (km s^{-1})	L_V ($L_\odot$)
Fornax	138 ± 8	-31.8 ± 1.7	196 ± 29	15.5×10^6
Sculptor	87 ± 4	79 ± 6	198 ± 50	2.2×10^6
Ursa Minor	76 ± 4	-75 ± 44	144 ± 50	0.29×10^6
Carina	101 ± 5	113 ± 52	46 ± 54	0.43×10^6

Note **:** the inner region of a satellite is affected by tides after significant tidal destruction of its outer parts (Kazantzidis et al. 2004).
I.e. the baryonic content (i.e. L_V) is a measure of the DMhalo mass according to LCDM theory.

Sales, Navarro et al. 2017, MNRAS, "The low-mass end of the baryonic Tully–Fisher relation" (EAGLE simulation)

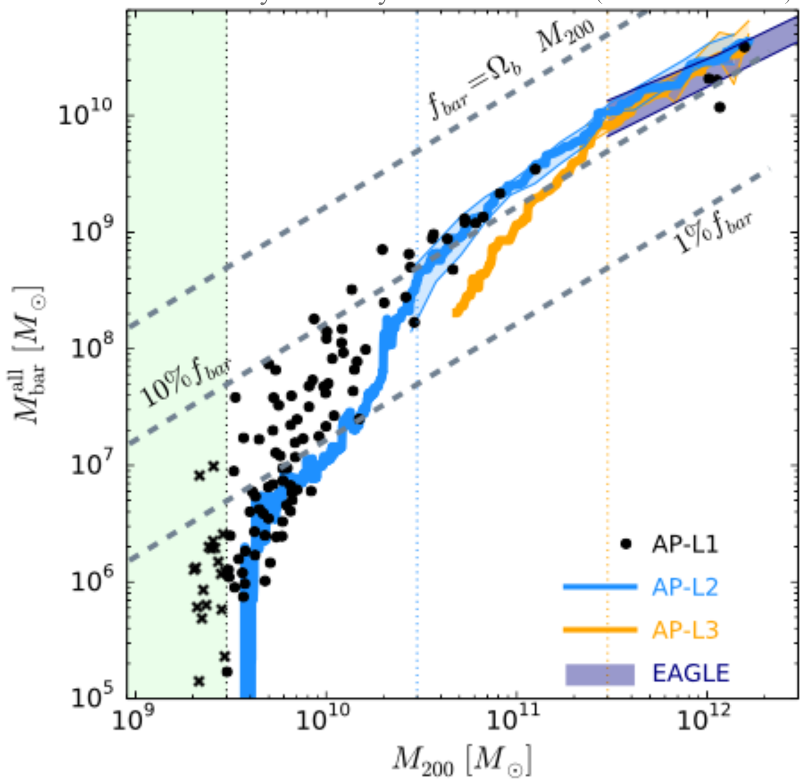

Chandrasekhar dynamical friction :

Orbits of satellite galaxies

Angus et al. 2011

Table 2. Galactocentric distances and velocities of the dSphs. For Fornax, Sculptor and Ursa Minor, our V_{x_0} corresponds to Piatek et al. (2003, 2005, 2006, 2007a) V_r and our V_{y_0} to their V_t. For Carina, the proper motion comes directly from Pasetto et al. (2011). Distances come from Mateo (1998).

dSph	r_0 (kpc)	V_{x_0} (km s^{-1})	V_{y_0} (km s^{-1})	L_V ($L_\odot$)
Fornax	138 ± 8	-31.8 ± 1.7	196 ± 29	15.5×10^6
Sculptor	87 ± 4	79 ± 6	198 ± 50	2.2×10^6
Ursa Minor	76 ± 4	-75 ± 44	144 ± 50	0.29×10^6
Carina	101 ± 5	113 ± 52	46 ± 54	0.43×10^6

Note : the inner region of a satellite is affected by tides after significant tidal destruction of its outer parts (Kazantzidis et al. 2004).

I.e. the baryonic content (i.e. L_V) is a measure of the DMhalo mass according to LCDM theory.

Sales, Navarro et al. 2017, MNRAS, "The low-mass end of the baryonic Tully–Fisher relation" (EAGLE simulation)

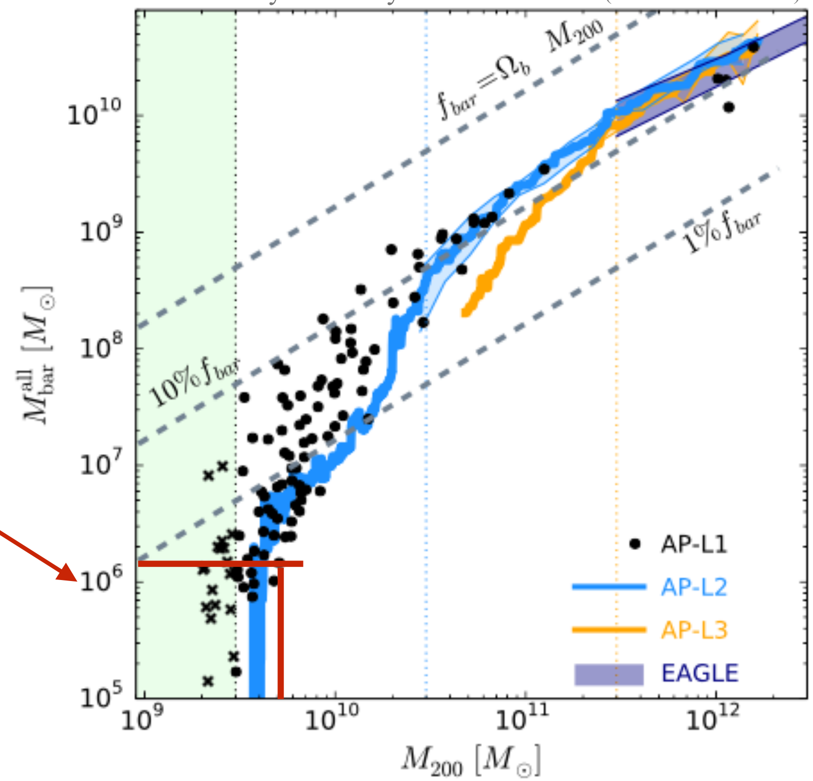

Chandrasekhar dynamical friction :

Orbits of satellite galaxies

Angus et al. 2011

Table 2. Galactocentric distances and velocities of the dSphs. For Fornax, Sculptor and Ursa Minor, our V_{x_0} corresponds to Piatek et al. (2003, 2005, 2006, 2007a) V_r and our V_{y_0} to their V_t. For Carina, the proper motion comes directly from Pasetto et al. (2011). Distances come from Mateo (1998).

dSph	r_0 (kpc)	V_{x_0} (km s^{-1})	V_{y_0} (km s^{-1})	L_V ($L_\odot$)
Fornax	138 ± 8	-31.8 ± 1.7	196 ± 29	15.5×10^6
Sculptor	87 ± 4	79 ± 6	198 ± 50	2.2×10^6
Ursa Minor	76 ± 4	-75 ± 44	144 ± 50	0.29×10^6
Carina	101 ± 5	113 ± 52	46 ± 54	0.43×10^6

Note : the inner region of a satellite is affected by tides after significant tidal destruction of its outer parts (Kazantzidis et al. 2004).
I.e. the baryonic content (i.e. L_V) is a measure of the DMhalo mass according to LCDM theory.

Sales, Navarro et al. 2017, MNRAS, "The low-mass end of the baryonic Tully–Fisher relation" (EAGLE simulation)

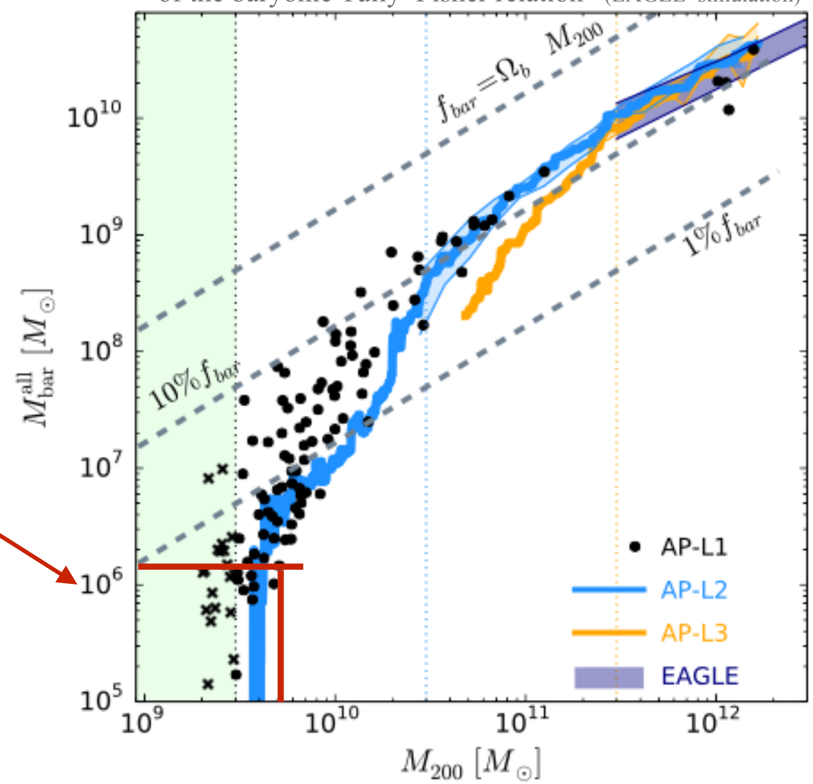

observed stellar masses

$\Rightarrow M_{\rm DMhalo} < 5 \times 10^9 \, M_\odot$

Chandrasekhar dynamical friction :

Orbits of satellite galaxies

Angus et al. 2011

Table 2. Galactocentric distances and velocities of the dSphs. For Fornax, Sculptor and Ursa Minor, our V_{x_0} corresponds to Piatek et al. (2003, 2005, 2006, 2007a) V_r and our V_{y_0} to their V_t. For Carina, the proper motion comes directly from Pasetto et al. (2011). Distances come from Mateo (1998).

dSph	r_0 (kpc)	V_{x_0} (km s^{-1})	V_{y_0} (km s^{-1})	L_V ($L_\odot$)
Fornax	138 ± 8	-31.8 ± 1.7	196 ± 29	15.5×10^6
Sculptor	87 ± 4	79 ± 6	198 ± 50	2.2×10^6
Ursa Minor	76 ± 4	-75 ± 44	144 ± 50	0.29×10^6
Carina	101 ± 5	113 ± 52	46 ± 54	0.43×10^6

Note : the inner region of a satellite is affected by tides after significant tidal destruction of its outer parts (Kazantzidis et al. 2004).

I.e. the baryonic content (i.e. L_V) is a measure of the DMhalo mass according to LCDM theory.

Sales, Navarro et al. 2017, MNRAS, "The low-mass end of the baryonic Tully–Fisher relation" (EAGLE simulation)

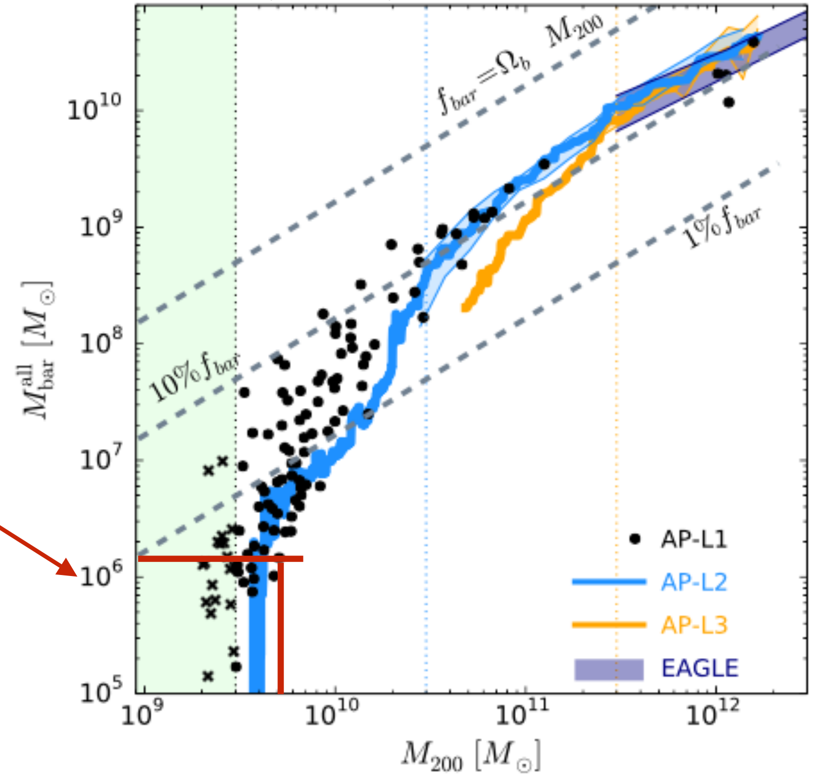

observed stellar masses

$M_{\rm DMhalo} < 5 \times 10^9 \, M_\odot$

$M_{\rm DMhalo} > 10^{10} \, M_\odot$

needed DMhalo masses for infall (for the satellite to get stuck)

Chandrasekhar dynamical friction :

Orbits of satellite galaxies

Angus et al. 2011

Table 2. Galactocentric distances and velocities of the dSphs. For Fornax, Sculptor and Ursa Minor, our V_{x_0} corresponds to Piatek et al. (2003, 2005, 2006, 2007a) V_r and our V_{y_0} to their V_t. For Carina, the proper motion comes directly from Pasetto et al. (2011). Distances come from Mateo (1998).

dSph	r_0 (kpc)	V_{x_0} (km s^{-1})	V_{y_0} (km s^{-1})	$L_V\,(L_\odot)$
Fornax	138 ± 8	-31.8 ± 1.7	196 ± 29	15.5×10^6
Sculptor	87 ± 4	79 ± 6	198 ± 50	2.2×10^6
Ursa Minor	76 ± 4	-75 ± 44	144 ± 50	0.29×10^6
Carina	101 ± 5	113 ± 52	46 ± 54	0.43×10^6

Note : the inner region of a satellite is affected by tides after significant tidal destruction of its outer parts
(Kazantzidis et al. 2004).
I.e. the baryonic content (i.e. L_V) is a measure of the DMhalo mass according to LCDM theory.

Sales, Navarro et al. 2017, MNRAS, "The low-mass end of the baryonic Tully–Fisher relation" (EAGLE simulation)

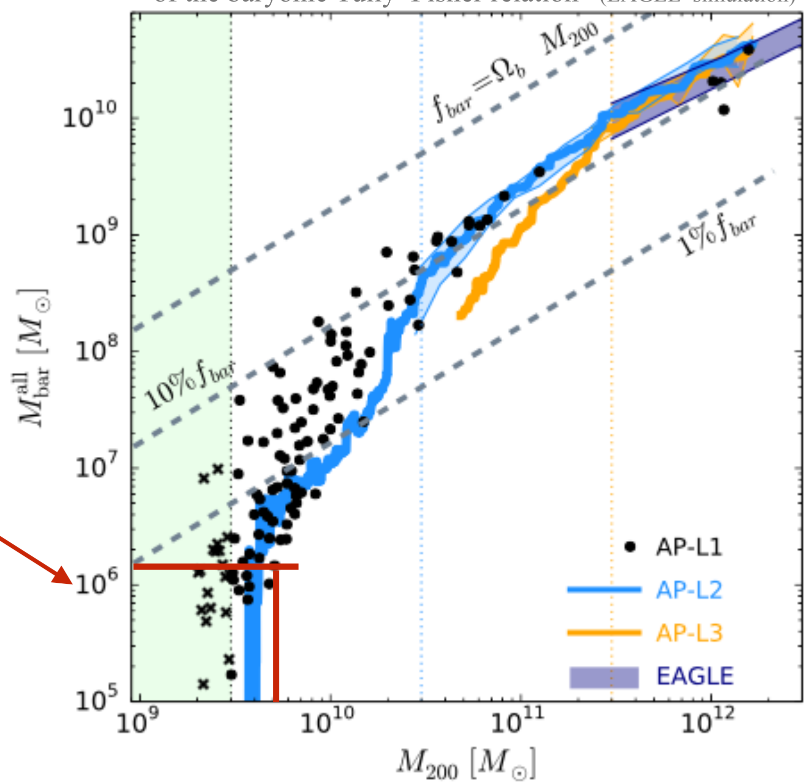

observed stellar masses

$M_{\rm DMhalo} < 5 \times 10^9\, M_\odot$ ⟷ incompatible ⟷ $M_{\rm DMhalo} > 10^{10}\, M_\odot$
needed DMhalo masses for infall (for the satellite to get stuck)

Chandrasekhar dynamical friction :

Orbits of satellite galaxies

Angus et al. 2011

Table 2. Galactocentric distances and velocities of the dSphs. For Fornax, Sculptor and Ursa Minor, our V_{x_0} corresponds to Piatek et al. (2003, 2005, 2006, 2007a) V_r and our V_{y_0} to their V_t. For Carina, the proper motion comes directly from Pasetto et al. (2011). Distances come from Mateo (1998).

dSph	r_0 (kpc)	V_{x_0} (km s^{-1})	V_{y_0} (km s^{-1})	L_V ($L_\odot$)
Fornax	138 ± 8	-31.8 ± 1.7	196 ± 29	15.5×10^6
Sculptor	87 ± 4	79 ± 6	198 ± 50	2.2×10^6
Ursa Minor	76 ± 4	-75 ± 44	144 ± 50	0.29×10^6
Carina	101 ± 5	113 ± 52	46 ± 54	0.43×10^6

Note : the inner region of a satellite is affected by tides after significant tidal destruction of its outer parts (Kazantzidis et al. 2004).

I.e. the baryonic content (i.e. L_V) is a measure of the DMhalo mass according to LCDM theory.

Sales, Navarro et al. 2017, MNRAS, "The low-mass end of the baryonic Tully–Fisher relation" (EAGLE simulation)

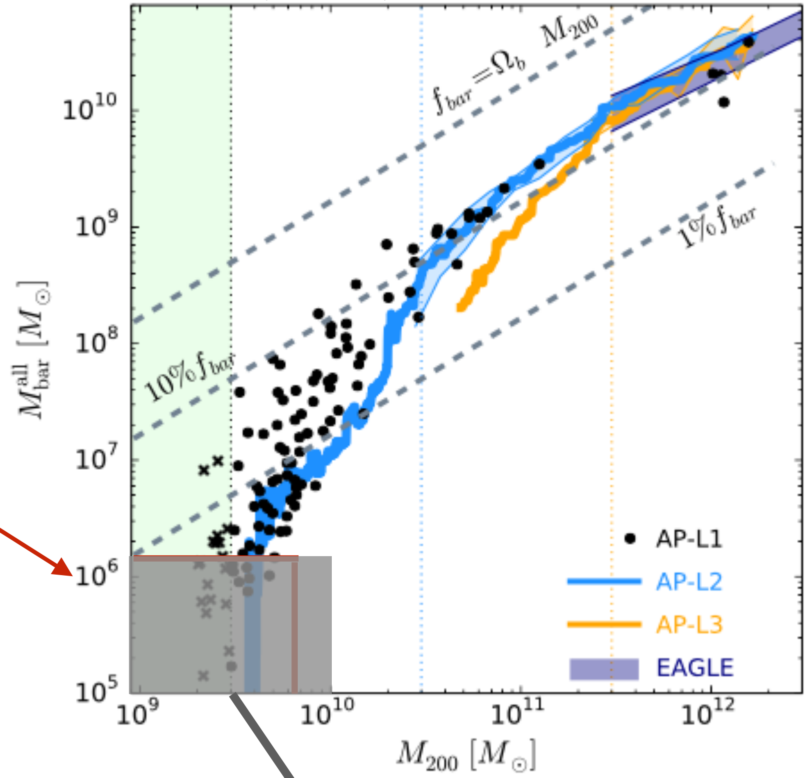

excluded by observational data.

observed stellar masses

$M_{\rm DMhalo} < 5 \times 10^9\, M_\odot$ incompatible $M_{\rm DMhalo} > 10^{10}\, M_\odot$

needed DMhalo masses for infall (for the satellite to get stuck)

Chandrasekhar dynamical friction :

Orbits of satellite galaxies

Angus et al. 2011

Table 2. Galactocentric distances and velocities of the dSphs. For Fornax, Sculptor and Ursa Minor, our V_{x0} corresponds to Piatek et al. (2003, 2005, 2006, 2007a) V_r and our V_{y0} to their V_t. For Carina, the proper motion comes directly from Pasetto et al. (2011). Distances come from Mateo (1998).

dSph	r_0 (kpc)	V_{x_0} (km s^{-1})	V_{y_0} (km s^{-1})	L_V ($L_\odot$)
Fornax	138 ± 8	-31.8 ± 1.7	196 ± 29	15.5×10^6
Sculptor	87 ± 4	79 ± 6	198 ± 50	2.2×10^6
Ursa Minor	76 ± 4	-75 ± 44	144 ± 50	0.29×10^6
Carina	101 ± 5	113 ± 52	46 ± 54	0.43×10^6

Note : the inner region of a satellite is affected by tides after significant tidal destruction of its outer parts (Kazantzidis et al. 2004).
I.e. the baryonic content (i.e. L_V) is a measure of the DMhalo mass according to LCDM theory.

Sales, Navarro et al. 2017, MNRAS, "The low-mass end of the baryonic Tully–Fisher relation" (EAGLE simulation)

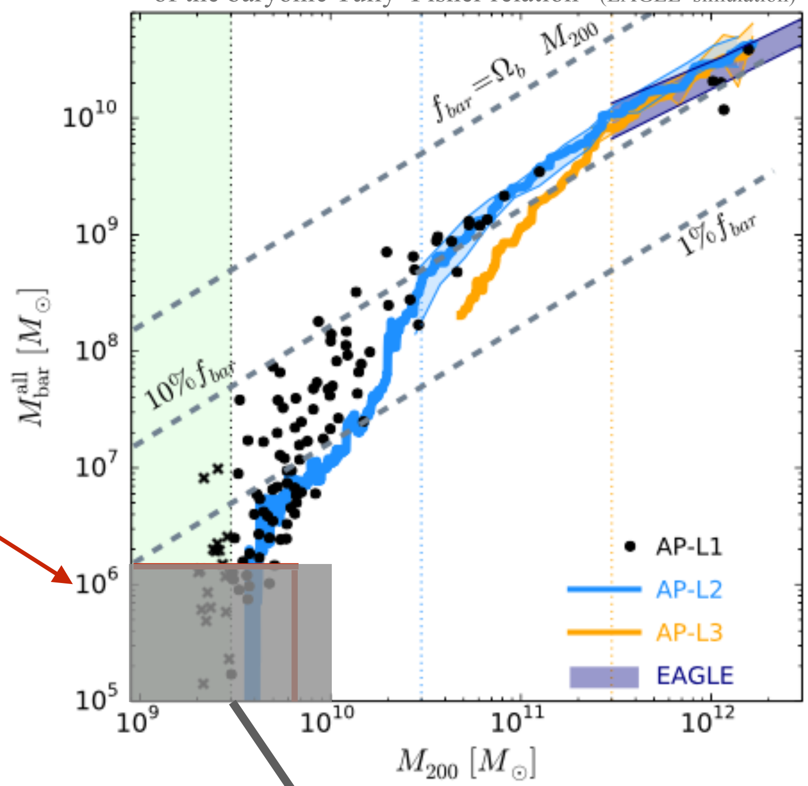

excluded by observational data.

observed stellar masses

$M_{\rm DMhalo} < 5 \times 10^9 \, M_\odot$ incompatible $M_{\rm DMhalo} > 10^{10} \, M_\odot$

needed DMhalo masses for infall (for the satellite to get stuck)

no SMoC infall solutions

Chandrasekhar dynamical friction :

Orbits of satellite galaxies

Angus et al. 2011

Table 2. Galactocentric distances and velocities of the dSphs. For Fornax, Sculptor and Ursa Minor, our V_{x_0} corresponds to Piatek et al. (2003, 2005, 2006, 2007a) V_r and our V_{y_0} to their V_t. For Carina, the proper motion comes directly from Pasetto et al. (2011). Distances come from Mateo (1998).

dSph	r_0 (kpc)	V_{x_0} (km s^{-1})	V_{y_0} (km s^{-1})	L_V ($L_\odot$)
Fornax	138 ± 8	-31.8 ± 1.7	196 ± 29	15.5×10^6
Sculptor	87 ± 4	79 ± 6	198 ± 50	2.2×10^6
Ursa Minor	76 ± 4	-75 ± 44	144 ± 50	0.29×10^6
Carina	101 ± 5	113 ± 52	46 ± 54	0.43×10^6

Note : the inner region of a satellite is affected by tides after significant tidal destruction of its outer parts (Kazantzidis et al. 2004).
I.e. the baryonic content (i.e. L_V) is a measure of the DMhalo mass according to LCDM theory.

Sales, Navarro et al. 2017, MNRAS, "The low-mass end of the baryonic Tully–Fisher relation" (EAGLE simulation)

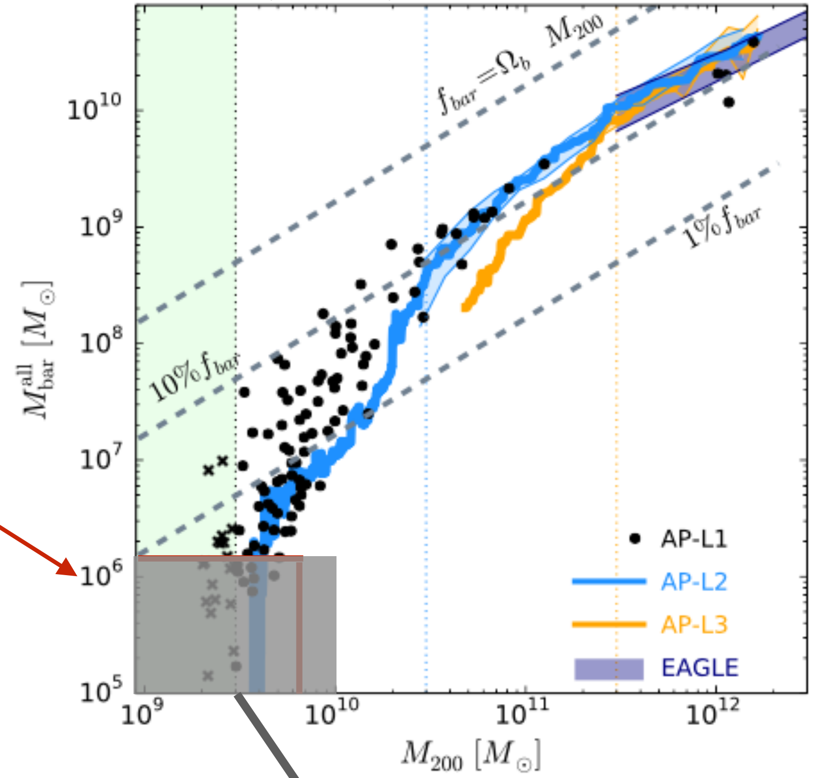

excluded by observational data.

observed stellar masses

$M_{\rm DMhalo} < 5 \times 10^9\, M_\odot$ incompatible $M_{\rm DMhalo} > 10^{10}\, M_\odot$

needed DMhalo masses for infall (for the satellite to get stuck)

no SMoC infall solutions

no dark matter halos

Case in point:
The orbits
of the
Large (LMC)
and
Small (SMC)
Magellanic Clouds

Magellanic clouds
Magellanic Stream began to form
about 1-2Gyr ago

e.g. Wang, Hammer...+2022

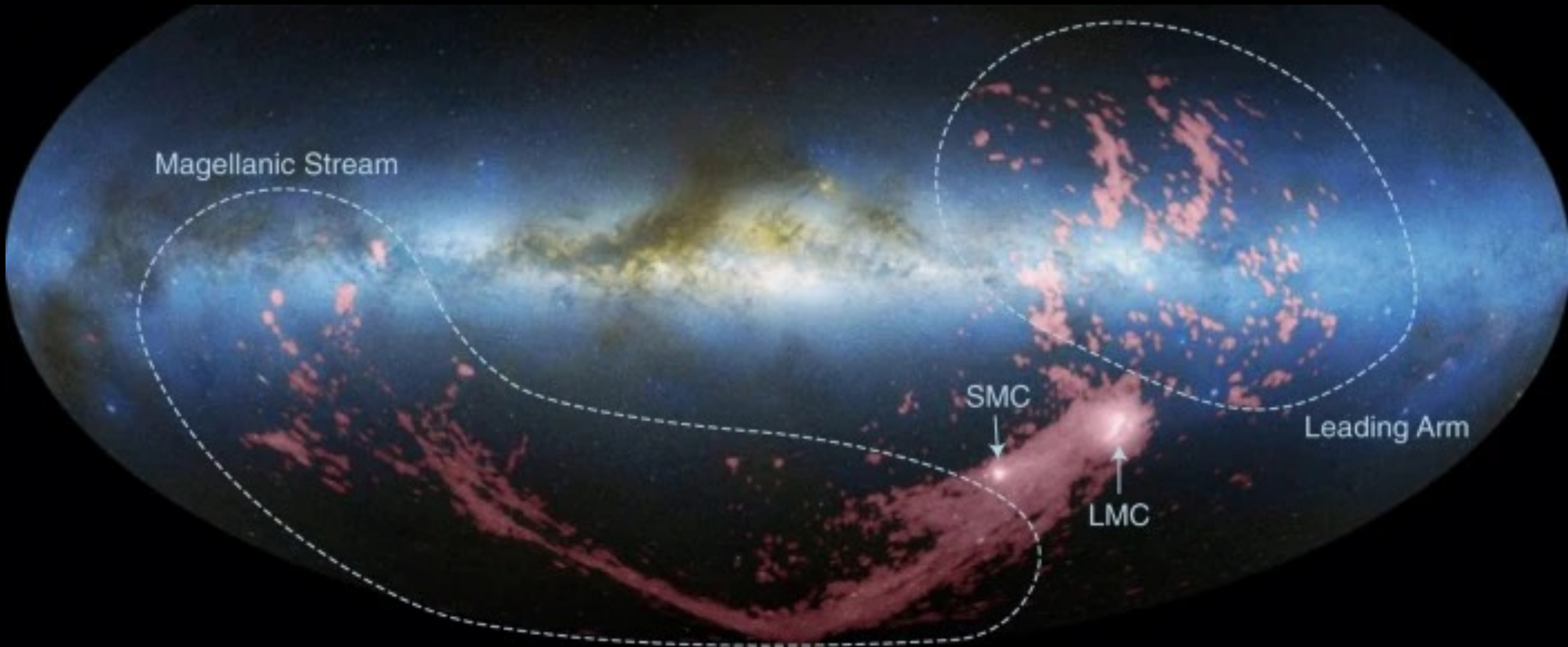

Credit: NASA/D. Nidever

Current distances : LMC-MW = 55kpc
SMC-LMC = 20kpc

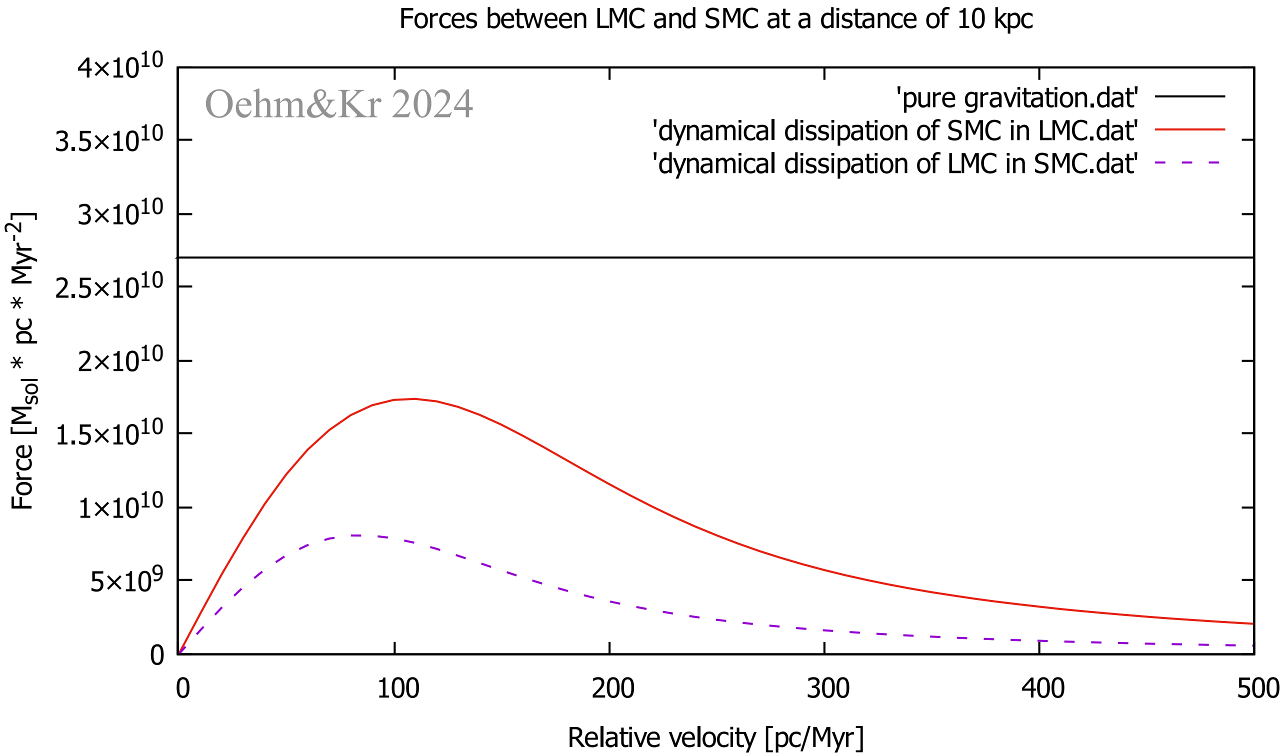

Applied to the LMC and SMC

Current distances : LMC-MW = 55kpc
SMC-LMC = 20kpc

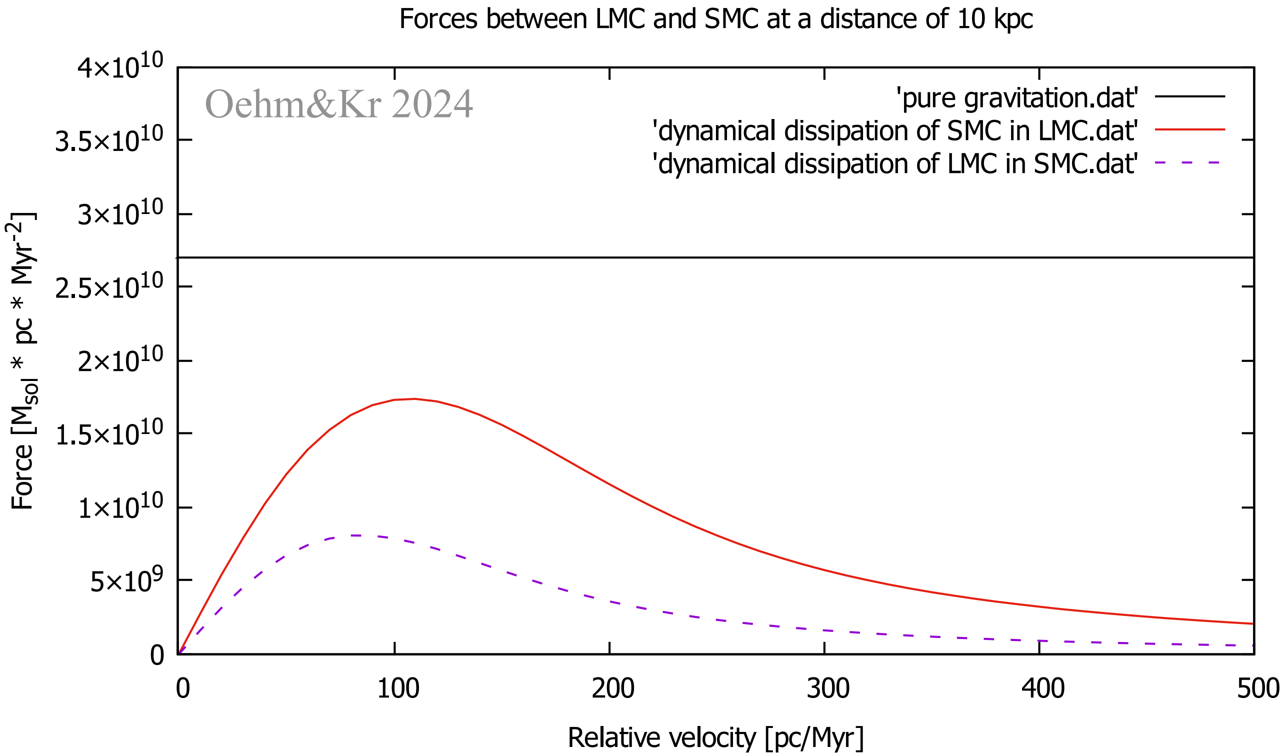

Applied to the LMC and SMC

The *frictional deceleration* of the LMC / SMC orbital motion due to Chandrasekhar dynamical friction is comparable to the gravitational *attraction* between the two.

Monthly Notices of the ROYAL ASTRONOMICAL SOCIETY

MNRAS **513,** L40–L45 (2022) https://doi.org/10.1093/mnrasl/slac030
Advance Access publication 2022 March 25

The synchronized dance of the magellanic clouds' star formation history

P. Massana,[1,2★] T. Ruiz-Lara,[3★] N. E. D. Noël,[1] C. Gallart,[4,5] D. L. Nidever,[6] Y. Choi,[7] J. D. Sakowska,[1] G. Besla,[8] K. A. G. Olsen,[9] M. Monelli,[4,5] A. Dorta,[4] G. S. Stringfellow,[10] S. Cassisi,[11,12] E. J. Bernard,[13] D. Zaritsky,[8] M.-R. L. Cioni,[14] A. Monachesi,[15,16] R. P. van der Marel,[7,17] T. J. L. de Boer[18] and A. R. Walker[19]

ABSTRACT

We use the SMASH survey to obtain unprecedented deep photometry reaching down to the oldest main-sequence turn-offs in the colour–magnitude diagrams (CMDs) of the Small Magellanic Cloud (SMC) and quantitatively derive its star formation history (SFH) using CMD fitting techniques. We identify five distinctive peaks of star formation in the last 3.5 Gyr, at ~3, ~2, ~1.1, ~0.45 Gyr ago, and one presently. We compare these to the SFH of the Large Magellanic Cloud (LMC), finding unequivocal synchronicity, with both galaxies displaying similar periods of enhanced star formation over the past ~3.5 Gyr. The parallelism between their SFHs indicates that tidal interactions between the MCs have recurrently played an important role in their evolution for at least the last ~3.5 Gyr, tidally truncating the SMC and shaping the LMC's spiral arm. We show, for the first time, an SMC–LMC correlated SFH at recent times in which enhancements of star formation are localized in the northern spiral arm of the LMC, and globally across the SMC. These novel findings should be used to constrain not only the orbital history of the MCs but also how star formation should be treated in simulations.

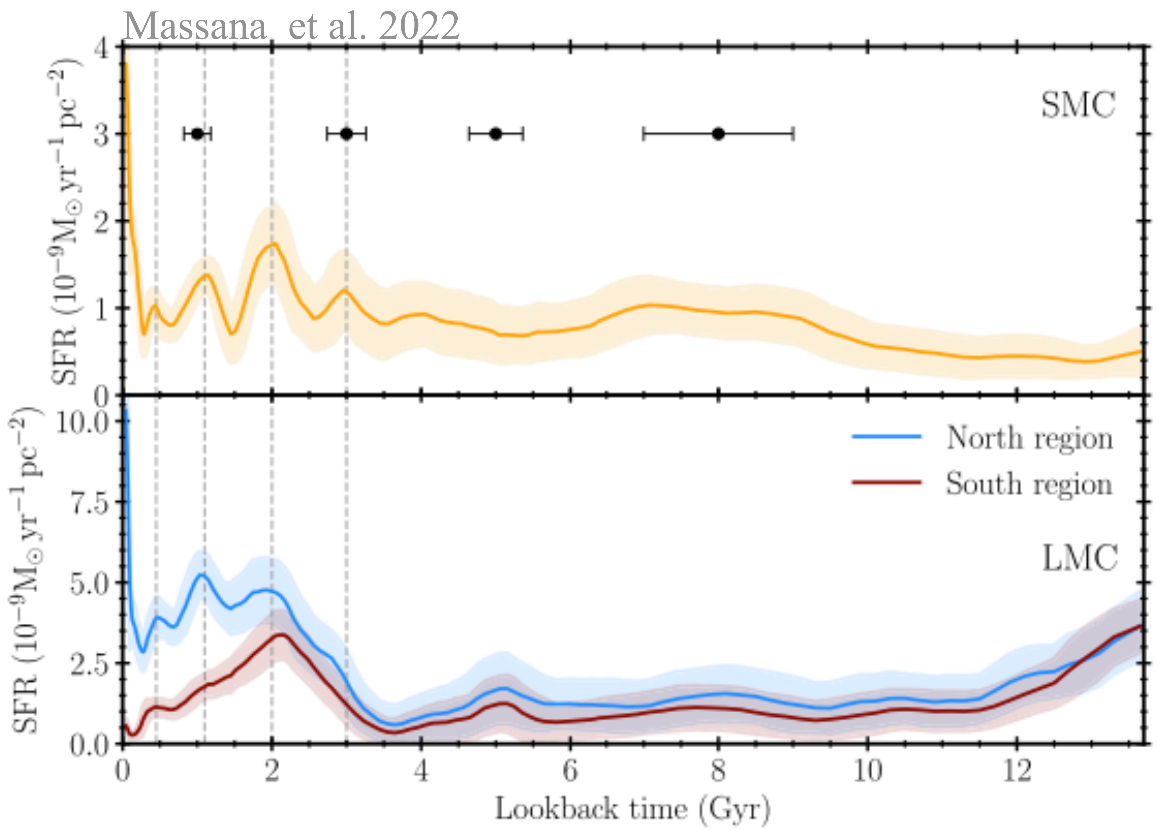

The LMC and SMC have peaks in the SFRs at very similar times because of their orbits about each other.

Figure 2. Comparison of the global SFRs for the SMC (this work) and the LMC (Ruiz-Lara et al. 2020b). Vertical dashed lines link the peaks at 0.45, 1.1, 2, and 3 Gyr ago in the SMC to those of the LMC. The horizontal bars in the top panel show the width of the SFH enhancement. Uncertainties in the SFHs (shaded regions) were calculated as in Hidalgo et al. (2011) and Rusakov et al. (2021).

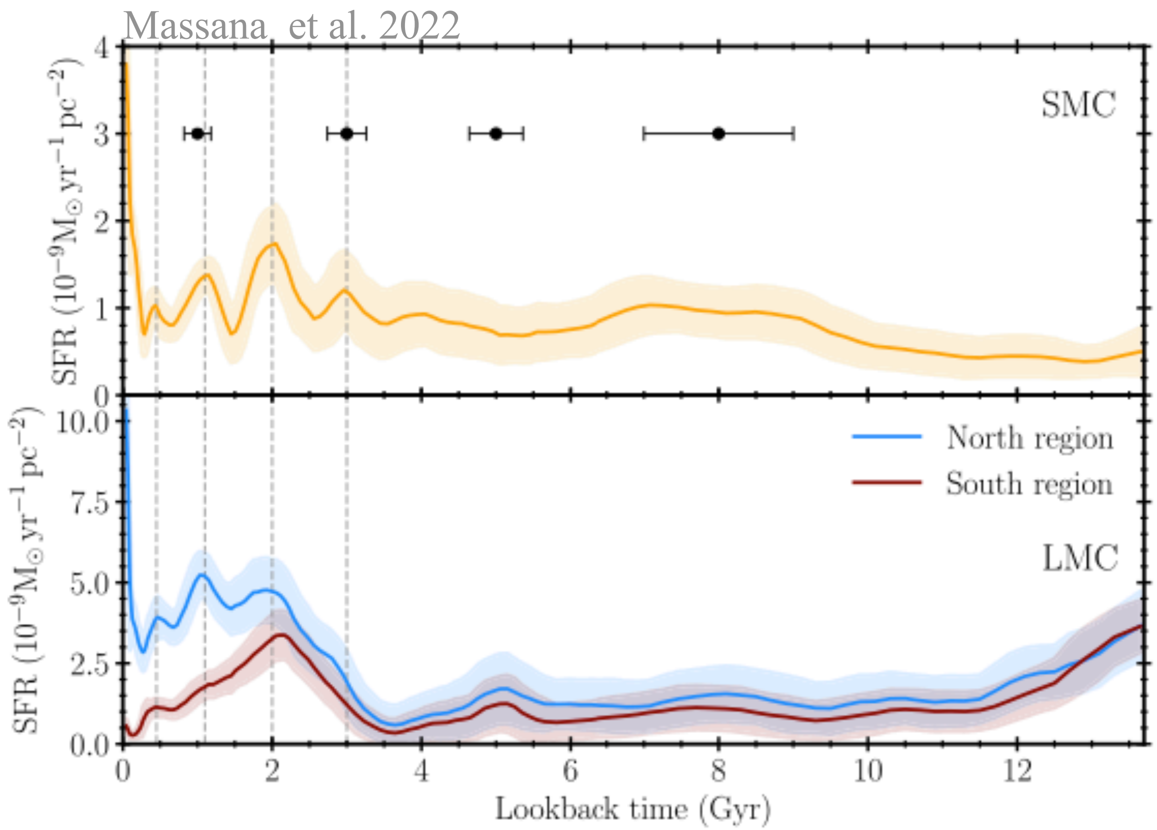

Figure 2. Comparison of the global SFRs for the SMC (this work) and the LMC (Ruiz-Lara et al. 2020b). Vertical dashed lines link the peaks at 0.45, 1.1, 2, and 3 Gyr ago in the SMC to those of the LMC. The horizontal bars in the top panel show the width of the SFH enhancement. Uncertainties in the SFHs (shaded regions) were calculated as in Hidalgo et al. (2011) and Rusakov et al. (2021).

The LMC and SMC have peaks in the SFRs at very similar times because of their orbits about each other.

This constrains the number of close encounters the SMC had with the LMC :

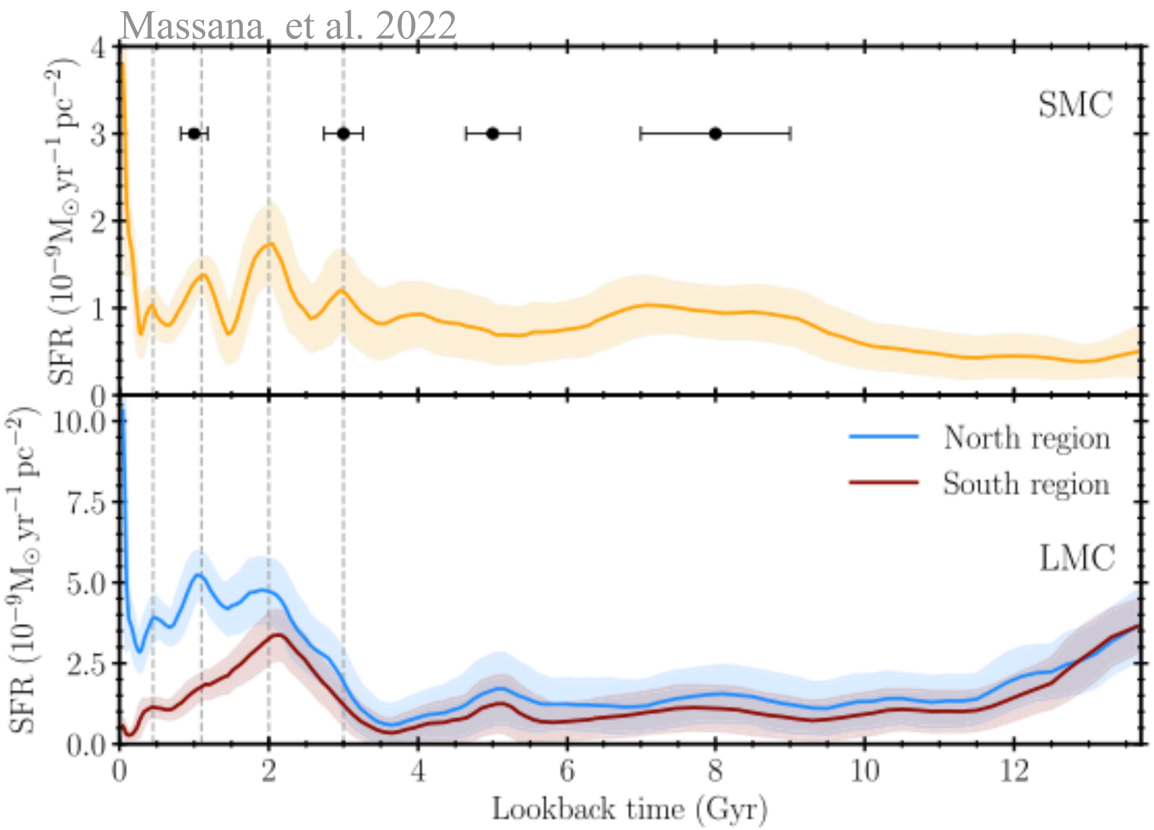

Figure 2. Comparison of the global SFRs for the SMC (this work) and the LMC (Ruiz-Lara et al. 2020b). Vertical dashed lines link the peaks at 0.45, 1.1, 2, and 3 Gyr ago in the SMC to those of the LMC. The horizontal bars in the top panel show the width of the SFH enhancement. Uncertainties in the SFHs (shaded regions) were calculated as in Hidalgo et al. (2011) and Rusakov et al. (2021).

The LMC and SMC have peaks in the SFRs at very similar times because of their orbits about each other.

This constrains the number of close encounters the SMC had with the LMC :

4 over the past 3Gyr !

Search for solutions using (i) genetic algorithm and (ii) Markov-Chain Monte-Carlo method
within the 5sigma uncertainty bounds of velocities
such that LMC and SMC had an encounter between 1 and 4 Gyr ago with a separation of 20kpc or smaller.

Search for solutions using (i) genetic algorithm and (ii) Markov-Chain Monte-Carlo method within the 5sigma uncertainty bounds of velocities such that LMC and SMC had an encounter between 1 and 4 Gyr ago with a separation of 20kpc or smaller.

Table 1. Stellar masses of the galaxies (model (o)), varied by −30% (model (m)) and +30% (model (p)), and the derived DM halo masses according to **Section 2.1**.

Object	Model	Stellar Mass $[M_\odot]$	DM Halo Mass $[M_\odot]$
MW	(o)	5×10^{10}	2.41×10^{12}
	−30% (m)	3.5×10^{10}	1.39×10^{12}
	+30% (p)	6.5×10^{10}	4.05×10^{12}
LMC	(o)	3.2×10^{9}	2.55×10^{11}
	−30% (m)	2.24×10^{9}	1.47×10^{11}
	+30% (p)	4.16×10^{9}	2.90×10^{11}
SMC	(o)	5.3×10^{8}	1.07×10^{11}
	−30% (m)	3.71×10^{8}	8.86×10^{10}
	+30% (p)	6.89×10^{8}	1.24×10^{11}

Oehm & Kroupa 2024

Table 3. Observational data for LMC and SMC and in parts for the Galactic centre.

Object	RA (EquJ2000)	DEC (EquJ2000)	Heliocentric Distance	Heliocentric Radial Velocity
LMC	80.894°	−69.756°	49.97 kpc	262.2 km/s
SMC	13.187°	−72.829°	60.6 kpc	145.6 km/s
MW	266.405°	−28.936°	8.122 kpc	

Table 4. Transverse velocity components for LMC and SMC.

Object	v_{RA} [mas/yr]	v_{RA} [km/s]	v_{DEC} [mas/yr]	v_{DEC} [km/s]
LMC	1.872 ± 0.045	443.3 ± 10.7	0.224 ± 0.054	53.0 ± 12.8
SMC	0.820 ± 0.060	235.5 ± 17.2	-1.230 ± 0.070	-353.3 ± 20.1

The LMC and SMC have dark-matter halos
according to the SMoC and
are integrated backwards in time
(i.e. the friction leads to an acceleration)
assuming their observed position and velocity
vectors
(Gaia data).

The LMC and SMC have dark-matter halos according to the SMoC and are integrated backwards in time (i.e. the friction leads to an acceleration) assuming their observed position and velocity vectors (Gaia data).

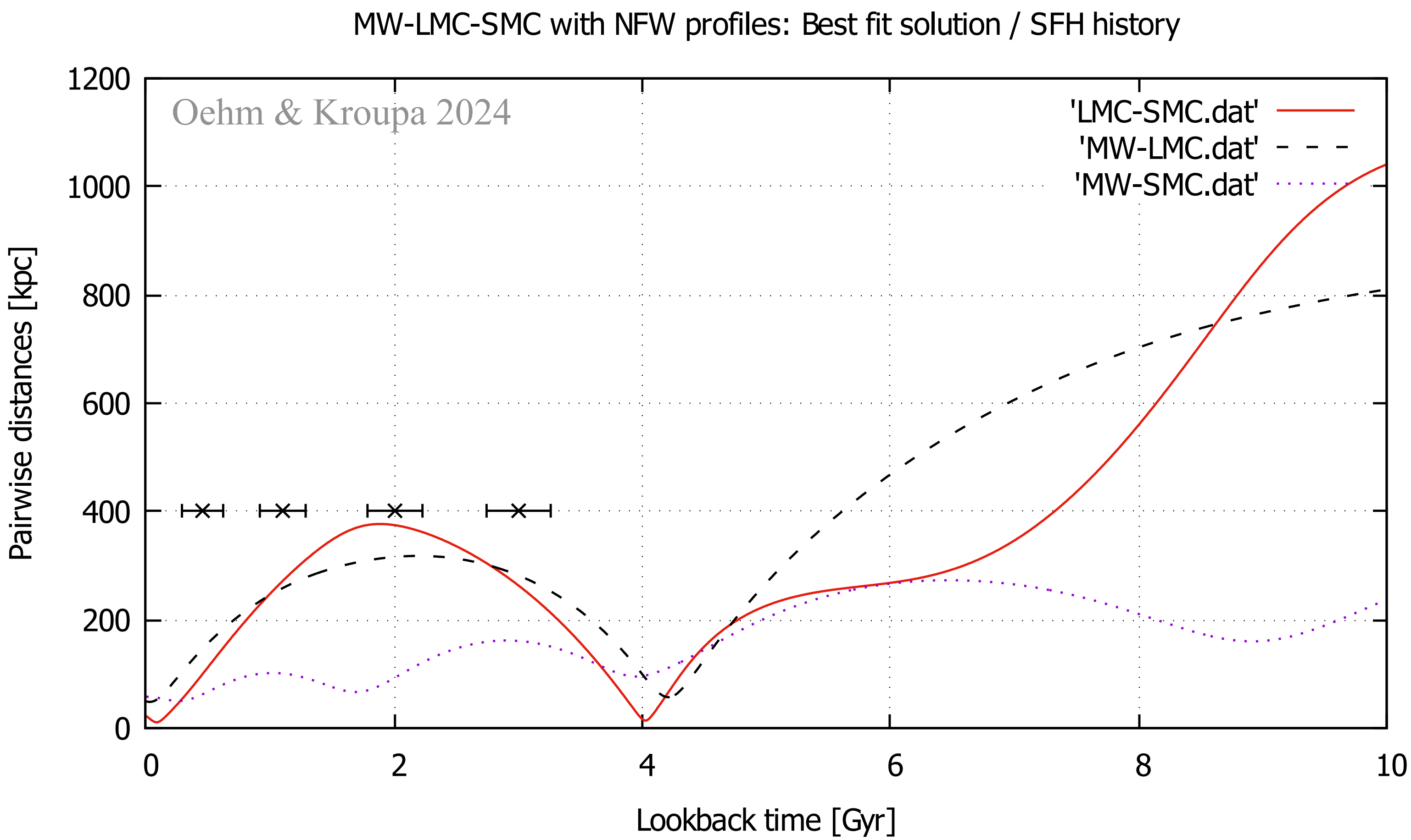

The LMC and SMC have dark-matter halos
according to the SMoC and
are integrated backwards in time
(i.e. the friction leads to an acceleration)
assuming their observed position and velocity
vectors
(Gaia data).

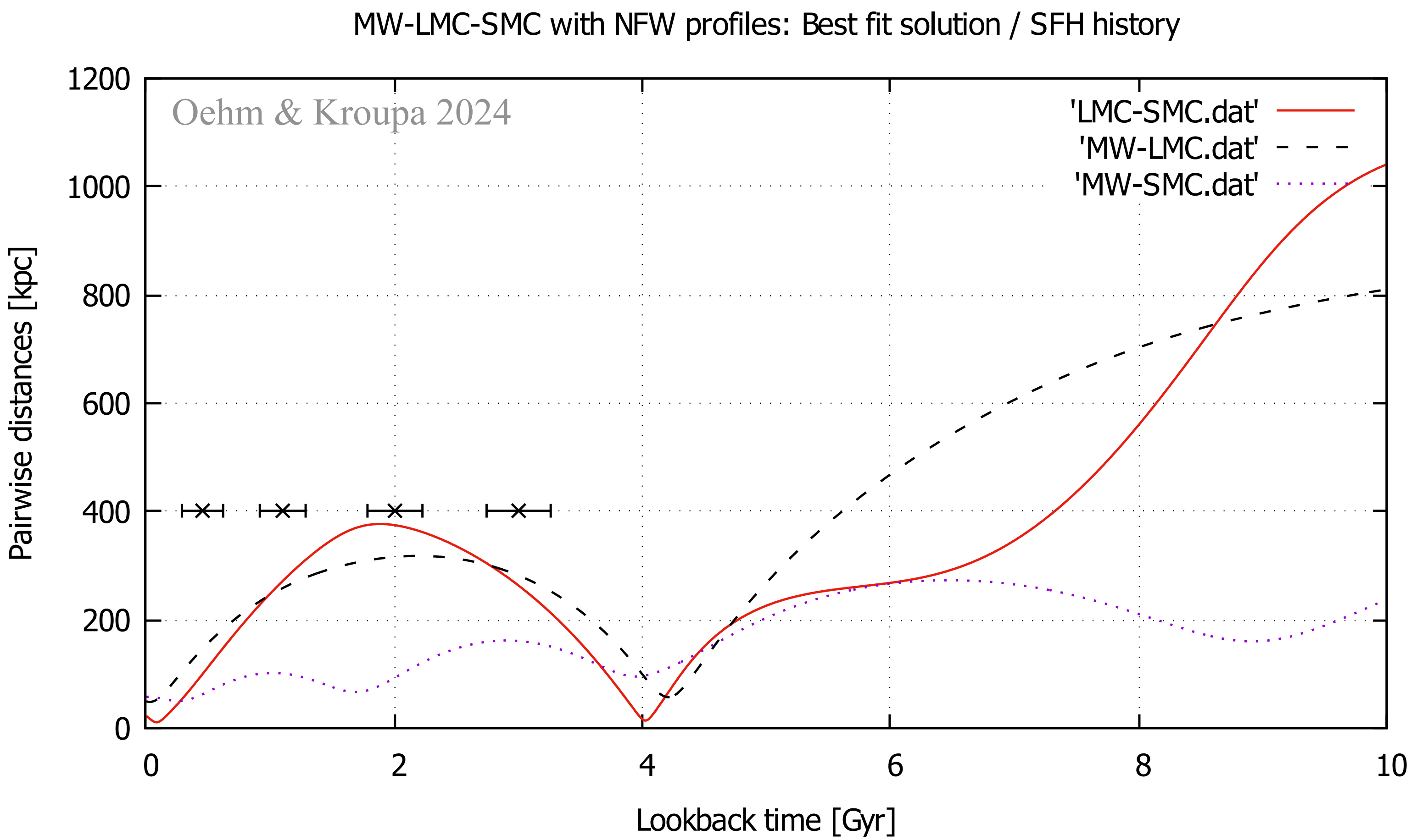

No solution of
SMC-LMC orbit
that explains
the synchronised
star-formation
history.

The LMC and SMC have dark-matter halos according to the SMoC and are integrated backwards in time (i.e. the friction leads to an acceleration) assuming their observed position and velocity vectors (Gaia data).

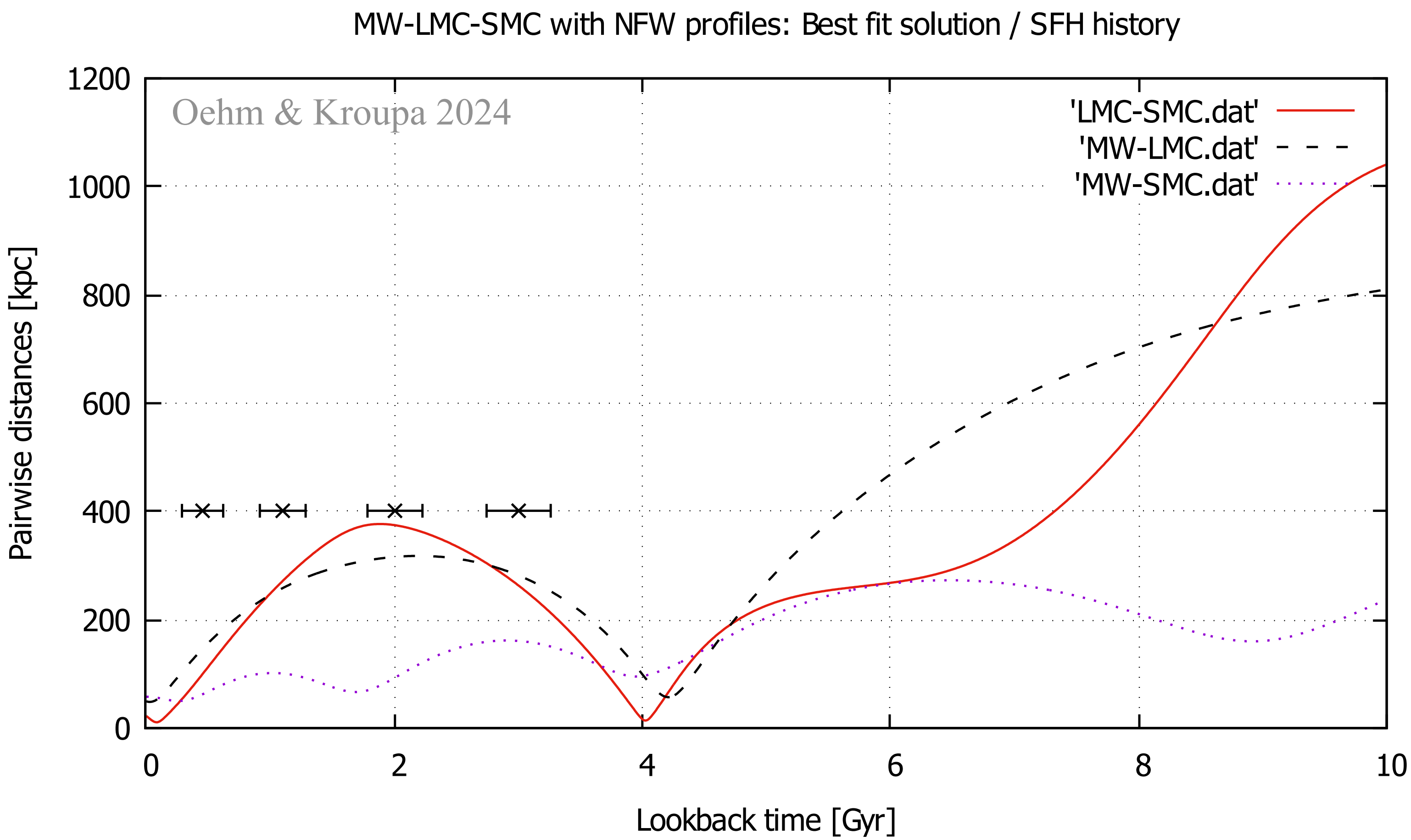

No solution of SMC-LMC orbit that explains the synchronised star-formation history.

A solution of the SMC / LMC / MW system is *not* possible in the SMoC.

The LMC and SMC have dark-matter halos according to the SMoC and are integrated backwards in time (i.e. the friction leads to an acceleration) assuming their observed position and velocity vectors (Gaia data).

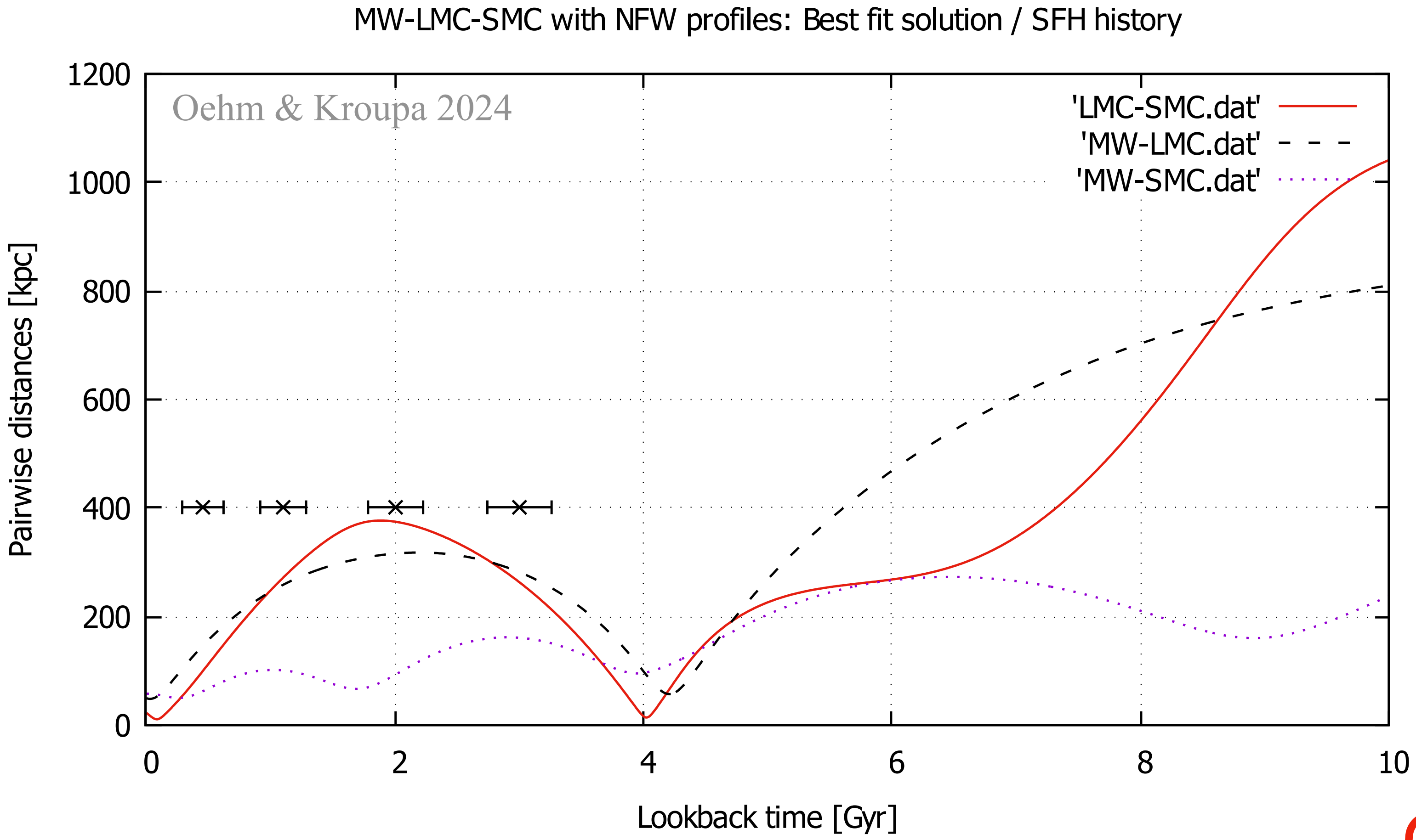

No solution of SMC-LMC orbit that explains the synchronised star-formation history.

A solution of the SMC / LMC / MW system is *not* possible in the SMoC.

no dark matter halos

Testing for the existence
of

Dark Matter

via

Chandrasekhar
dynamical friction

With galaxy bars

Chandrasekhar dynamical friction :

Bars slow down due to dynamical friction on DM halo

NGC1300 - Hubble/Wikipedia

Chandrasekhar dynamical friction :

Bars slow down due to dynamical friction on DM halo

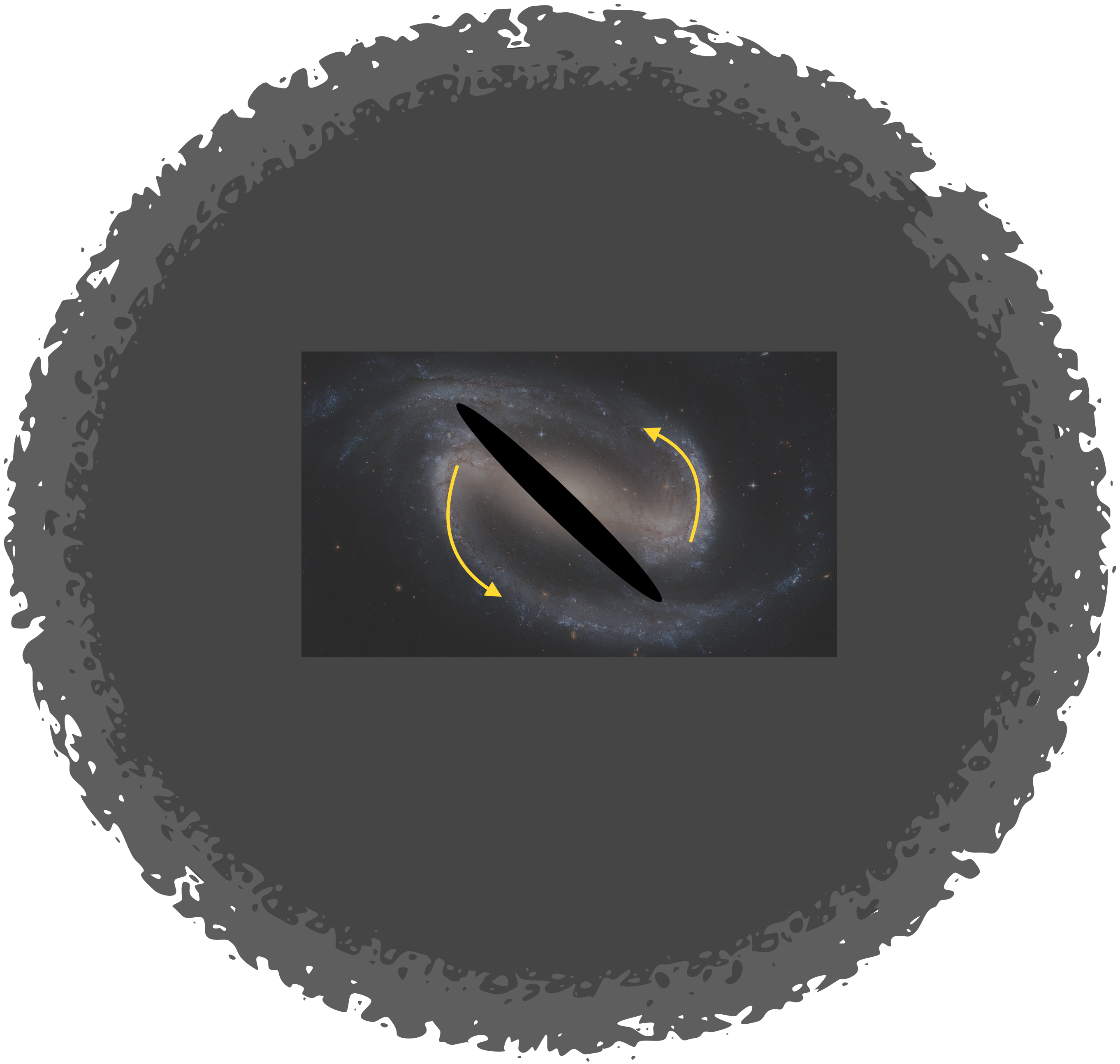

Chandrasekhar dynamical friction :

Bars slow down due to dynamical friction on DM halo

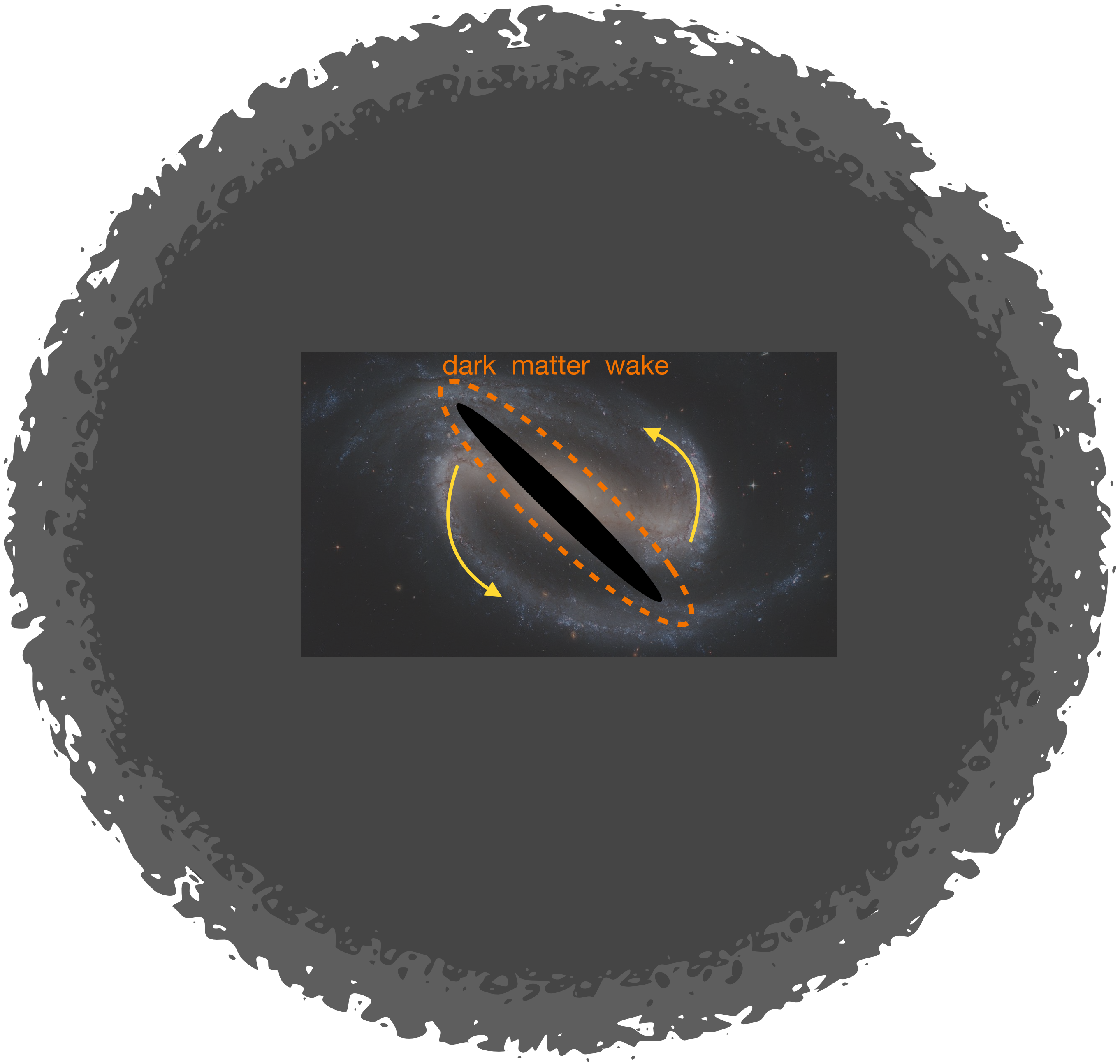

Chandrasekhar dynamical friction :

Bars slow down due to dynamical friction on DM halo

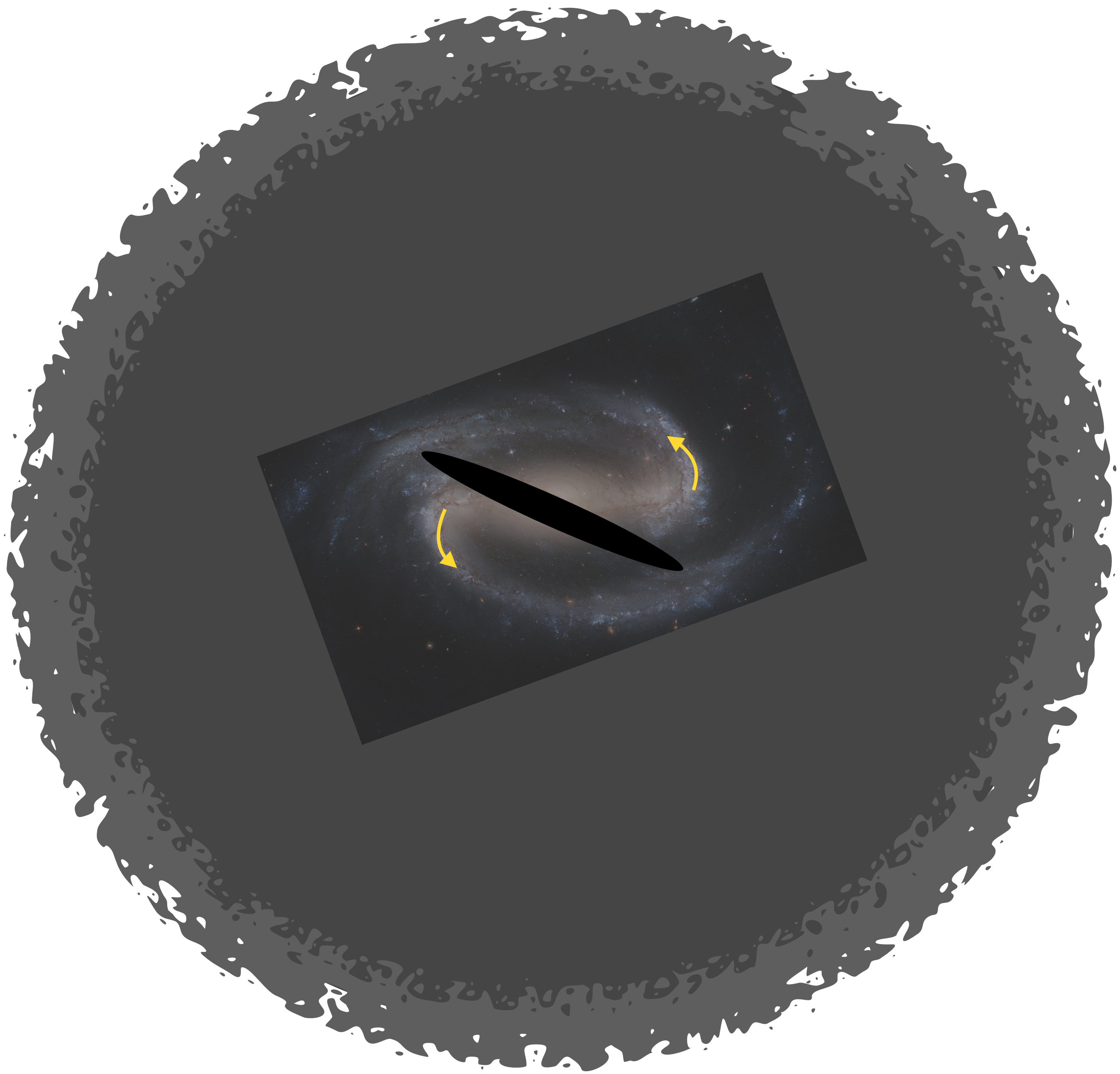

Chandrasekhar dynamical friction :

Bars slow down due to dynamical friction on DM halo

If dark matter halos exist,
then bars *must* slow down

Chandrasekhar dynamical friction :

Bars slow down due to dynamical friction on DM halo

If dark matter halos exist,
then bars *must* slow down

Bar rotates like rigid body,
it's length thus is measure of
rotation speed.

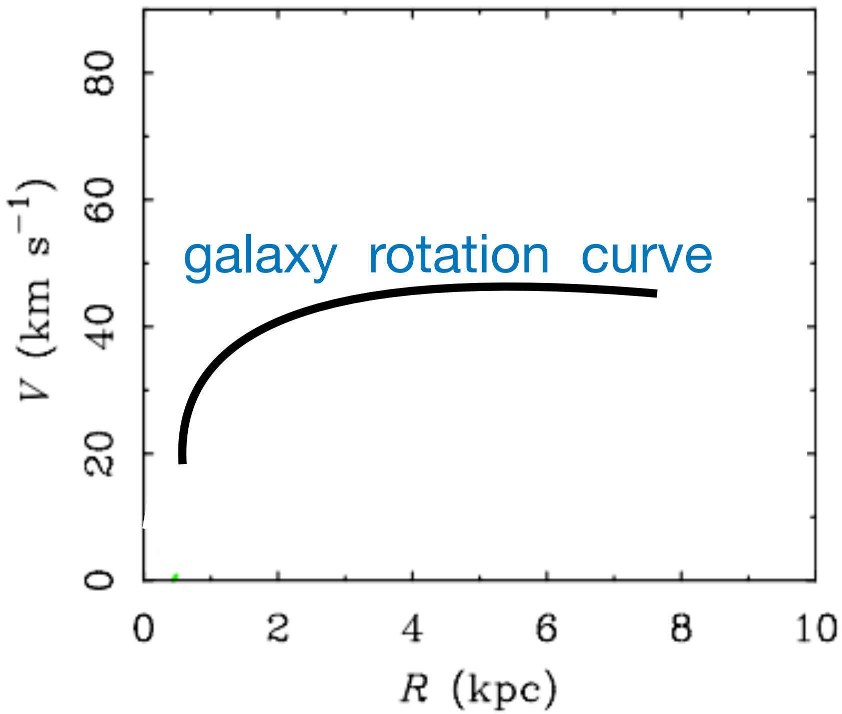

Chandrasekhar dynamical friction :

Bars slow down due to dynamical friction on DM halo

$$\mathcal{R} = \frac{R_{\rm corotation}}{R_{\rm bar\ length}}$$

$$\mathcal{R} > 1.4 \quad \Rightarrow \quad \text{slow bar}$$
$$\mathcal{R} < 1.4 \quad \Rightarrow \quad \text{fast bar}$$

Chandrasekhar dynamical friction :

Bars slow down due to dynamical friction on DM halo

Roshan, Ghafourian et al. 2021

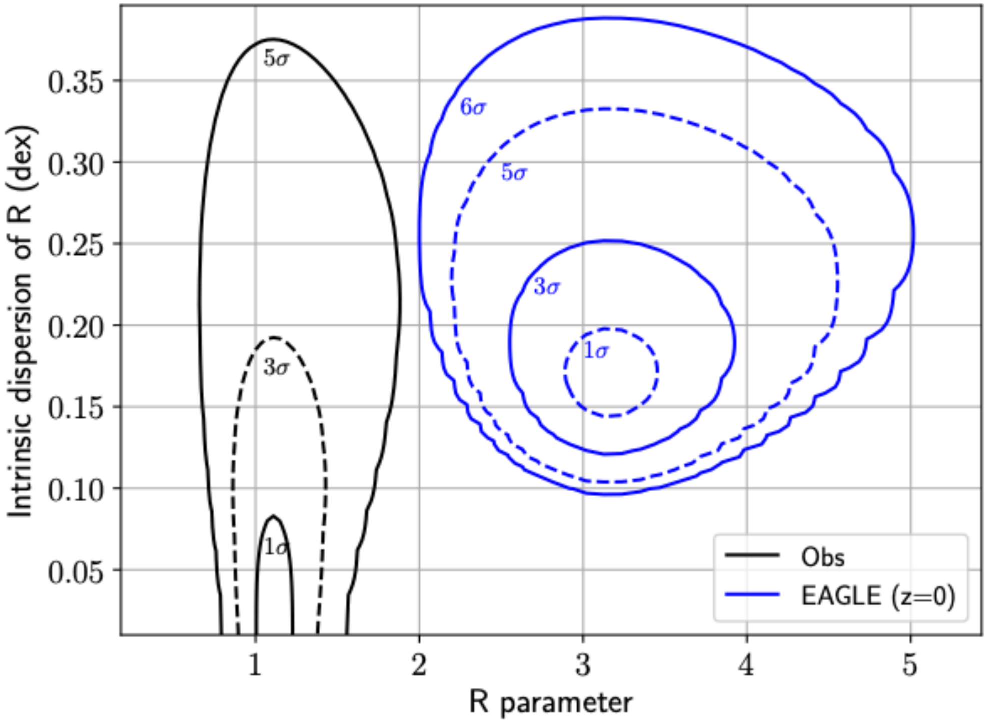

Figure 19. The posterior inference on $\mathcal{R}$ and the intrinsic dispersion of $\log_{10}\mathcal{R}$, found by applying Equation 28 to our compilation of observational results (Table 2) and to the EAGLE simulation at $z = 0$ based on figure 9 of Algorry et al. (2017). Although the calculations are done in the space of $\log_{10}\mathcal{R}$, we change the x-axis to a linear scale when plotting so the results are more intuitive (i.e. we plot $10^{\overline{\widetilde{\mathcal{R}}}}$). The black (blue) contours correspond to 1σ, 3σ, and 5σ outliers from the observed (EAGLE) posterior. Due to the significant mismatch, the 6σ contour is also shown for the EAGLE simulation.

$$\mathcal{R} = \frac{R_{\text{corotation}}}{R_{\text{bar length}}}$$

$$\mathcal{R} > 1.4 \quad \Rightarrow \quad \text{slow bar}$$
$$\mathcal{R} < 1.4 \quad \Rightarrow \quad \text{fast bar}$$

Chandrasekhar dynamical friction :

Bars slow down due to dynamical friction on DM halo

Roshan, Ghafourian et al. 2021

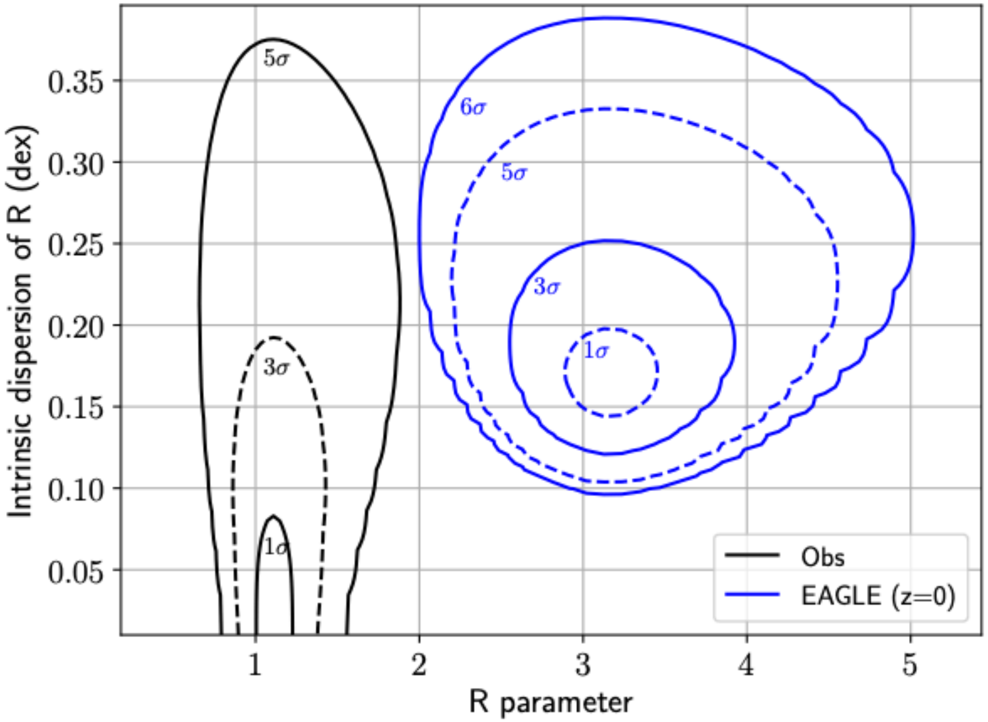

Figure 19. The posterior inference on $\mathcal{R}$ and the intrinsic dispersion of $\log_{10}\mathcal{R}$, found by applying Equation 28 to our compilation of observational results (Table 2) and to the EAGLE simulation at $z = 0$ based on figure 9 of Algorry et al. (2017). Although the calculations are done in the space of $\log_{10}\mathcal{R}$, we change the x-axis to a linear scale when plotting so the results are more intuitive (i.e. we plot $10^{\overline{\widetilde{\mathcal{R}}}}$). The black (blue) contours correspond to 1σ, 3σ, and 5σ outliers from the observed (EAGLE) posterior. Due to the significant mismatch, the 6σ contour is also shown for the EAGLE simulation.

$$\mathcal{R} = \frac{R_{\text{corotation}}}{R_{\text{bar length}}}$$

$\mathcal{R} > 1.4 \quad \Rightarrow \quad$ slow bar

$\mathcal{R} < 1.4 \quad \Rightarrow \quad$ fast bar

Real galaxies have fast bars.

Chandrasekhar dynamical friction :

Bars slow down due to dynamical friction on DM halo

$$\mathcal{R} = \frac{R_{\text{corotation}}}{R_{\text{bar length}}}$$

$\mathcal{R} > 1.4 \quad \Rightarrow \quad$ slow bar

$\mathcal{R} < 1.4 \quad \Rightarrow \quad$ fast bar

Roshan, Ghafourian et al. 2021

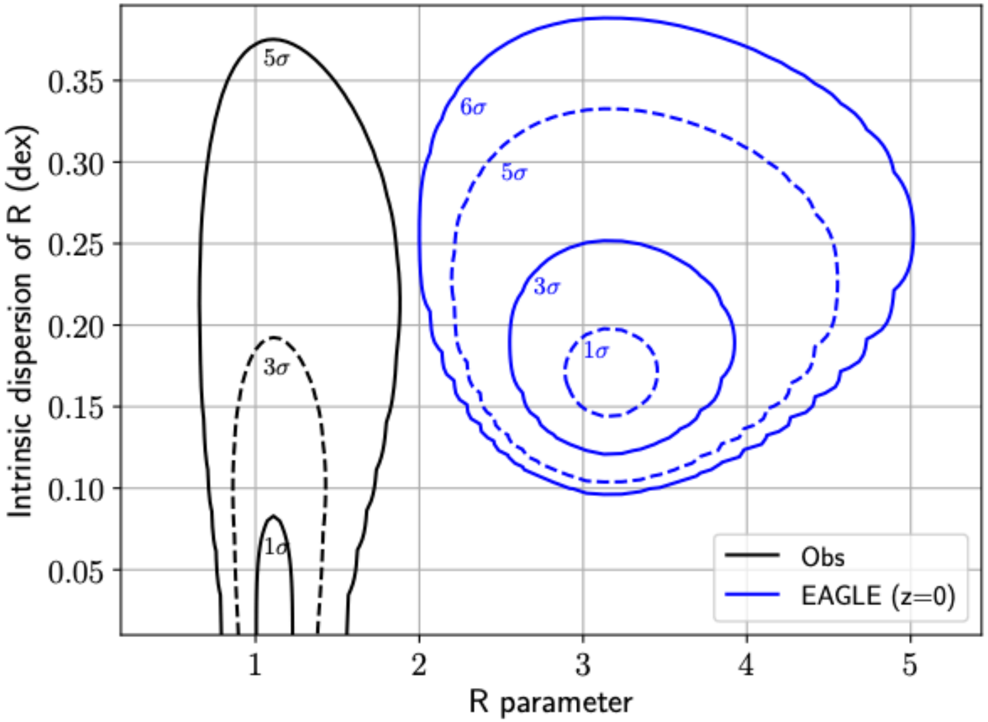

Figure 19. The posterior inference on $\mathcal{R}$ and the intrinsic dispersion of $\log_{10}\mathcal{R}$, found by applying Equation 28 to our compilation of observational results (Table 2) and to the EAGLE simulation at $z = 0$ based on figure 9 of Algorry et al. (2017). Although the calculations are done in the space of $\log_{10}\mathcal{R}$, we change the x-axis to a linear scale when plotting so the results are more intuitive (i.e. we plot $10^{\overline{\widetilde{\mathcal{R}}}}$). The black (blue) contours correspond to 1σ, 3σ, and 5σ outliers from the observed (EAGLE) posterior. Due to the significant mismatch, the 6σ contour is also shown for the EAGLE simulation.

Real galaxies have fast bars.
Dark-matter-galaxies have slow bars.

Chandrasekhar dynamical friction :

Bars slow down due to dynamical friction on DM halo

Roshan, Ghafourian et al. 2021

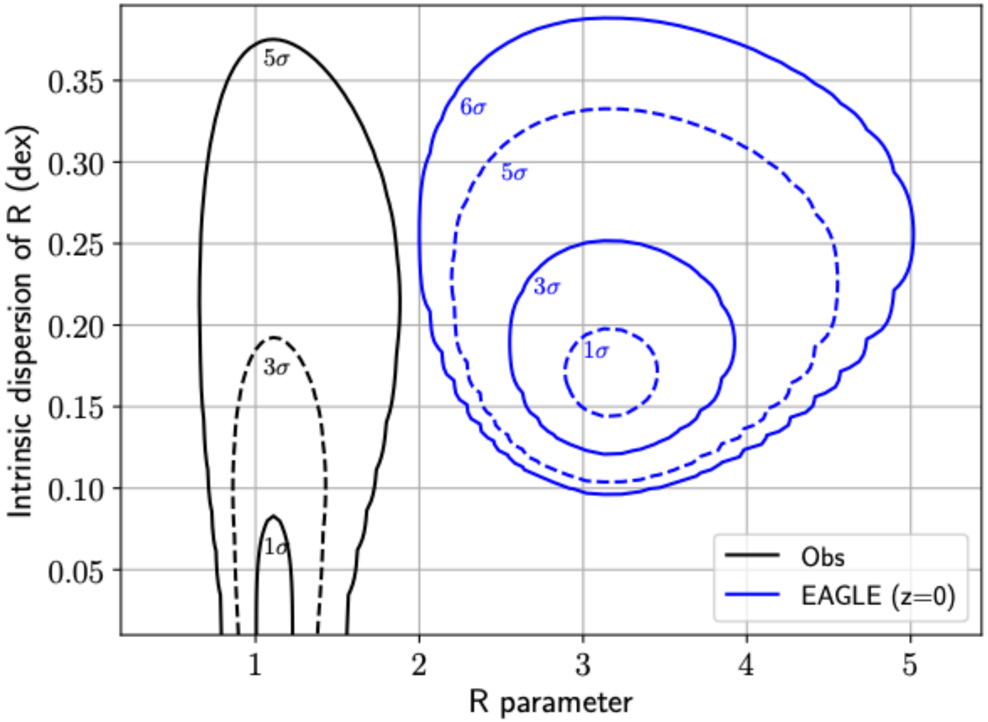

Figure 19. The posterior inference on $\mathcal{R}$ and the intrinsic dispersion of $\log_{10}\mathcal{R}$, found by applying Equation 28 to our compilation of observational results (Table 2) and to the EAGLE simulation at $z = 0$ based on figure 9 of Algorry et al. (2017). Although the calculations are done in the space of $\log_{10}\mathcal{R}$, we change the x-axis to a linear scale when plotting so the results are more intuitive (i.e. we plot $10^{\overline{\widetilde{\mathcal{R}}}}$). The black (blue) contours correspond to 1σ, 3σ, and 5σ outliers from the observed (EAGLE) posterior. Due to the significant mismatch, the 6σ contour is also shown for the EAGLE simulation.

$$\mathcal{R} = \frac{R_{\text{corotation}}}{R_{\text{bar length}}}$$

$$\mathcal{R} > 1.4 \quad \Rightarrow \quad \text{slow bar}$$
$$\mathcal{R} < 1.4 \quad \Rightarrow \quad \text{fast bar}$$

Real galaxies have fast bars.
Dark-matter-galaxies have slow bars.

8 sigma tension

no significant dark matter halo in nature

Thus, other applications of

Chandrasekhar dynamical friction :

Thus, other applications of

Chandrasekhar dynamical friction **:**

The bars of galaxies are too long

Thus, other applications of

Chandrasekhar dynamical friction :

The bars of galaxies are too long

Existence of dark matter halos falsified with $> 5\sigma$ confidence

Roshan, Ghafourian et al. 2021

Thus, other applications of

Chandrasekhar dynamical friction :

The bars of galaxies are too long

Existence of dark matter halos falsified with $> 5\sigma$ confidence

Roshan, Ghafourian et al. 2021

The observed configuration of the M81 group of galaxies *cannot exist* in the SMoC

Yun 1999
Thomson, Laine & Turnbull 1999
Oehm et al. 2017; 2018

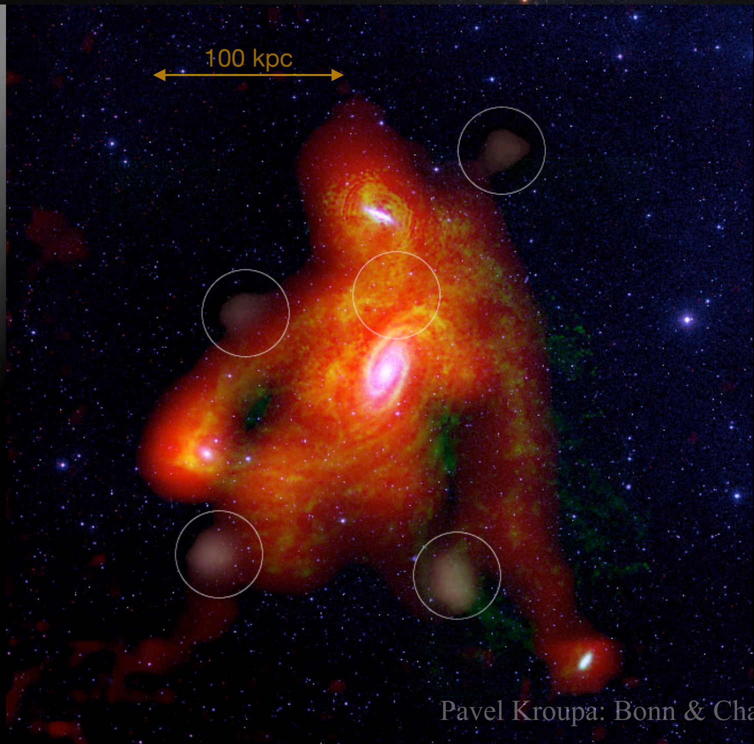

Thus, other applications of

Chandrasekhar dynamical friction :

The bars of galaxies are too long

Existence of dark matter halos
falsified with $> 5\sigma$ confidence

Roshan, Ghafourian et al. 2021

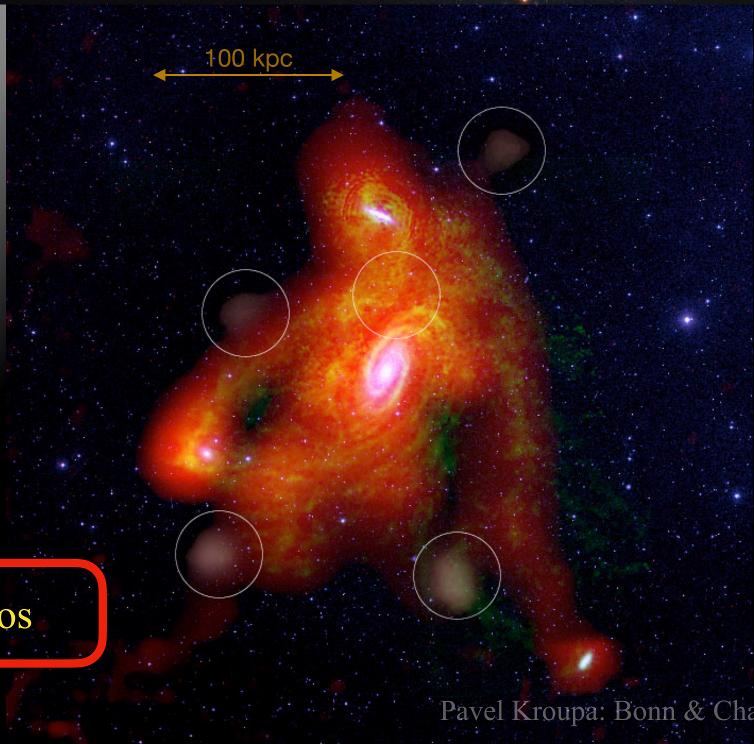

The observed configuration of
the M81 group of galaxies
cannot exist in the SMoC

Yun 1999
Thomson, Laine & Turnbull 1999
Oehm et al. 2017; 2018

no dark matter halos

Chandrasekhar dynamical friction :

All tests performed demonstrate

with >>5 sigma confidence

that dark matter halos
made of particles
of any mass
are ruled out.

Other tests,

not based

on

Chandrasekhar dynamical friction

If there is no C/W dark matter,

If there is no C/W dark matter,

then Newtonian / Einsteinian gravitation ought to break down,

If there is no C/W dark matter,

then Newtonian / Einsteinian gravitation ought to break down,

no ?

$$\dot{M}_{\rm cluster} < 0$$

Open star clusters
as tests of
gravitational theory

Open star clusters as tests of gravitational theory

How do star clusters loose their stars ?

Ejection

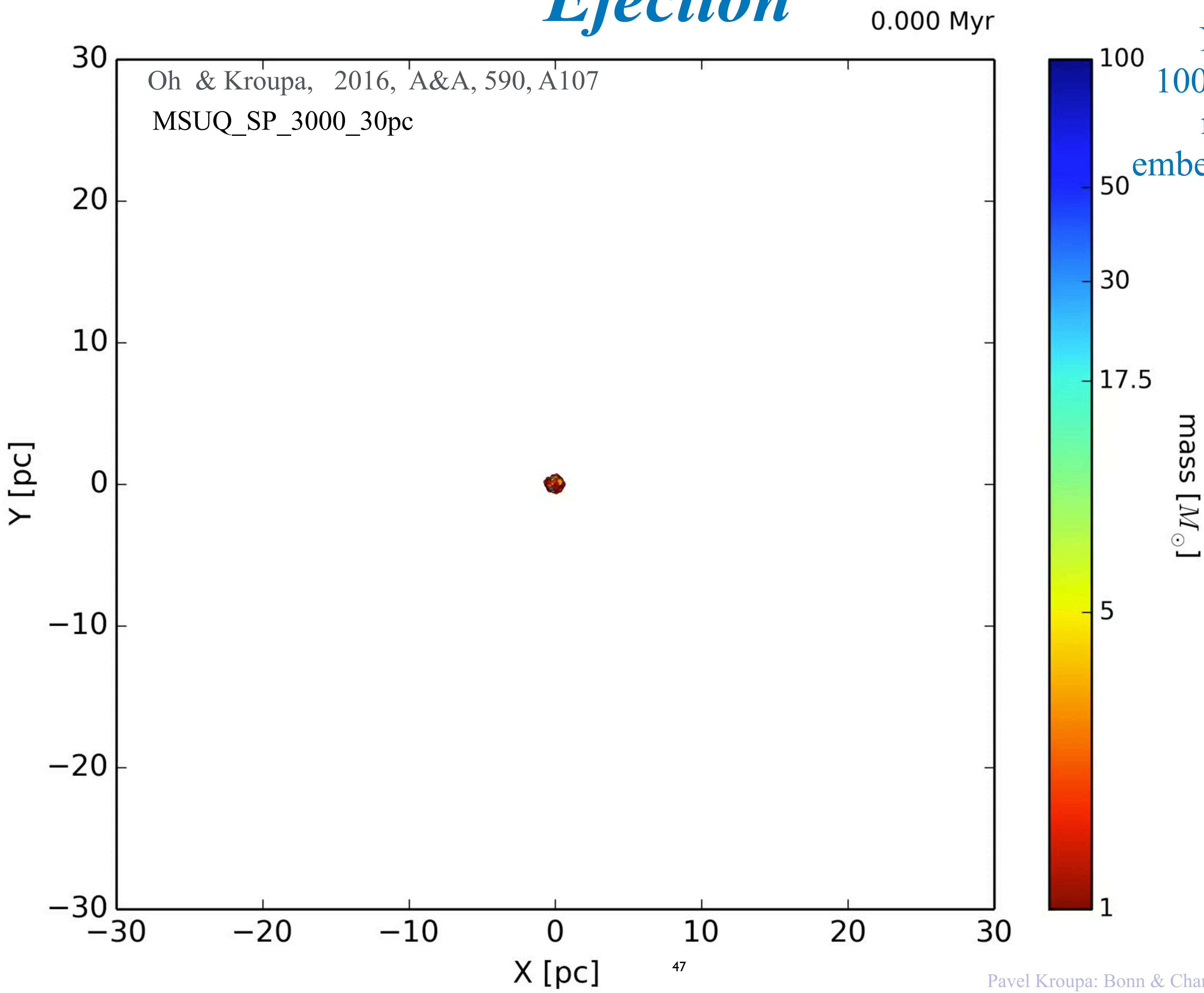

Nbody6
100% binaries
realistic
embedded cluster

Ejection

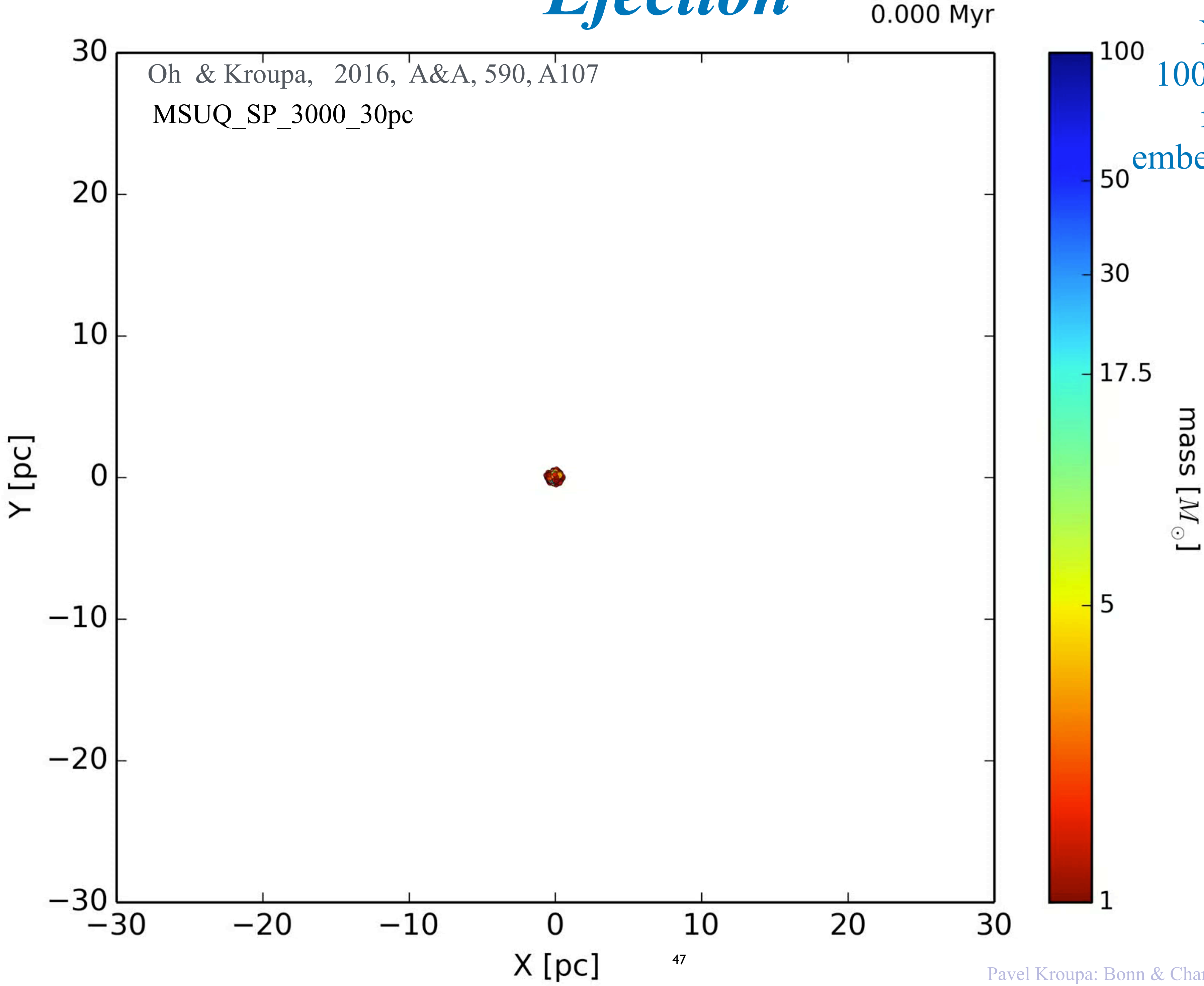

Nbody6
100% binaries
realistic
embedded cluster

Ejection

Oh & Kroupa, 2016, A&A, 590, A107

MSUQ_SP_3000_30pc Nbody models

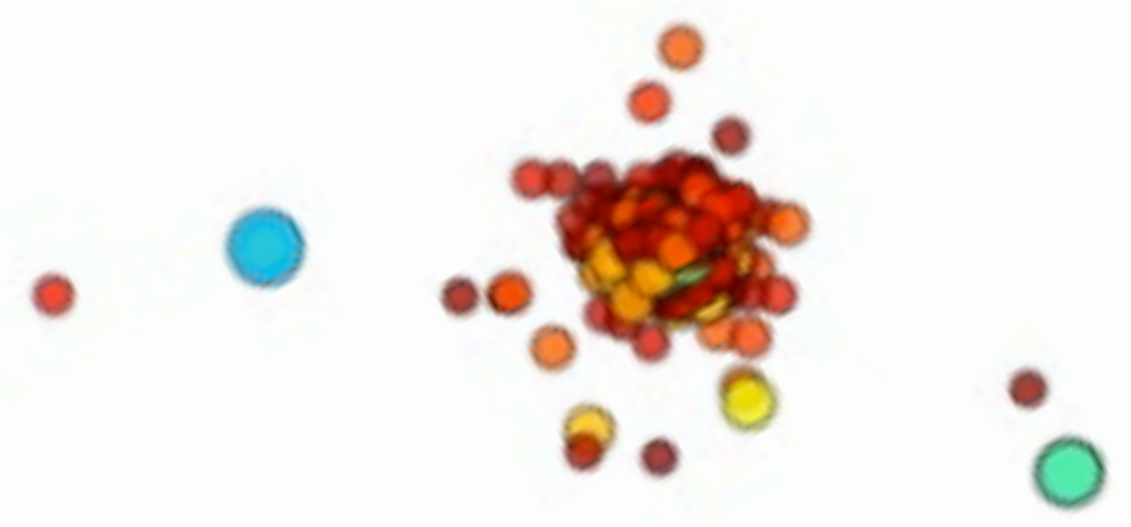

Monoceros R2 cluster

(Carpenter et al. 1997, AJ 114, 198)

Evaporation

Assume, for simplicity : the cluster consists of single stars of equal mass m.

Evaporation

Assume, for simplicity : the cluster consists of single stars of equal mass m.

At a given radius r in the cluster the stars have, approximately, a *Maxwell-Boltzmann* distribution of speeds :

$$\mathcal{V}(v)\,dv = dN = F(v)\,4\,\pi\,v^2\,dv = N_{\rm tot}\,\frac{1}{(2\pi\,\sigma^2)^{\frac{3}{2}}}\,e^{-\frac{v^2}{2\,\sigma^2}}\,4\,\pi\,v^2\,dv$$

Evaporation

Assume, for simplicity : the cluster consists of single stars of equal mass m.

At a given radius r in the cluster the stars have, approximately, a *Maxwell-Boltzmann* distribution of speeds :

$$\mathcal{V}(v)\,dv = dN = F(v)\,4\,\pi\,v^2\,dv = N_{\rm tot}\,\frac{1}{(2\pi\,\sigma^2)^{\frac{3}{2}}}\,e^{-\frac{v^2}{2\,\sigma^2}}\,4\,\pi\,v^2\,dv$$

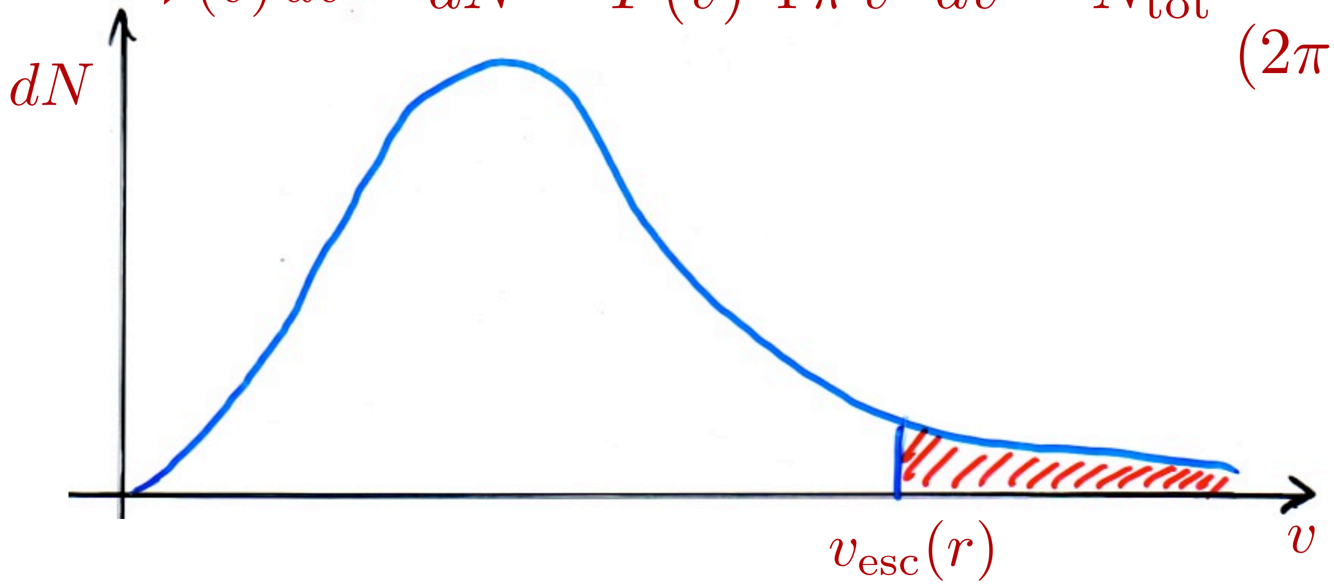

Evaporation

Assume, for simplicity : the cluster consists of single stars of equal mass *m*.

At a given radius *r* in the cluster the stars have, approximately, a *Maxwell-Boltzmann* distribution of speeds :

$$\mathcal{V}(v)\,dv = dN = F(v)\,4\,\pi\,v^2\,dv = N_{\rm tot}\,\frac{1}{(2\pi\,\sigma^2)^{\frac{3}{2}}}\,e^{-\frac{v^2}{2\,\sigma^2}}\,4\,\pi\,v^2\,dv$$

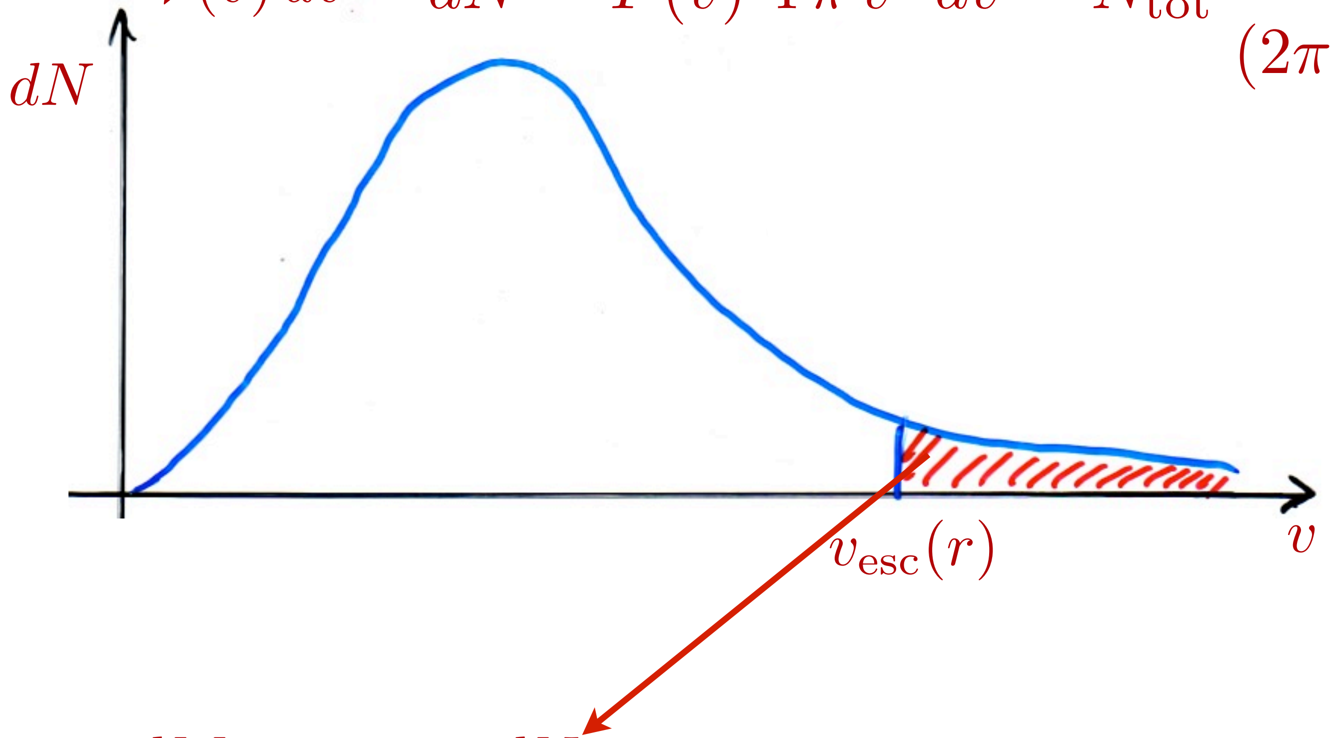

$$\frac{dM_{\rm cl}}{dt}(t) = m\,\frac{dN}{dt}(t)$$

Evaporated stars
leave their
open clusters
through
tidal tails

New method developed by Tereza Jerabkova in 2021 allowing *the tidal tails of open clusters* to be mapped to their tips.

New method developed by Tereza Jerabkova in 2021 allowing *the tidal tails of open clusters* to be mapped to their tips.

The Jerabkova Compact Convergent Point (CCP) method.

(Jerabkova et al. 2021)

https://www.cosmos.esa.int/web/gaia/iow_20221026

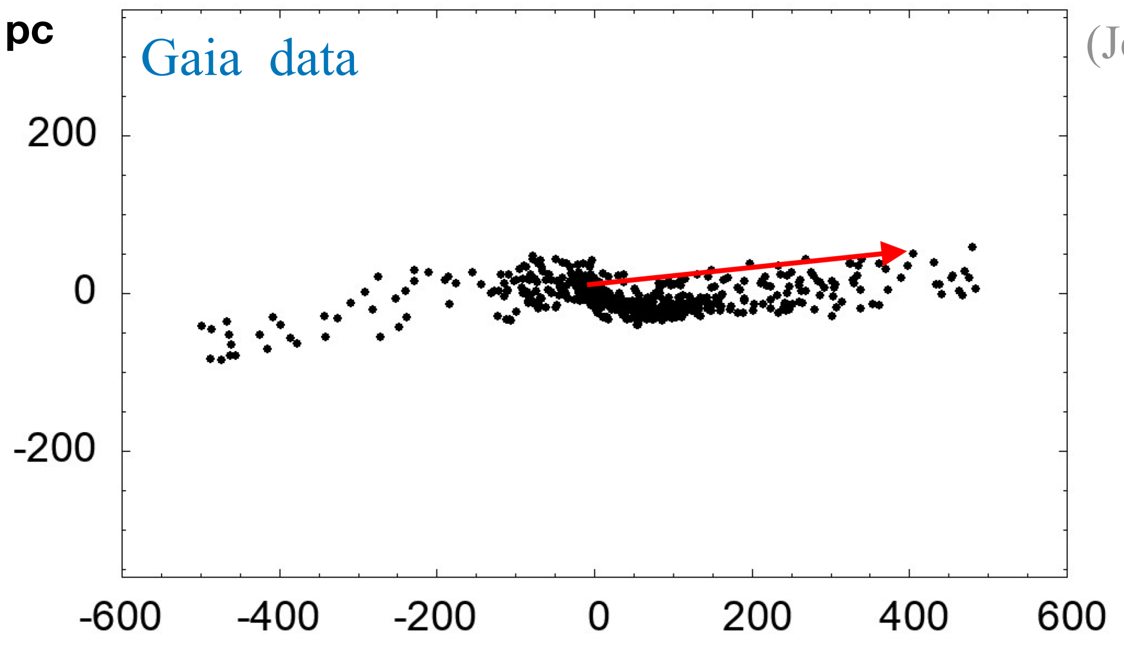

(Jerabkova et al. 2021)

Hyades

(Kroupa, Jerabkova et al. 2022)

The asymmetry in number of stars between leading and trailing tail is a 6.5sigma deviation from Newtonian predictions.

https://www.cosmos.esa.int/web/gaia/iow_20221026

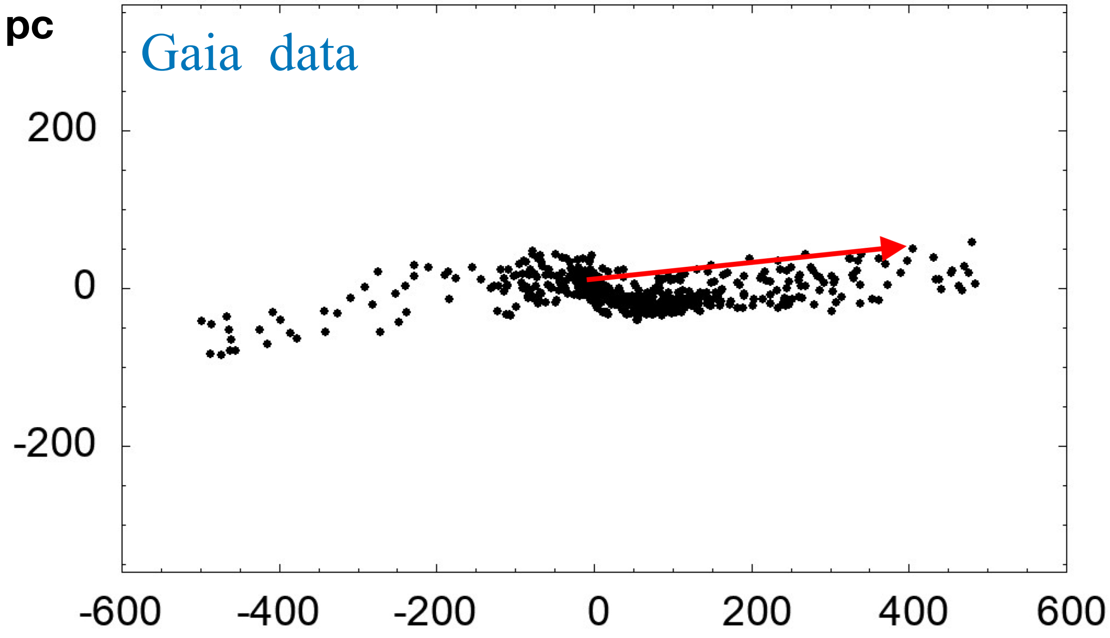

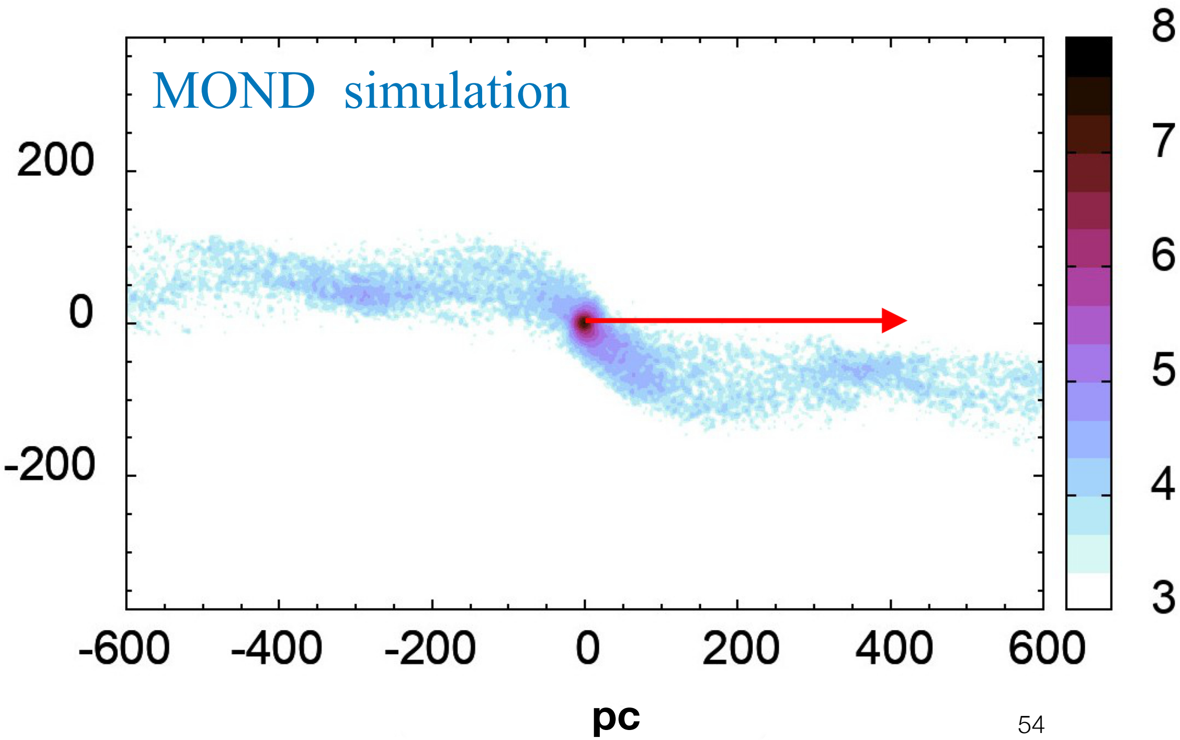

Hyades

(Kroupa, Jerabkova et al. 2022)

The asymmetry in number of stars between leading and trailing tail is a 6.5sigma deviation from Newtonian predictions.

https://www.cosmos.esa.int/web/gaia/iow_20221026

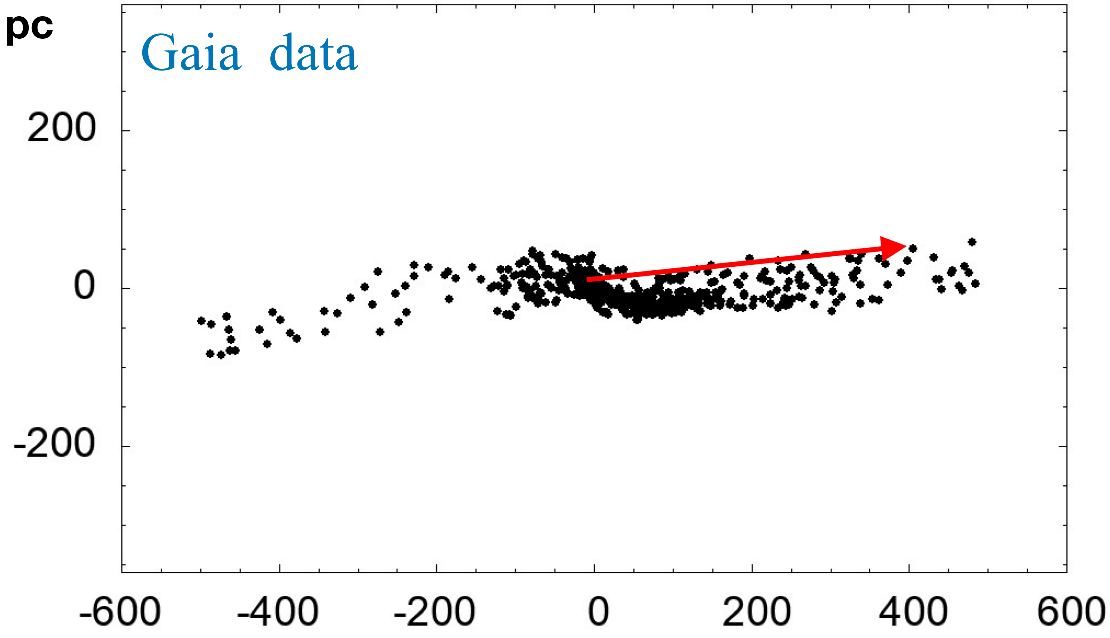

Hyades

(Kroupa, Jerabkova et al. 2022)

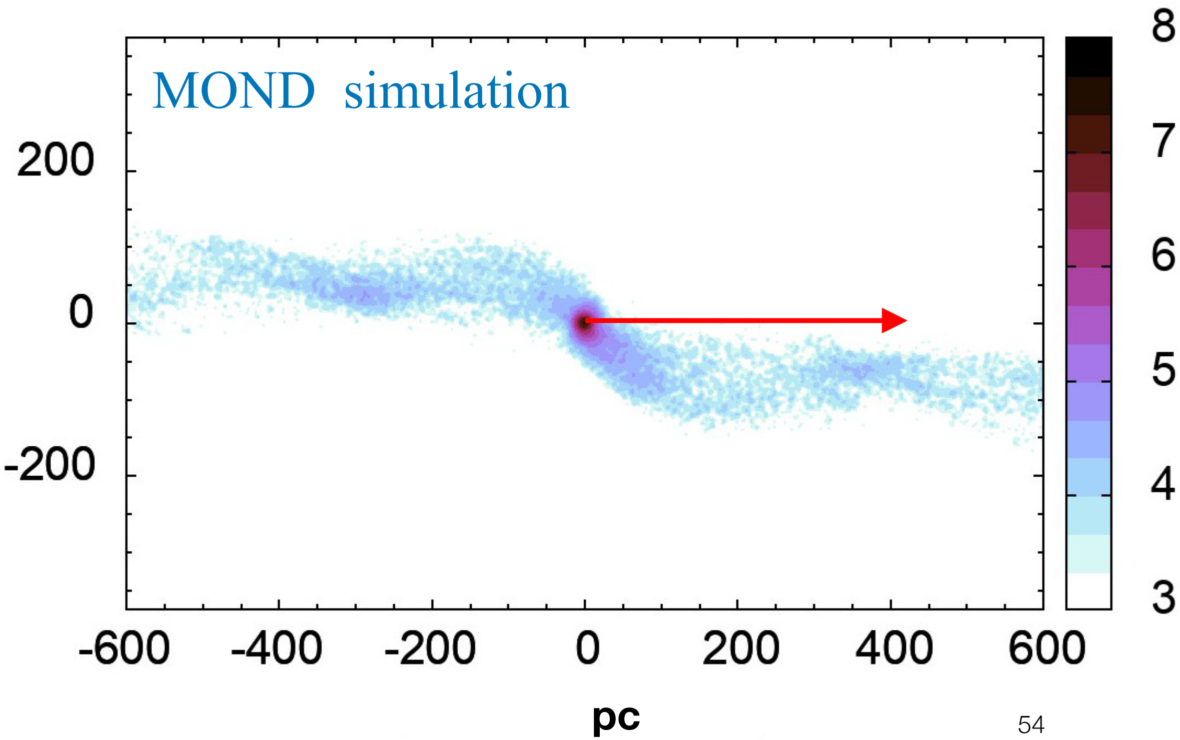

The asymmetry in number of stars between leading and trailing tail is a 6.5sigma deviation from Newtonian predictions.

Evaporation in Newtonian and Milgromian gravitation

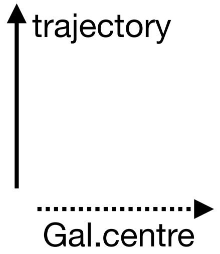

(Kroupa, Jerabkova et al. 2022)

open star cluster

Evaporation in Newtonian and Milgromian gravitation

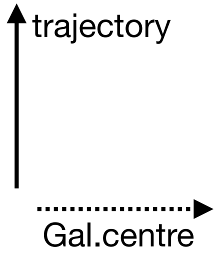

(Kroupa, Jerabkova et al. 2022)

open star cluster

MOND radius :

$$r_M = \left(\frac{G\, M_{oc}}{a_0} \right)^{\frac{1}{2}}$$

Newtonian case

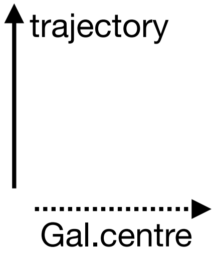

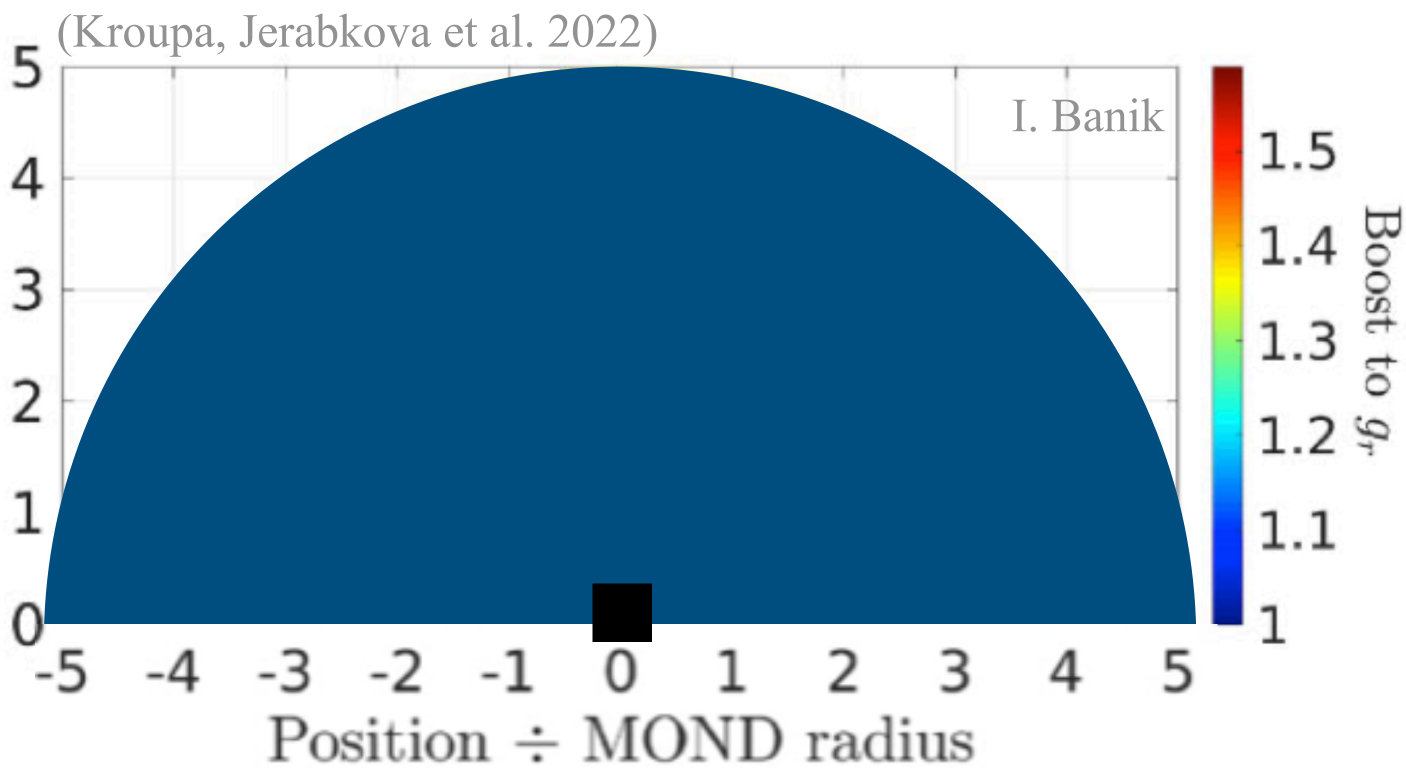

MOND radius :

$$r_{\mathrm{M}} = \left(\frac{G\, M_{\mathrm{oc}}}{a_0} \right)^{\frac{1}{2}}$$

Newtonian case

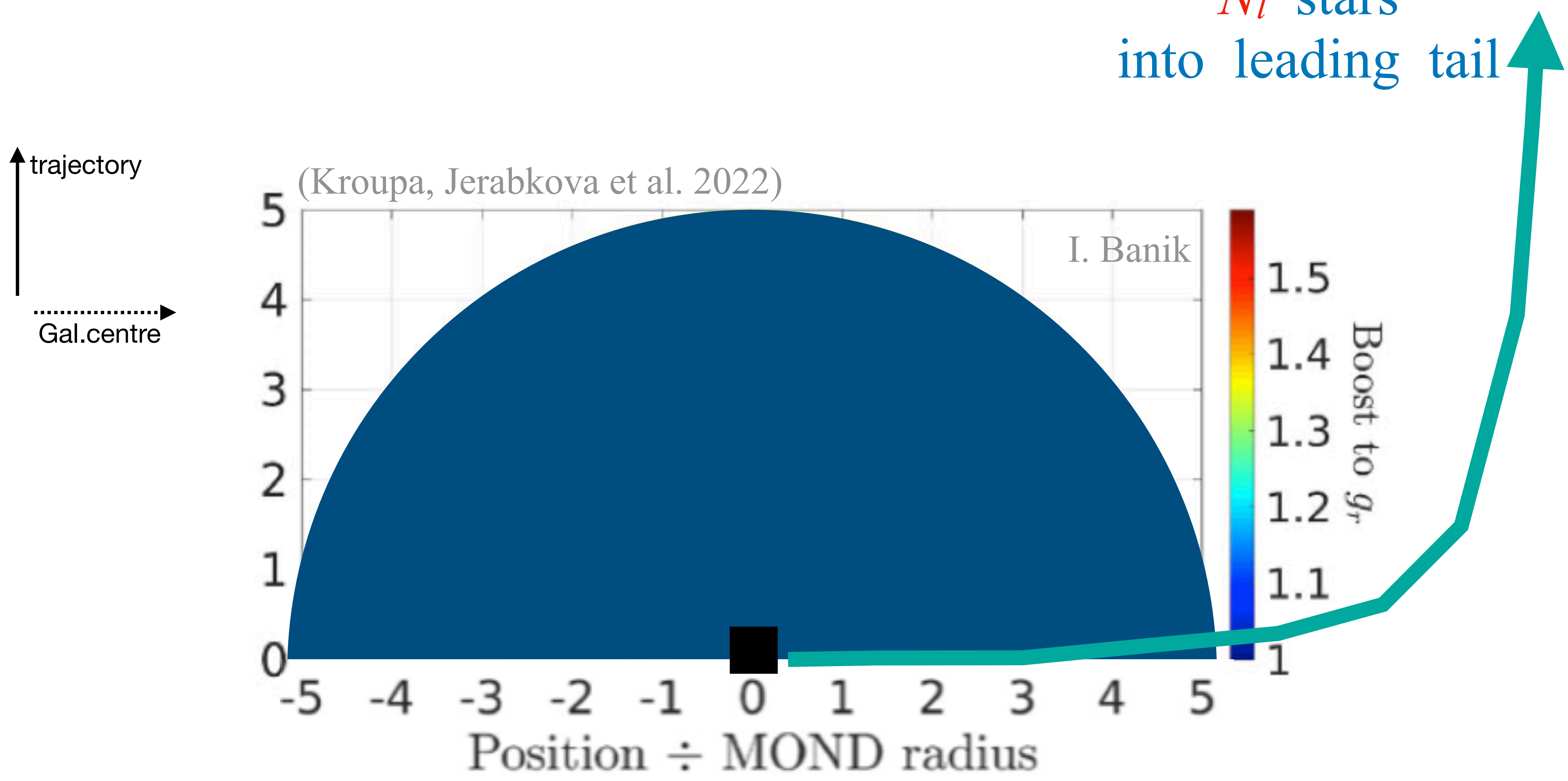

MOND radius :

$$r_M = \left(\frac{G\, M_{oc}}{a_0} \right)^{\frac{1}{2}}$$

Newtonian case

N_l stars
into leading tail

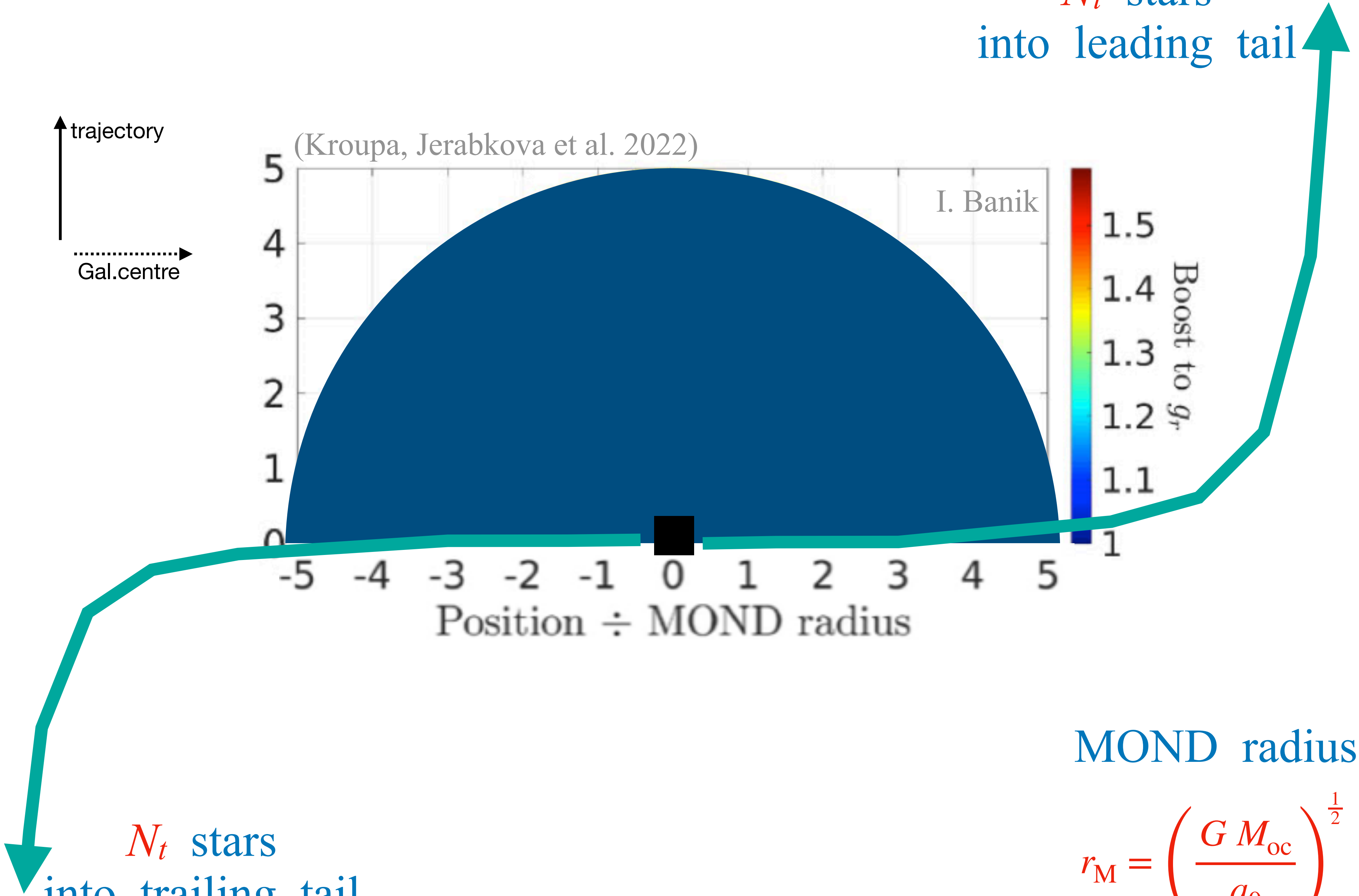

N_t stars
into trailing tail

MOND radius :

$$r_M = \left(\frac{G\, M_{oc}}{a_0} \right)^{\frac{1}{2}}$$

Newtonian case

N_l stars
into leading tail

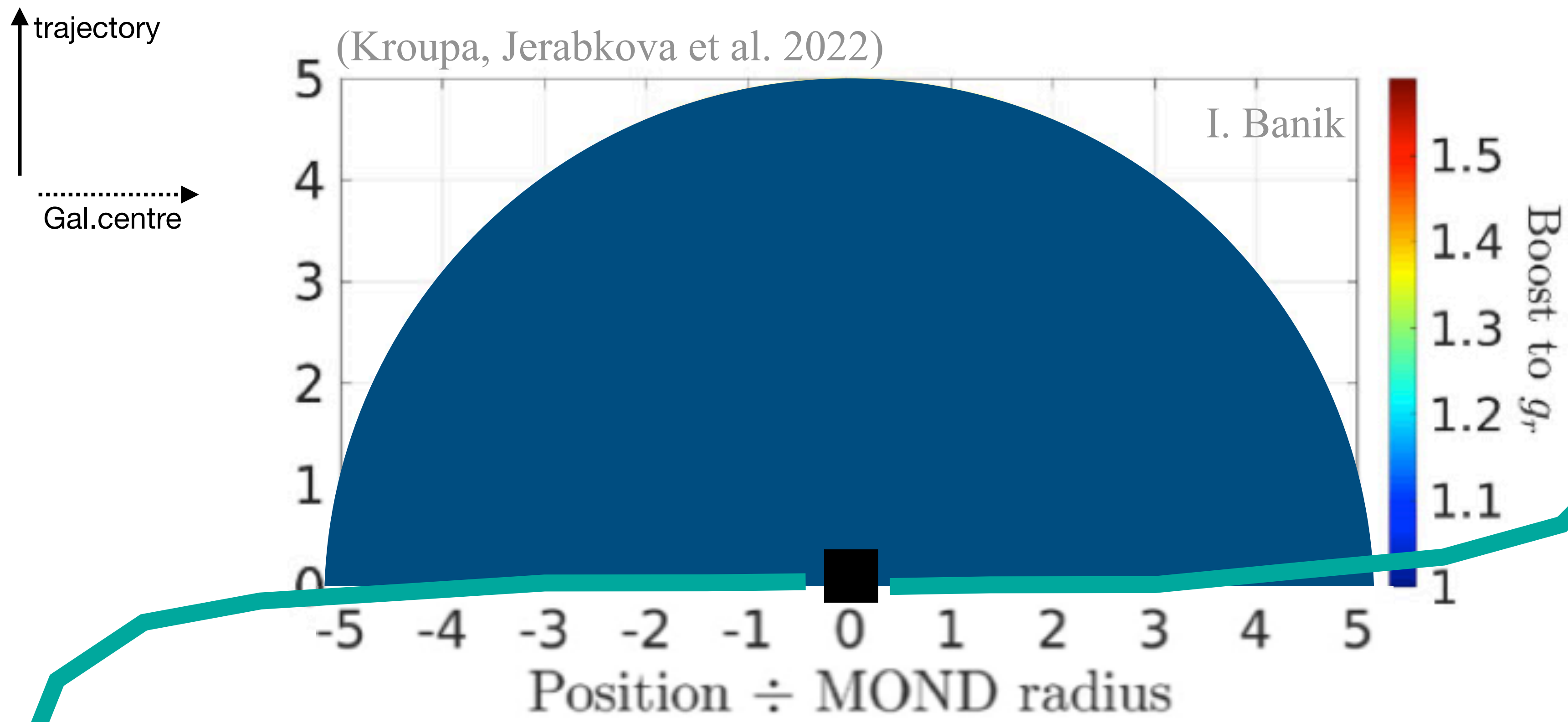

N_t stars
into trailing tail

$$\boxed{N_l = N_t}$$

(Pflamm-Altenburg et al. 2023)

MOND radius :

$$r_M = \left(\frac{G\, M_{oc}}{a_0} \right)^{\frac{1}{2}}$$

MOND predictions

of new phenomena

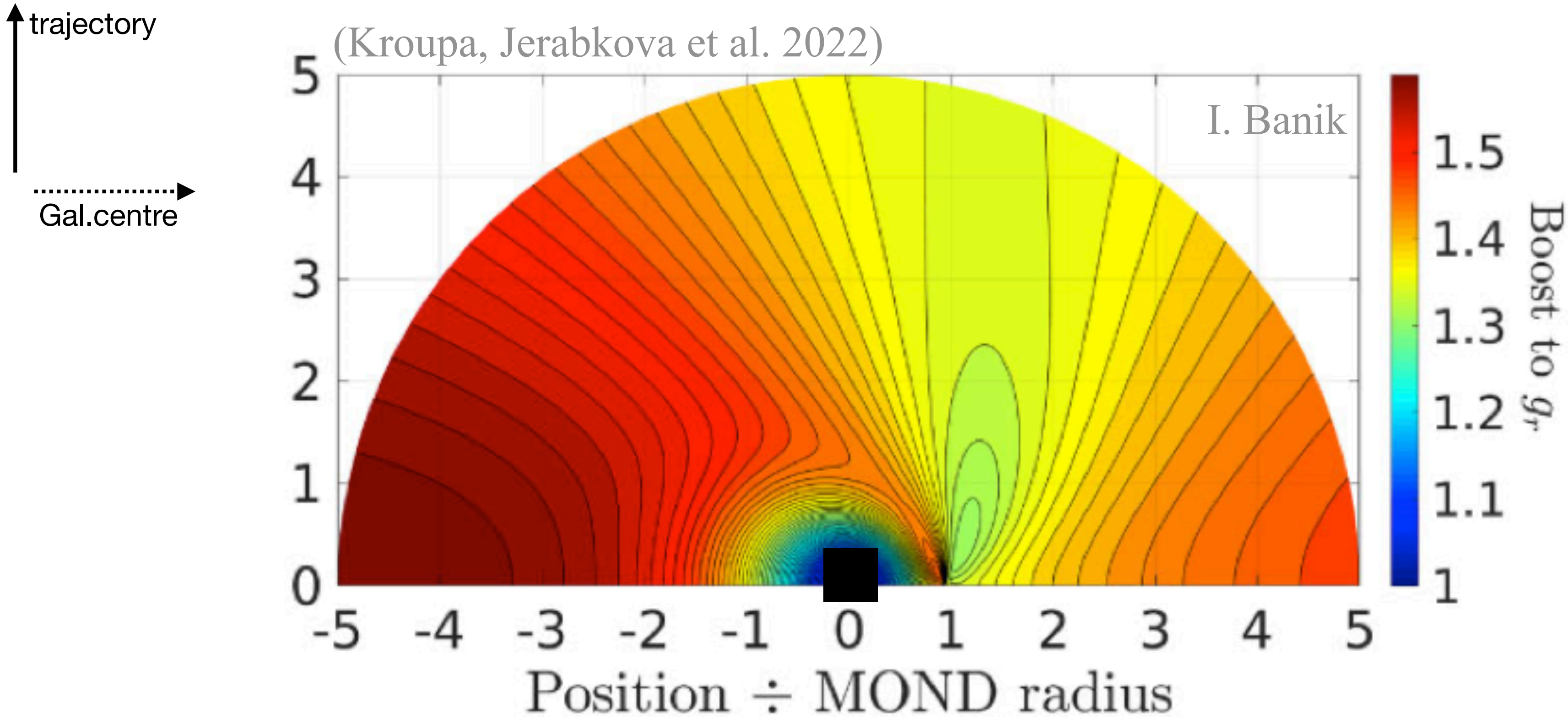

MOND radius :

$$r_M = \left(\frac{G\, M_{oc}}{a_0} \right)^{\frac{1}{2}}$$

MOND predictions

of new phenomena

N_l stars into leading tail

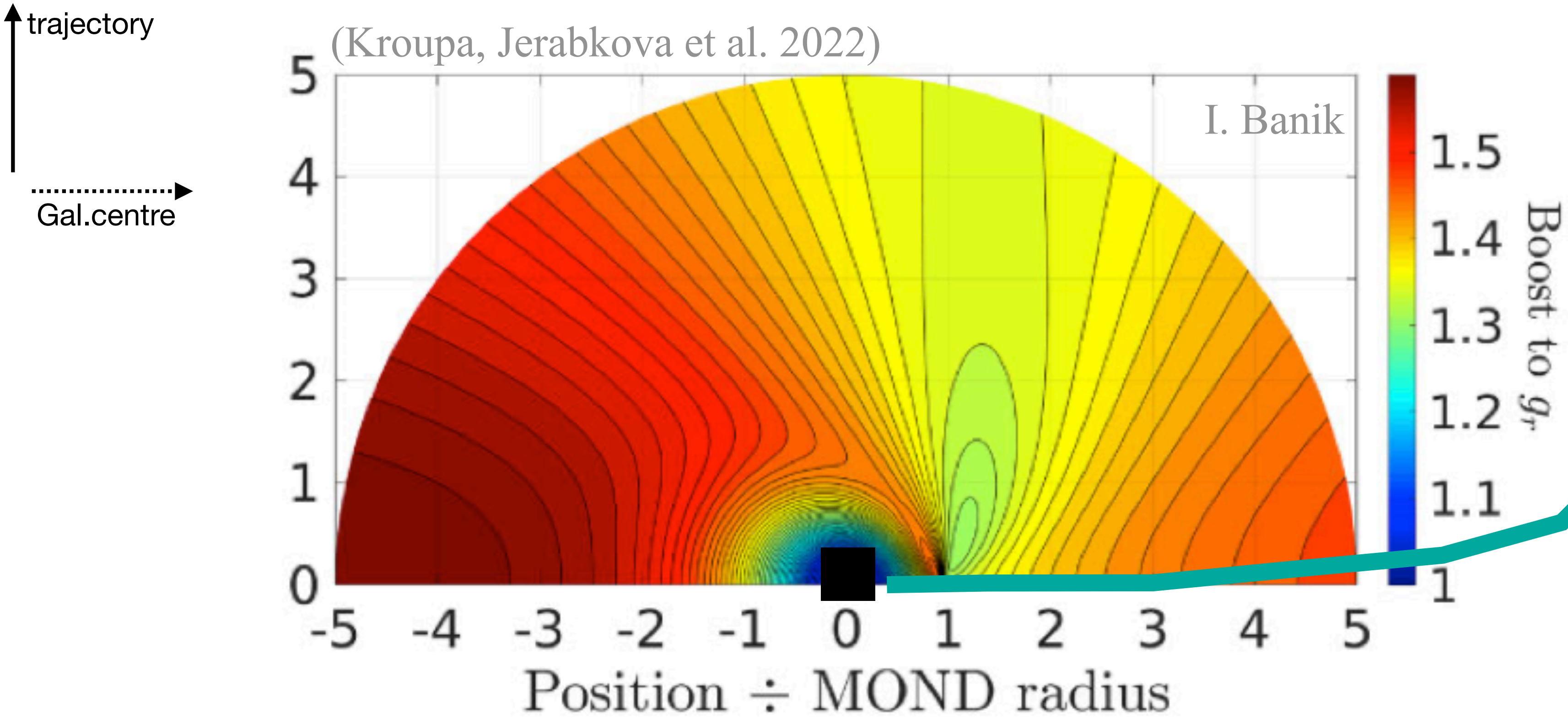

MOND radius :

$$r_M = \left(\frac{G\,M_{oc}}{a_0} \right)^{\frac{1}{2}}$$

MOND predictions

of new phenomena

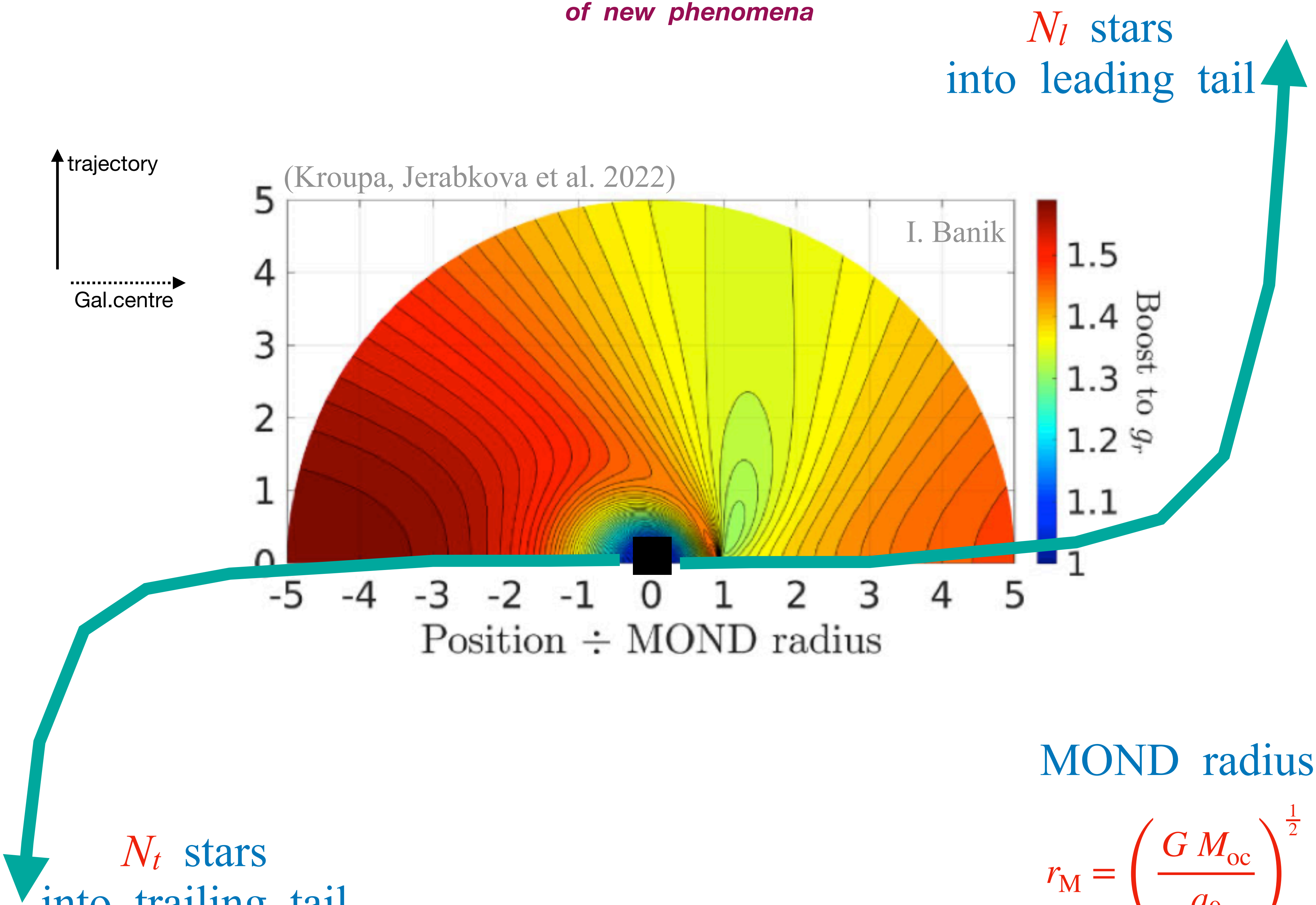

MOND radius :

$$r_{\mathrm{M}} = \left(\frac{G\, M_{\mathrm{oc}}}{a_0} \right)^{\frac{1}{2}}$$

MOND predictions

of new phenomena

N_l stars
into leading tail

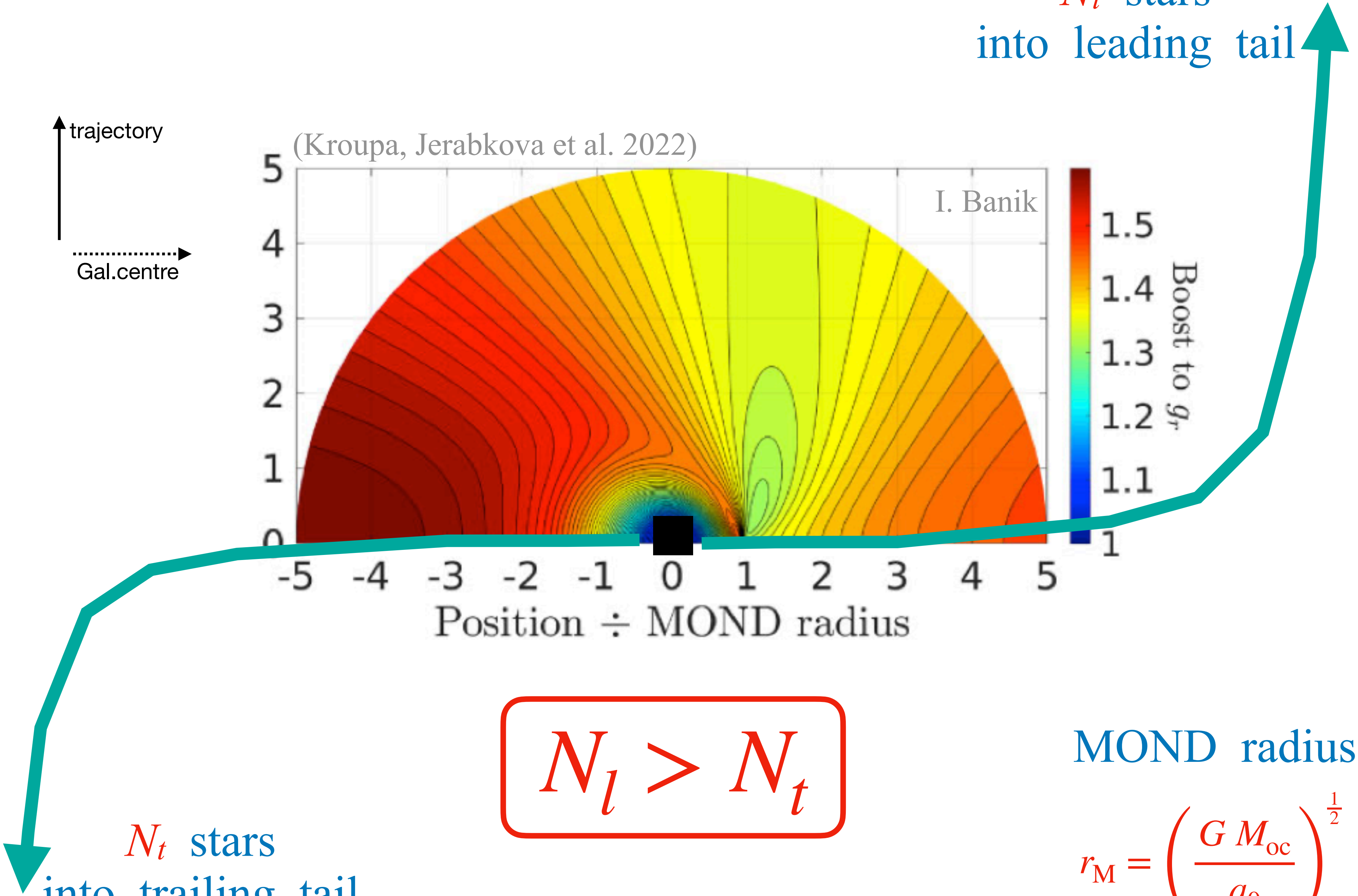

N_t stars
into trailing tail

$$\boxed{N_l > N_t}$$

MOND radius :

$$r_M = \left(\frac{G\, M_{oc}}{a_0} \right)^{\frac{1}{2}}$$

(Kroupa, Jerabkova et al. 2022)

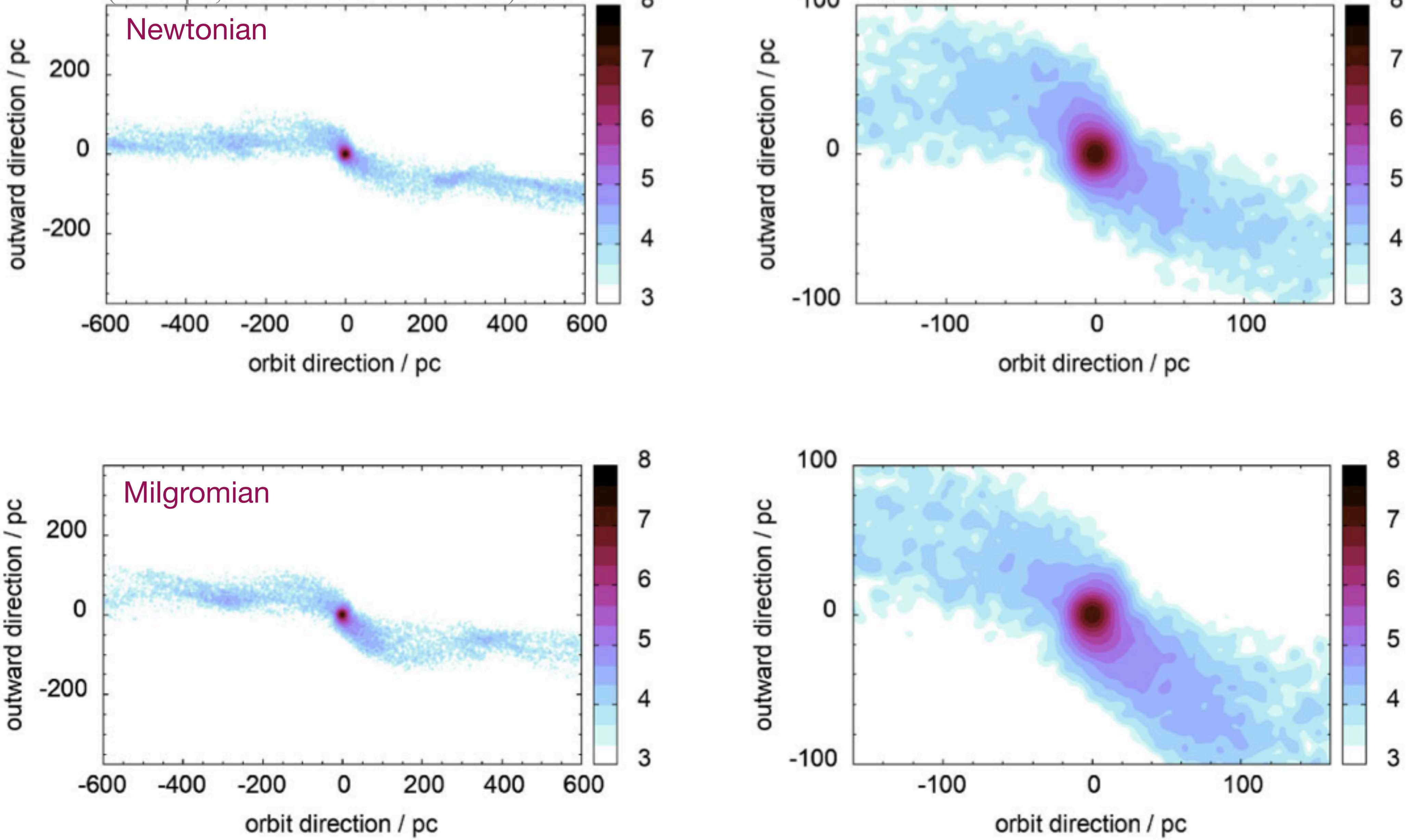

(Kroupa, Jerabkova et al. 2022)

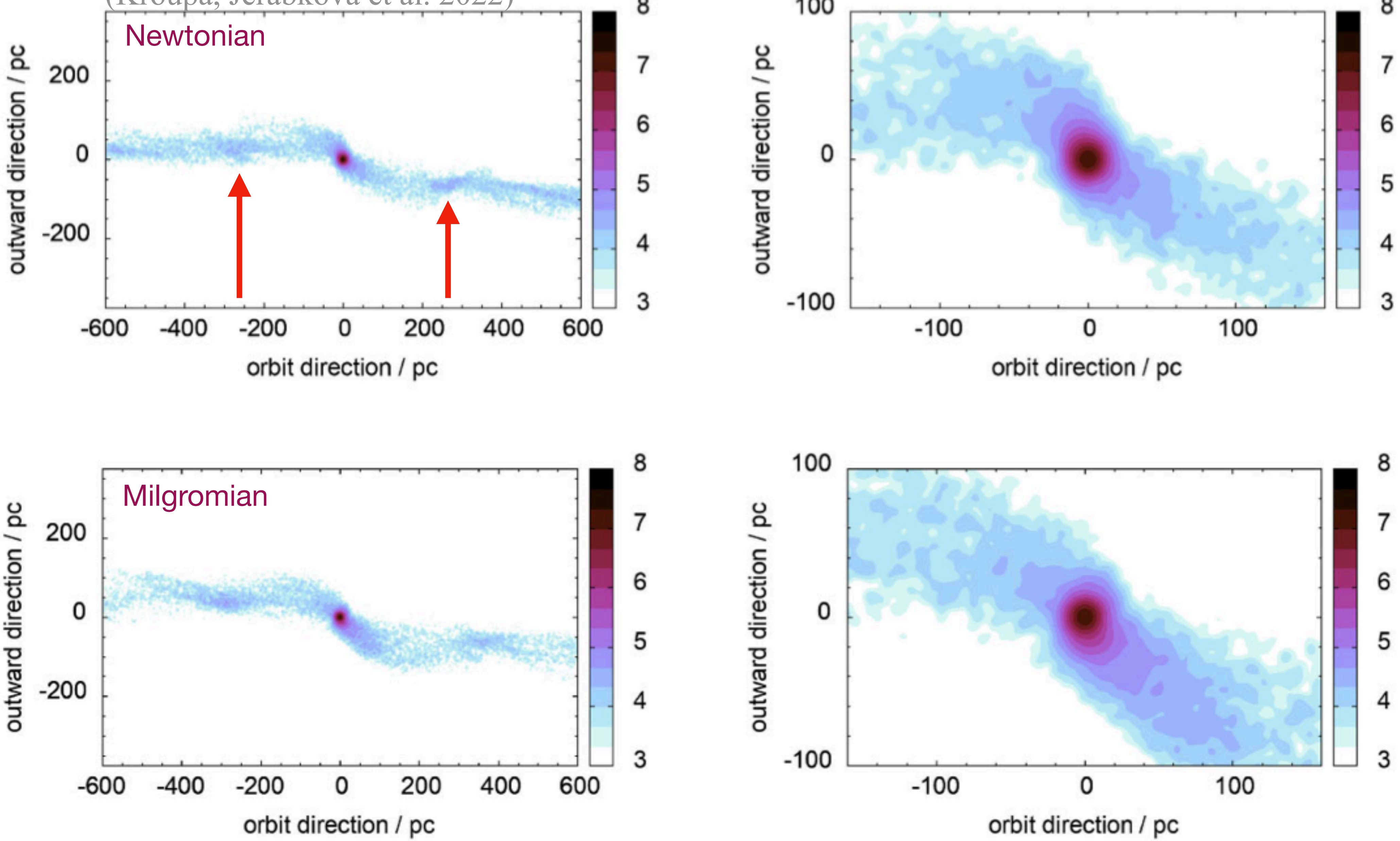

(Kroupa, Jerabkova et al. 2022)

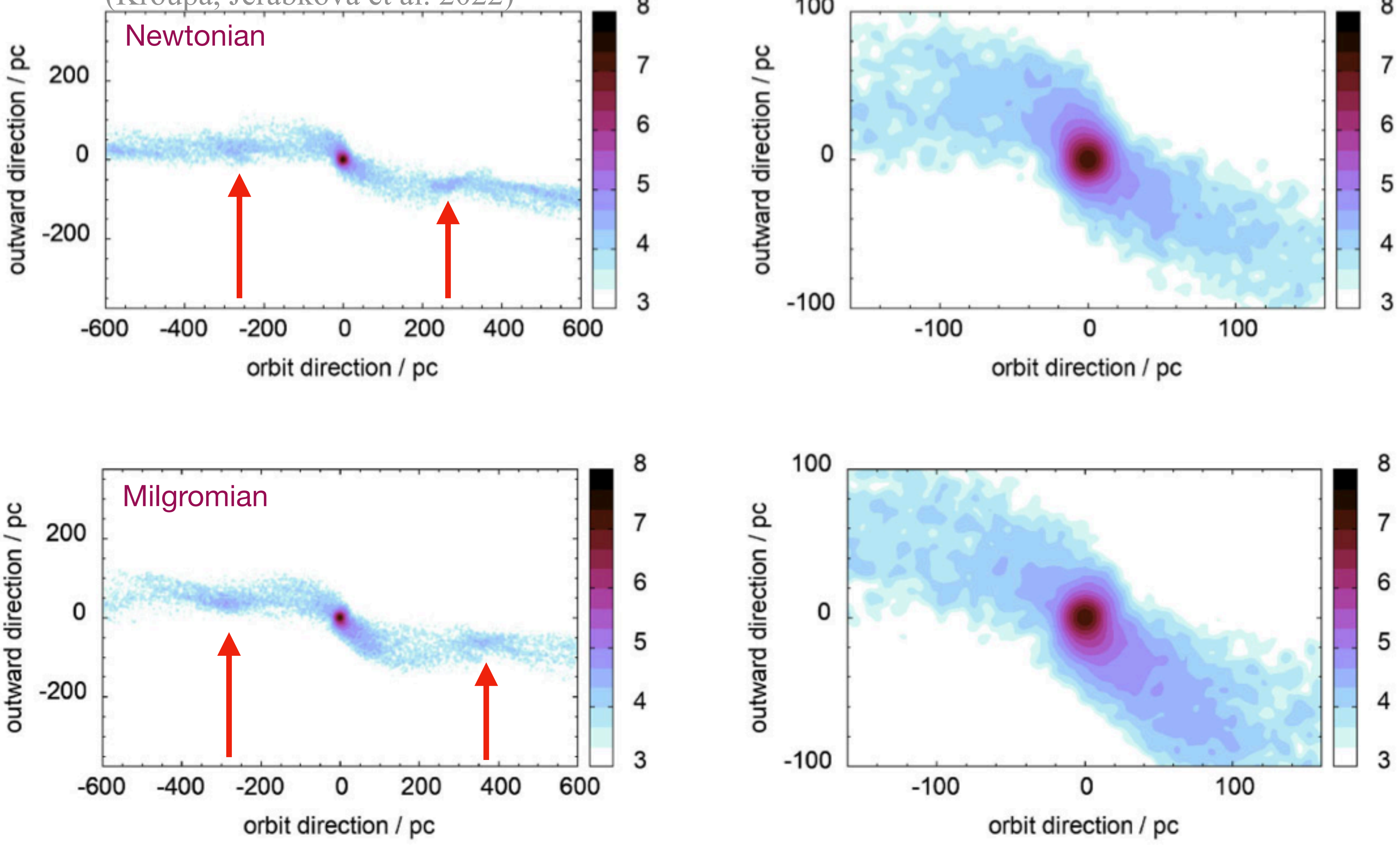

(Kroupa, Jerabkova et al. 2022)

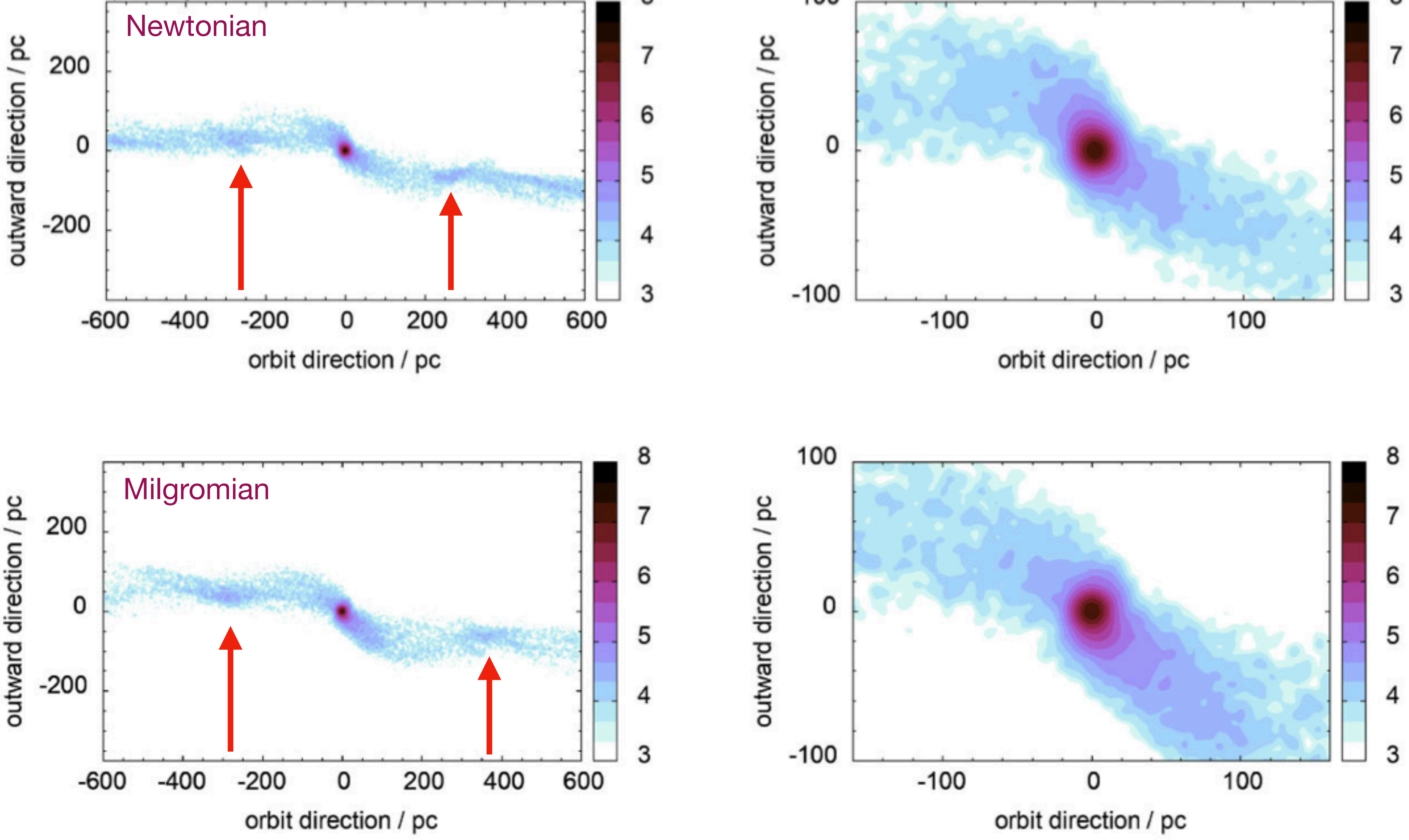

Leading Kuepper-overdensity further from cluster in Milgromian case

Above applied the new CCP method
to extract the extended tidal tails.

Above applied the new CCP method
to extract the extended tidal tails.

Four nearby open star clusters analysed
by 6 different teams using
the older / traditional CP method.

(Kroupa, Pflamm-Altenburg et al. 2024)

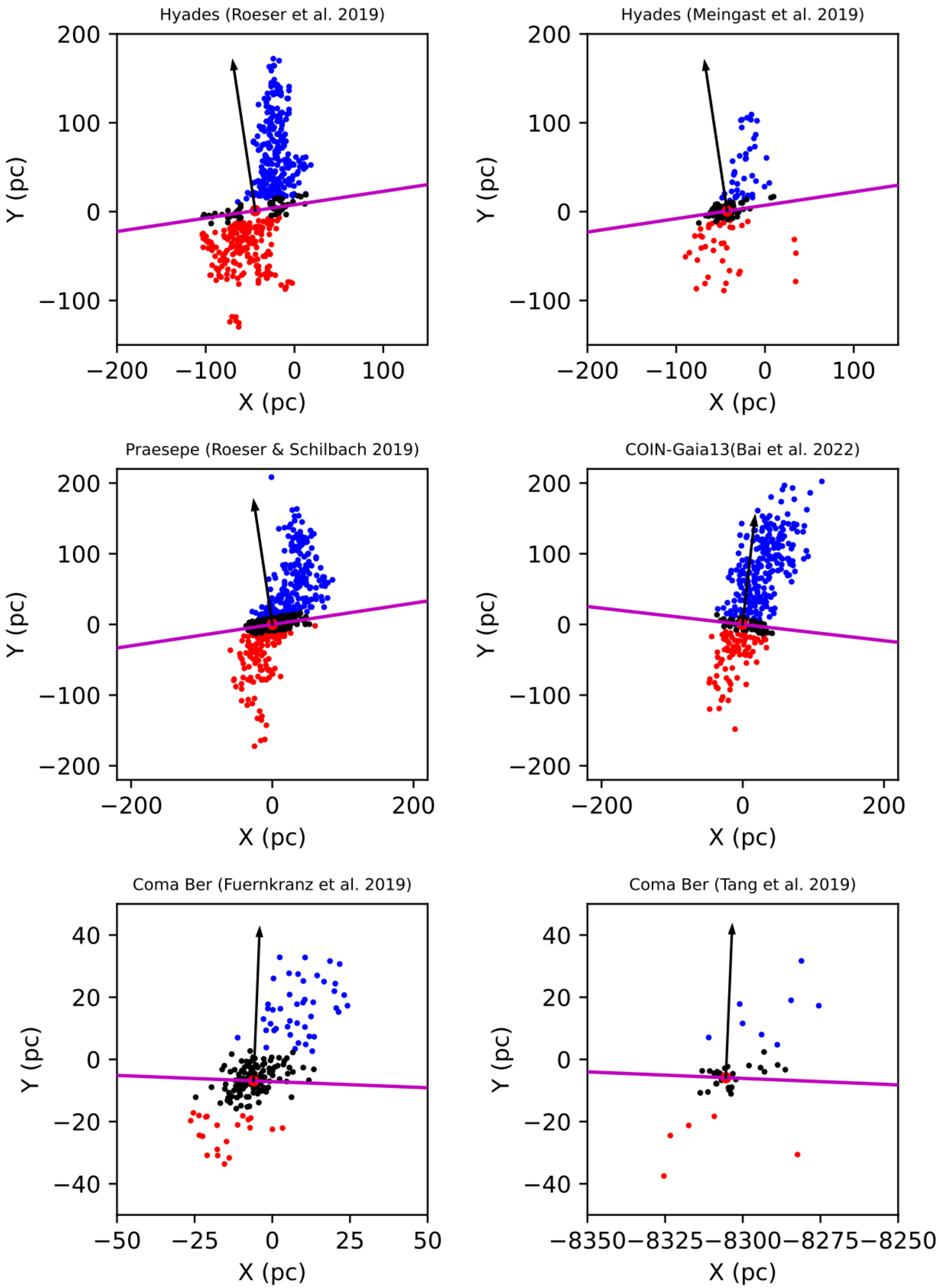

Above applied the new CCP method to extract the extended tidal tails.

Four nearby open star clusters analysed by 6 different teams using the older / traditional CP method.

(Kroupa, Pflamm-Altenburg et al. 2024)

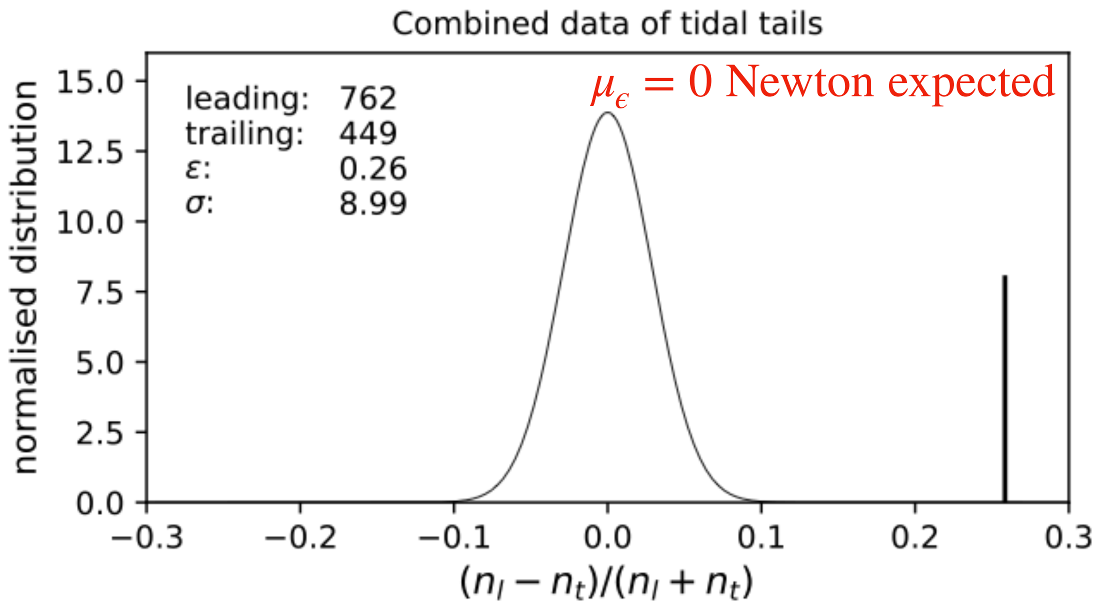

Figure 9. As Fig. 4, but here the number of stars in the leading and trailing tails are combined from all observed tidal tails to assess the probability whether all measurements are one-sided asymmetric with $n_{\mathrm{l,sum}} > n_{\mathrm{t,sum}}$.

(Kroupa, Pflamm-Altenburg et al. 2024)

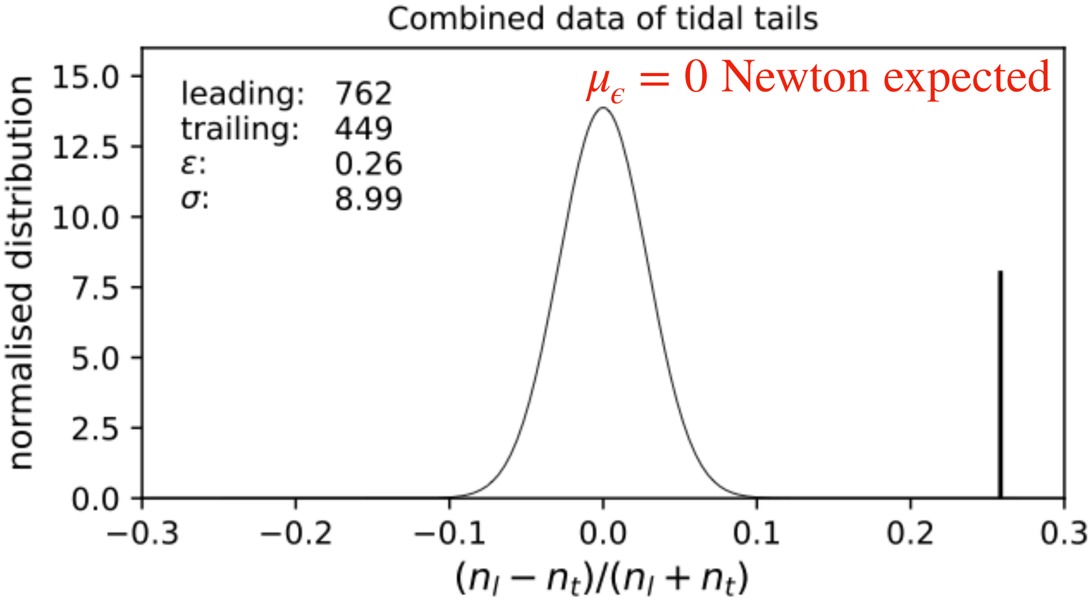

Figure 9. As Fig. 4, but here the number of stars in the leading and trailing tails are combined from all observed tidal tails to assess the probability whether all measurements are one-sided asymmetric with $n_{\mathrm{l,sum}} > n_{\mathrm{t,sum}}$.

$$\epsilon = \frac{n_\mathrm{l} - n_\mathrm{t}}{n_\mathrm{l} + n_\mathrm{t}}$$ asymmetry parameter

$$\sigma_\epsilon = \frac{1}{\sqrt{n_\mathrm{l} + n_\mathrm{t}}}$$ its variance

$$\sigma = \frac{|\mu_\epsilon - \epsilon|}{\sigma_\epsilon}$$ asymmetry significance

(Kroupa, Pflamm-Altenburg et al. 2024)

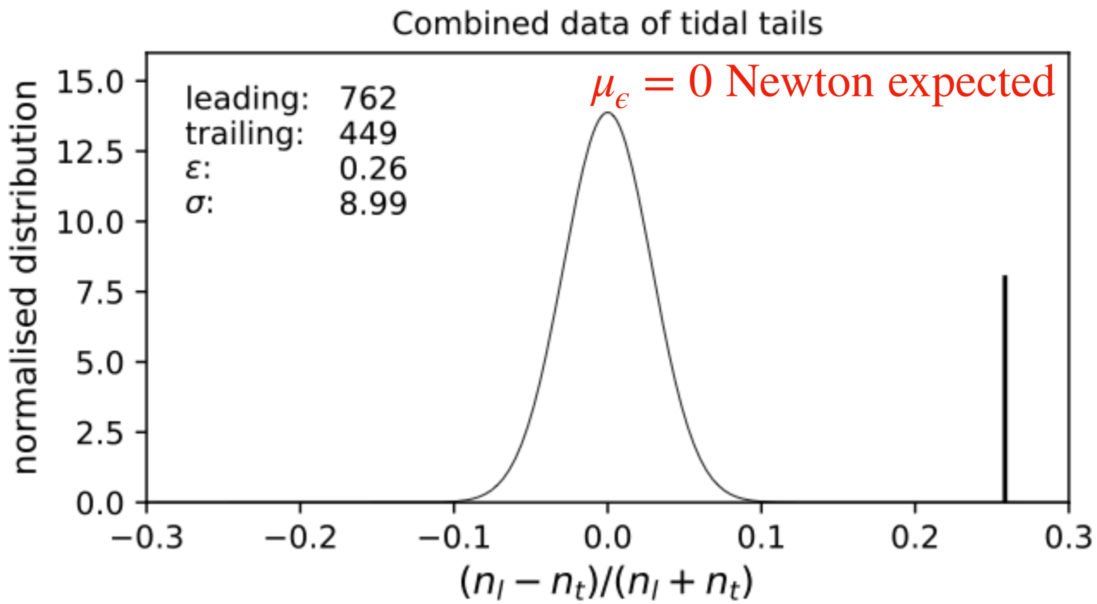

Figure 9. As Fig. 4, but here the number of stars in the leading and trailing tails are combined from all observed tidal tails to assess the probability whether all measurements are one-sided asymmetric with $n_{\mathrm{l,sum}} > n_{\mathrm{t,sum}}$.

$$\epsilon = \frac{n_\mathrm{l} - n_\mathrm{t}}{n_\mathrm{l} + n_\mathrm{t}}$$ asymmetry parameter

$$\sigma_\epsilon = \frac{1}{\sqrt{n_\mathrm{l} + n_\mathrm{t}}}$$ its variance

$$\sigma = \frac{|\mu_\epsilon - \epsilon|}{\sigma_\epsilon}$$ asymmetry significance

Observed tidal tails are in 8.99sigma tension with Newtonian symmetry.

(Kroupa, Pflamm-Altenburg et al. 2024)

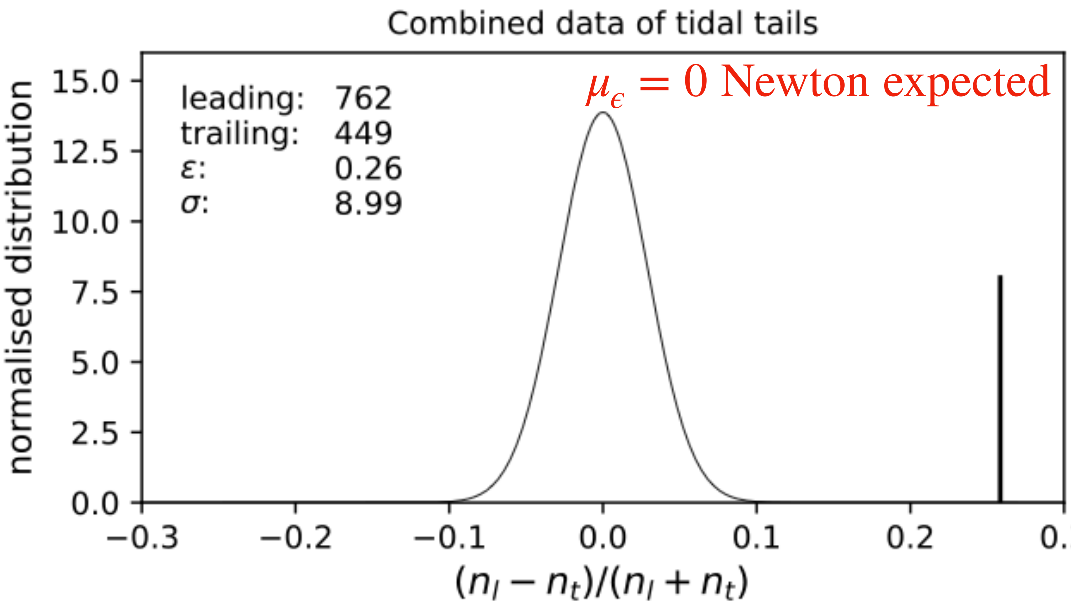

$$\epsilon = \frac{n_\mathrm{l} - n_\mathrm{t}}{n_\mathrm{l} + n_\mathrm{t}}$$ asymmetry parameter

$$\sigma_\epsilon = \frac{1}{\sqrt{n_\mathrm{l} + n_\mathrm{t}}}$$ its variance

$$\sigma = \frac{|\mu_\epsilon - \epsilon|}{\sigma_\epsilon}$$ asymmetry significance

Observed tidal tails are in 8.99sigma tension with Newtonian symmetry.

Figure 9. As Fig. 4, but here the number of stars in the leading and trailing tails are combined from all observed tidal tails to assess the probability whether all measurements are one-sided asymmetric with $n_{\mathrm{l,sum}} > n_{\mathrm{t,sum}}$.

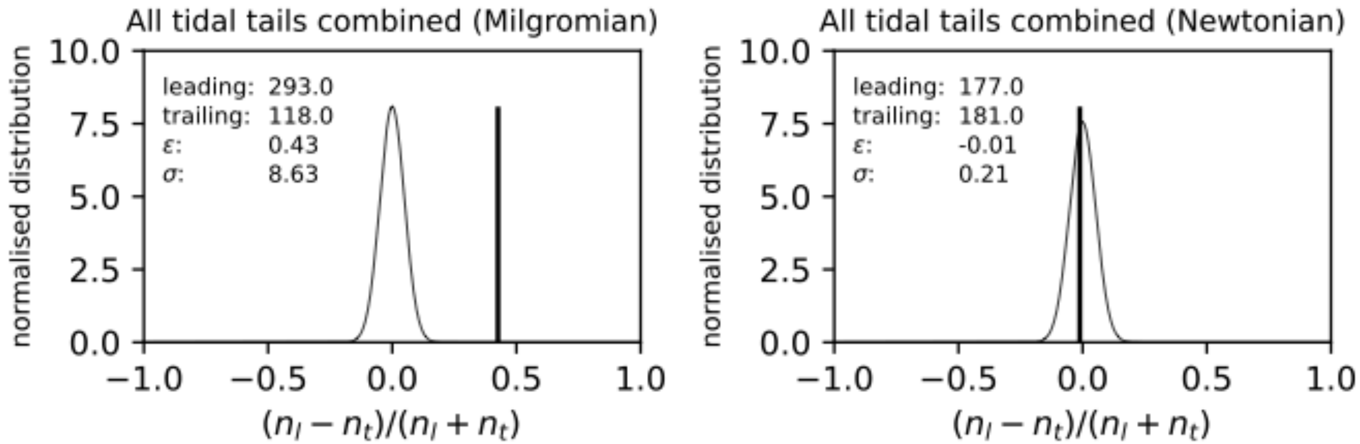

Figure 14. Similar to Fig. 13. Here the leading and trailing tail numbers of all models are combined to assess the probability if all measurements are one-sided asymmetric with $n_\mathrm{l} > n_\mathrm{t}$. The left panel depicts the combined stacked Milgromian models and shows a similar and extremely significant asymmetry that is very comparable to that observed (Fig. 9), while the combined stacked Newtonian models (right panel) are consistent with the leading and trailing tail having a similar number of stars.

(Kroupa, Pflamm-Altenburg et al. 2024)

$$\epsilon = \frac{n_{\rm l} - n_{\rm t}}{n_{\rm l} + n_{\rm t}}$$ asymmetry parameter

$$\sigma_\epsilon = \frac{1}{\sqrt{n_{\rm l} + n_{\rm t}}}$$ its variance

$$\sigma = \frac{|\mu_\epsilon - \epsilon|}{\sigma_\epsilon}$$ asymmetry significance

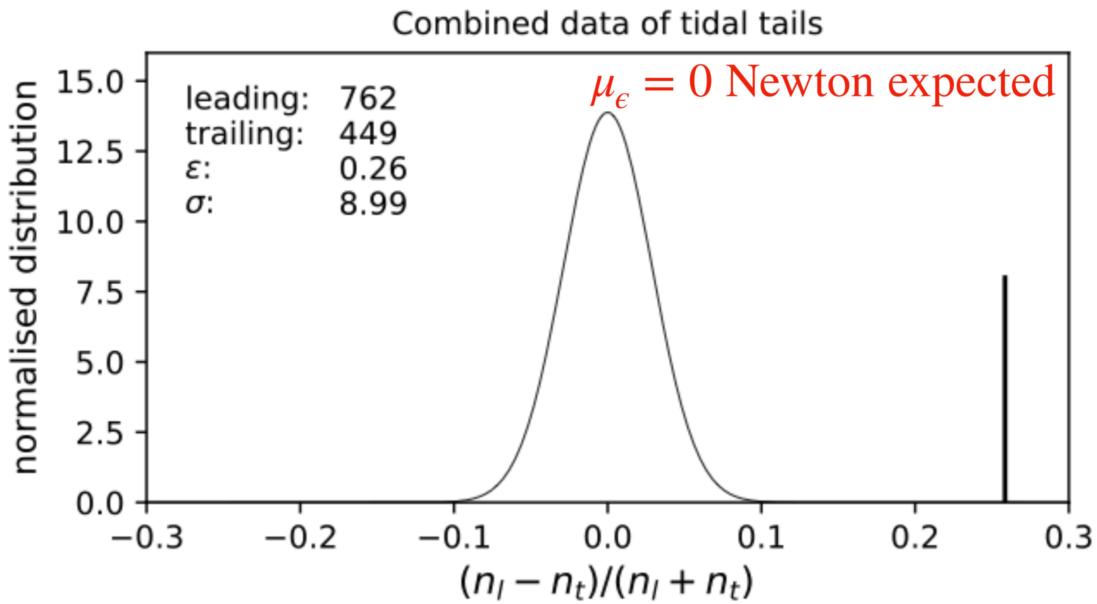

Observed tidal tails are in 8.99sigma tension with Newtonian symmetry.

Figure 9. As Fig. 4, but here the number of stars in the leading and trailing tails are combined from all observed tidal tails to assess the probability whether all measurements are one-sided asymmetric with $n_{\rm l,sum} > n_{\rm t,sum}$.

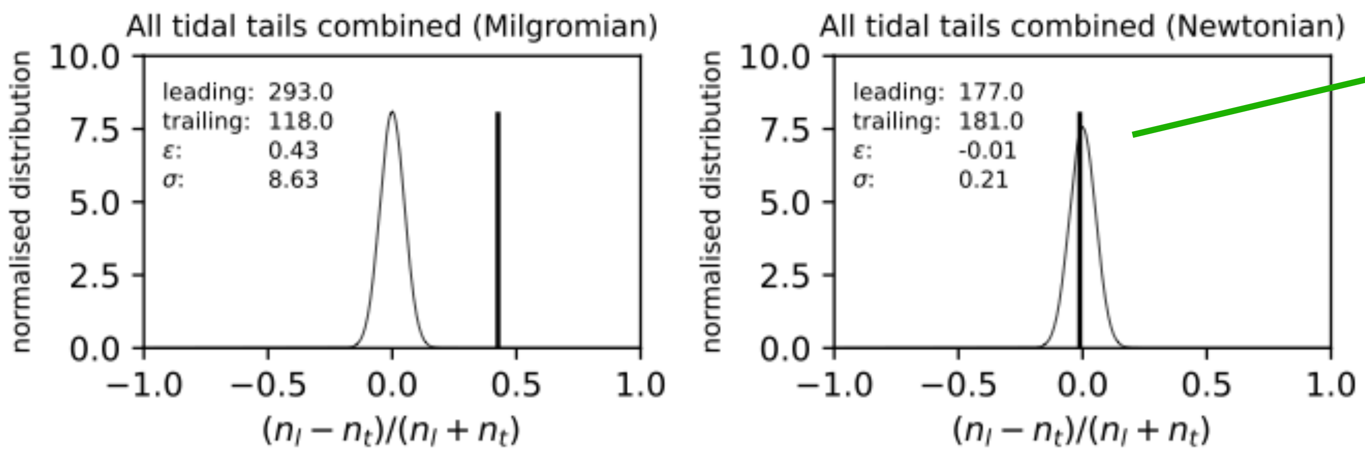

Modelled Newtonian tidal tails are in 0.21sigma tension with Newtonian symmetry.

Figure 14. Similar to Fig. 13. Here the leading and trailing tail numbers of all models are combined to assess the probability if all measurements are one-sided asymmetric with $n_{\rm l} > n_{\rm t}$. The left panel depicts the combined stacked Milgromian models and shows a similar and extremely significant asymmetry that is very comparable to that observed (Fig. 9), while the combined stacked Newtonian models (right panel) are consistent with the leading and trailing tail having a similar number of stars.

(Kroupa, Pflamm-Altenburg et al. 2024)

$$\epsilon = \frac{n_{\rm l} - n_{\rm t}}{n_{\rm l} + n_{\rm t}}$$ asymmetry parameter

$$\sigma_\epsilon = \frac{1}{\sqrt{n_{\rm l} + n_{\rm t}}}$$ its variance

$$\sigma = \frac{|\mu_\epsilon - \epsilon|}{\sigma_\epsilon}$$ asymmetry significance

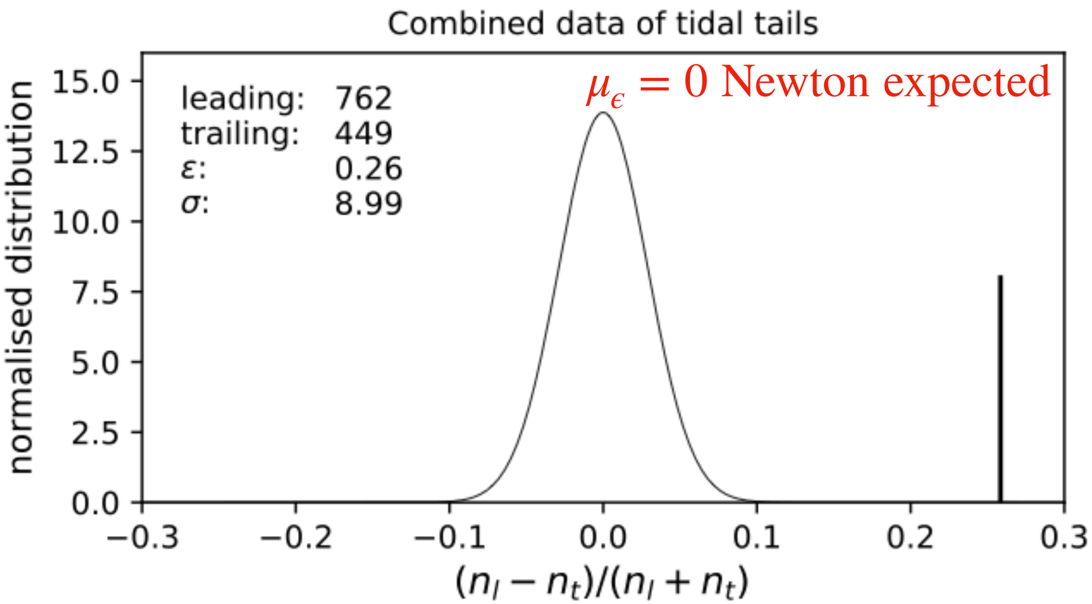

Observed tidal tails are in 8.99sigma tension with Newtonian symmetry.

Figure 9. As Fig. 4, but here the number of stars in the leading and trailing tails are combined from all observed tidal tails to assess the probability whether all measurements are one-sided asymmetric with $n_{\rm l,sum} > n_{\rm t,sum}$.

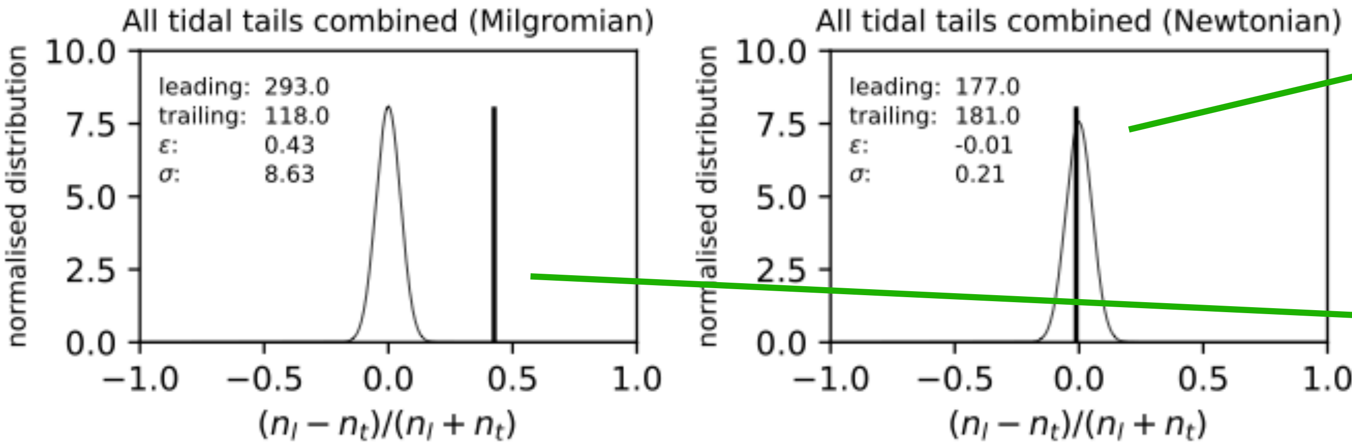

Modelled Newtonian tidal tails are in 0.21sigma tension with Newtonian symmetry.

Modelled Milgromian tidal tails are in 8.63sigma tension with Newtonian symmetry.

Figure 14. Similar to Fig. 13. Here the leading and trailing tail numbers of all models are combined to assess the probability if all measurements are one-sided asymmetric with $n_{\rm l} > n_{\rm t}$. The left panel depicts the combined stacked Milgromian models and shows a similar and extremely significant asymmetry that is very comparable to that observed (Fig. 9), while the combined stacked Newtonian models (right panel) are consistent with the leading and trailing tail having a similar number of stars.

The evaporation of stars from their star clusters

unambiguously

compellingly

absolutely

falsify Newtonian gravitation

The evaporation of stars from their star clusters
unambiguously
compellingly
absolutely
falsify Newtonian gravitation

Consistency of test results :

The evaporation of stars from their star clusters
unambiguously
compellingly
absolutely
falsify Newtonian gravitation

Consistency of test results :

Falsification of cold and warm dark matter particles
(dynamical friction test on 100kpc scale)

The evaporation of stars from their star clusters
unambiguously
compellingly
absolutely
falsify Newtonian gravitation

Consistency of test results :

Falsification of cold and warm dark matter particles
(dynamical friction test on 100kpc scale)

Gravitational potential cannot be Newtonian

The evaporation of stars from their star clusters
unambiguously
compellingly
absolutely
falsify Newtonian gravitation

Consistency of test results :

Falsification of cold and warm dark matter particles
(dynamical friction test on 100kpc scale)

Gravitational potential cannot be Newtonian

The tidal tail asymmetry confirms this !

Other tests,

not based

on

Chandrasekhar dynamical friction

The distribution of matter on scales of Mpc

Structure of and correlations in Local group

Frighteningly symmetric structure of the Local Group

Structure of and correlations in Local group

Frighteningly symmetric structure of the Local Group

Everything we know about the Local Group today :

Structure of and correlations in Local group

Frighteningly symmetric structure of the Local Group

Everything we know about the Local Group today :

Pawlowski, Kroupa & Jerjen (2013) **:**

"***The discovery of symmetric structures in the Local Group***"

Structure of and correlations in Local group

Frighteningly symmetric structure of the Local Group

Looking along the line between Milky Way and Andromeda

Everything we know about the Local Group today :

Pawlowski, Kroupa & Jerjen (2013) **:**

"***The discovery of symmetric structures in the Local Group***"

Structure of and correlations in Local group

Frighteningly symmetric structure of the Local Group

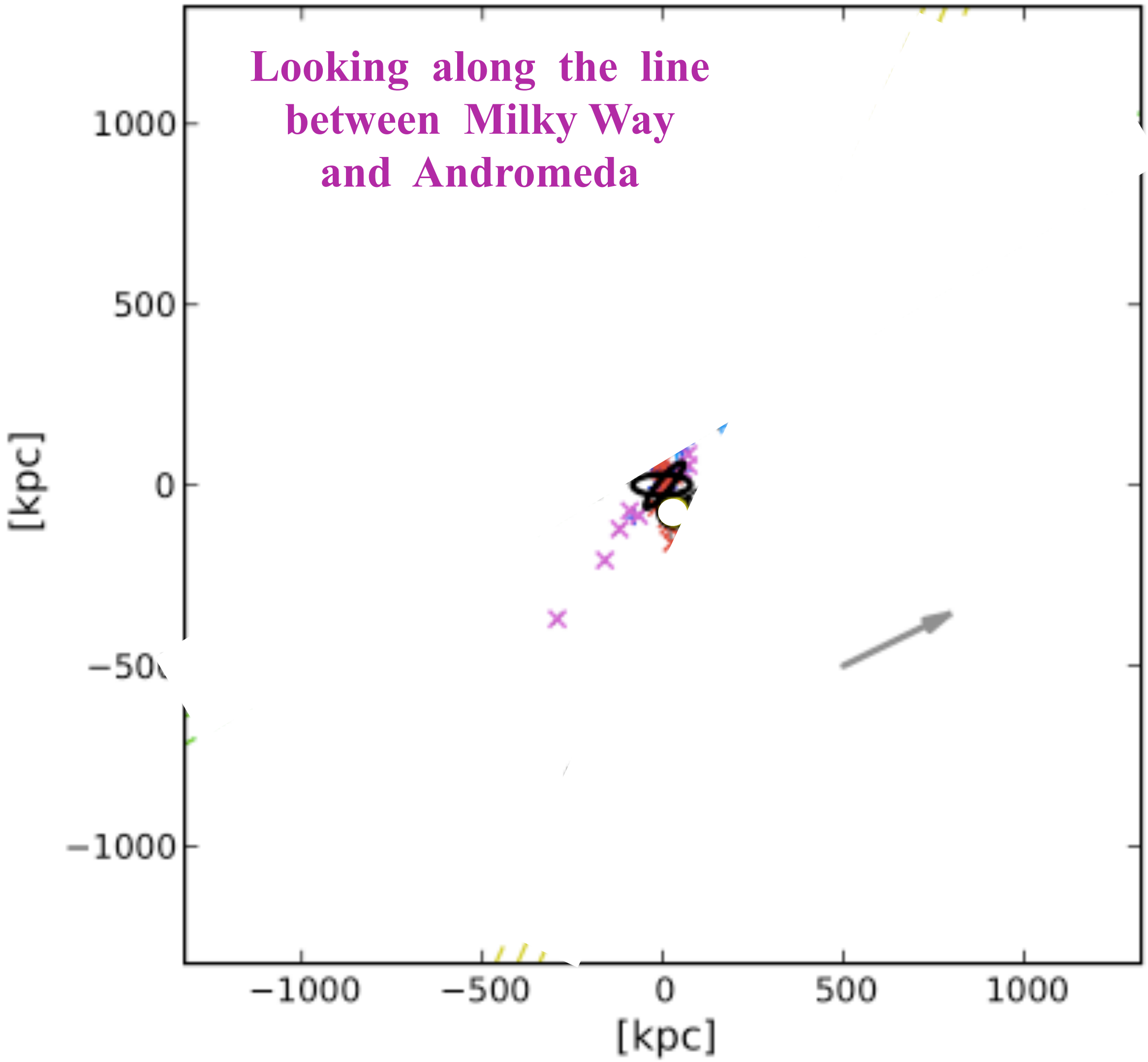

Figure 9. Edge-on view of both LG planes. The orientation of the MW and M31 are indicted as black ellipses in the centre. Members of the LGP1 are plotted as yellow points, those of LGP2 as green points. MW galaxies are plotted as plus signs (+), all other galaxies as crosses (×), the colours code their plane membership as in Fig. 6. The best-fitting planes are plotted as

Everything we know about the Local Group today :

Pawlowski, Kroupa & Jerjen (2013) :

"The discovery of symmetric structures in the Local Group"

Structure of and correlations in Local group

Frighteningly symmetric structure of the Local Group

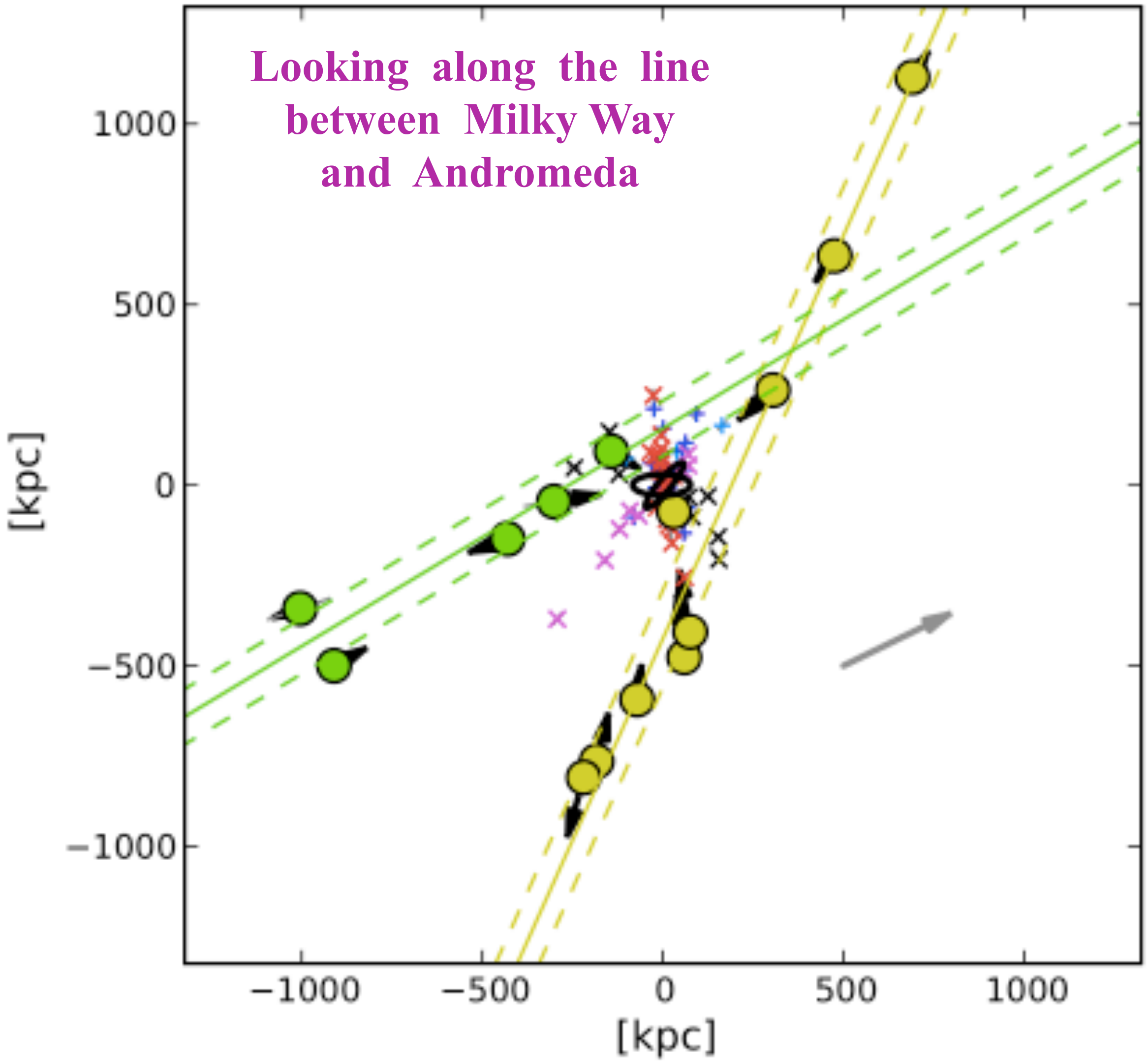

Figure 9. Edge-on view of both LG planes. The orientation of the MW and M31 are indicted as black ellipses in the centre. Members of the LGP1 are plotted as yellow points, those of LGP2 as green points. MW galaxies are plotted as plus signs (+), all other galaxies as crosses (×), the colours code their plane membership as in Fig. 6. The best-fitting planes are plotted as

Everything we know about the Local Group today :

Pawlowski, Kroupa & Jerjen (2013) :

"The discovery of symmetric structures in the Local Group"

Structure of and correlations in Local group

Frighteningly symmetric structure of the Local Group

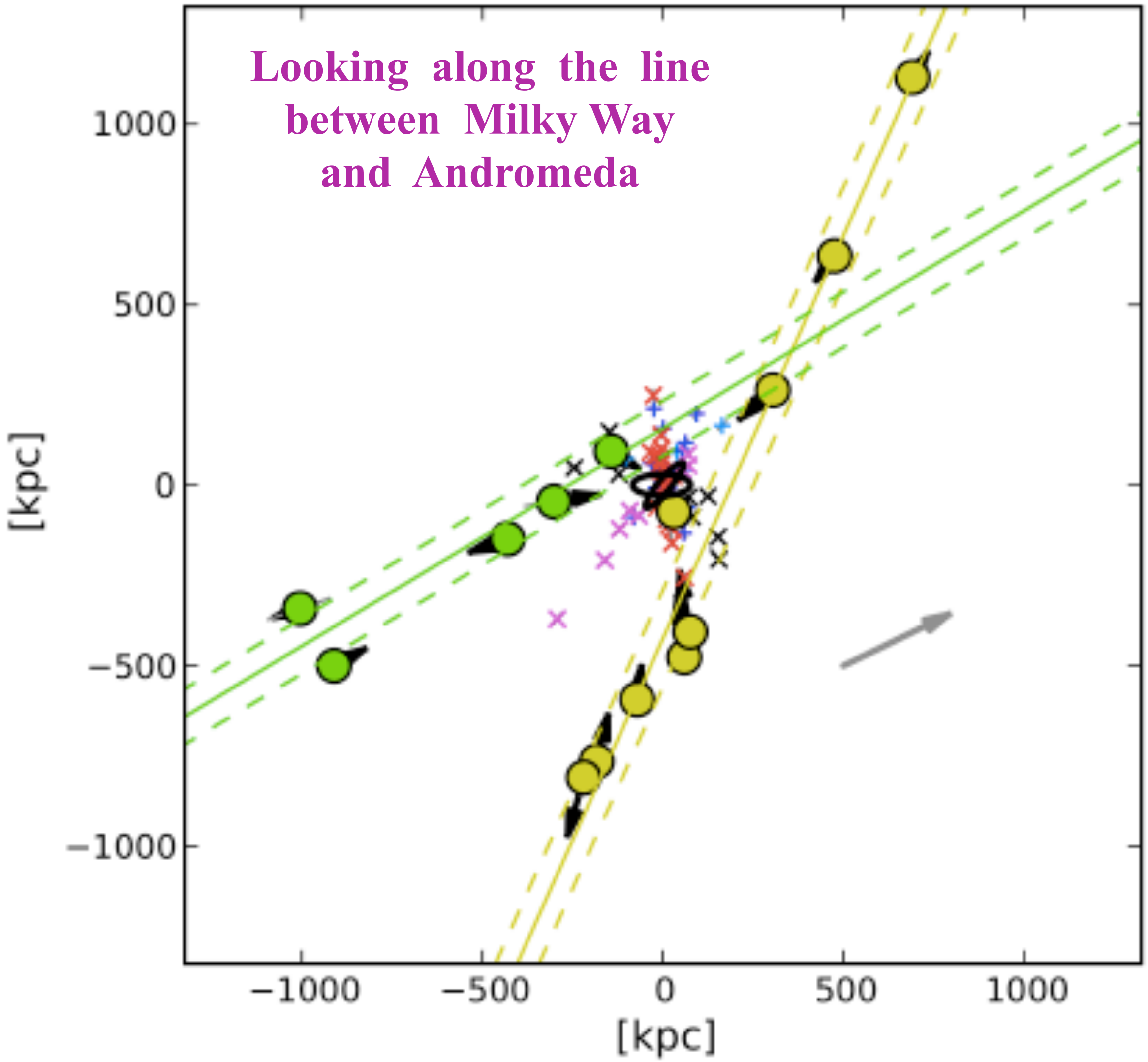

Figure 9. Edge-on view of both LG planes. The orientation of the MW and M31 are indicted as black ellipses in the centre. Members of the LGP1 are plotted as yellow points, those of LGP2 as green points. MW galaxies are plotted as plus signs (+), all other galaxies as crosses (×), the colours code their plane membership as in Fig. 6. The best-fitting planes are plotted as

Everything we know about the Local Group today :

Pawlowski, Kroupa & Jerjen (2013) :

"The discovery of symmetric structures in the Local Group"

A frightening symmetry

NOT SMoC at ∞ sigma

The distribution of
matter on scales
of
a Gpc

KBC void and Hubble Tension

The Cosmological Scale

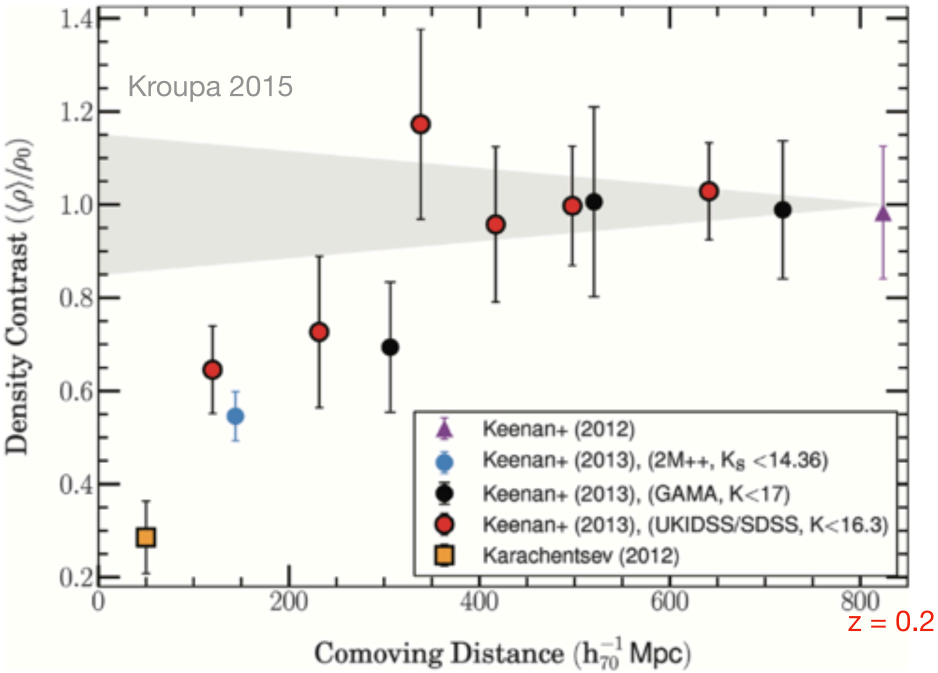

Figure 1. The KBC void: the actual density of normal matter divided by the mean cosmological density is plotted in dependence of the distance from the position of the Sun (which is in the Local Group of galaxies). The grey area indicates the density fluctuations allowed by the ΛCDM model. Taken from fig. 1 in Kroupa (2015).

KBC void and Hubble Tension

The Cosmological Scale

Haslbauer, Banik & Kroupa 2020 :

The under-density is evident in

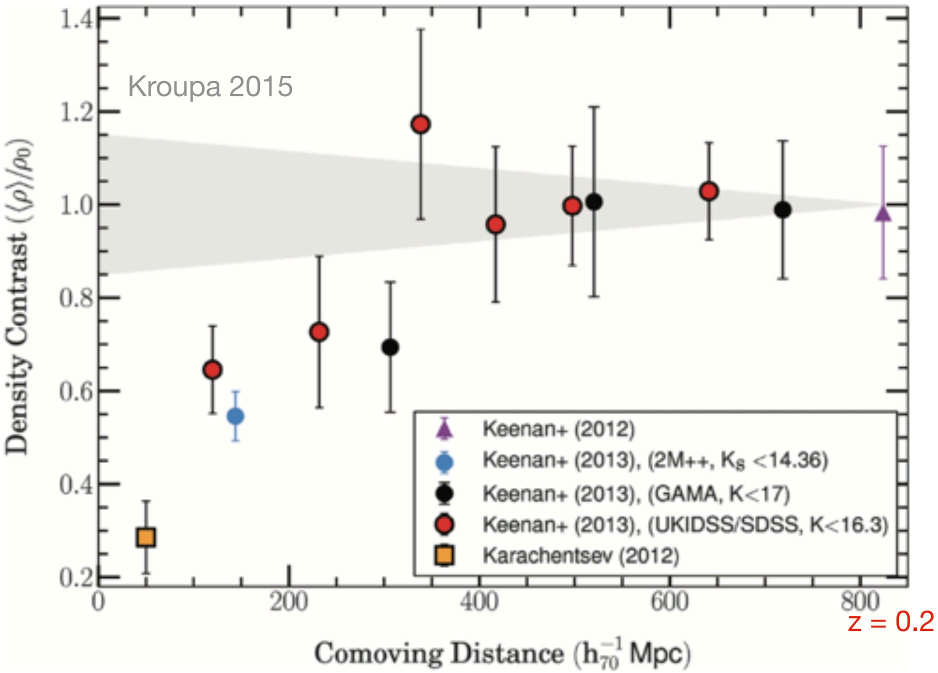

Figure 1. The KBC void: the actual density of normal matter divided by the mean cosmological density is plotted in dependence of the distance from the position of the Sun (which is in the Local Group of galaxies). The grey area indicates the density fluctuations allowed by the ΛCDM model. Taken from fig. 1 in Kroupa (2015).

KBC void and Hubble Tension

The Cosmological Scale

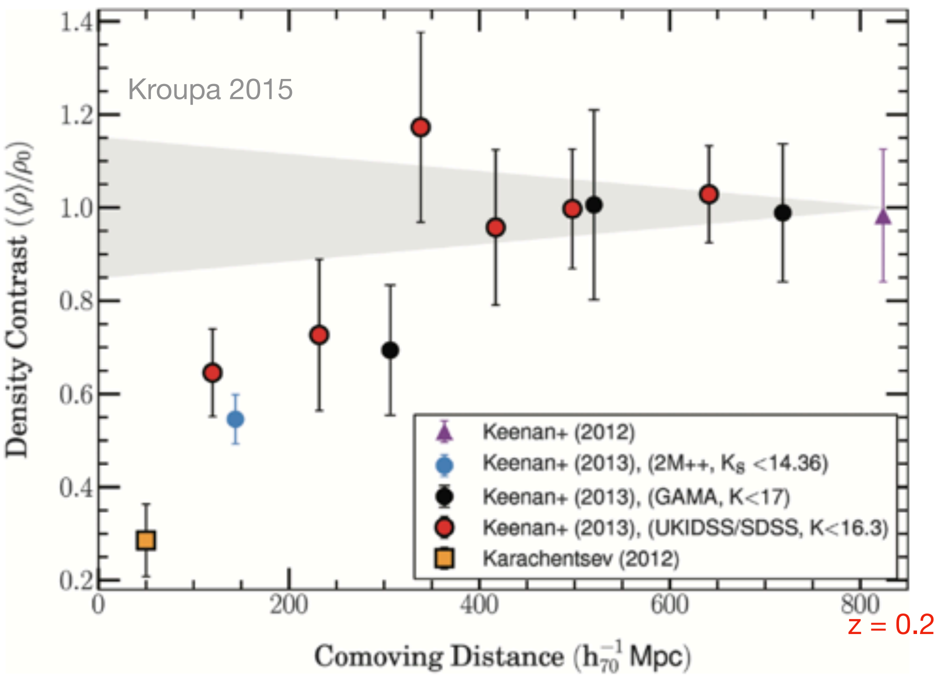

Figure 1. The KBC void: the actual density of normal matter divided by the mean cosmological density is plotted in dependence of the distance from the position of the Sun (which is in the Local Group of galaxies). The grey area indicates the density fluctuations allowed by the ΛCDM model. Taken from fig. 1 in Kroupa (2015).

Haslbauer, Banik & Kroupa 2020 :

The under-density is evident in

optical galaxy surveys
Maddox+1990; Zucca+1997

near-infrared galaxy surveys
Keenan, Barger & Cowie'13 (KBC)

X-ray cluster surveys
Böhringer+2015; Böhringer, Chan, Collins 2020; Migkas+21

CMB dipole indicating large-scale bulk flows as expected for such a void (radio observations)

Rubart & Schwarz 2013; Rubart, Bacon & Schwarz 2014; Javanmardi+ 2015; Secrest+ 2020

KBC void and Hubble Tension

The Cosmological Scale

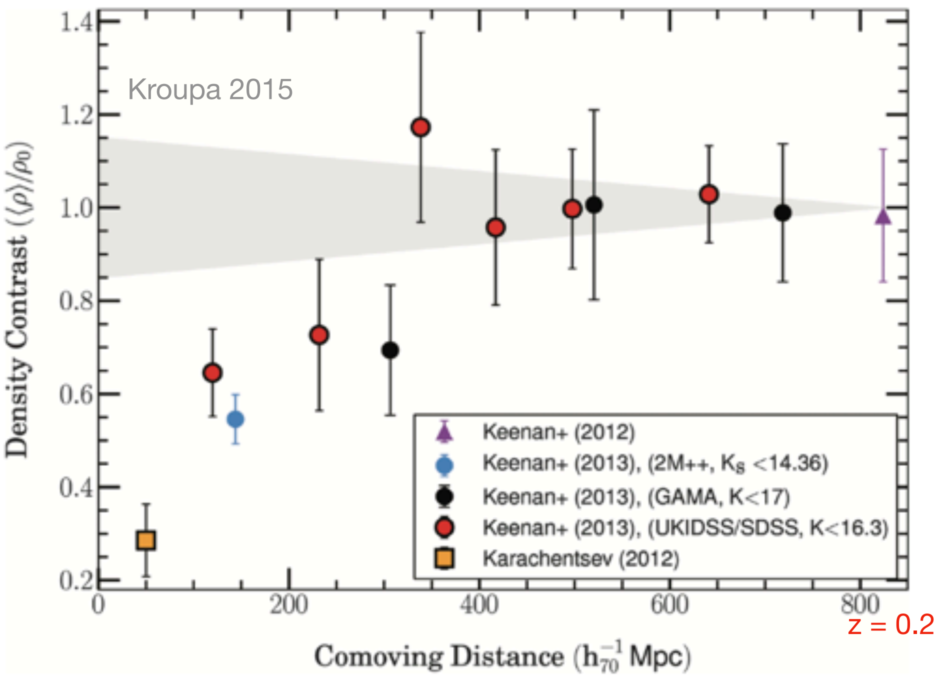

Figure 1. The KBC void: the actual density of normal matter divided by the mean cosmological density is plotted in dependence of the distance from the position of the Sun (which is in the Local Group of galaxies). The grey area indicates the density fluctuations allowed by the ΛCDM model. Taken from fig. 1 in Kroupa (2015).

Haslbauer, Banik & Kroupa 2020 :

The under-density is evident in

optical galaxy surveys

Maddox+1990; Zucca+1997

near-infrared galaxy surveys

Keenan, Barger & Cowie'13 (KBC)

X-ray cluster surveys

Böhringer+2015; Böhringer, Chan, Collins 2020; Migkas+21

CMB dipole indicating large-scale bulk flows as expected for such a void (radio observations)

Rubart & Schwarz 2013; Rubart, Bacon & Schwarz 2014; Javanmardi+ 2015; Secrest+ 2020

Additionally :

Strong evidence for highly significant over- and under-densities in galaxy-cluster data

Migkas & Reiprich (2018); Migkas et al. (2021)

4.9 sigma exclusion of cosmological principle based on distribution of 10^6 quasars Secrest+... Sarkar et al. (2021)

KBC void and Hubble Tension

The Cosmological Scale

Can the KBC void
grow in the SMoC **?**

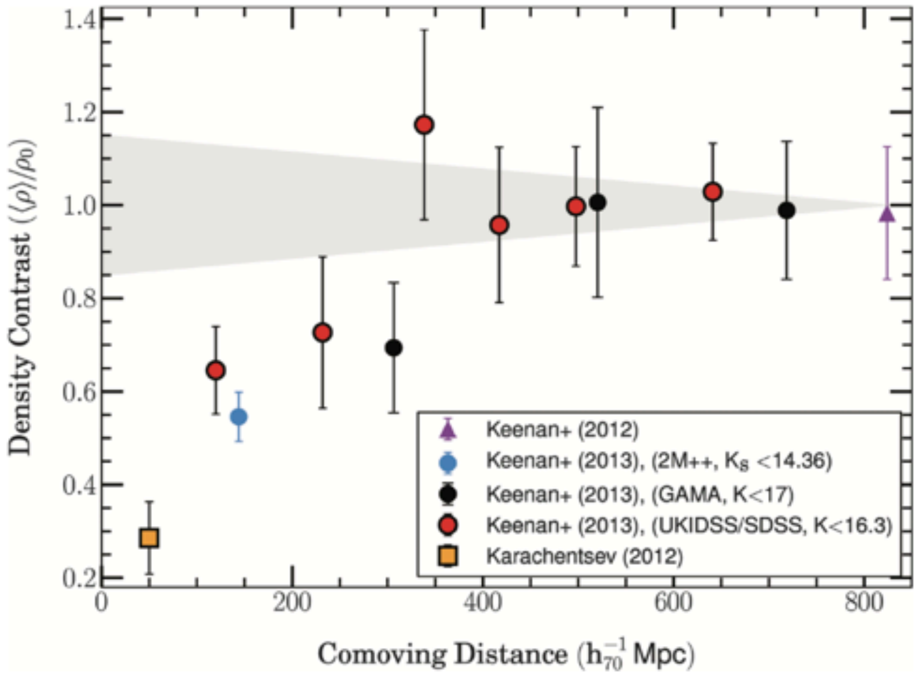

Figure 1. The KBC void: the actual density of normal matter divided by the mean cosmological density is plotted in dependence of the distance from the position of the Sun (which is in the Local Group of galaxies). The grey area indicates the density fluctuations allowed by the ΛCDM model. Taken from fig. 1 in Kroupa (2015).

KBC void and Hubble Tension

The Cosmological Scale

Can the KBC void grow in the SMoC ?

CMB at z = 1100
density contrast ≈ 1e-5

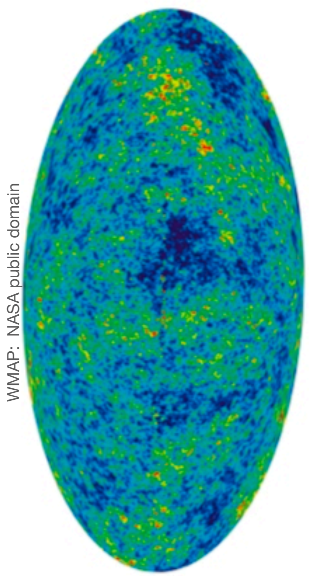

?

Use Millenium XXL SMoC/LCDM simulation (Angulo et al. 2012

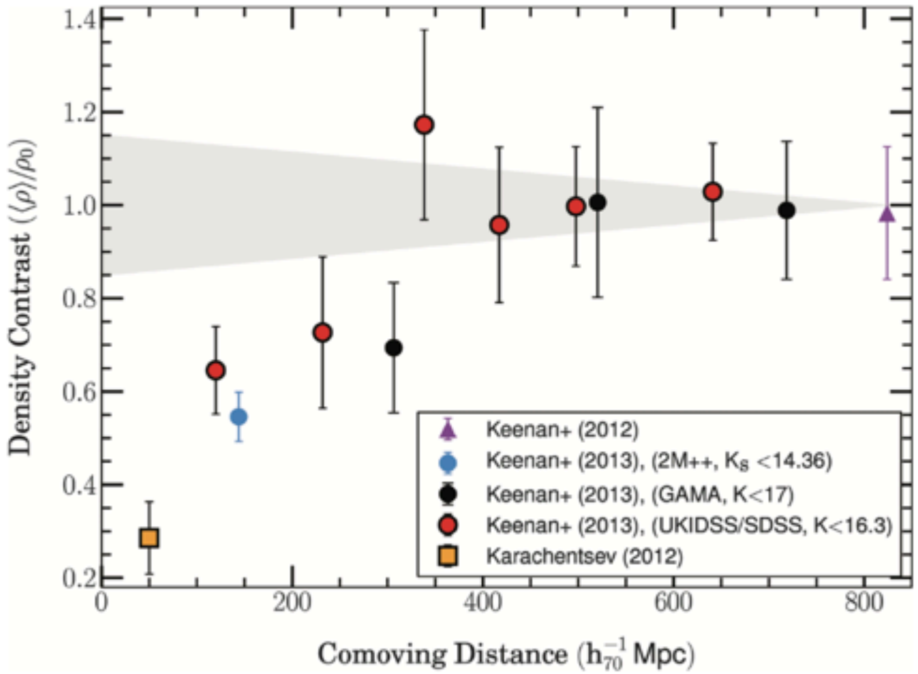

Figure 1. The KBC void: the actual density of normal matter divided by the mean cosmological density is plotted in dependence of the distance from the position of the Sun (which is in the Local Group of galaxies). The grey area indicates the density fluctuations allowed by the ΛCDM model. Taken from fig. 1 in Kroupa (2015).

KBC void and Hubble Tension

The Cosmological Scale

Test how often does a KBC void occur ?

Haslbauer, Banik & Kroupa 2020

https://www.h-its.org/wp-content/uploads/2014/10/inSiDE_autumn2010_p20.pdf

KBC void and Hubble Tension

The Cosmological Scale

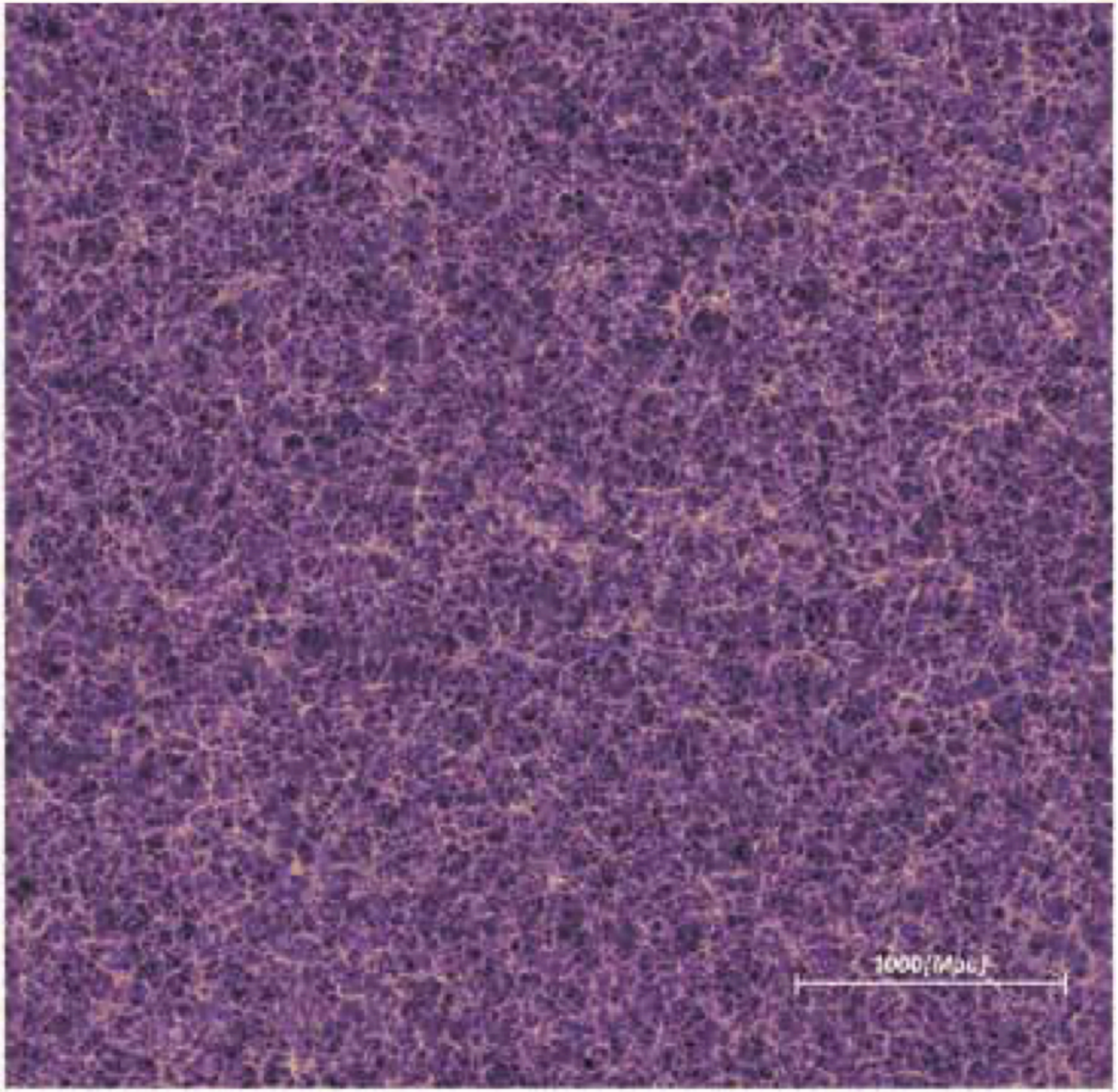

https://www.h-its.org/wp-content/uploads/2014/10/inSiDE_autumn2010_p20.pdf

The Millennium XXL (MXXL) simulation (SMoC)

Angulo et al. 2012

Test how often does a KBC void occur ?

Haslbauer, Banik & Kroupa 2020

KBC void and Hubble Tension

The Cosmological Scale

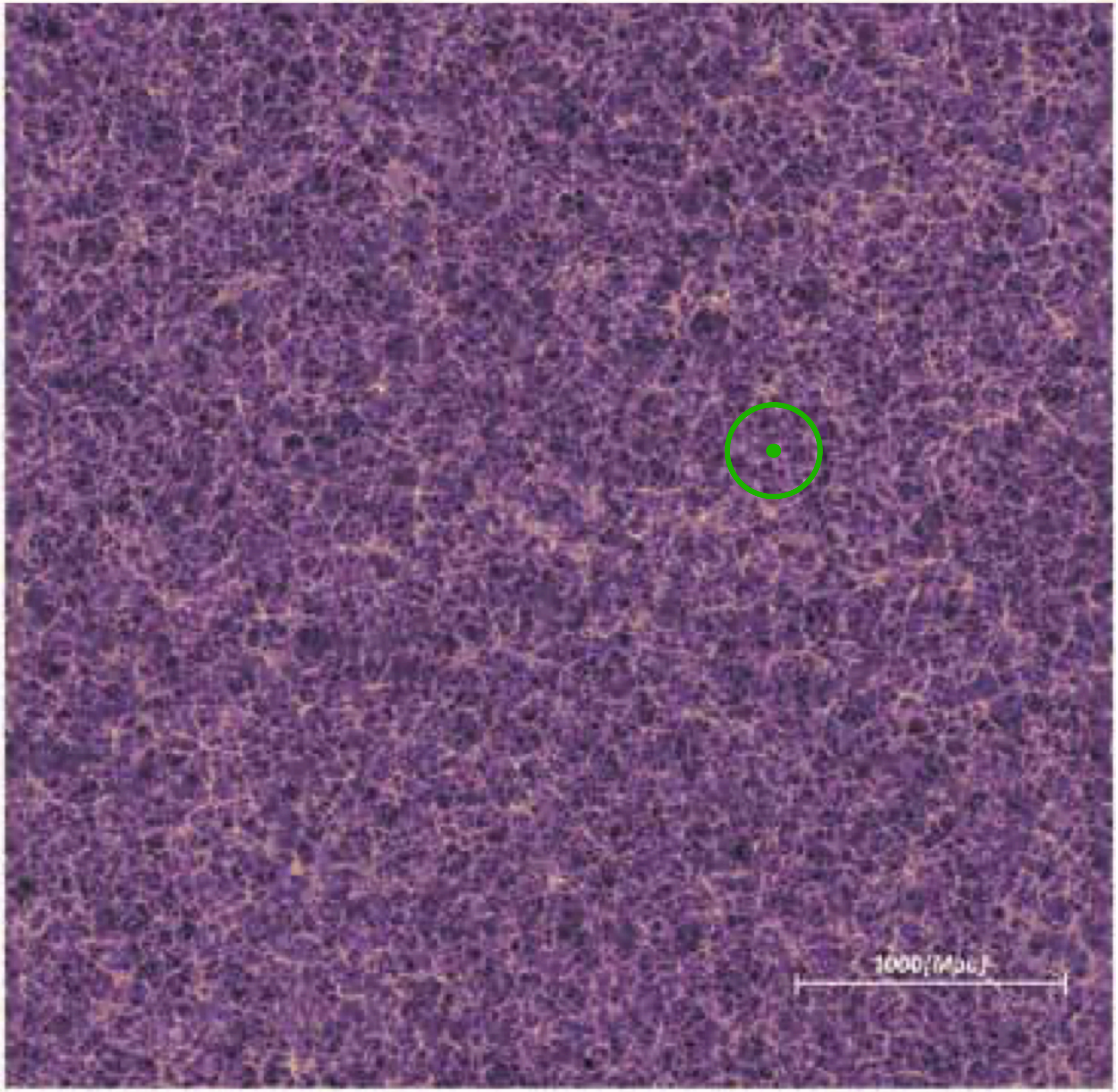

https://www.h-its.org/wp-content/uploads/2014/10/inSiDE_autumn2010_p20.pdf

The Millennium XXL (MXXL) simulation (SMoC)

Angulo et al. 2012

Test how often does a KBC void occur ?

Haslbauer, Banik & Kroupa 2020

KBC void and Hubble Tension

The Cosmological Scale

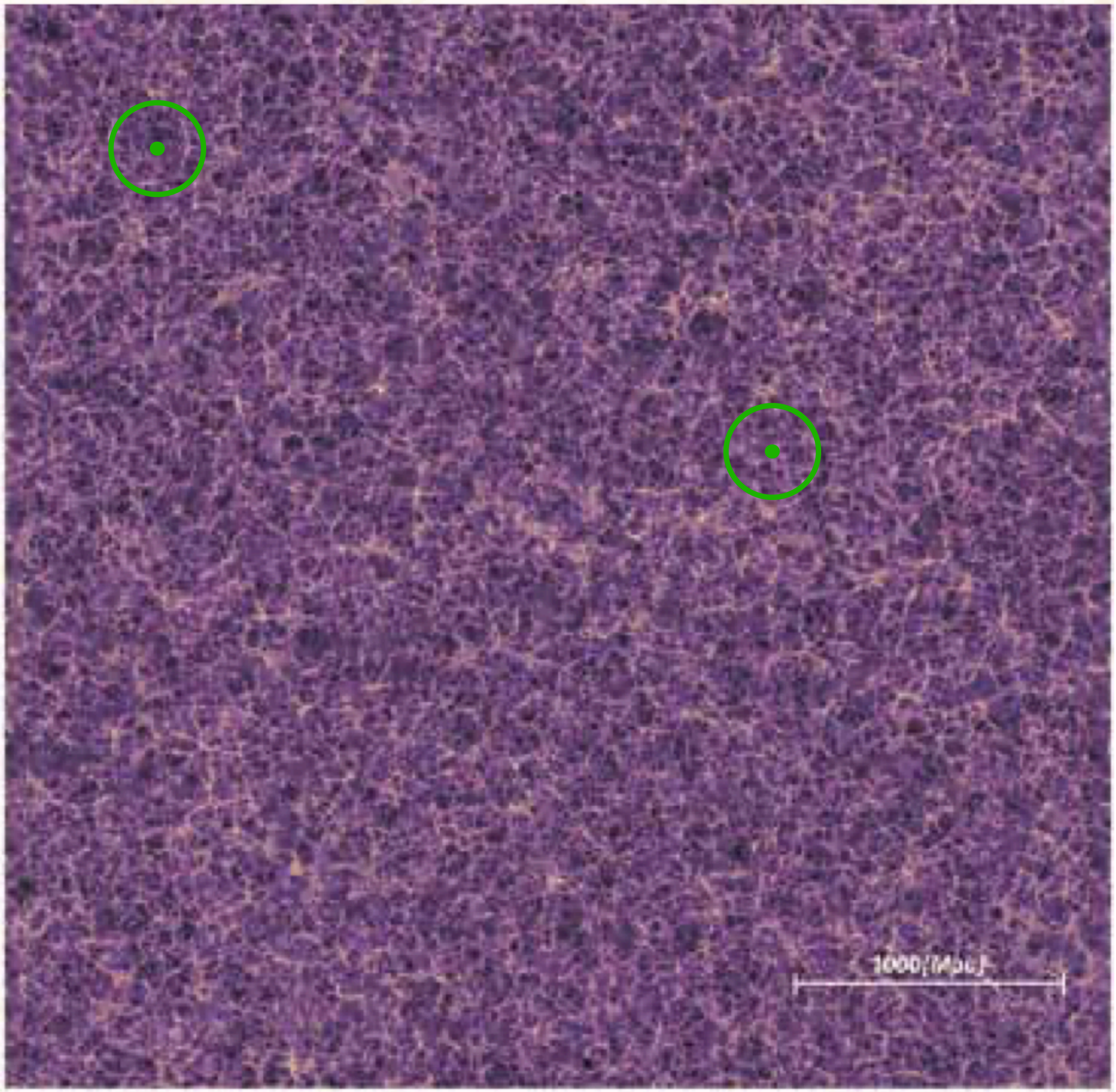

https://www.h-its.org/wp-content/uploads/2014/10/inSiDE_autumn2010_p20.pdf

The Millennium XXL (MXXL) simulation (SMoC)

Angulo et al. 2012

Test how often does a KBC void occur ?

Haslbauer, Banik & Kroupa 2020

KBC void and Hubble Tension

The Cosmological Scale

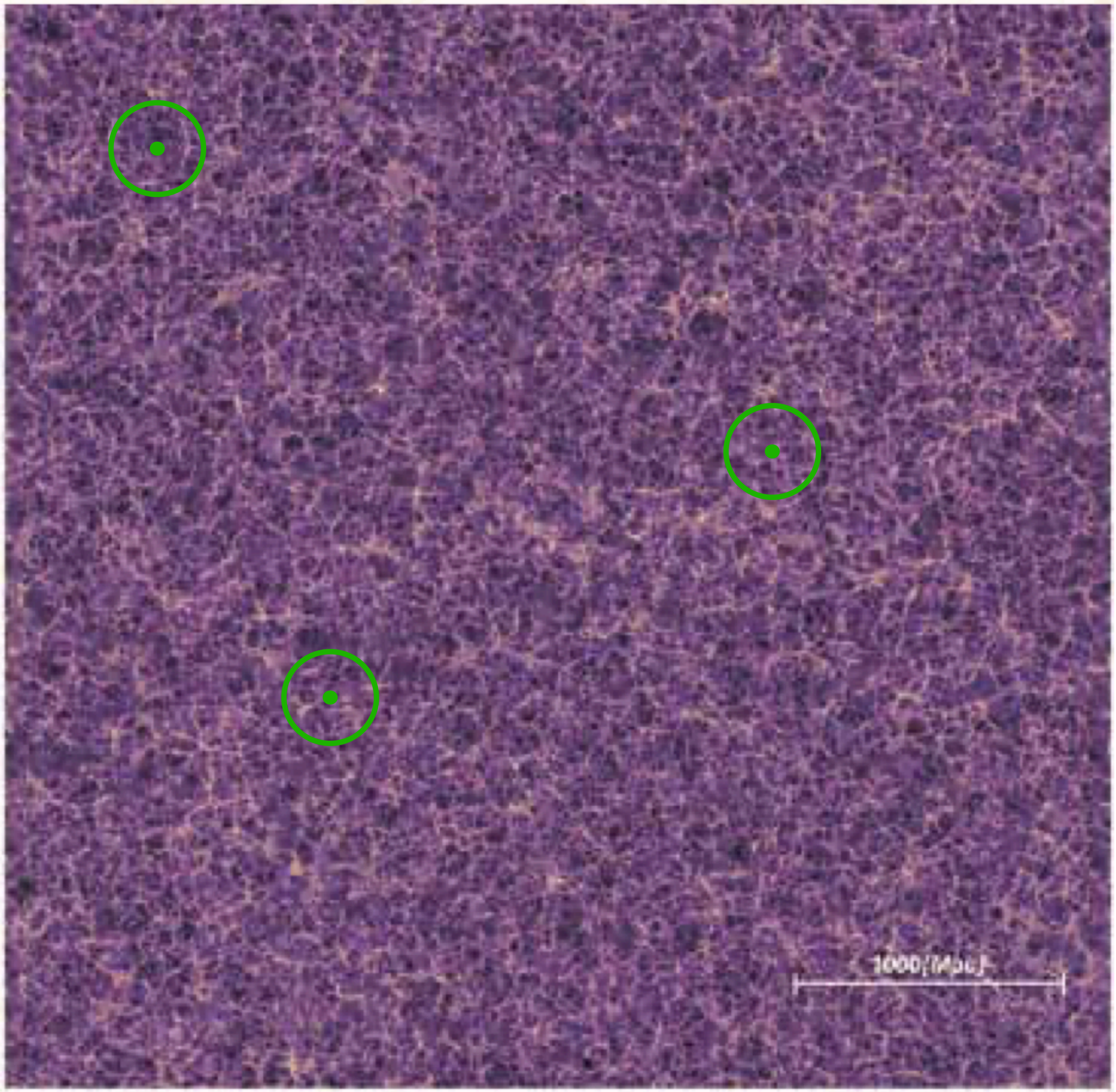

https://www.h-its.org/wp-content/uploads/2014/10/inSiDE_autumn2010_p20.pdf

The Millennium XXL (MXXL) simulation (SMoC)

Angulo et al. 2012

Test how often does a KBC void occur ?

Haslbauer, Banik & Kroupa 2020

KBC void and Hubble Tension

The Cosmological Scale

The KBC Void + Hubble Tension

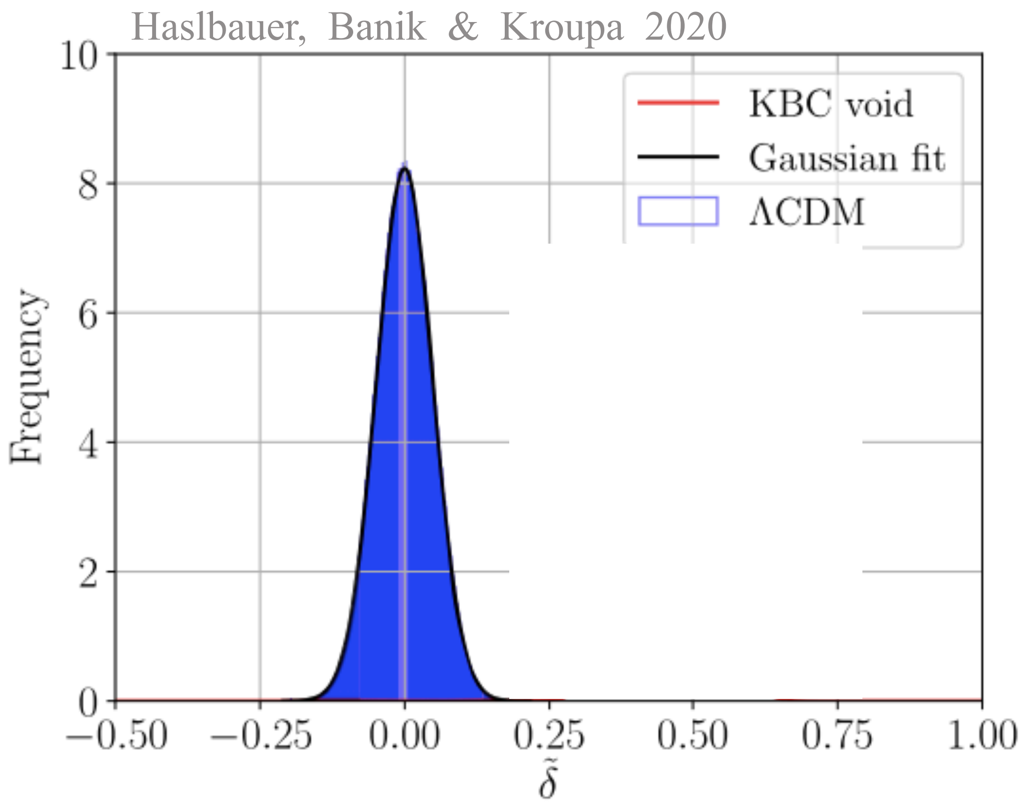

Figure 1. Distribution of the apparent relative density contrast $\tilde{\delta}$ (equation 22) of spheres with a 300 Mpc radius less an inner 40 Mpc hole in the ΛCDM MXXL simulation, calculated at redshift $z = 0$ (Section 2.1). The red solid curve shows the observed density contrast of $\delta_{\rm obs} = 0.46 \pm 0.06$ with Gaussian errors (see also fig. 11 and table 1 in Keenan et al. 2013). The $\tilde{\delta}$ values closely follow a Gaussian distribution with a dispersion of $\sigma_{\Lambda\rm CDM} = 0.048$ (the black curve). A more detailed Gaussianity test is performed in Appendix A. Both curves are normalized to the same area.

KBC void and Hubble Tension

The Cosmological Scale

The KBC Void + Hubble Tension

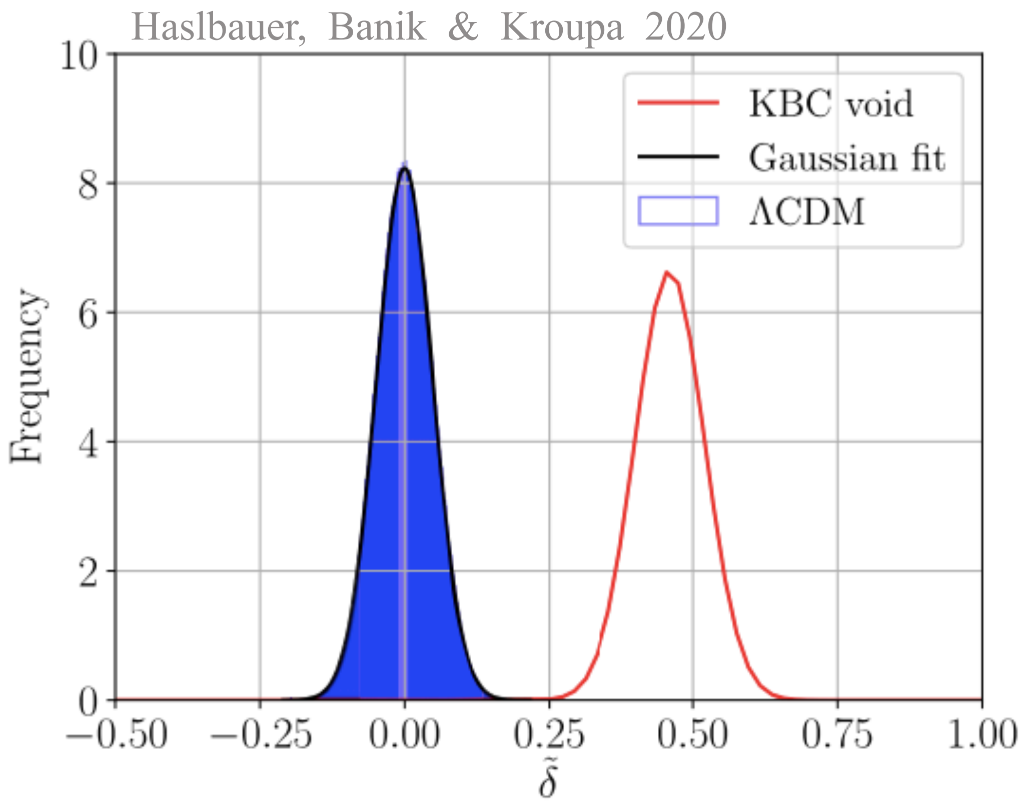

Figure 1. Distribution of the apparent relative density contrast $\tilde{\delta}$ (equation 22) of spheres with a 300 Mpc radius less an inner 40 Mpc hole in the ΛCDM MXXL simulation, calculated at redshift $z = 0$ (Section 2.1). The red solid curve shows the observed density contrast of $\delta_{\mathrm{obs}} = 0.46 \pm 0.06$ with Gaussian errors (see also fig. 11 and table 1 in Keenan et al. 2013). The $\tilde{\delta}$ values closely follow a Gaussian distribution with a dispersion of $\sigma_{\Lambda\mathrm{CDM}} = 0.048$ (the black curve). A more detailed Gaussianity test is performed in Appendix A. Both curves are normalized to the same area.

KBC void and Hubble Tension

The Cosmological Scale

The KBC Void + Hubble Tension

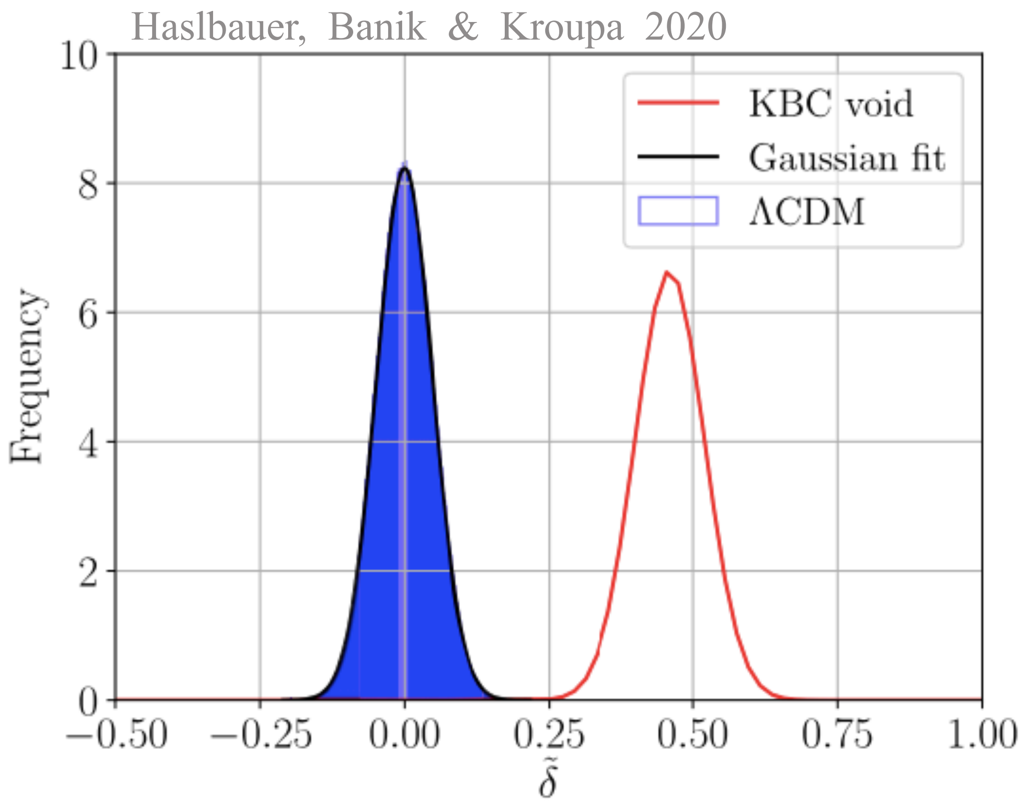

Figure 1. Distribution of the apparent relative density contrast $\tilde{\delta}$ (equation 22) of spheres with a 300 Mpc radius less an inner 40 Mpc hole in the ΛCDM MXXL simulation, calculated at redshift $z = 0$ (Section 2.1). The red solid curve shows the observed density contrast of $\delta_{obs} = 0.46 \pm 0.06$ with Gaussian errors (see also fig. 11 and table 1 in Keenan et al. 2013). The $\tilde{\delta}$ values closely follow a Gaussian distribution with a dispersion of $\sigma_{\Lambda CDM} = 0.048$ (the black curve). A more detailed Gaussianity test is performed in Appendix A. Both curves are normalized to the same area.

Difference of >6 sigma

KBC void and Hubble Tension

The Cosmological Scale

Haslbauer, Banik & Kroupa 2020

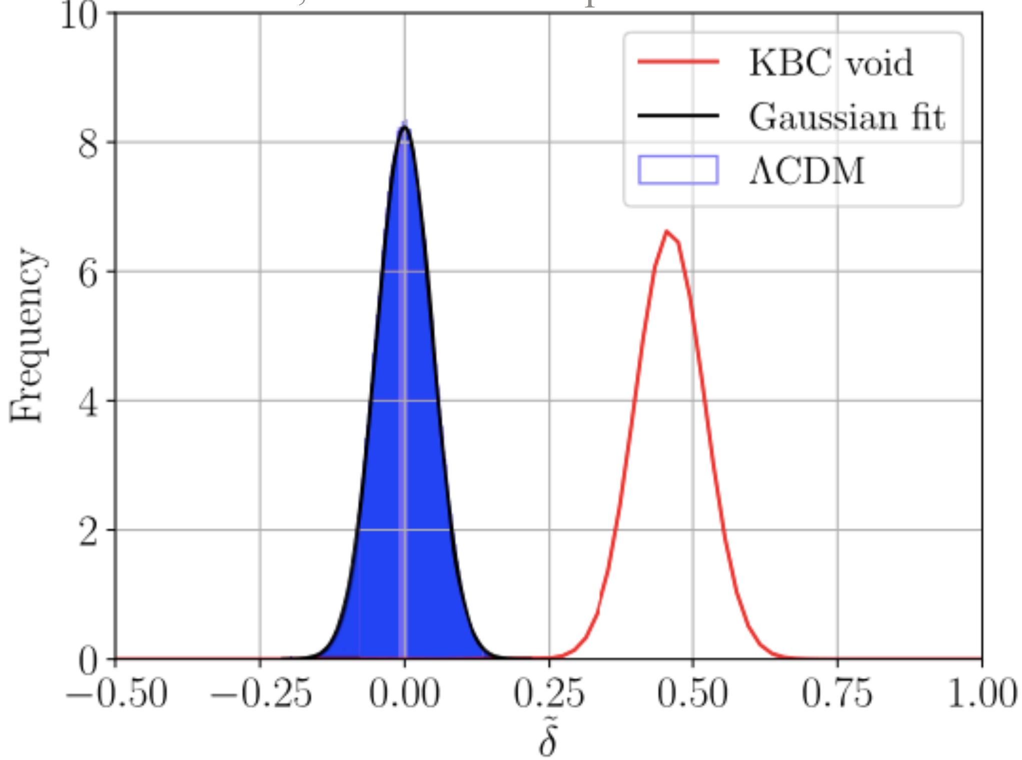

Figure 1. Distribution of the apparent relative density contrast $\tilde{\delta}$ (equation 22) of spheres with a 300 Mpc radius less an inner 40 Mpc hole in the ΛCDM MXXL simulation, calculated at redshift $z = 0$ (Section 2.1). The red solid curve shows the observed density contrast of $\delta_{obs} = 0.46 \pm 0.06$ with Gaussian errors (see also fig. 11 and table 1 in Keenan et al. 2013). The $\tilde{\delta}$ values closely follow a Gaussian distribution with a dispersion of $\sigma_{\Lambda CDM} = 0.048$ (the black curve). A more detailed Gaussianity test is performed in Appendix A. Both curves are normalized to the same area.

The KBC Void + Hubble Tension

Difference of >6 sigma

Not SMoC at $> 6\,\sigma$ confidence .

KBC void and Hubble Tension

The Cosmological Scale

Haslbauer, Banik & Kroupa 2020 ; Mazurenko, Banik et al. 2023

KBC void and Hubble Tension

The Cosmological Scale

Haslbauer, Banik & Kroupa 2020 ;
Mazurenko, Banik et al. 2023

observed KBC void

diameter: ≈1 Gpc

density contrast: ≈50%

KBC void and Hubble Tension

The Cosmological Scale

Haslbauer, Banik & Kroupa 2020 ; Mazurenko, Banik et al. 2023

observed KBC void

diameter: ≈1 Gpc

density contrast: ≈50%

there exists no Hubble Tension !!!

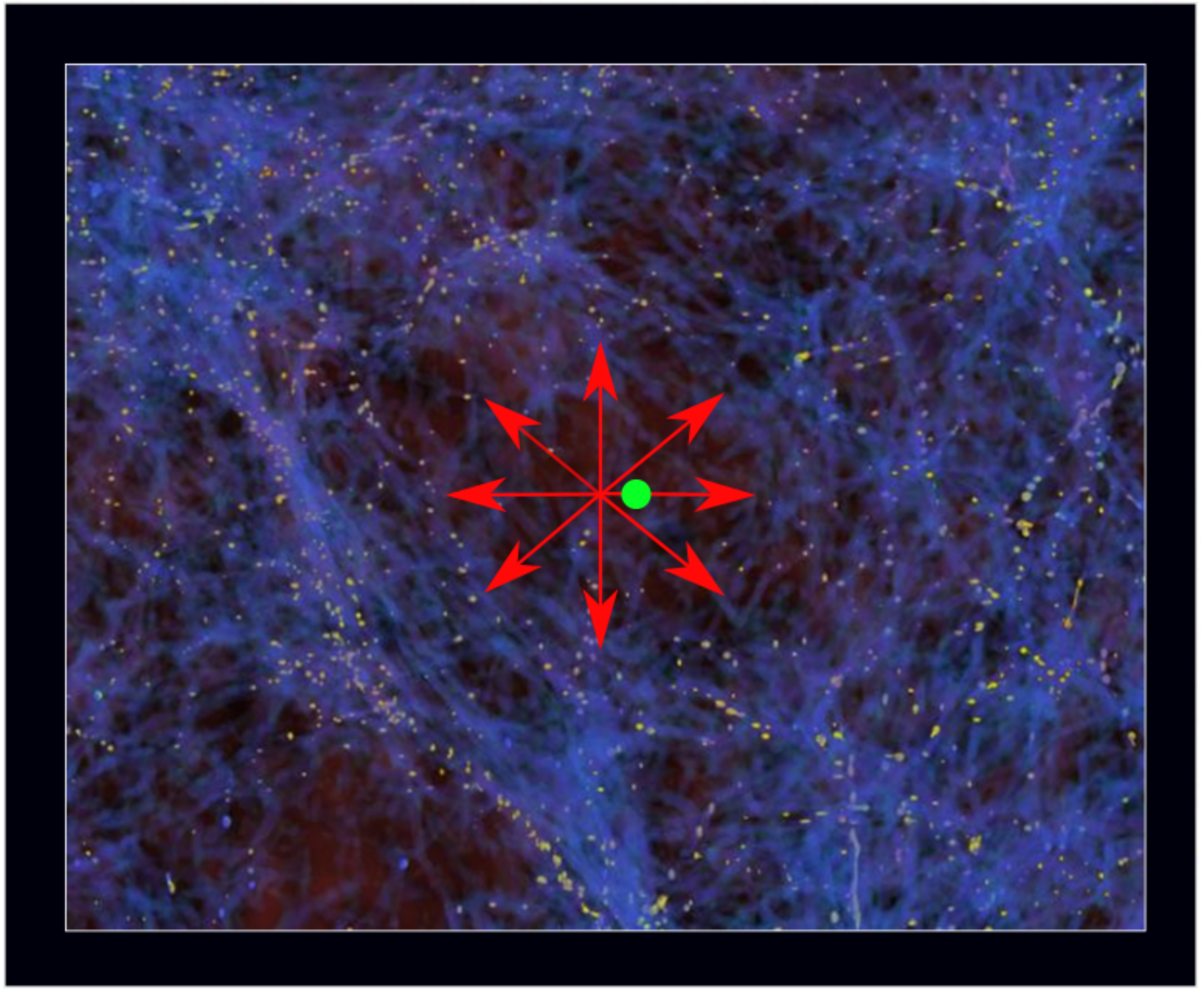

KBC void and Hubble Tension

The Cosmological Scale

Haslbauer, Banik & Kroupa 2020 ; Mazurenko, Banik et al. 2023

observed KBC void

diameter: ≈1 Gpc

density contrast: ≈50%

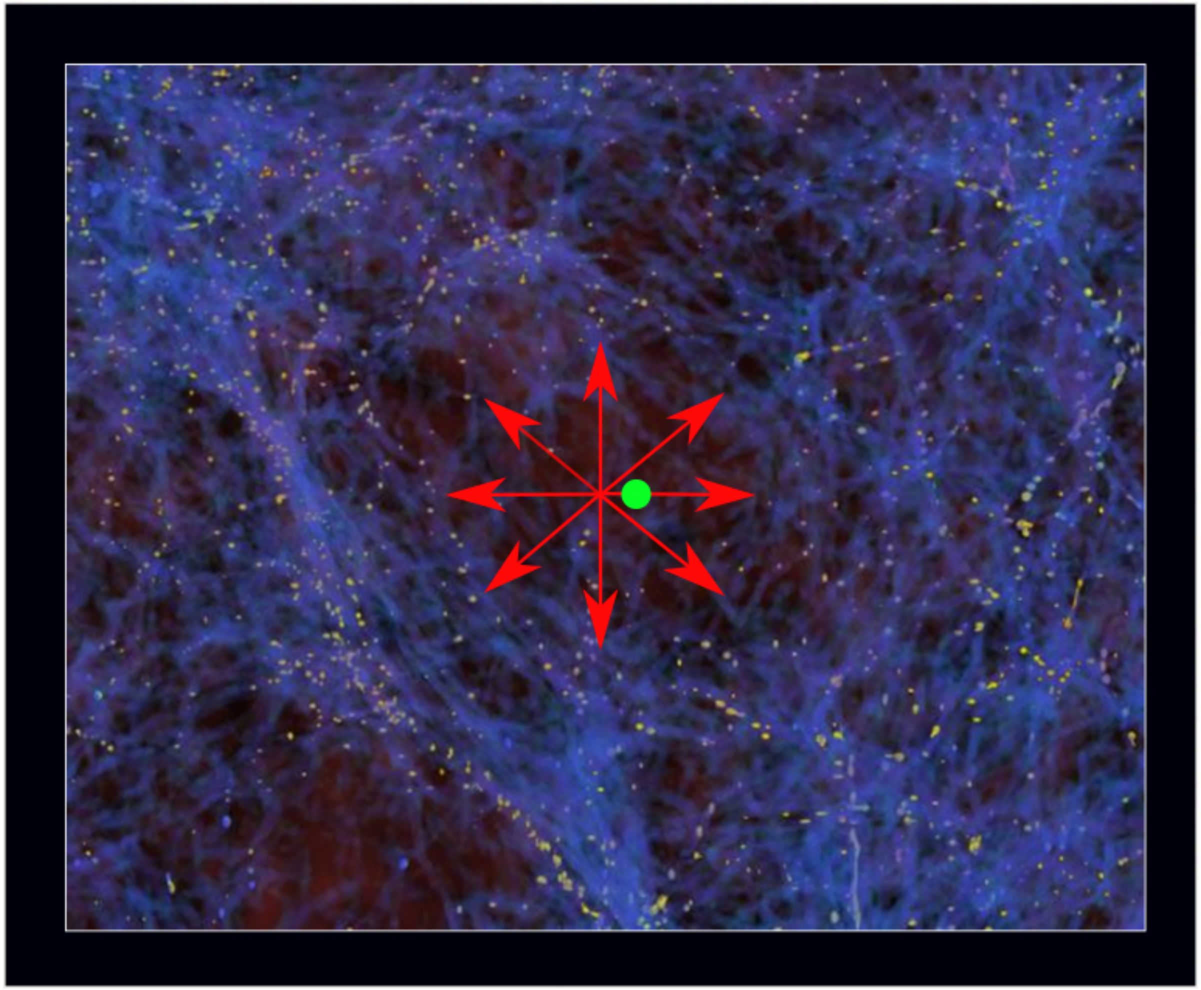

there exists no Hubble Tension !!!

The KBC void automatically solves the **Hubble Tension**,

but KBC void not possible in LCDM

KBC void and Hubble Tension

The Cosmological Scale

Haslbauer, Banik & Kroupa 2020 ; Mazurenko, Banik et al. 2023

observed KBC void

diameter: ≈1 Gpc

density contrast: ≈50%

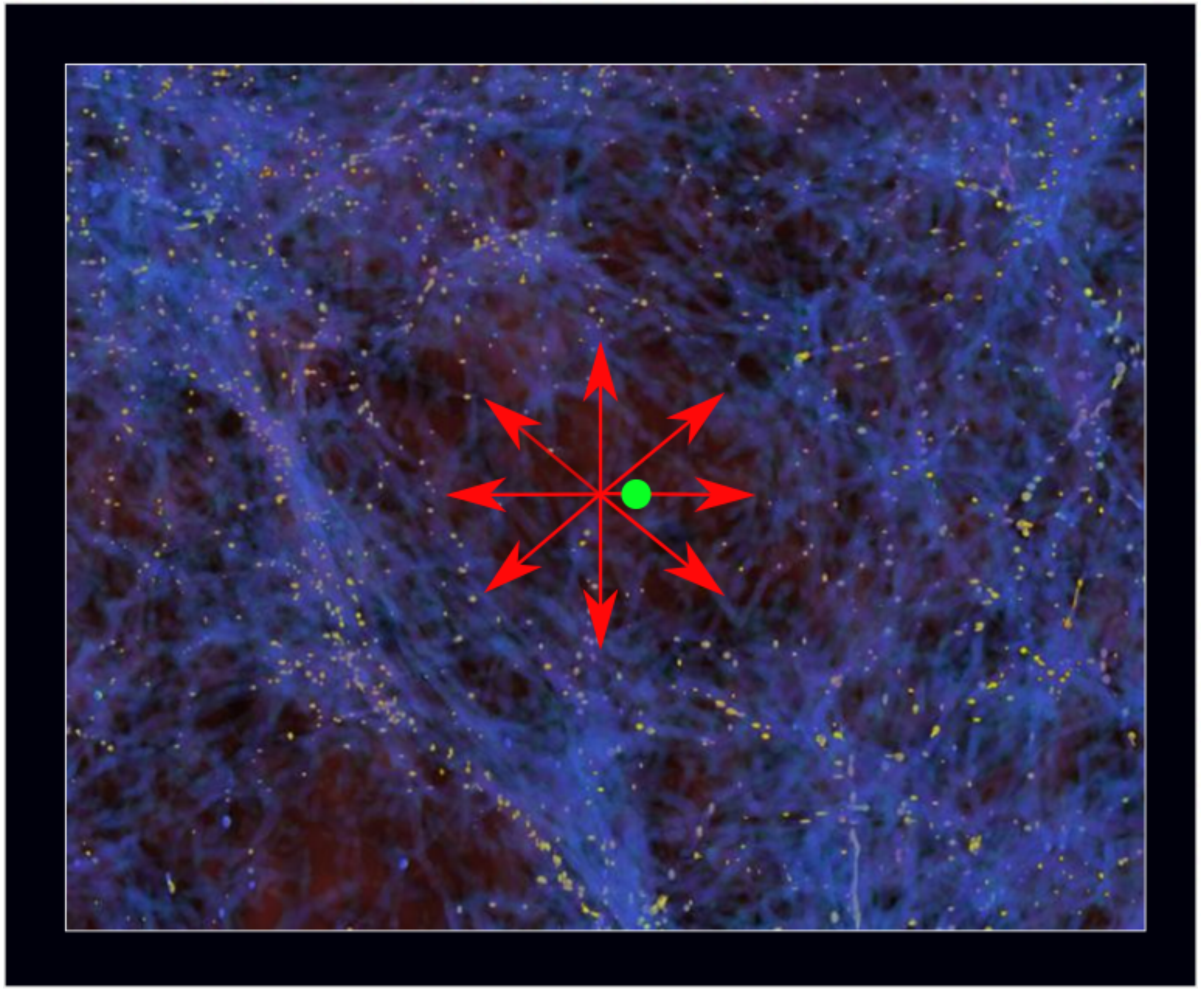

there exists no Hubble Tension !!!

The KBC void automatically solves the **Hubble Tension**,

but KBC void not possible in LCDM

Bulk flows of galaxies correctly predicted in this model

Mazurenko, Banik et al. 2023

KBC void and Hubble Tension

The Cosmological Scale

Haslbauer, Banik & Kroupa 2020 ; Mazurenko, Banik et al. 2023

Mazurenko, Banik et al. 2023

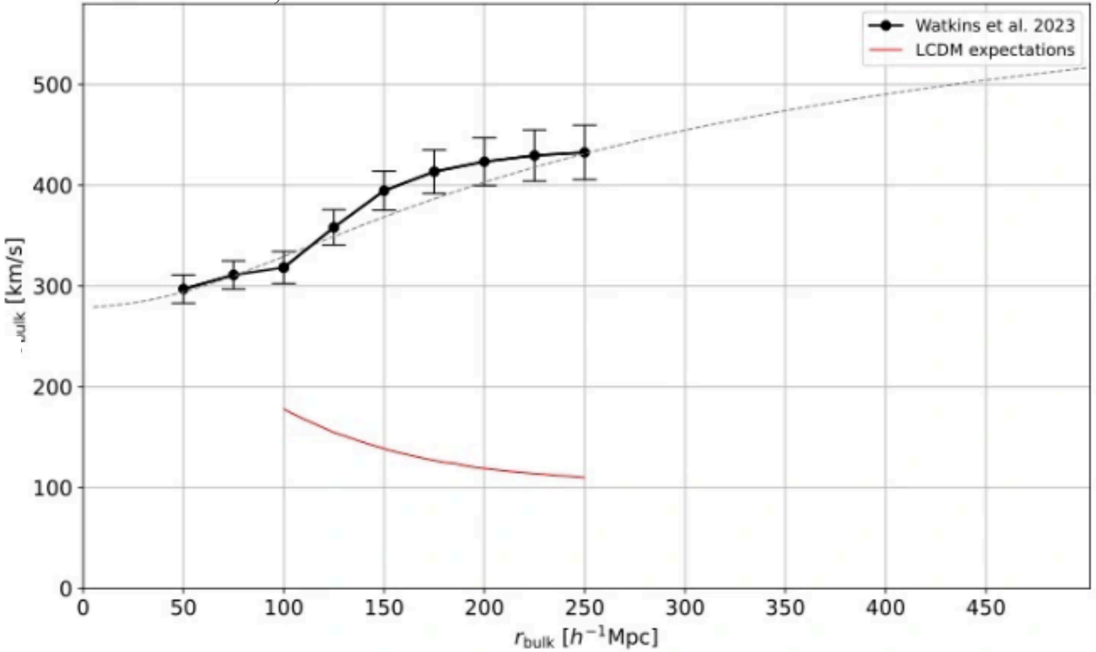

3: The bulk flow of galaxies (the average speed of many galaxies, y-axis) is plotted versus the e from the observer on the x-axis. The data from Watkins et al. (2023) are shown as solid black ıe MOND-based cosmological model is shown as the dotted line assuming the local void has a ın density profile, that the Local Group is located 116 Mpc (about 380 million light years) away from the void centre and that the Local Group is moving with 627 km/s relative to the CMB and about 200 km/s slower than the local bulk flow (within some 150 million light years). In other words, the Local Group's velocity relative to the CMB has been reduced to 627 km/s by small-scale flows in the local region. Thus, the MOND-cosmology-based bulk flow (dotted black line) is in (stunning) agreement with the data in terms of its amplitude and shape, while the LCDM model predicts bulk velocities (solid red line) that are in major disagreement with the observations. Adapted from Mazurenko et al. (2023).

From The Dark Matter Crisis #86

there exists no Hubble Tension !!!

The KBC void automatically solves the **Hubble Tension**,

but KBC void not possible in LCDM

Bulk flows of galaxies correctly predicted in this model

Mazurenko, Banik et al. 2023

KBC void and Hubble Tension

The Cosmological Scale

Haslbauer, Banik & Kroupa 2020 ; Mazurenko, Banik et al. 2023

Mazurenko, Banik et al. 2023

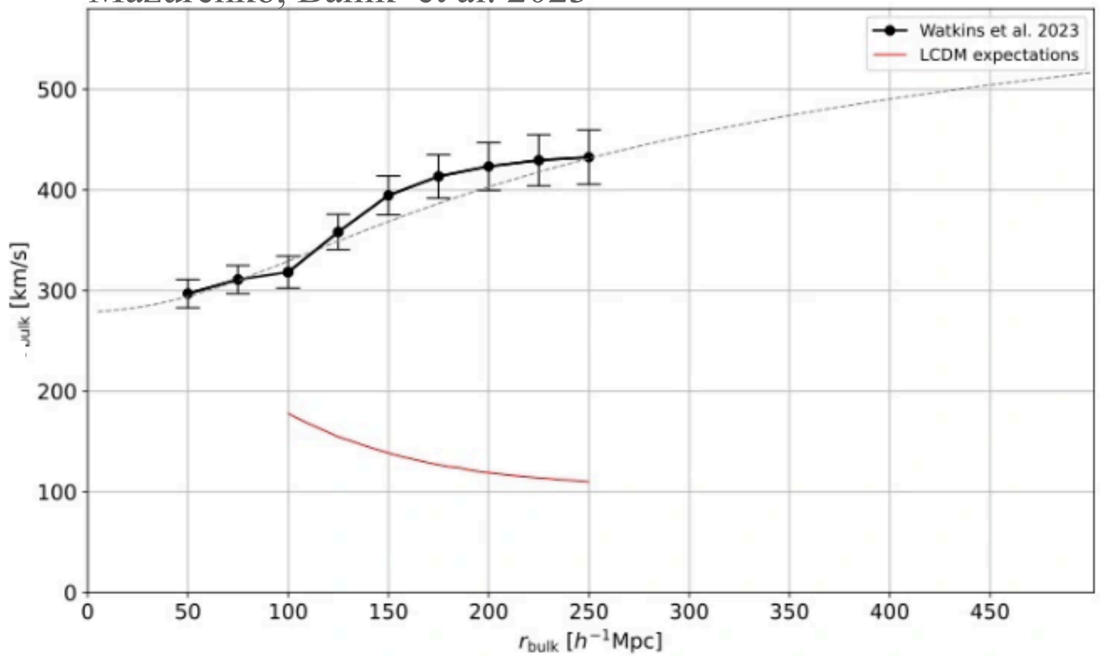

3: The bulk flow of galaxies (the average speed of many galaxies, y-axis) is plotted versus the
e from the observer on the x-axis. The data from Watkins et al. (2023) are shown as solid black
ne MOND-based cosmological model is shown as the dotted line assuming the local void has a
an density profile, that the Local Group is located 116 Mpc (about 380 million light years) away from the void centre and that the Local Group is moving with 627 km/s relative to the CMB and about 200 km/s slower than the local bulk flow (within some 150 million light years). In other words, the Local Group's velocity relative to the CMB has been reduced to 627 km/s by small-scale flows in the local region. Thus, the MOND-cosmology-based bulk flow (dotted black line) is in (stunning) agreement with the data in terms of its amplitude and shape, while the LCDM model predicts bulk velocities (solid red line) that are in major disagreement with the observations. Adapted from Mazurenko et al. (2023).

From The Dark Matter Crisis #86

there exists no Hubble Tension !!!

The KBC void automatically solves the **Hubble Tension**,

but KBC void not possible in LCDM

Bulk flows of galaxies correctly predicted in this model

Mazurenko, Banik et al. 2023

----> talk by Indranil Banik on Wed.

The distribution of
matter on scales
of
many Gpc

Assume the ≈ 500 galaxies in our 11Mpc neighbourhood are representative of all galaxies in the Universe.

(*cf*: the stars in the Solar neighbourhood are representative of all stars in the Milky Way and in the Universe)

Assume the ≈ 500 galaxies in our 11Mpc neighbourhood are representative of all galaxies in the Universe.

(*cf*: the stars in the Solar neighbourhood are representative of all stars in the Milky Way and in the Universe)

The 11 Mpc galaxies have nearly constant star formation histories.

(*i.e.* present-day SFR $\approx$ average SFR)

Assume the ≈ 500 galaxies in our 11Mpc neighbourhood
are representative of all galaxies in the Universe.
(*cf*: the stars in the Solar neighbourhood are representative of all stars in the Milky Way and in the Universe)

The 11 Mpc galaxies have nearly constant star formation histories.
(*i.e.* present-day SFR $\approx$ average SFR)

The maximum in the observed cosmic star-formation rate density
near $z \approx 1.8$
thus implies a massive matter-overdensity about 5 Gpc away

Assume the ≈ 500 galaxies in our 11Mpc neighbourhood are representative of all galaxies in the Universe.

(*cf*: the stars in the Solar neighbourhood are representative of all stars in the Milky Way and in the Universe)

The 11 Mpc galaxies have nearly constant star formation histories.

(*i.e.* present-day SFR $\approx$ average SFR)

The maximum in the observed cosmic star-formation rate density near $z \approx 1.8$ thus implies a massive matter-overdensity about 5 Gpc away

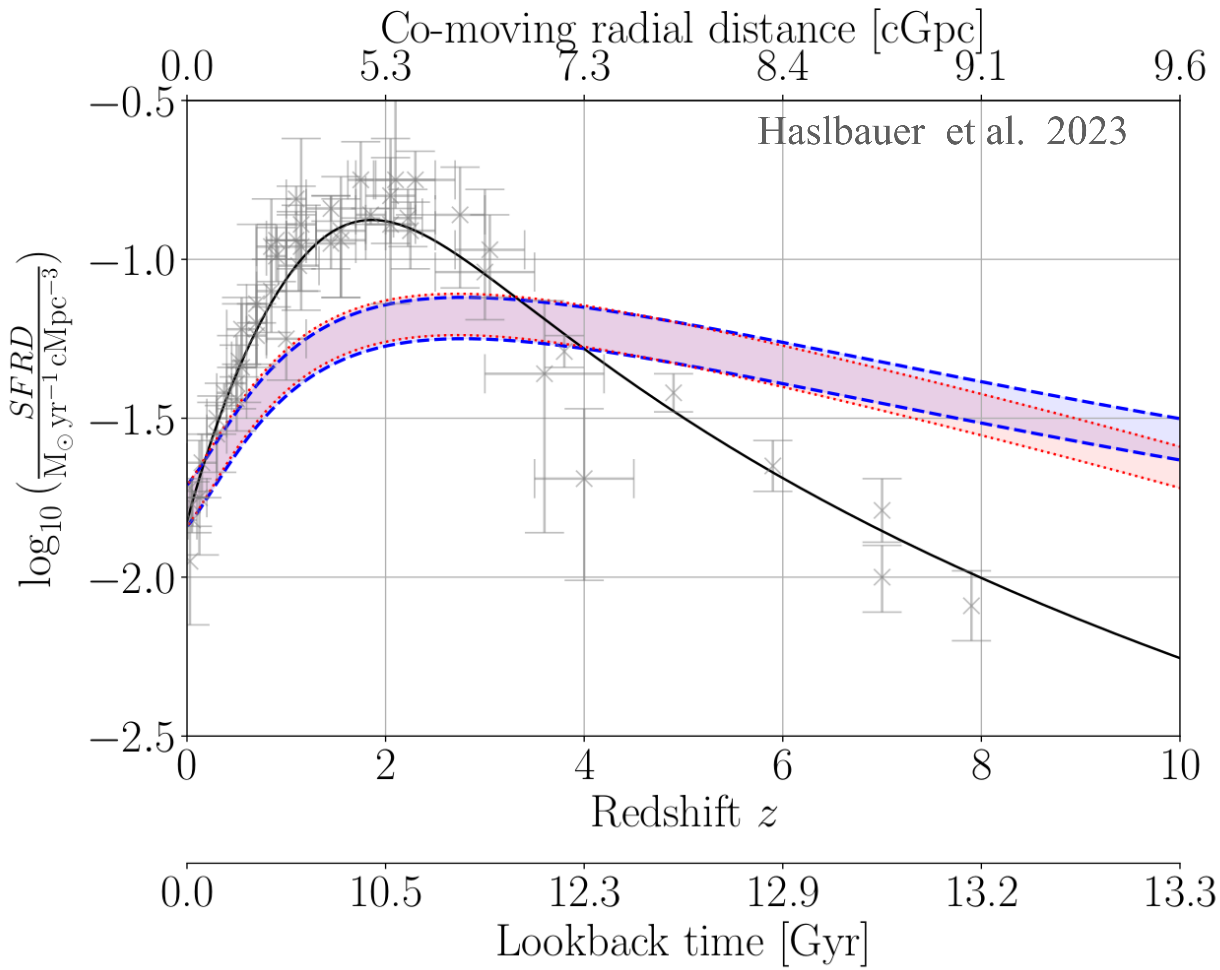

Assume the ≈ 500 galaxies in our 11Mpc neighbourhood are representative of all galaxies in the Universe.

(*cf*: the stars in the Solar neighbourhood are representative of all stars in the Milky Way and in the Universe)

The 11 Mpc galaxies have nearly constant star formation histories.

(*i.e.* present-day SFR $\approx$ average SFR)

The maximum in the observed cosmic star-formation rate density near $z \approx 1.8$ thus implies a massive matter-overdensity about 5 Gpc away

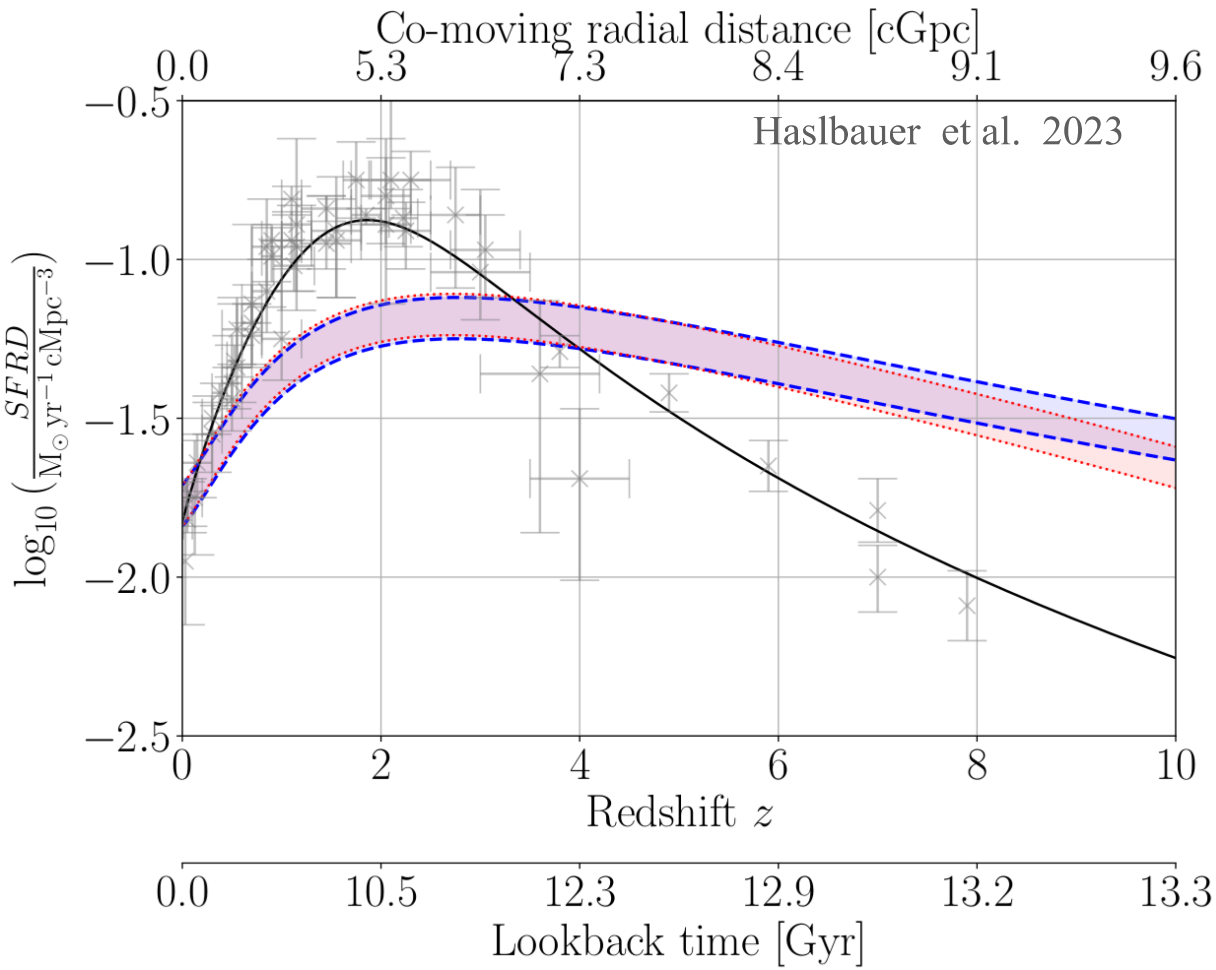

A 5 Gpc-scale inhomogeneity suggests that the Universe is structured on all scales.

Assume the ≈ 500 galaxies in our 11Mpc neighbourhood are representative of all galaxies in the Universe.

(*cf*: the stars in the Solar neighbourhood are representative of all stars in the Milky Way and in the Universe)

The 11 Mpc galaxies have nearly constant star formation histories.

(*i.e.* present-day SFR $\approx$ average SFR)

The maximum in the observed cosmic star-formation rate density near $z \approx 1.8$ thus implies a massive matter-overdensity about 5 Gpc away

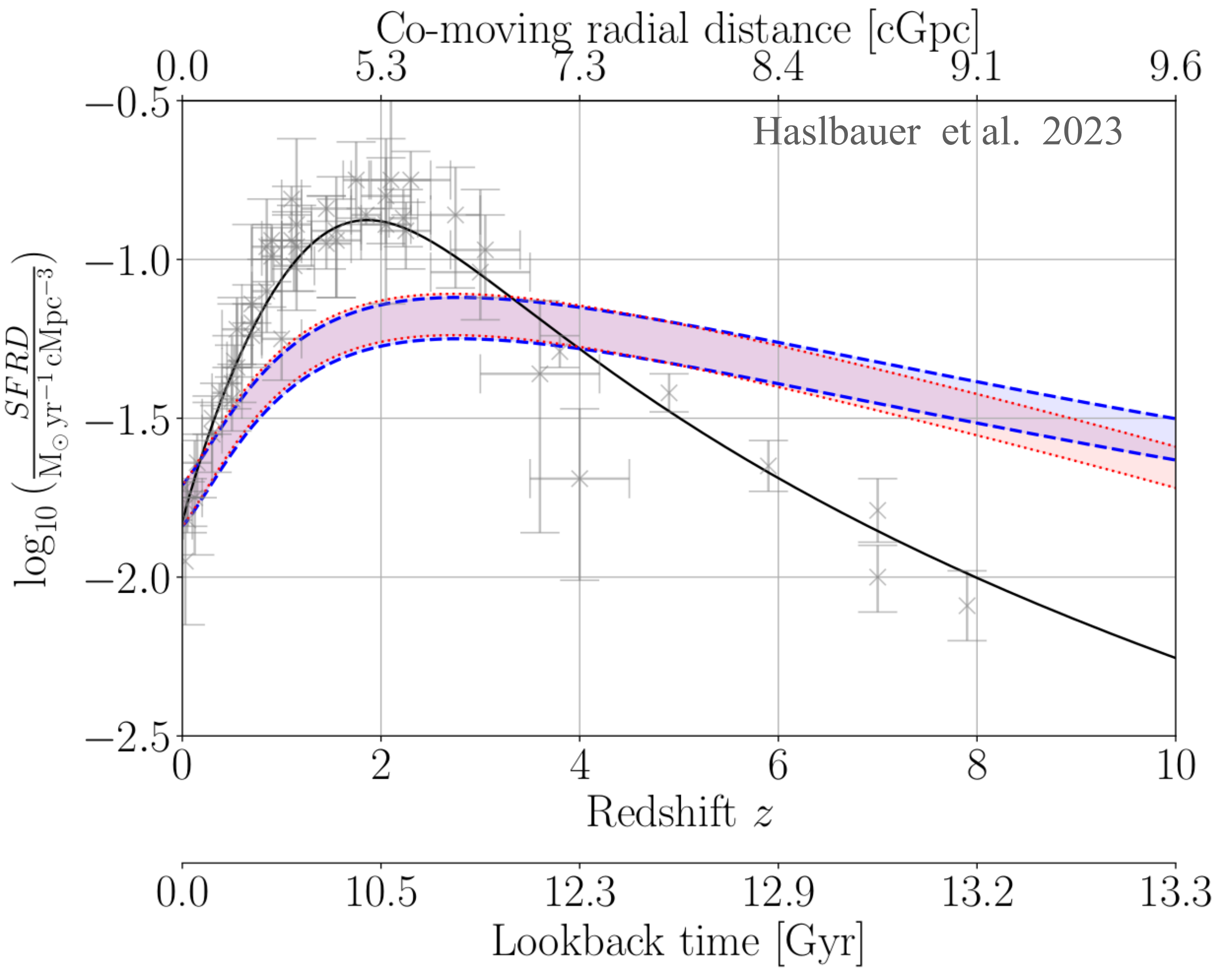

A 5 Gpc-scale inhomogeneity suggests that the Universe is structured on all scales.

Not SMoC at $\infty\sigma$ confidence .

Additional

The real Universe
is thus highly orderly structured on Mpc scales
and highly inhomogeneous on all larger scales,
up the the horizon
(CMB hemispherical anisotropy)

Schwarz et al. 2016

The real Universe
is thus highly orderly structured on Mpc scales
and highly inhomogeneous on all larger scales,
up the the horizon
(CMB hemispherical anisotropy)
Schwarz et al. 2016

Additional constraints (and stress for the LC/WDM models) :

- Ages of the oldest stars = 14.05 +- 0.25 (Cimatti & Moresco 2023)
  (add 200 Myr for time before star formation);

The real Universe
is thus highly orderly structured on Mpc scales
and highly inhomogeneous on all larger scales,
up the the horizon
(CMB hemispherical anisotropy)
Schwarz et al. 2016

Additional constraints (and stress for the LC/WDM models) :

- Ages of the oldest stars = 14.05 +- 0.25 (Cimatti & Moresco 2023)
  (add 200 Myr for time before star formation);

- z>10 galaxies too massive for LC/WDM (Haslbauer, Kr+2022);

The real Universe
is thus highly orderly structured on Mpc scales
and highly inhomogeneous on all larger scales,
up the the horizon
(CMB hemispherical anisotropy)
Schwarz et al. 2016

Additional constraints (and stress for the LC/WDM models) :

- Ages of the oldest stars = 14.05 +- 0.25 (Cimatti & Moresco 2023)
  (add 200 Myr for time before star formation);
- z>10 galaxies too massive for LC/WDM (Haslbauer, Kr+2022);
- e.g. z=14 galaxies with masses $\log_{10}(M_*/M_{sun}) = 10^8$ and $10^{8.7}$
  (Carniani+2024).

The real Universe
is thus highly orderly structured on Mpc scales
and highly inhomogeneous on all larger scales,
up the the horizon
(CMB hemispherical anisotropy)
Schwarz et al. 2016

Additional constraints (and stress for the LC/WDM models) :

- Ages of the oldest stars = 14.05 +- 0.25 (Cimatti & Moresco 2023)
  (add 200 Myr for time before star formation);
- z>10 galaxies too massive for LC/WDM (Haslbauer, Kr+2022);
- e.g. z=14 galaxies with masses $\log_{10}(M_*/M_{sun}) = 10^8$ and $10^{8.7}$
  (Carniani+2024).
  Caveat : most authors use *incorrect stellar IMF* to
  infer the stellar mass given the received flux.

The real Universe
is thus highly orderly structured on Mpc scales
and highly inhomogeneous on all larger scales,
up the the horizon
(CMB hemispherical anisotropy)
Schwarz et al. 2016

Additional constraints (and stress for the LC/WDM models) :

- Ages of the oldest stars = 14.05 +- 0.25 (Cimatti & Moresco 2023)
  (add 200 Myr for time before star formation);

- z>10 galaxies too massive for LC/WDM (Haslbauer, Kr+2022);

- e.g. z=14 galaxies with masses $\log_{10}(M_*/M_{sun}) = 10^8$ and $10^{8.7}$
  (Carniani+2024).

  Caveat : most authors use *incorrect stellar IMF* to infer the stellar mass given the received flux.

Major research programme
in Bonn, Garching, Nanjing
to understand the
variation of the
stellar IMF
--- the IGIMF theory --

The real Universe
is thus highly orderly structured on Mpc scales
and highly inhomogeneous on all larger scales,
up the the horizon
(CMB hemispherical anisotropy)
Schwarz et al. 2016

Additional constraints (and stress for the LC/WDM models) :

- Ages of the oldest stars = 14.05 +- 0.25 (Cimatti & Moresco 2023)
  (add 200 Myr for time before star formation);

- z>10 galaxies too massive for LC/WDM (Haslbauer, Kr+2022);

- e.g. z=14 galaxies with masses $\log_{10}(M_*/M_{sun}) = 10^8$ and $10^{8.7}$
  (Carniani+2024).
  Caveat : most authors use *incorrect stellar IMF* to infer the stellar mass given the received flux.

Major research programme
in Bonn, Garching, Nanjing
to understand the
variation of the
stellar IMF
--- the IGIMF theory --

- e.g. elliptical galaxies formed extremely early and rapidly
  (Yan, Jerabkova+2021 ; Eappen & Kr 2022).

Overview of SMoC constraints

Many tests made. All independent. Kroupa, Gjergo et al. 2023

E.g. : (there are more tests)

Many tests made. All independent. Kroupa, Gjergo et al. 2023

E.g. : (there are more tests)

I) Mutually independent tests for the existence of dark matter particles :

- The orbits of the Large and Small Magellanic Clouds Oehm+Kr 2024
- The lengths of galactic bars Roshan+ 2021
- The backsplash NGC3109 group of galaxies (at distance of a Mpc) Pawlowski&McGaugh 2018; Banik+2021
- The M81 group of galaxies (at distance of 3.6 Mpc) Oehm+ 2017
- No dark matter in dwarf galaxies in Fornax galaxy cluster Asencio+ 2022

Many tests made. All independent. Kroupa, Gjergo et al. 2023

E.g. : (there are more tests)

I) Mutually independent tests for the existence of dark matter particles :

- The orbits of the Large and Small Magellanic Clouds Oehm+Kr 2024
- The lengths of galactic bars Roshan+ 2021
- The backsplash NGC3109 group of galaxies (at distance of a Mpc) Pawlowski&McGaugh 2018; Banik+2021
- The M81 group of galaxies (at distance of 3.6 Mpc) Oehm+ 2017
- No dark matter in dwarf galaxies in Fornax galaxy cluster Asencio+ 2022

Based mostly on Chandrasekhar dynamical friction and dynamical dissipation

Many tests made. All independent. Kroupa, Gjergo et al. 2023

E.g. : (there are more tests)

I) Mutually independent tests for the existence of dark matter particles :

- The orbits of the Large and Small Magellanic Clouds Oehm+Kr 2024
- The lengths of galactic bars Roshan+ 2021
- The backsplash NGC3109 group of galaxies (at distance of a Mpc) Pawlowski&McGaugh 2018; Banik+2021
- The M81 group of galaxies (at distance of 3.6 Mpc) Oehm+ 2017
- No dark matter in dwarf galaxies in Fornax galaxy cluster Asencio+ 2022

Based mostly on Chandrasekhar dynamical friction and dynamical dissipation

II) Tests for validity of Newtonian gravitation : Kroupa+ 2022; Kroupa+2024

Many tests made. All independent. Kroupa, Gjergo et al. 2023

E.g. : (there are more tests)

I) Mutually independent tests for the existence of dark matter particles :

- The orbits of the Large and Small Magellanic Clouds Oehm+Kr 2024
- The lengths of galactic bars Roshan+ 2021
- The backsplash NGC3109 group of galaxies (at distance of a Mpc) Pawlowski&McGaugh 2018; Banik+2021
- The M81 group of galaxies (at distance of 3.6 Mpc) Oehm+ 2017
- No dark matter in dwarf galaxies in Fornax galaxy cluster Asencio+ 2022

Based mostly on Chandrasekhar dynamical friction and dynamical dissipation

II) Tests for validity of Newtonian gravitation : Kroupa+ 2022; Kroupa+2024

III) Tests for the matter-distribution predicted by the dark matter models :

- Disks of Satellites around 6 nearby galaxies Kroupa+ 2005; Pawlowski+; Asencio+ 2022
- The 3d structure of the Local Group of galaxies (within one Mpc) Pawlowski+ 2013
- The KBC void (within one Gpc) Haslbauer+ 2020
- The Hubble Tension (within one Gpc) Haslbauer+ 2020
- The Lilly-Madau plot (5 Gpc scale) Haslbauer+ 2023
- The over-massive El Gordo galaxy cluster (8 Gyr away) Asencio+ 2021
- Bulk flows on cosmological scales Migkas+ 2021; Secrest +2022
- CMB anomalies (hemispherical power and temp. difference, lack of correlation on large angular scales, cold spot). Schwarz+ 2016

Many tests made. All independent. Kroupa, Gjergo et al. 2023

E.g. : (there are more tests)

I) Mutually independent tests for the existence of dark matter particles :

- The orbits of the Large and Small Magellanic Clouds Oehm+Kr 2024
- The lengths of galactic bars Roshan+ 2021
- The backsplash NGC3109 group of galaxies (at distance of a Mpc) Pawlowski&McGaugh 2018; Banik+2021
- The M81 group of galaxies (at distance of 3.6 Mpc) Oehm+ 2017
- No dark matter in dwarf galaxies in Fornax galaxy cluster Asencio+ 2022

Based mostly on Chandrasekhar dynamical friction and dynamical dissipation

II) Tests for validity of Newtonian gravitation : Kroupa+ 2022; Kroupa+2024

III) Tests for the matter-distribution predicted by the dark matter models :

- Disks of Satellites around 6 nearby galaxies Kroupa+ 2005; Pawlowski+; Asencio+ 2022
- The 3d structure of the Local Group of galaxies (within one Mpc) Pawlowski+ 2013
- The KBC void (within one Gpc) Haslbauer+ 2020
- The Hubble Tension (within one Gpc) Haslbauer+ 2020
- The Lilly-Madau plot (5 Gpc scale) Haslbauer+ 2023
- The over-massive El Gordo galaxy cluster (8 Gyr away) Asencio+ 2021
- Bulk flows on cosmological scales Migkas+ 2021; Secrest +2022
- CMB anomalies (hemispherical power and temp. difference, lack of correlation on large angular scales, cold spot). Schwarz+ 2016

Based on the predicted stochastic merger histories and large-scale homogeneity of matter distribution

Many tests made. All independent. Kroupa, Gjergo et al. 2023

E.g. : (there are more tests)

I) Mutually independent tests for the existence of dark matter particles :

- The orbits of the Large and Small Magellanic Clouds Oehm+Kr 2024
- The lengths of galactic bars Roshan+ 2021
- The backsplash NGC3109 group of galaxies (at distance of a Mpc) Pawlowski&McGaugh 2018; Banik+2021
- The M81 group of galaxies (at distance of 3.6 Mpc) Oehm+ 2017
- No dark matter in dwarf galaxies in Fornax galaxy cluster Asencio+ 2022

Based mostly on Chandrasekhar dynamical friction and dynamical dissipation

II) Tests for validity of Newtonian gravitation : Kroupa+ 2022; Kroupa+2024

III) Tests for the matter-distribution predicted by the dark matter models :

- Disks of Satellites around 6 nearby galaxies Kroupa+ 2005; Pawlowski+; Asencio+ 2022
- The 3d structure of the Local Group of galaxies (within one Mpc) Pawlowski+ 2013
- The KBC void (within one Gpc) Haslbauer+ 2020
- The Hubble Tension (within one Gpc) Haslbauer+ 2020
- The Lilly-Madau plot (5 Gpc scale) Haslbauer+ 2023
- The over-massive El Gordo galaxy cluster (8 Gyr away) Asencio+ 2021
- Bulk flows on cosmological scales Migkas+ 2021; Secrest +2022
- CMB anomalies (hemispherical power and temp. difference, lack of correlation on large angular scales, cold spot). Schwarz+ 2016

Banik

Based on the predicted stochastic merger histories and large-scale homogeneity of matter distribution

Many tests made. All independent. Kroupa, Gjergo et al. 2023

E.g. : (there are more tests)

I) Mutually independent tests for the existence of dark matter particles :

- The orbits of the Large and Small Magellanic Clouds Oehm+Kr 2024
- The lengths of galactic bars Roshan+ 2021
- The backsplash NGC3109 group of galaxies (at distance of a Mpc) Pawlowski&McGaugh 2018; Banik+2021
- The M81 group of galaxies (at distance of 3.6 Mpc) Oehm+ 2017
- No dark matter in dwarf galaxies in Fornax galaxy cluster Asencio+ 2022

Based mostly on Chandrasekhar dynamical friction and dynamical dissipation

II) Tests for validity of Newtonian gravitation : Kroupa+ 2022; Kroupa+2024

III) Tests for the matter-distribution predicted by the dark matter models :

- Disks of Satellites around 6 nearby galaxies Kroupa+ 2005; Pawlowski+; Asencio+ 2022
- The 3d structure of the Local Group of galaxies (within one Mpc) Pawlowski+ 2013
- The KBC void (within one Gpc) Haslbauer+ 2020
- The Hubble Tension (within one Gpc) Haslbauer+ 2020
- The Lilly-Madau plot (5 Gpc scale) Haslbauer+ 2023
- The over-massive El Gordo galaxy cluster (8 Gyr away) Asencio+ 2021
- Bulk flows on cosmological scales Migkas+ 2021; Secrest +2022
- CMB anomalies (hemispherical power and temp. difference, lack of correlation on large angular scales, cold spot). Schwarz+ 2016

Banik

Based on the predicted stochastic merger histories and large-scale homogeneity of matter distribution

Kroupa, Gjergo et al. 2023

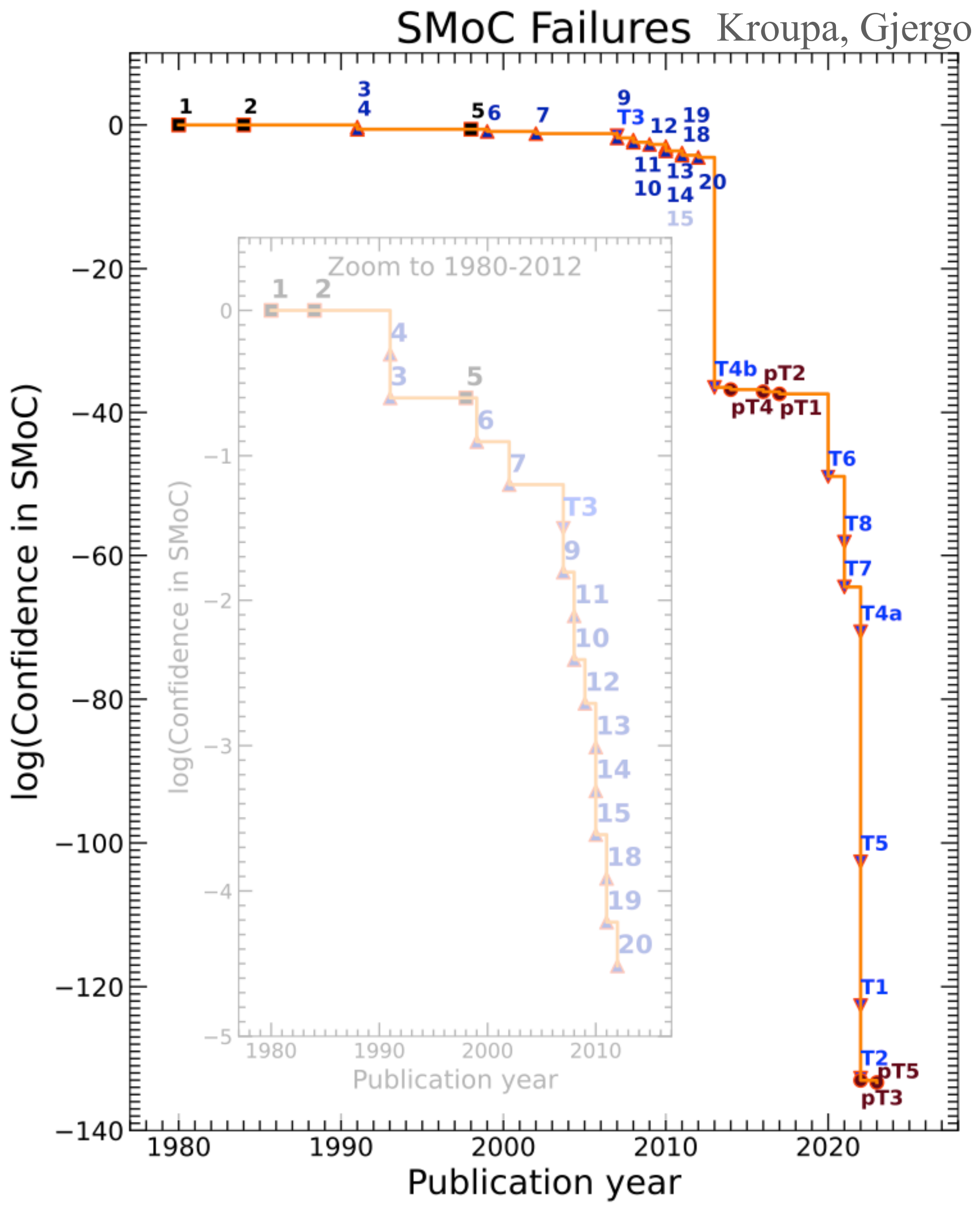

Figure 8: The SMoC-Confidence Graph: the cumulative loss in confidence that the Standard Model of Cosmology (SMoC) is a valid description of nature. The numbers 1-20 are based on a previous review (Kroupa, 2012, [6]), where an original form of the current plot appeared. Black squares (1, 2, and 5, representing inflation, dark matter, and dark energy, respectively) are treated in the SMoC as "new physics", so they are not assigned a loss of confidence. Upward blue triangles indicate failures, still current, already recognized in [6], while downward blue triangles (T1–T8) represent newly identified tensions where the loss of confidence was computed formally, as presented in Section 2.2. From the same section come the possible tensions (pT1–pT5), shown with red circles. Wherever the loss of confidence was not computed formally, we assign a drop in confidence by 50%. The inset graph zooms into the falsifications up to 2012.

Kroupa, Gjergo et al. 2023

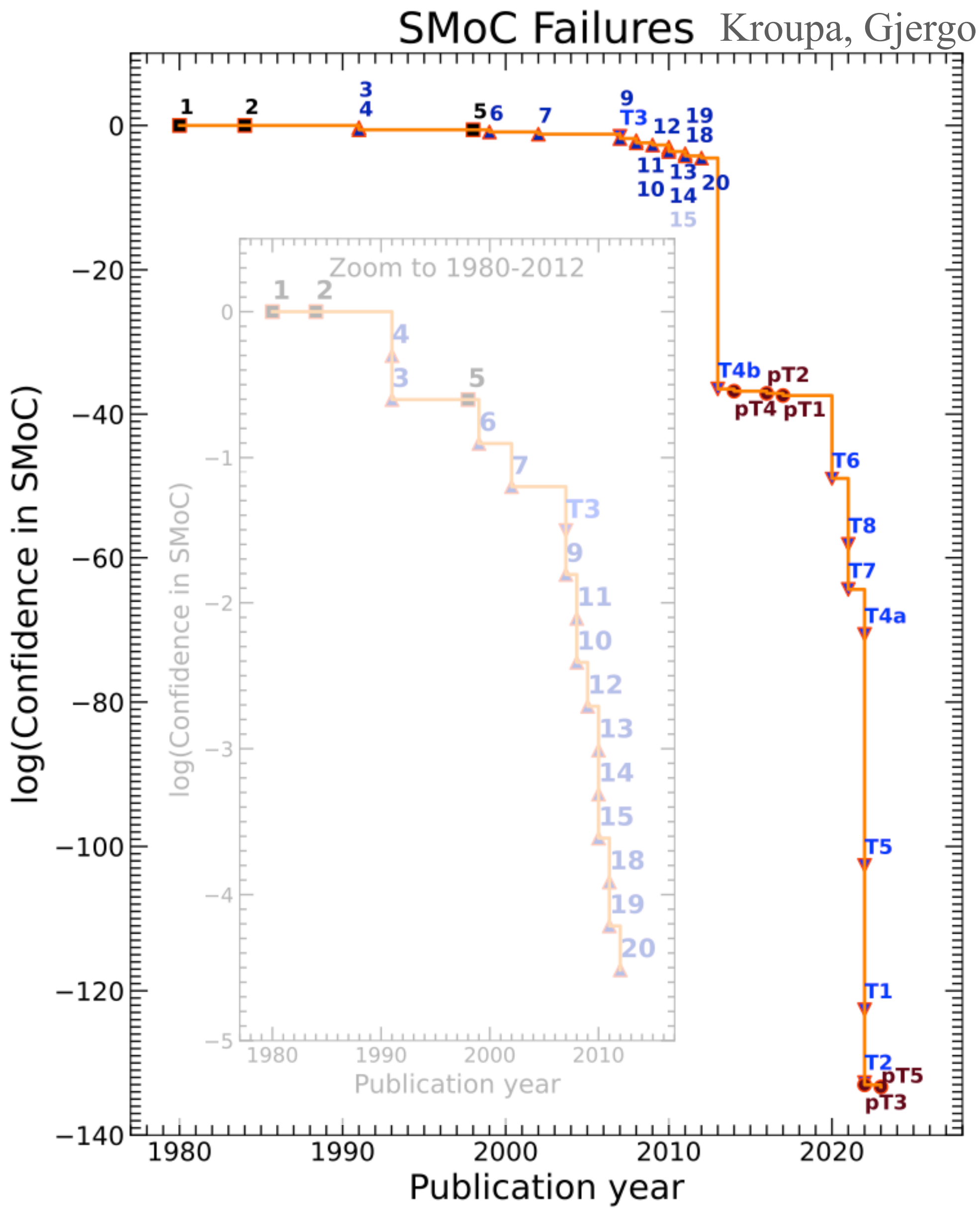

Figure 8: The SMoC-Confidence Graph: the cumulative loss in confidence that the Standard Model of Cosmology (SMoC) is a valid description of nature. The numbers 1-20 are based on a previous review (Kroupa, 2012, [6]), where an original form of the current plot appeared. Black squares (1, 2, and 5, representing inflation, dark matter, and dark energy, respectively) are treated in the SMoC as "new physics", so they are not assigned a loss of confidence. Upward blue triangles indicate failures, still current, already recognized in [6], while downward blue triangles (T1–T8) represent newly identified tensions where the loss of confidence was computed formally, as presented in Section 2.2. From the same section come the possible tensions (pT1–pT5), shown with red circles. Wherever the loss of confidence was not computed formally, we assign a drop in confidence by 50%. The inset graph zooms into the falsifications up to 2012.

The LC/WDM model is valid with a **confidence of $<10^{-140}$**

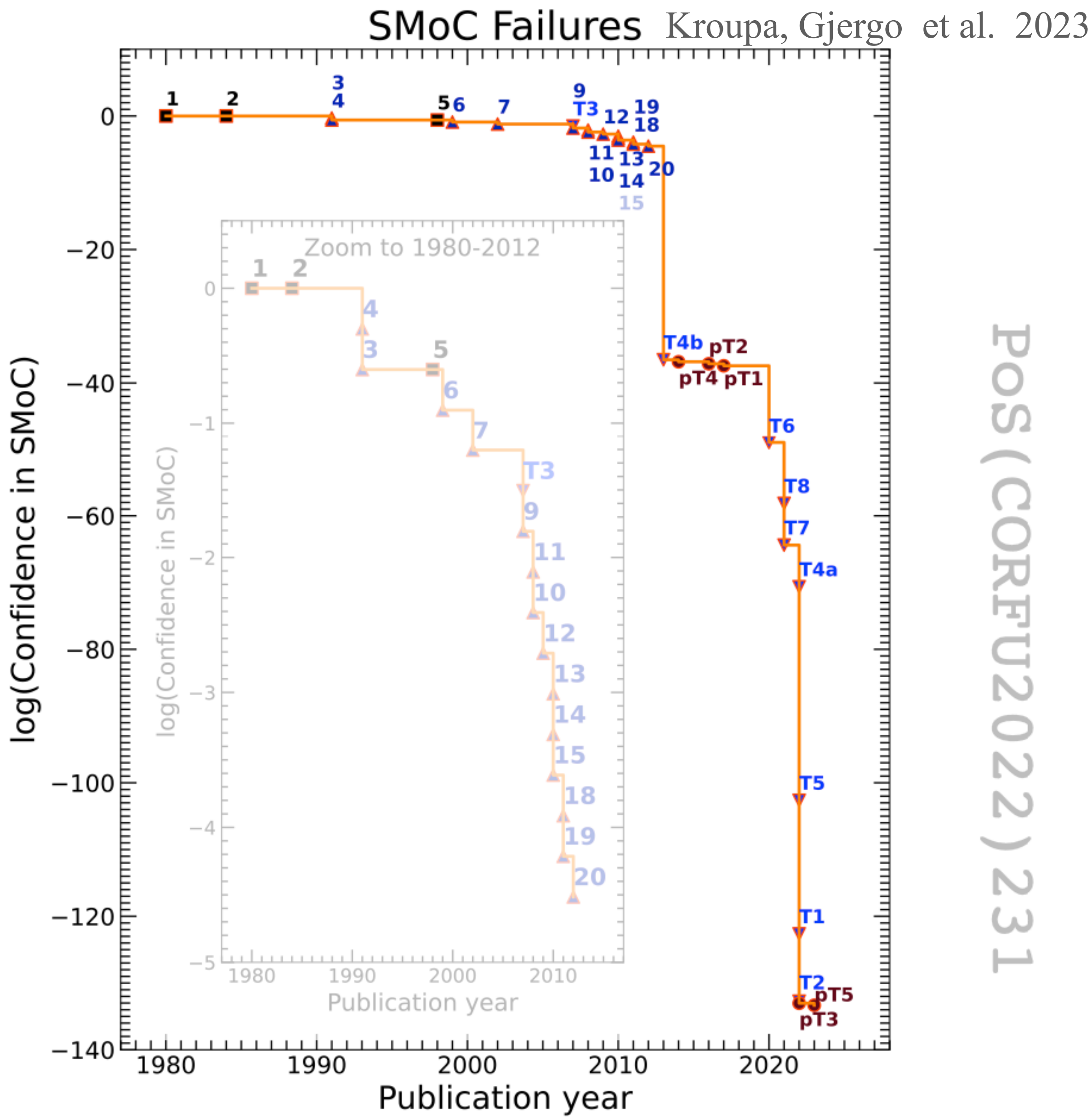

Figure 8: The SMoC-Confidence Graph: the cumulative loss in confidence that the Standard Model of Cosmology (SMoC) is a valid description of nature. The numbers 1-20 are based on a previous review (Kroupa, 2012, [6]), where an original form of the current plot appeared. Black squares (1, 2, and 5, representing inflation, dark matter, and dark energy, respectively) are treated in the SMoC as "new physics", so they are not assigned a loss of confidence. Upward blue triangles indicate failures, still current, already recognized in [6], while downward blue triangles (T1–T8) represent newly identified tensions where the loss of confidence was computed formally, as presented in Section 2.2. From the same section come the possible tensions (pT1–pT5), shown with red circles. Wherever the loss of confidence was not computed formally, we assign a drop in confidence by 50%. The inset graph zooms into the falsifications up to 2012.

\+ Magellanic Clouds 2024

==> no dark matter

\+ tidal tails of open star clusters 2024

==> not Newton

The LC/WDM model is valid
with a
confidence of $<10^{-140}$

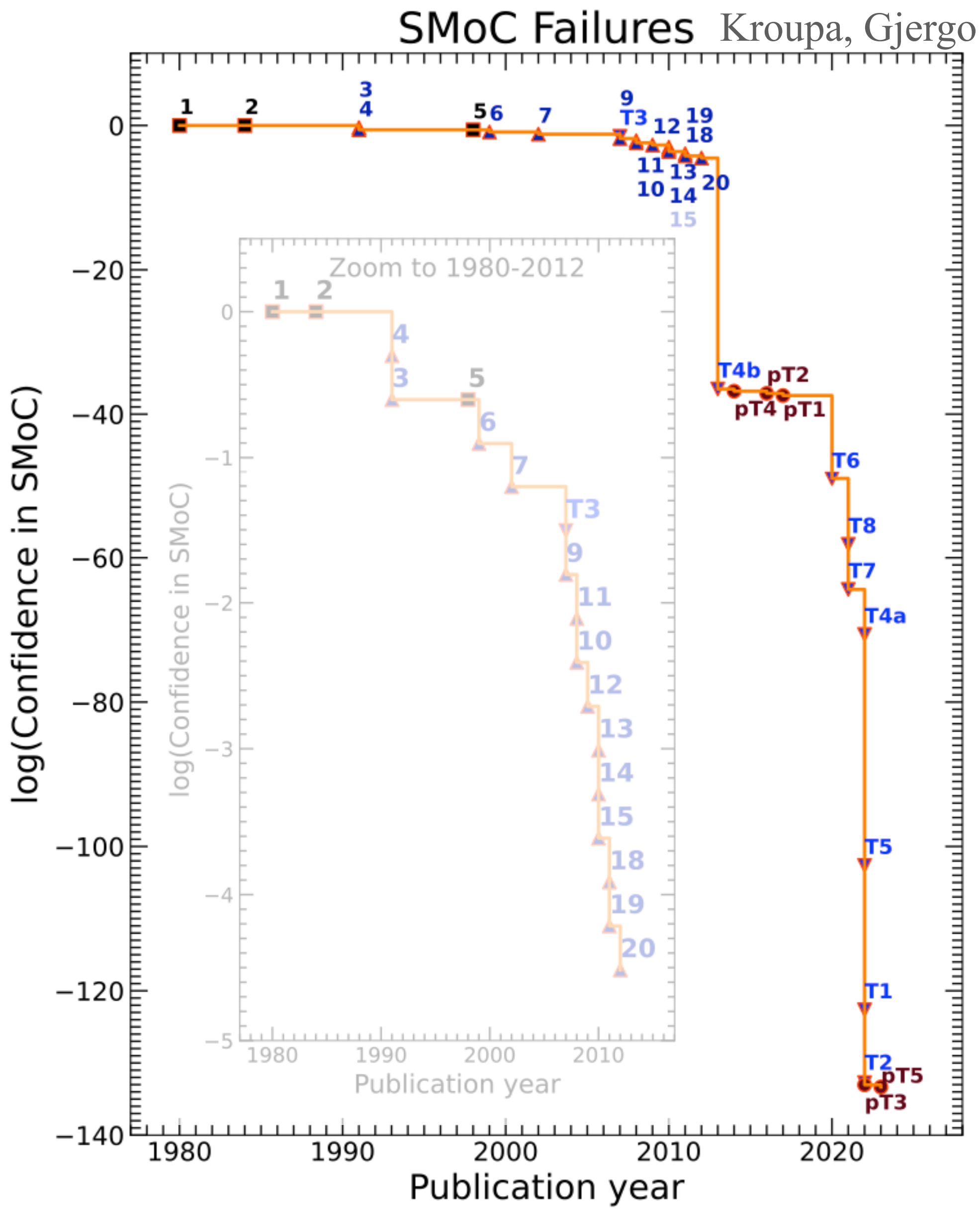

Kroupa, Gjergo et al. 2023

+ Magellanic Clouds 2024

==> no dark matter

+ tidal tails of open star clusters 2024

==> not Newton

The LC/WDM model is valid
with a
confidence of <<10^{-140}

Figure 8: The SMoC-Confidence Graph: the cumulative loss in confidence that the Standard Model of Cosmology (SMoC) is a valid description of nature. The numbers 1-20 are based on a previous review (Kroupa, 2012, [6]), where an original form of the current plot appeared. Black squares (1, 2, and 5, representing inflation, dark matter, and dark energy, respectively) are treated in the SMoC as "new physics", so they are not assigned a loss of confidence. Upward blue triangles indicate failures, still current, already recognized in [6], while downward blue triangles (T1–T8) represent newly identified tensions where the loss of confidence was computed formally, as presented in Section 2.2. From the same section come the possible tensions (pT1–pT5), shown with red circles. Wherever the loss of confidence was not computed formally, we assign a drop in confidence by 50%. The inset graph zooms into the falsifications up to 2012.

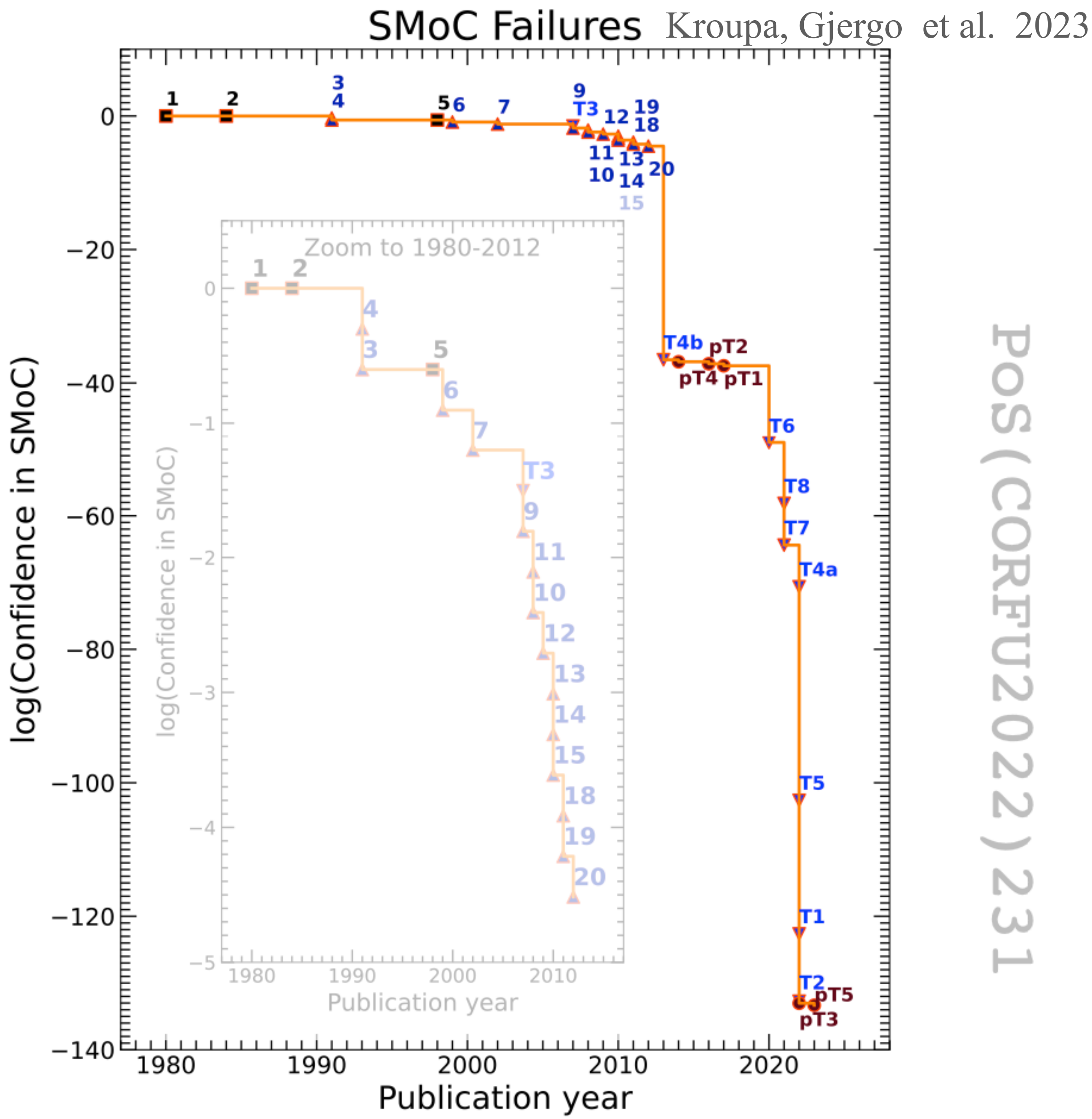

+ Magellanic Clouds 2024

==> no dark matter

+ tidal tails of open star clusters 2024

==> not Newton

The LC/WDM model is valid
with a
confidence of <<10^{-140}

The SMoC
(standard model of cosmology)
is the
most falsified
but
believed-to-be-true
model ever
in the history of
woman / man / them
kind.

Figure 8: The SMoC-Confidence Graph: the cumulative loss in confidence that the Standard Model of Cosmology (SMoC) is a valid description of nature. The numbers 1-20 are based on a previous review (Kroupa, 2012, [6]), where an original form of the current plot appeared. Black squares (1, 2, and 5, representing inflation, dark matter, and dark energy, respectively) are treated in the SMoC as "new physics", so they are not assigned a loss of confidence. Upward blue triangles indicate failures, still current, already recognized in [6], while downward blue triangles (T1–T8) represent newly identified tensions where the loss of confidence was computed formally, as presented in Section 2.2. From the same section come the possible tensions (pT1–pT5), shown with red circles. Wherever the loss of confidence was not computed formally, we assign a drop in confidence by 50%. The inset graph zooms into the falsifications up to 2012.

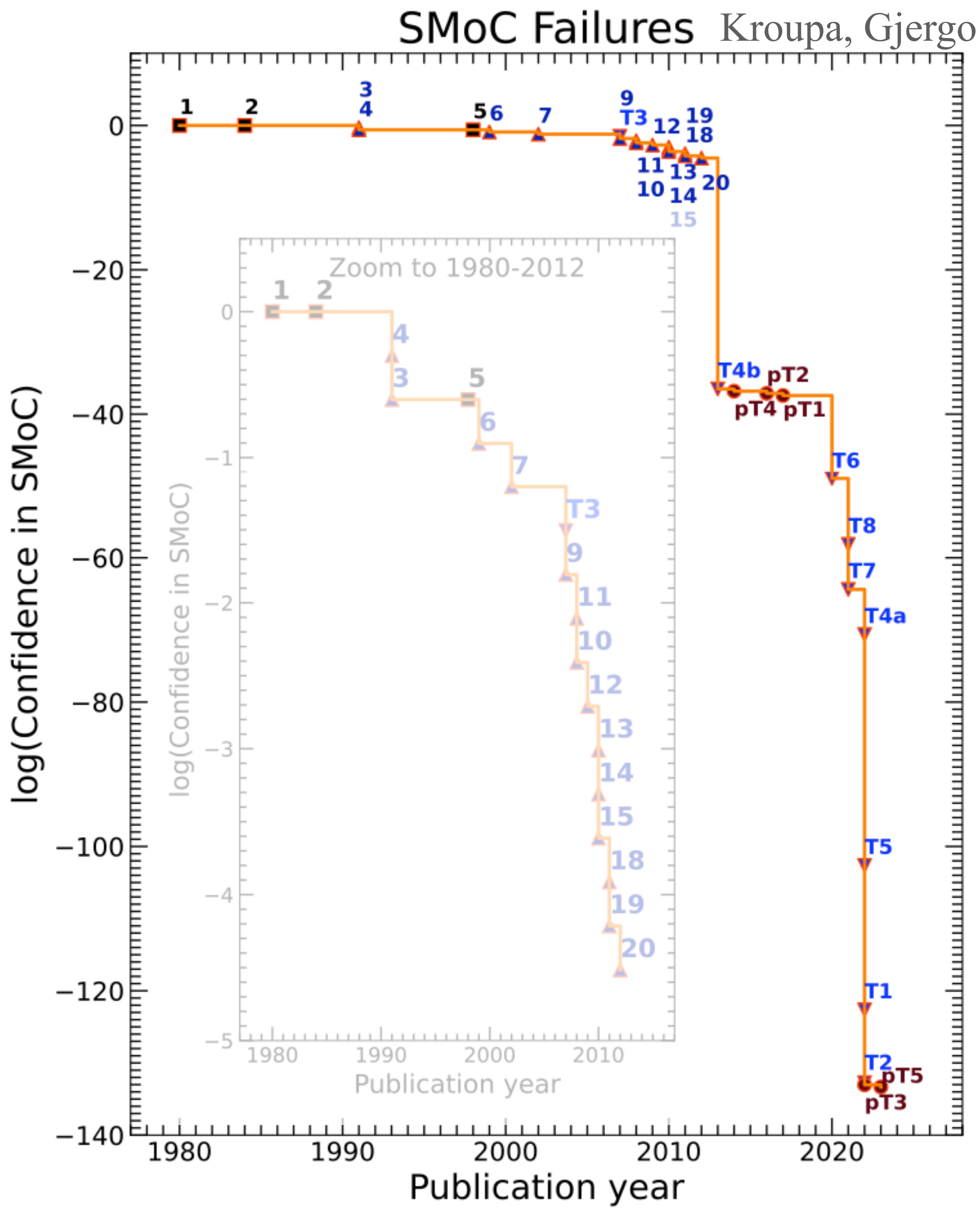

Kroupa, Gjergo et al. 2023

Figure 8: The SMoC-Confidence Graph: the cumulative loss in confidence that the Standard Model of Cosmology (SMoC) is a valid description of nature. The numbers 1-20 are based on a previous review (Kroupa, 2012, [6]), where an original form of the current plot appeared. Black squares (1, 2, and 5, representing inflation, dark matter, and dark energy, respectively) are treated in the SMoC as "new physics", so they are not assigned a loss of confidence. Upward blue triangles indicate failures, still current, already recognized in [6], while downward blue triangles (T1–T8) represent newly identified tensions where the loss of confidence was computed formally, as presented in Section 2.2. From the same section come the possible tensions (pT1–pT5), shown with red circles. Wherever the loss of confidence was not computed formally, we assign a drop in confidence by 50%. The inset graph zooms into the falsifications up to 2012.

\+ Magellanic Clouds 2024

==> no dark matter

\+ tidal tails of open star clusters 2024

==> not Newton

The LC/WDM model is valid with a **confidence of $<<10^{-140}$**

The SMoC
(standard model of cosmology)
is the
most falsified
but
believed-to-be-true
model ever
in the history of
woman / man / them
kind.

The greatest crisis in physics ever.

Future outlook

LC/WDM is not on the table any longer !

LC/WDM is not on the table any longer!

Need a new cosmological model!

LC/WDM is not on the table any longer !

Need a new cosmological model !

Success of MOND → it needs to be essentially MONDian

LC/WDM is not on the table any longer !

Need a new cosmological model !

Success of MOND → it needs to be essentially MONDian
Much work on this in Bonn and Prague

LC/WDM is not on the table any longer !

Need a new cosmological model !

Success of MOND → it needs to be essentially MONDian

Much work on this in Bonn and Prague

1) The **nuHDM model** :
with *inflation, dark energy* and *sterile neutrinos* as hot dark matter

LC/WDM is not on the table any longer !

Need a new cosmological model !

Success of MOND → it needs to be essentially MONDian
Much work on this in Bonn and Prague

1) The **nuHDM model** :
with *inflation, dark energy* and *sterile neutrinos* as hot dark matter
Simulations : Katz, McGaugh et al. 2013 -- pure Nbody
Wittenburg, Kroupa et al. 2023 -- hydrodynamical

LC/WDM is not on the table any longer !

Need a new cosmological model !

Success of MOND → it needs to be essentially MONDian
Much work on this in Bonn and Prague

1) The **nuHDM model** :
with *inflation, dark energy* and *sterile neutrinos* as hot dark matter
Simulations : Katz, McGaugh et al. 2013 -- pure Nbody
Wittenburg, Kroupa et al. 2023 -- hydrodynamical

→ e.g. Nikolaos Samaras in Prague

Comparison on the Cosmological Scale

A nuHDM simulation

Wittenburg et al. 2023

400Mpc x 400Mpc

The Millennium XXL (MXXL) simulation (SMoC)

Angulo et al. 2012

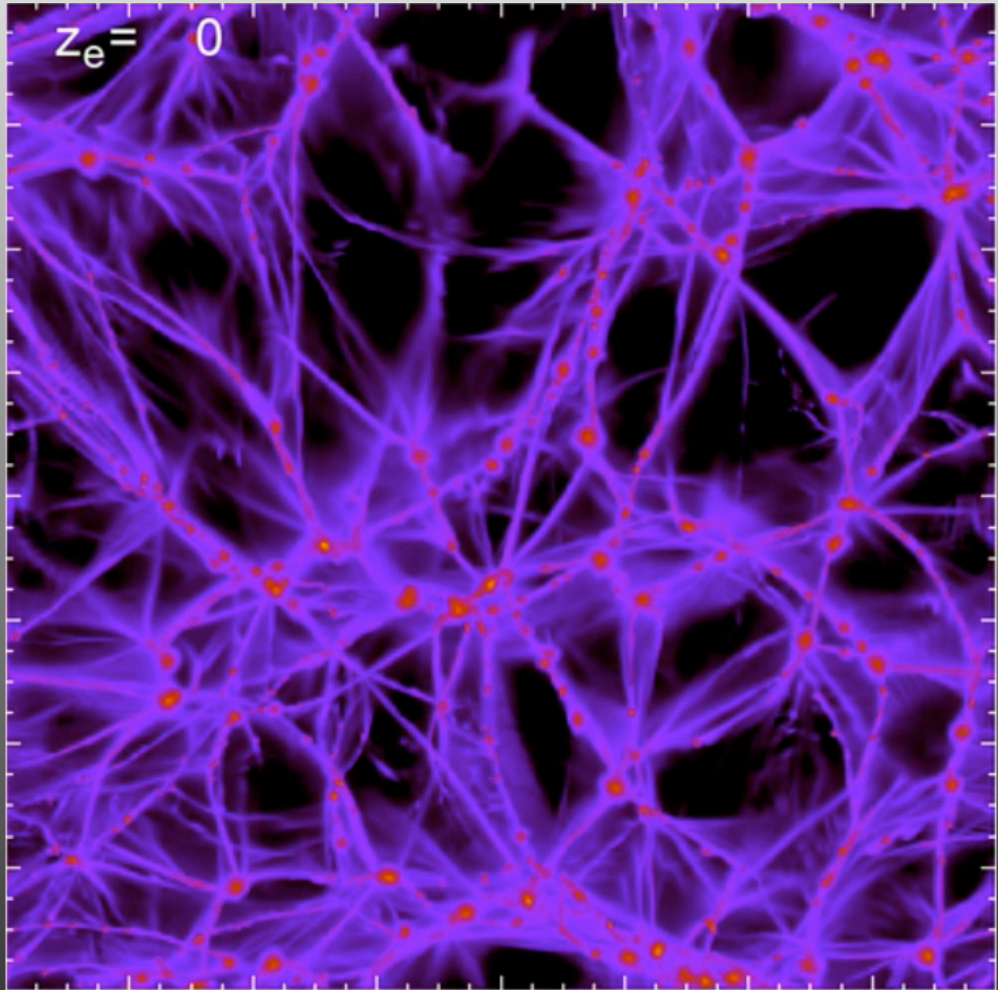

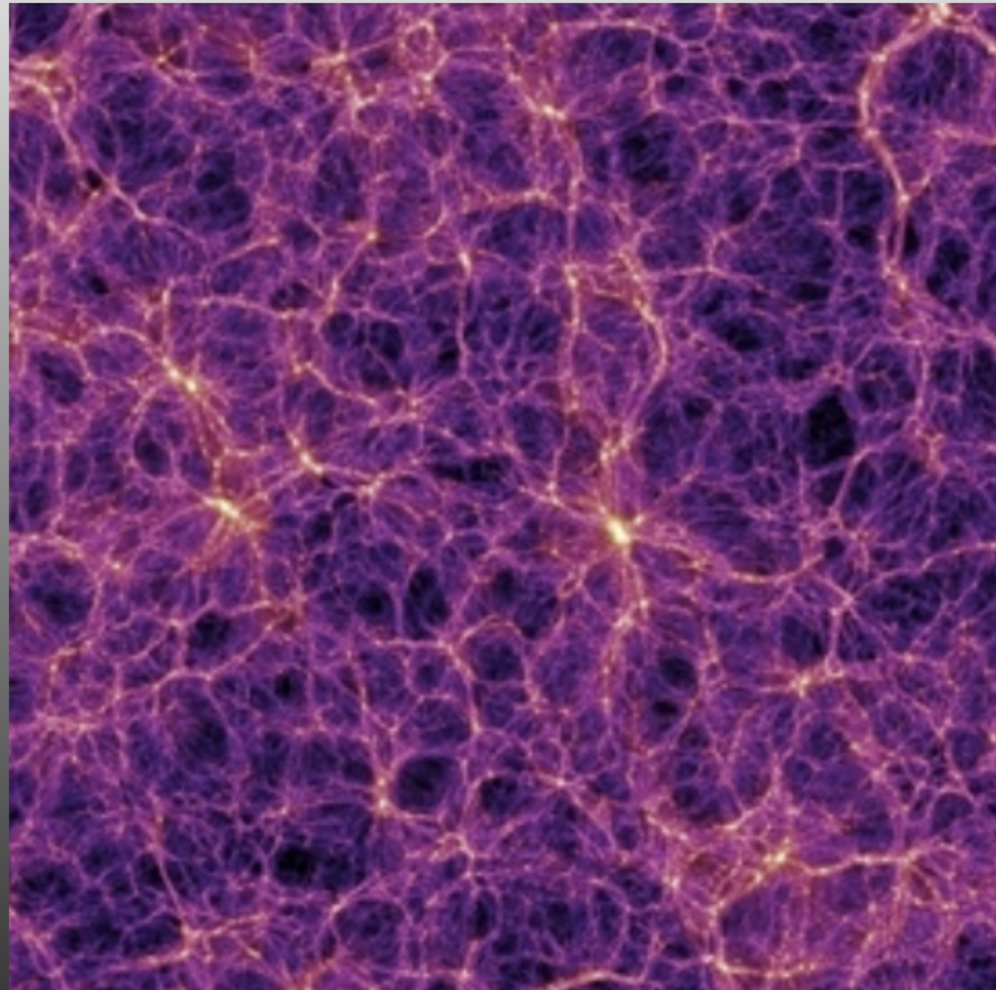

Comparison on the Cosmological Scale

A nuHDM simulation

Wittenburg et al. 2023

400Mpc x 400Mpc

The Millennium XXL (MXXL) simulation (SMoC)

Angulo et al. 2012

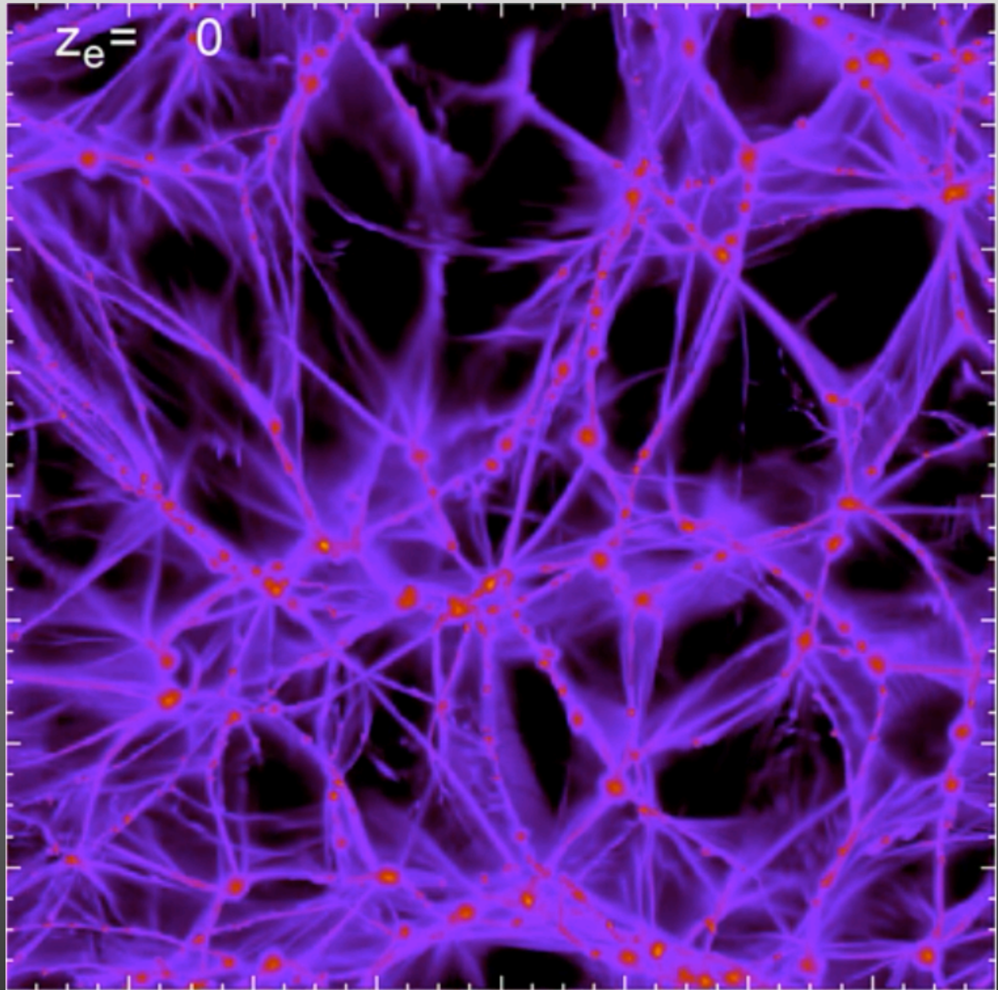

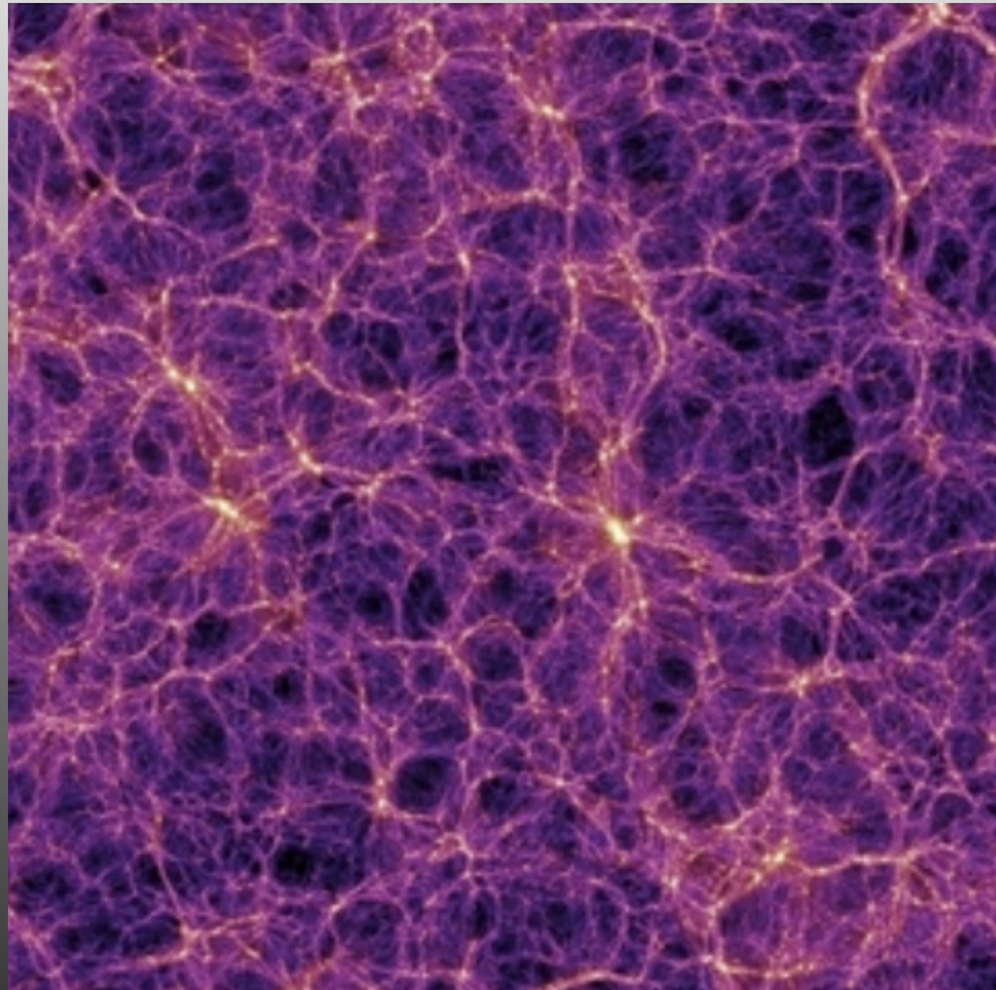

In the Milgromian model, the density contrasts are larger ----> this points into the correct direction
(the real universe being inhomogeneous on all scales)

Comparison on the Cosmological Scale

A nuHDM simulation

Wittenburg et al. 2023

400Mpc x 400Mpc

The Millennium XXL (MXXL) simulation (SMoC)

Angulo et al. 2012

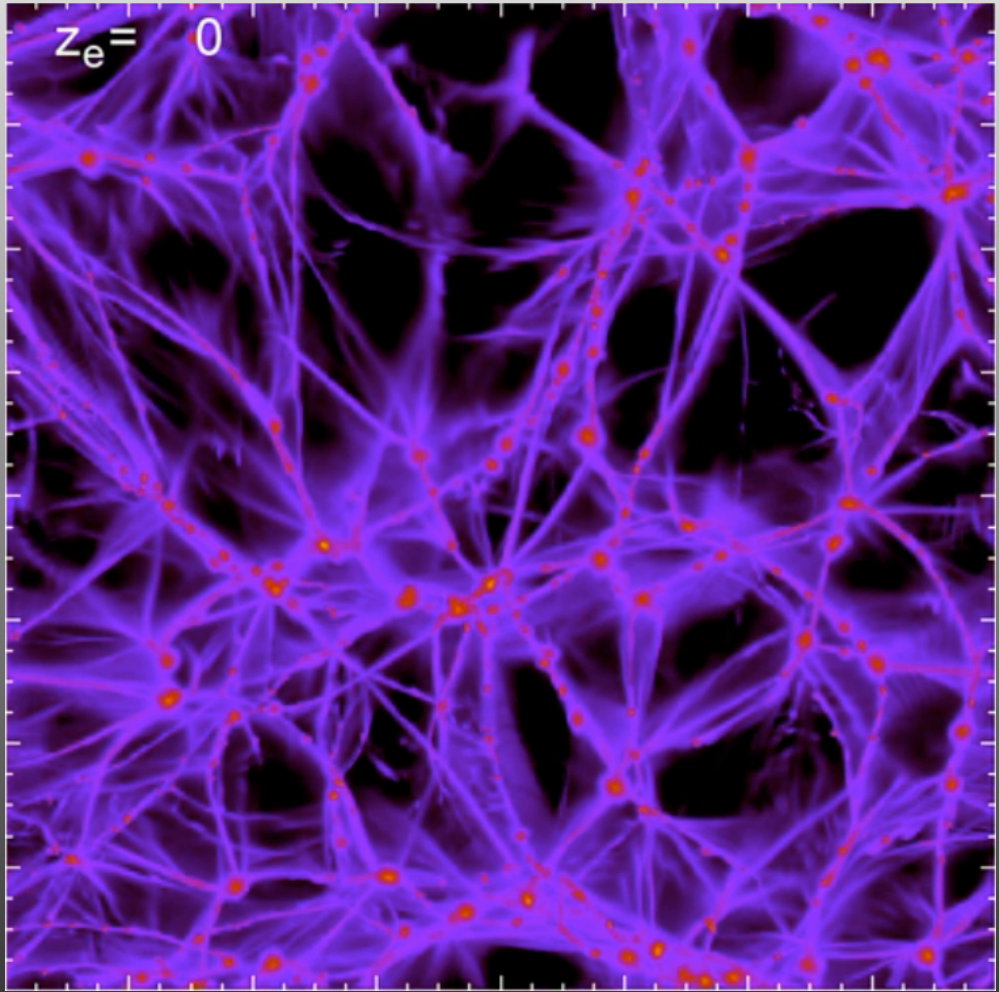

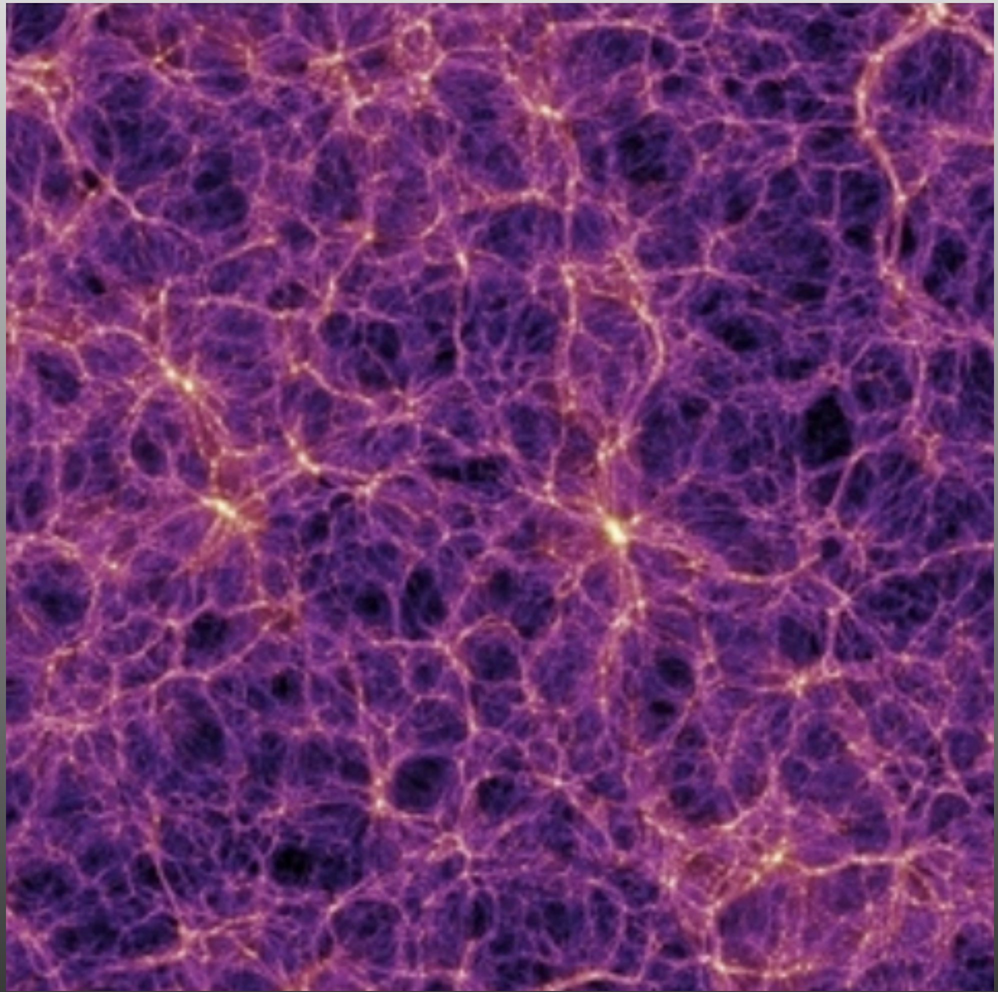

In the Milgromian model, the density contrasts are larger ----> this points into the correct direction (the real universe being inhomogeneous on all scales)

But, the model may be too homogeneous on scales >300Mpc (compared to real Universe which is inhomogeneous on 5Gpc scales)

LC/WDM is not on the table any longer !

Need a new cosmological model !

Success of MOND → it needs to be essentially MONDian
Much work on this in Bonn and Prague

1) The **nuHDM model :**
with *inflation, dark energy* and *sterile neutrinos* as hot dark matter
Simulations : Katz, McGaugh et al. 2013 -- pure Nbody
Wittenburg, Kroupa et al. 2023 -- hydrodynamical

→ e.g. Nikolaos Samaras in Prague

LC/WDM is not on the table any longer !

Need a new cosmological model !

Success of MOND → it needs to be essentially MONDian
Much work on this in Bonn and Prague

1) The **nuHDM model** :
with *inflation, dark energy* and *sterile neutrinos* as hot dark matter
Simulations : Katz, McGaugh et al. 2013 -- pure Nbody
Wittenburg, Kroupa et al. 2023 -- hydrodynamical

→ e.g. Nikolaos Samaras in Prague

2) The **Bohemian Model of Cosmology** :
no *inflation, dark energy* nor *dark matter*
(no yet published : Eda Gjergo)

LC/WDM is not on the table any longer !

Need a new cosmological model !

Success of MOND → it needs to be essentially MONDian
Much work on this in Bonn and Prague

1) The **nuHDM model** :
with *inflation, dark energy* and *sterile neutrinos* as hot dark matter
Simulations : Katz, McGaugh et al. 2013 -- pure Nbody
Wittenburg, Kroupa et al. 2023 -- hydrodynamical

→ e.g. Nikolaos Samaras in Prague

2) The **Bohemian Model of Cosmology** :
no *inflation, dark energy* nor *dark matter*
(no yet published : Eda Gjergo)

→ e.g. Nikolaos Samaras in Prague

Comparison on the Cosmological Scale

The Millennium XXL (MXXL) simulation (SMoC)

z=0

1Gpc x 1Gpc

Angulo et al. 2012

A Bohemian simulation

0.64Gpc x 0.64Gpc

by I.Thies

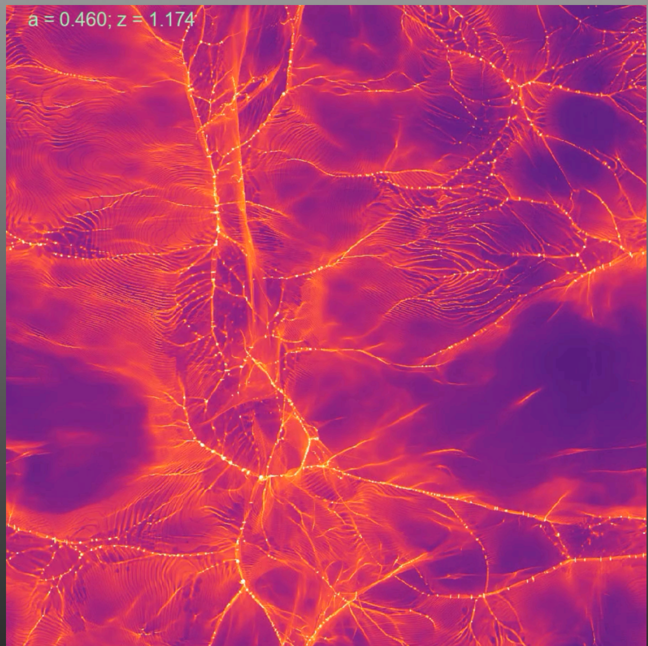

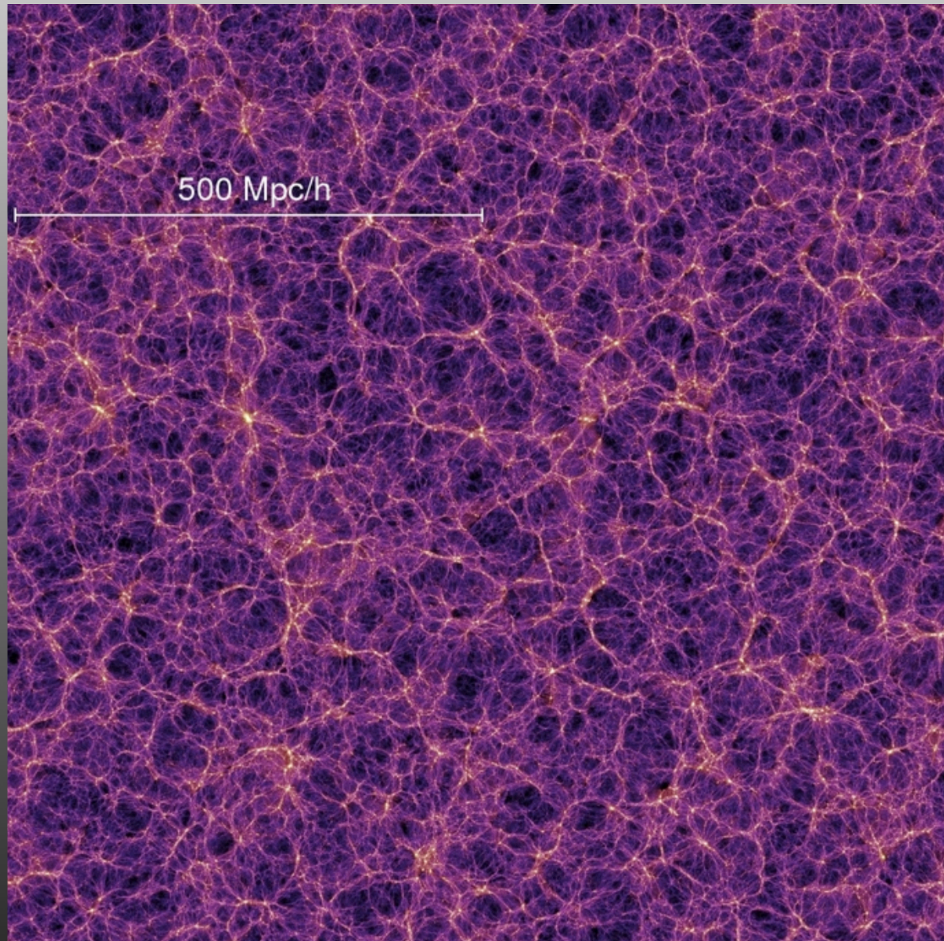

Comparison on the Cosmological Scale

A Bohemian simulation

0.64Gpc x 0.64Gpc by I.Thies

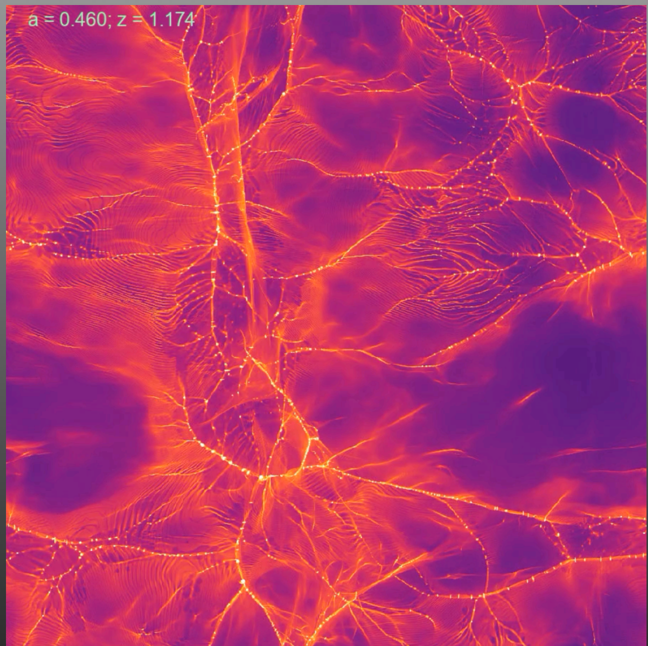

The Millennium XXL (MXXL) simulation (SMoC)

z=0
1Gpc x 1Gpc

Angulo et al. 2012

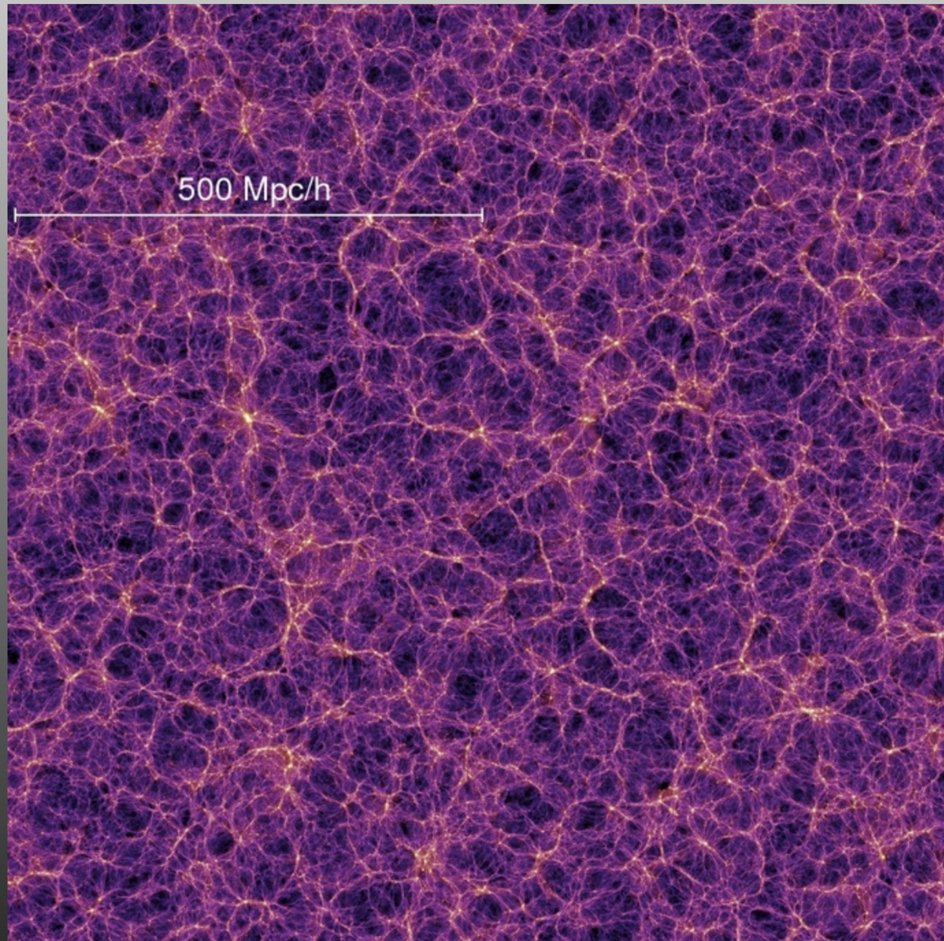

In the Bohemian model, the density contrasts are significantly larger ----> this points into the correct direction (the real universe being inhomogeneous on all scales)

Conclusion

With the LC/WDM standard model of cosmology model
being completely ruled out,
being entirely *off* the table,
being fundamentally irrelevant,
being the completely *wrong and invalid* description of cosmological physics

Conclusion

With the LC/WDM standard model of cosmology model
being completely ruled out,
being entirely *off* the table,
being fundamentally irrelevant,
being the completely *wrong and invalid* description of cosmological physics

--- dark matter does not exist
and
gravitation is not Newtonian but Milgromian(-like) ---

we need a new model that allows structure formation simulations.

Conclusion

With the LC/WDM standard model of cosmology model
being completely ruled out,
being entirely *off* the table,
being fundamentally irrelevant,
being the completely *wrong and invalid* description of cosmological physics

--- dark matter does not exist
and
gravitation is not Newtonian but Milgromian(-like) ---

we need a new model that allows structure formation simulations.

This is an active area of research in
Bonn & *Prague* & *Nanjing*

The END

Different-than-Newtonian dynamics or gravitation

Should one expect an empirical law to hold over an extrapolation of orders of magnitude ?

Gedankenexperiment

by Indranil Banik
(St. Andrews)

Gedankenexperiment

by Indranil Banik
(St. Andrews)

Depth of a trampolin with increasing weight :

Depth

0.0000001g 1g 10g 100g

Weight

Gedankenexperiment

by Indranil Banik
(St. Andrews)

Depth of a trampolin with increasing weight :

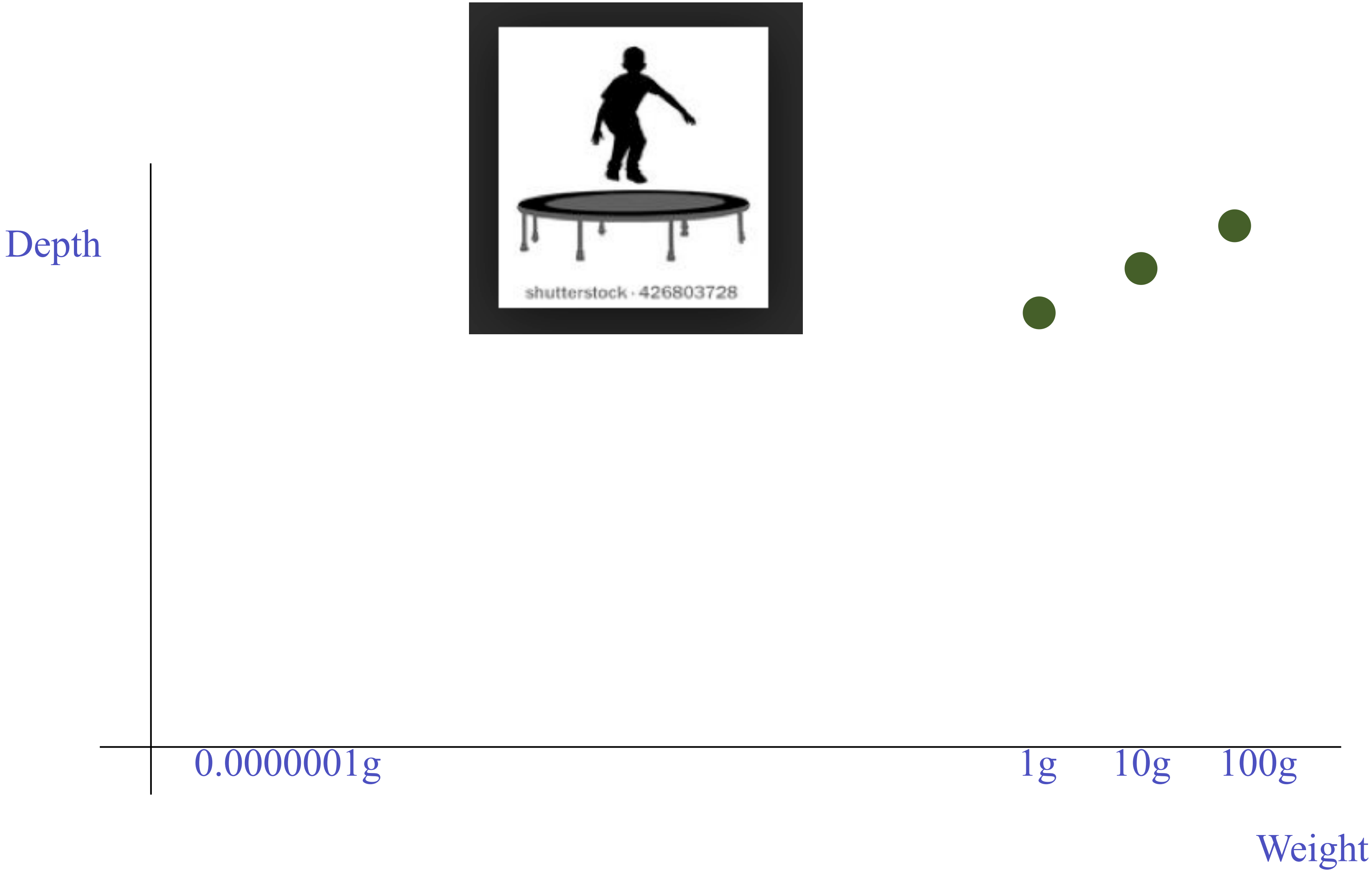

Gedankenexperiment

by Indranil Banik
(St. Andrews)

Depth of a trampolin with increasing weight :

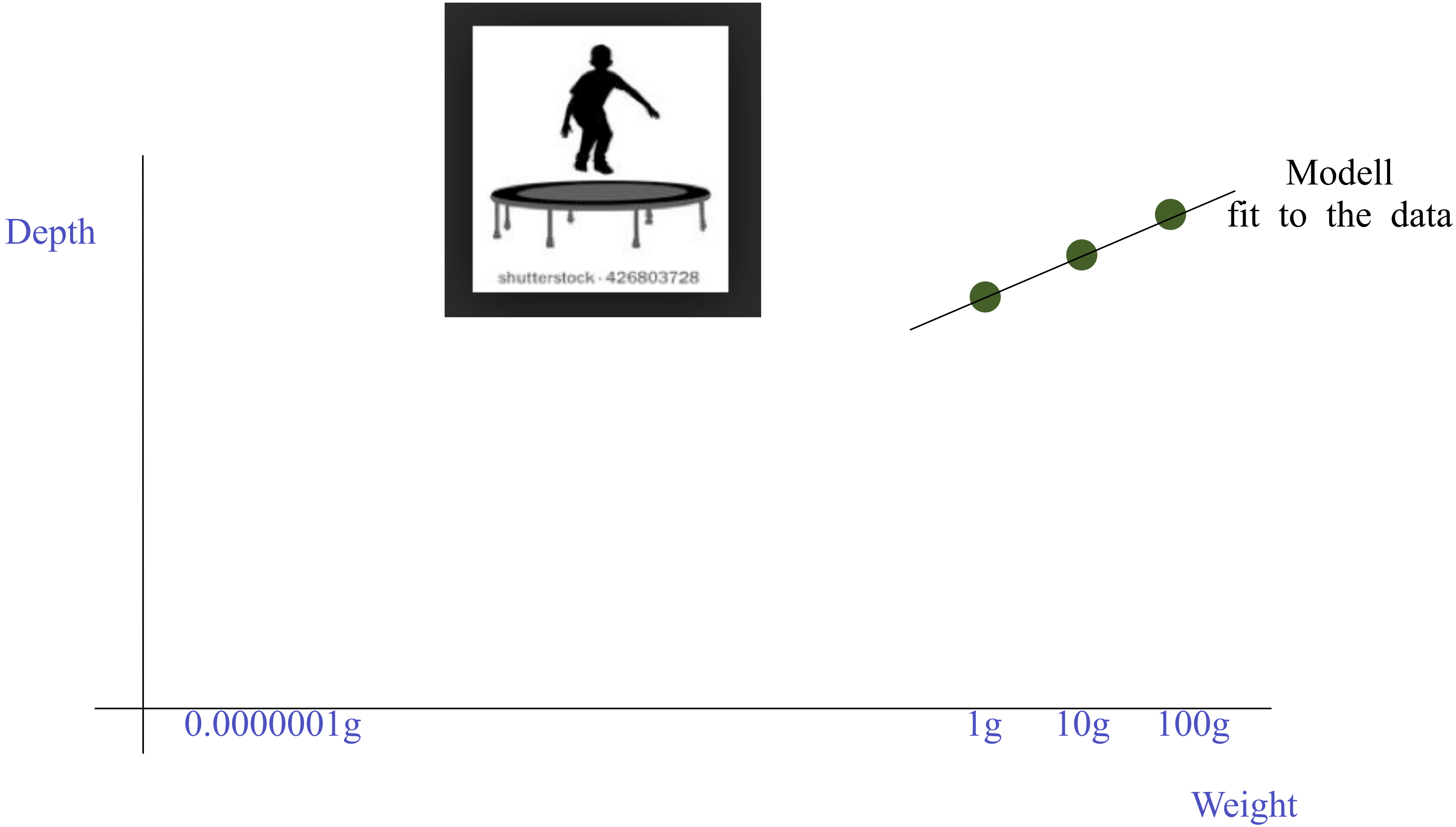

Gedankenexperiment

by Indranil Banik
(St. Andrews)

Depth of a trampolin with increasing weight :

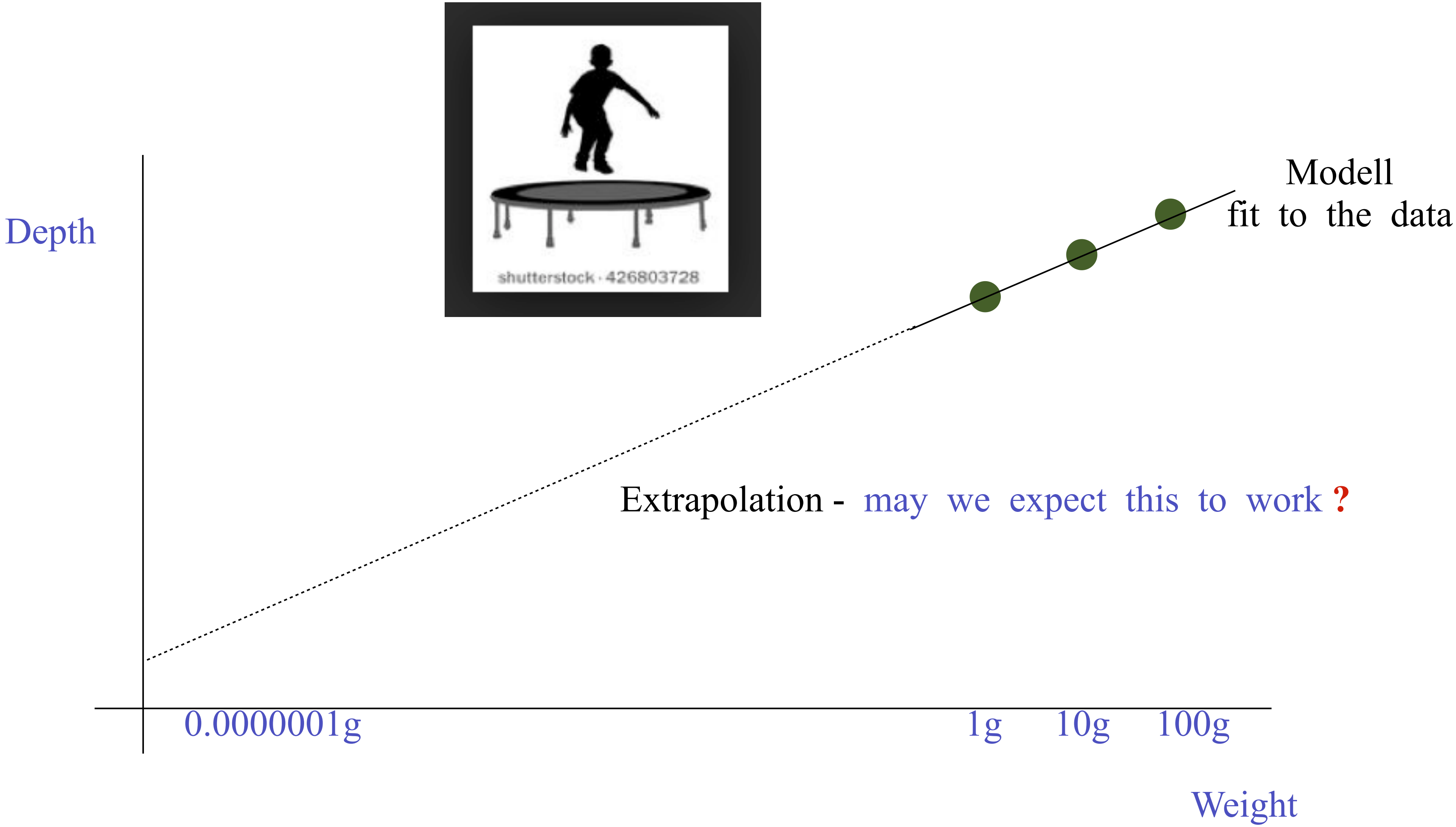

Gedankenexperiment

by Indranil Banik
(St. Andrews)

Depth of a trampolin with increasing weight :

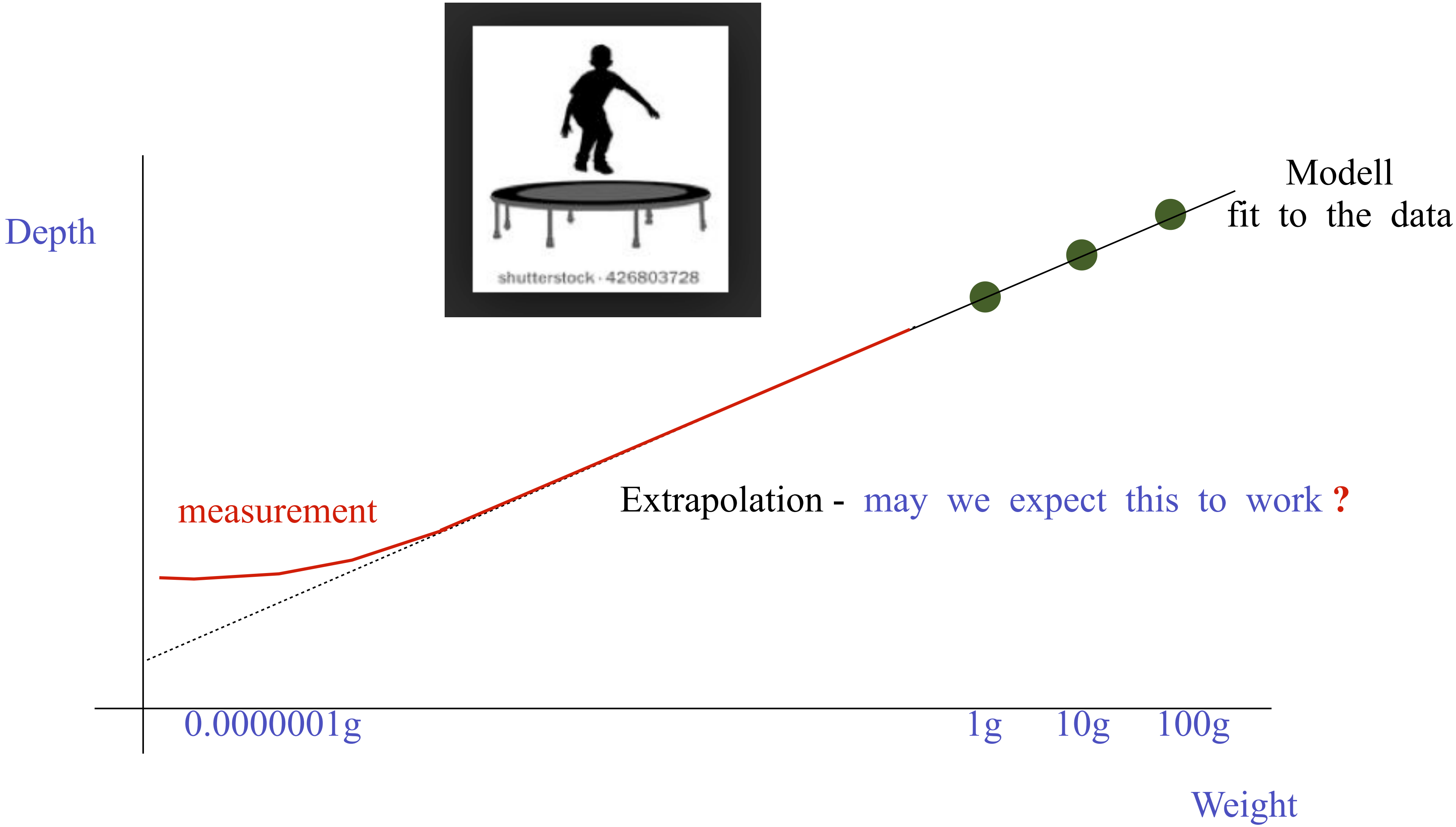

Gedankenexperiment

by Indranil Banik
(St. Andrews)

Depth of a trampolin with increasing weight :

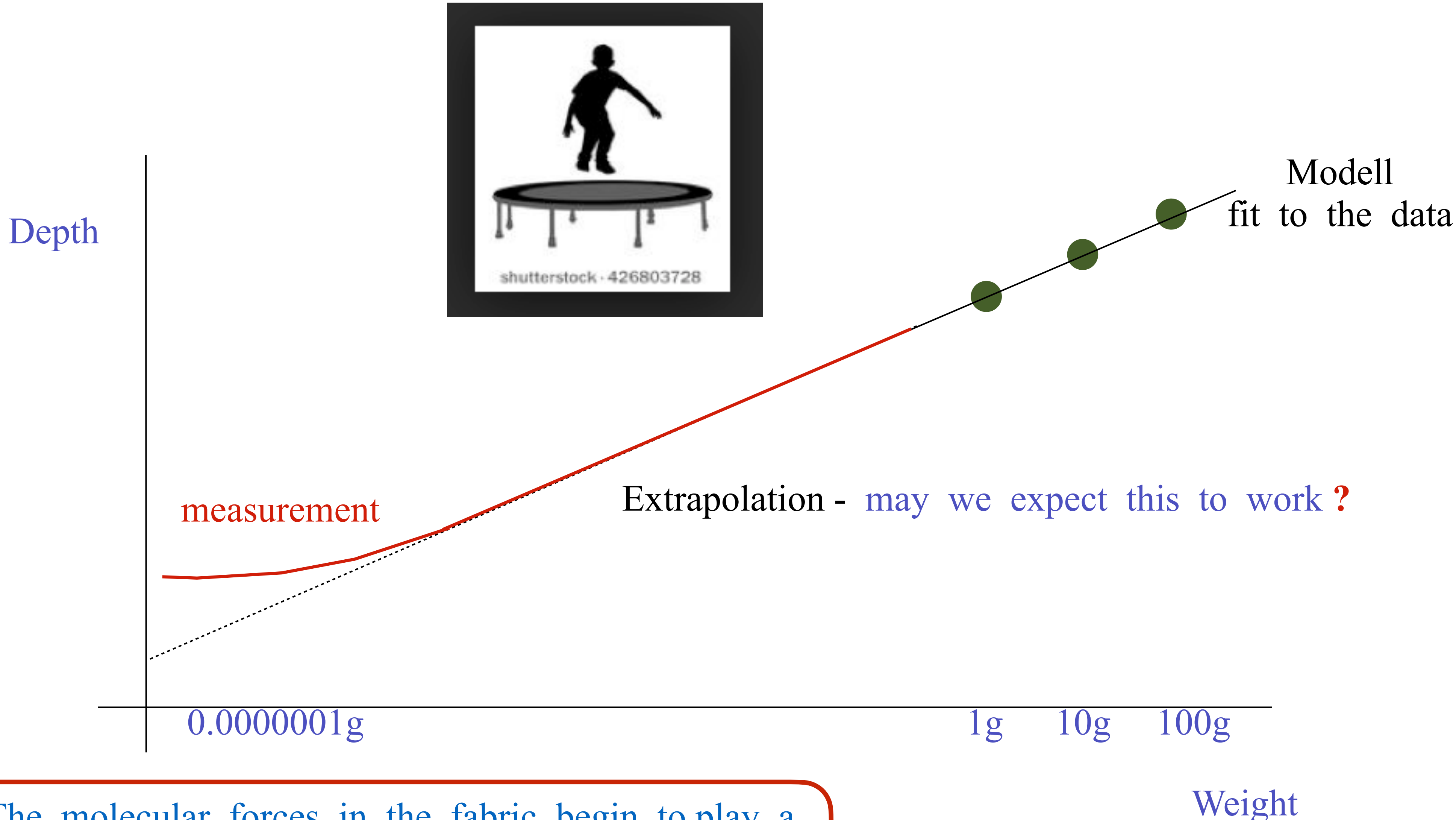

The molecular forces in the fabric begin to play a role and the system shifts from bulk properties to molecular-based behaviour.

Disc galaxies

Balance between
gravitation
and
centrifugal force

Disc galaxies

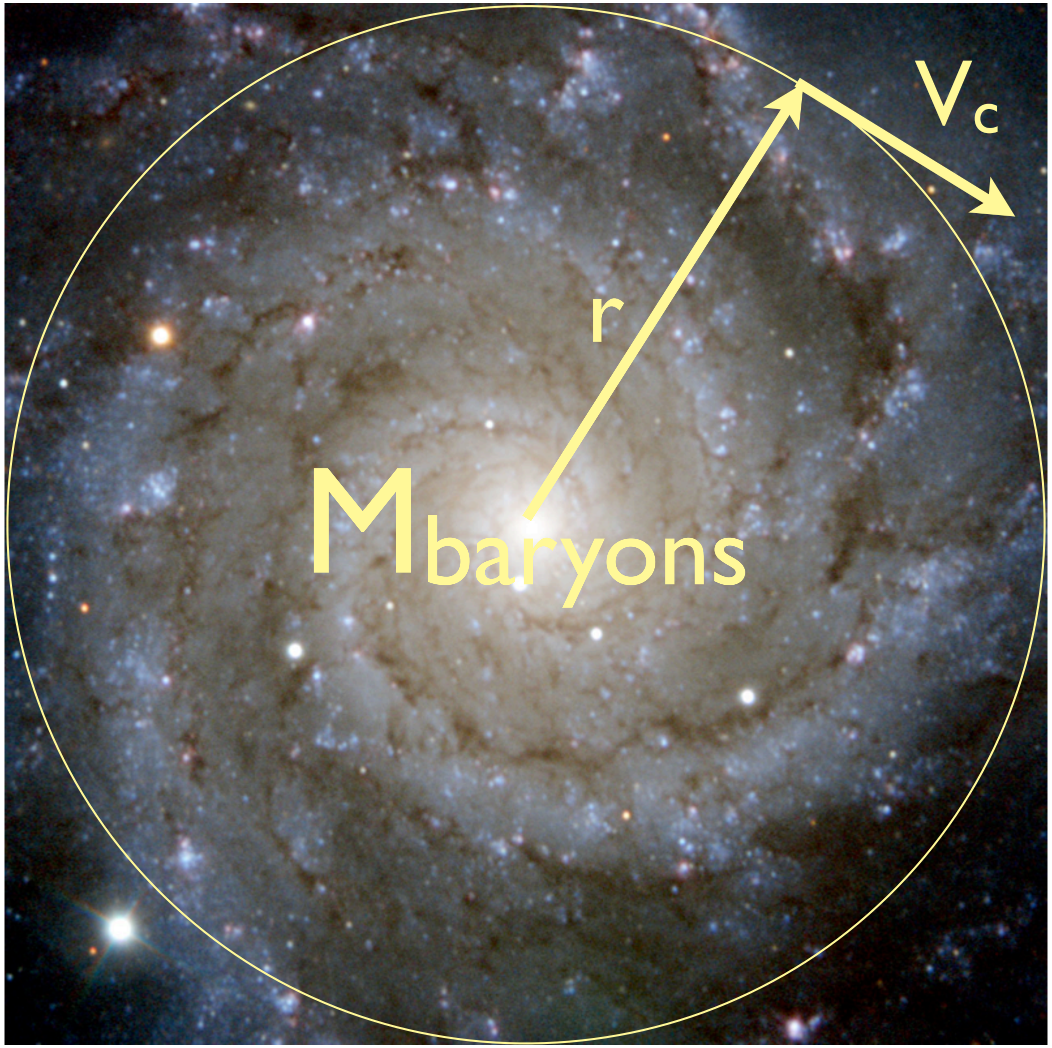

Balance between
gravitation
and
centrifugal force

According to Newton :

$$g_{\mathrm{N}} = G\,\frac{M_{\mathrm{baryons}}}{r^2}$$

Measured :

$$g = \frac{V_{\mathrm{c}}^2}{r}$$

Disc galaxies

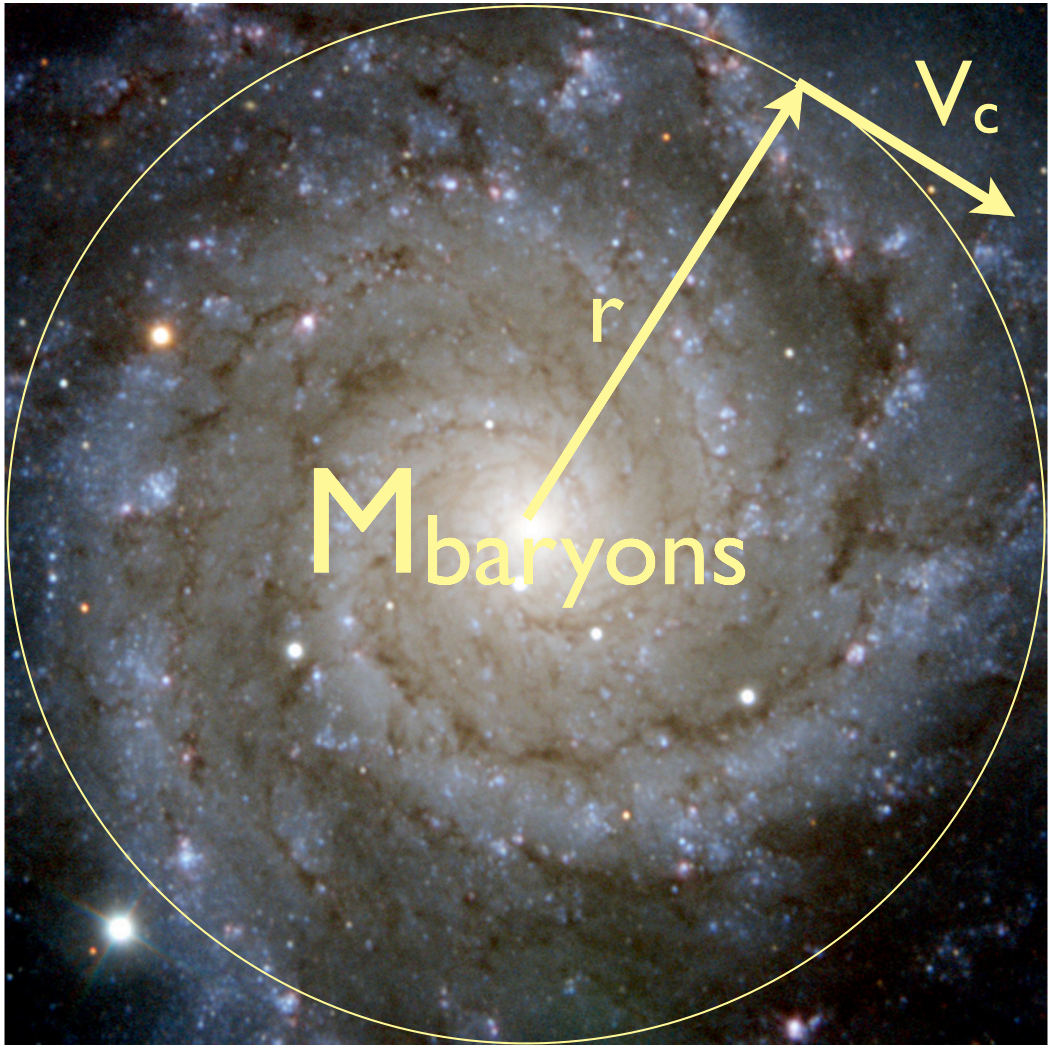

Balance between gravitation and centrifugal force

According to Newton :

$$g_{\mathrm{N}} = G\,\frac{M_{\mathrm{baryons}}}{r^2}$$

Measured :

$$g = \frac{V_{\mathrm{c}}^2}{r}$$

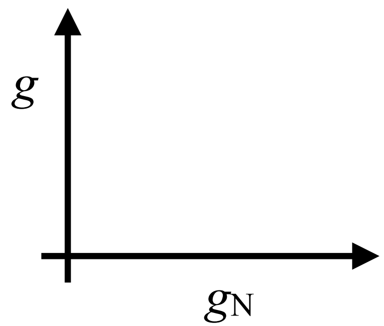

Disc galaxies

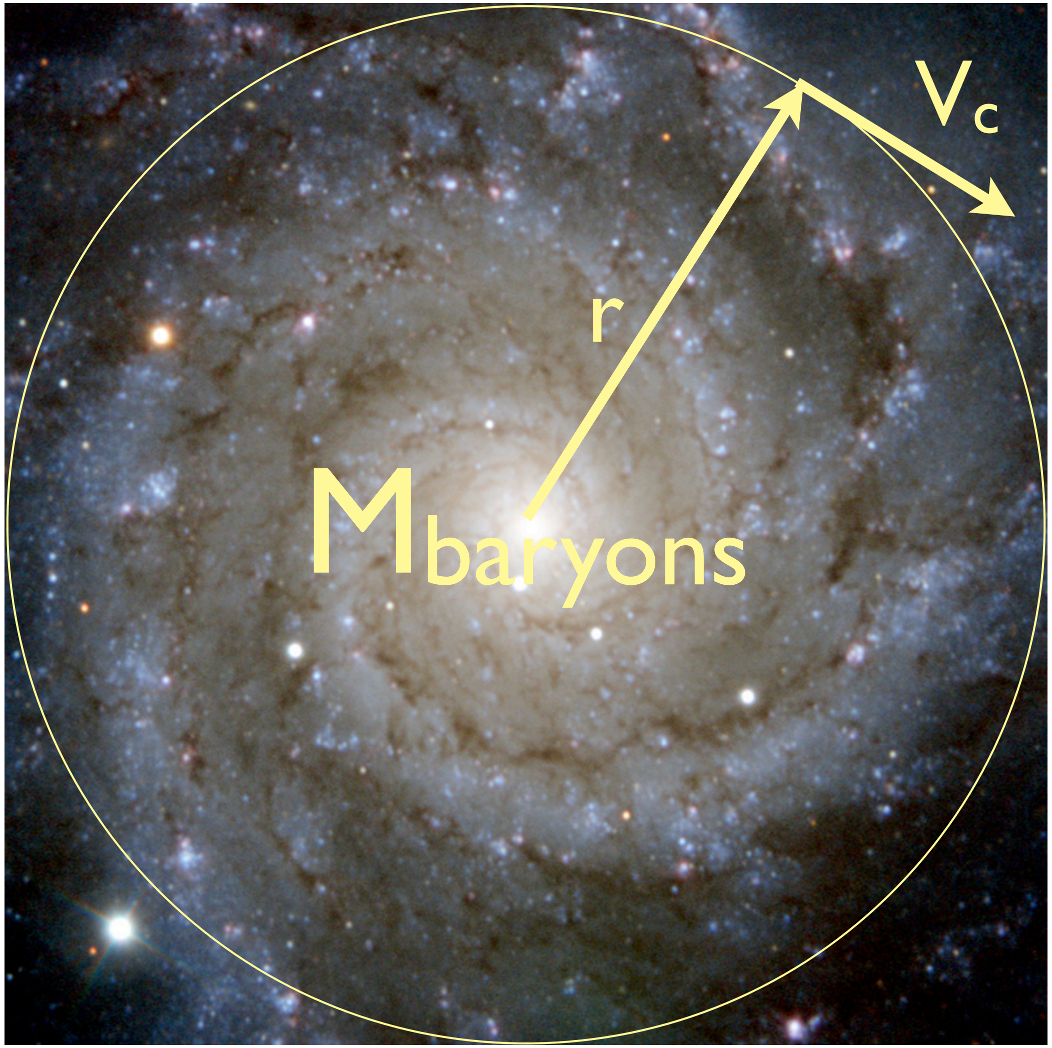

Balance between
gravitation
and
centrifugal force

According to Newton :

$$g_N = G\,\frac{M_{\rm baryons}}{r^2}$$

Measured :

$$g = \frac{V_c^2}{r}$$

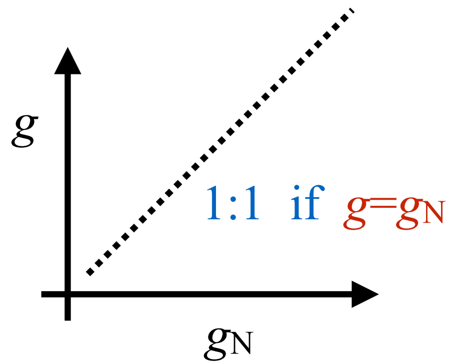

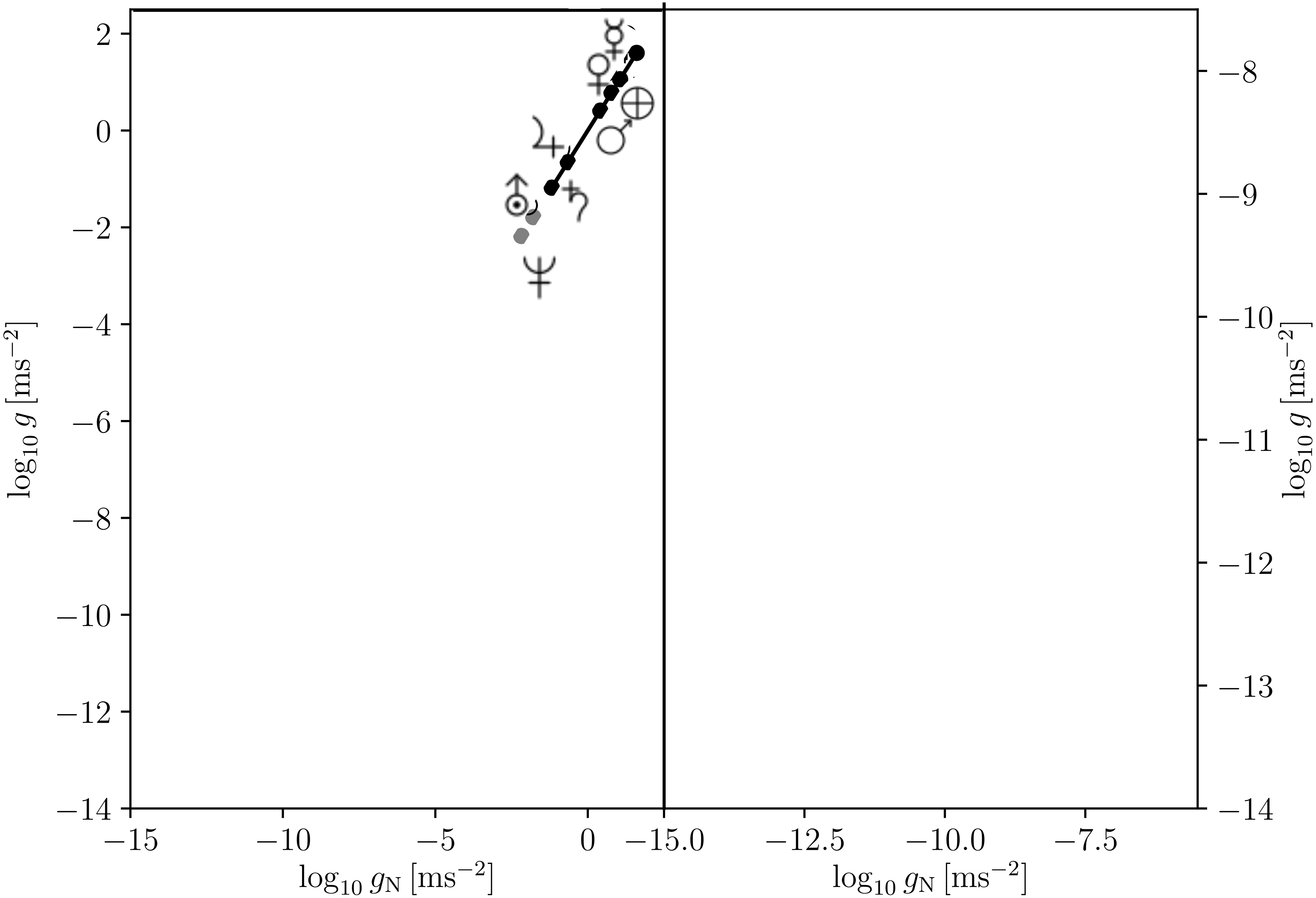

g = observed acceleration from rotation curve
g_N = expected acceleration from observed matter distribution

D2016 =
Dabringhausen&Kroupa2023
see also
Lelli et al. (2017)

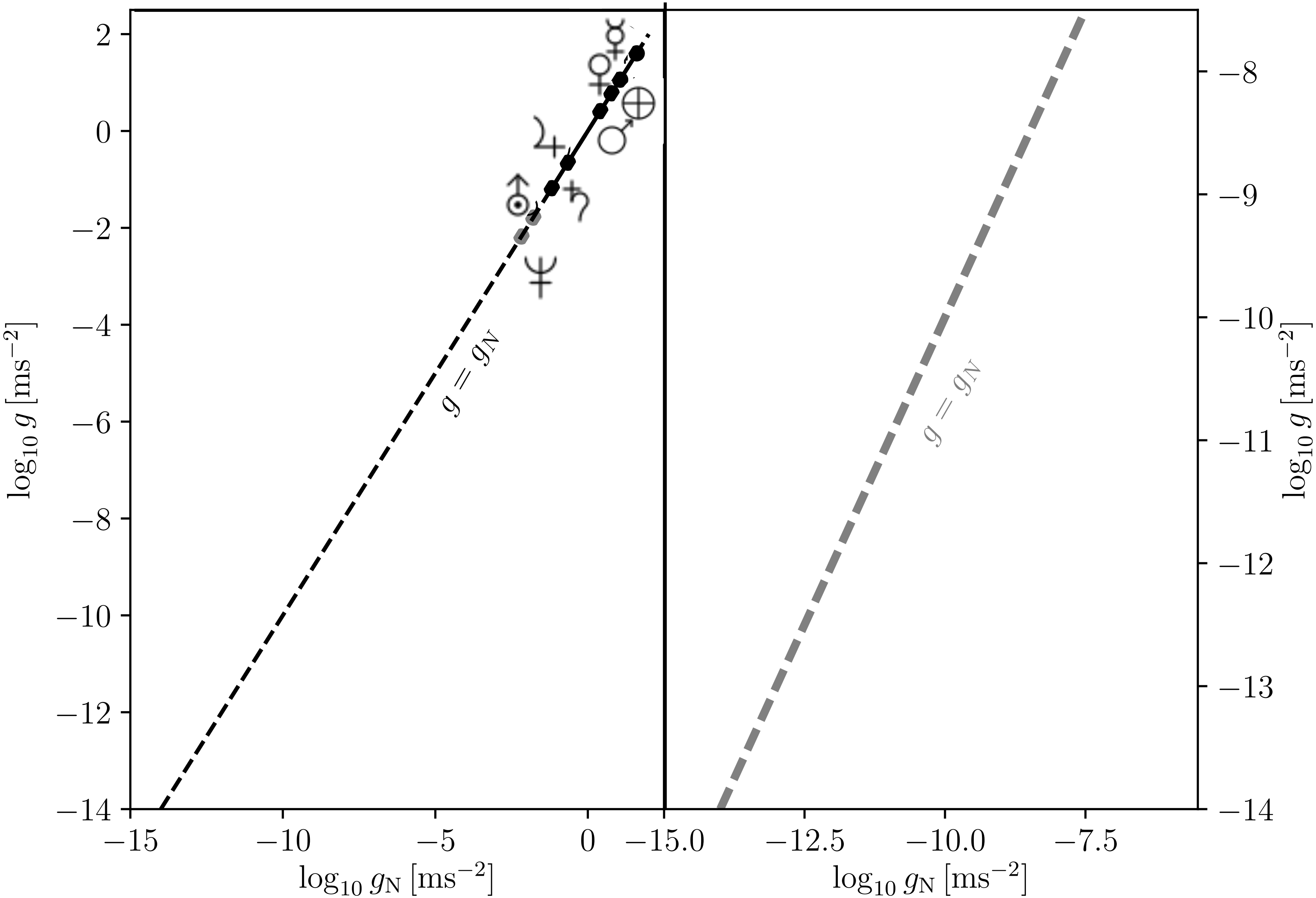

g = observed acceleration from rotation curve
g_N = expected acceleration from observed matter distribution

D2016 =
Dabringhausen&Kroupa2023
see also
Lelli et al. (2017)

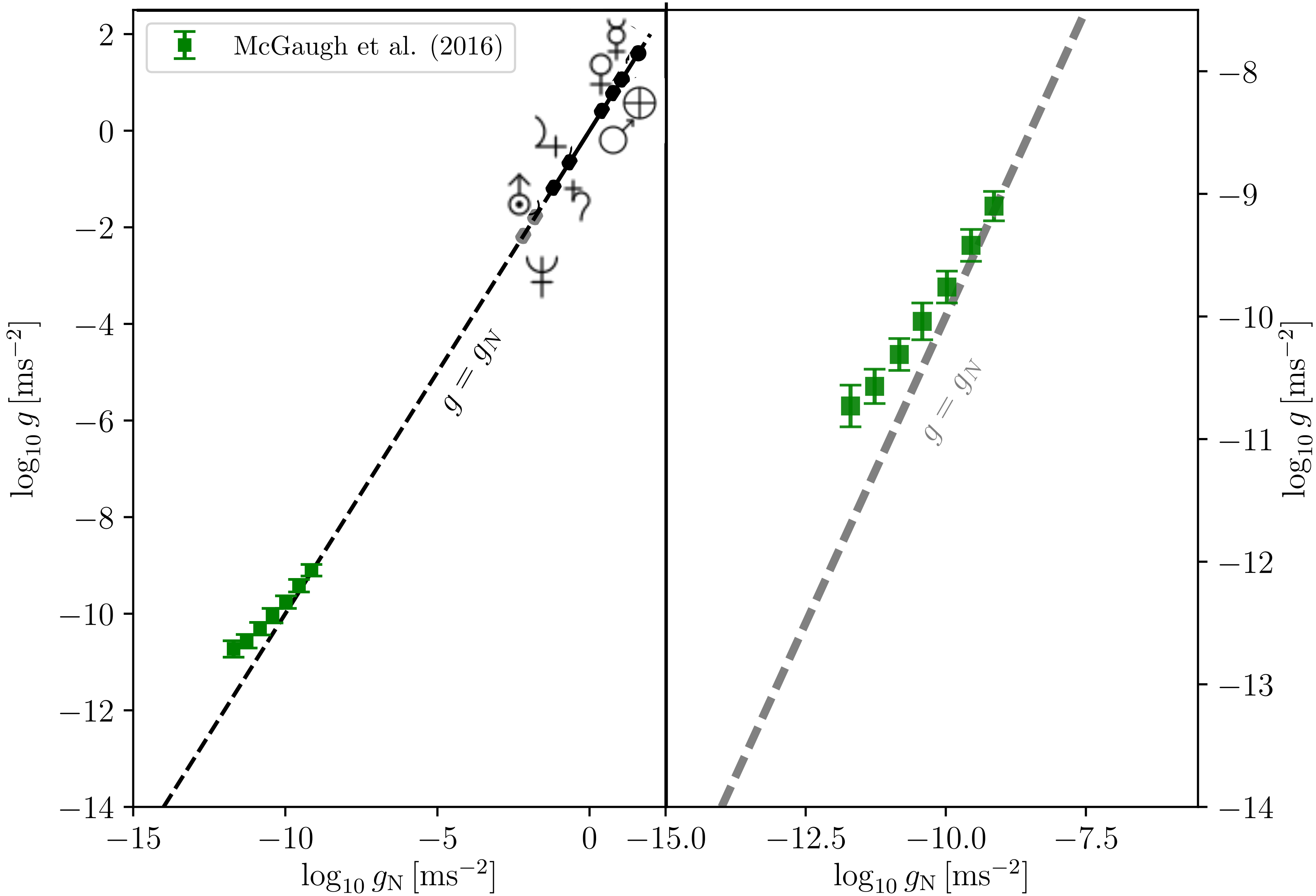

g = observed acceleration from rotation curve
g_N = expected acceleration from observed matter distribution

D2016 =
Dabringhausen&Kroupa2023
see also
Lelli et al. (2017)

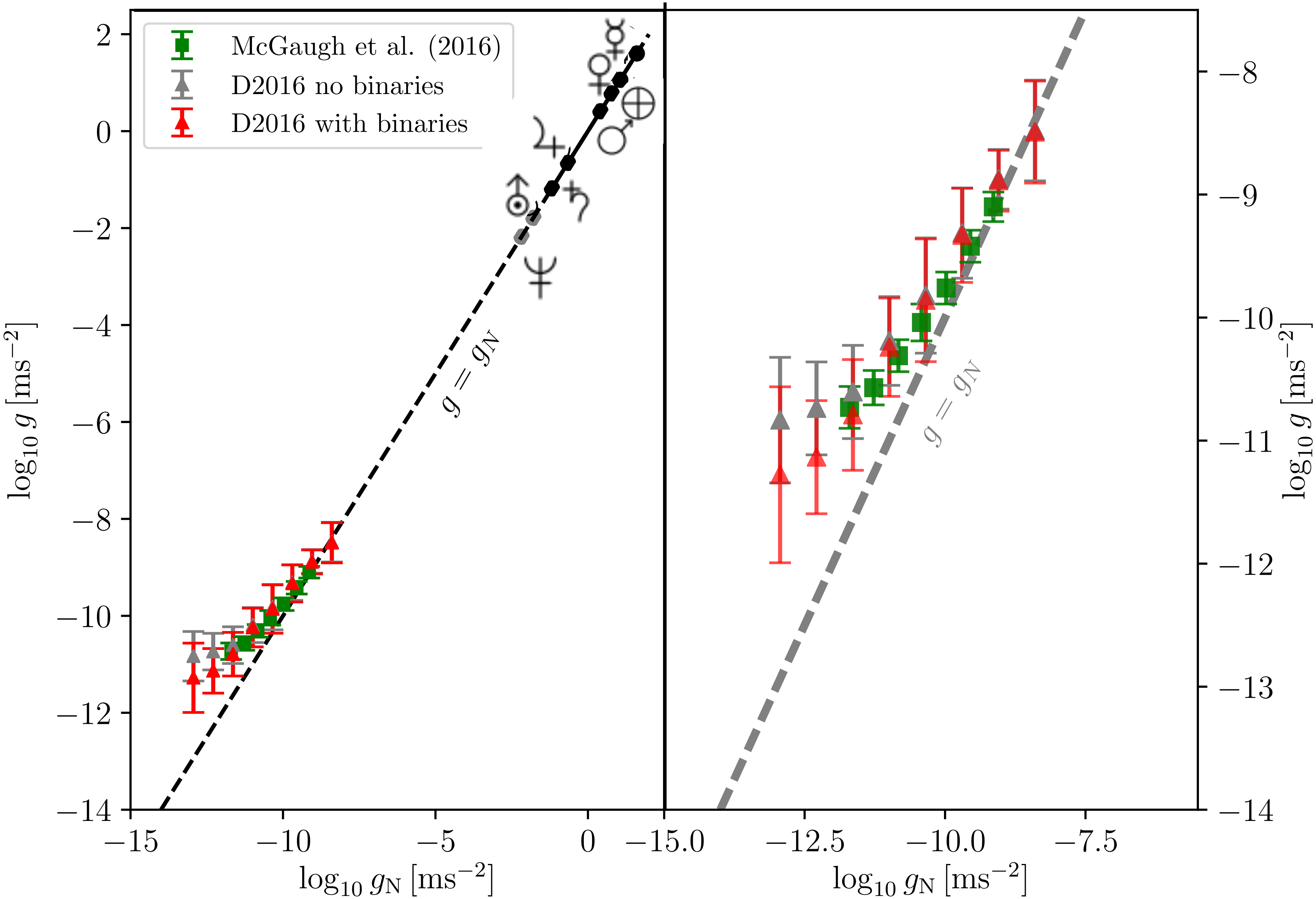

g = observed acceleration from rotation curve
g_N = expected acceleration from observed matter distribution

D2016 =
Dabringhausen&Kroupa2023
see also
Lelli et al. (2017)

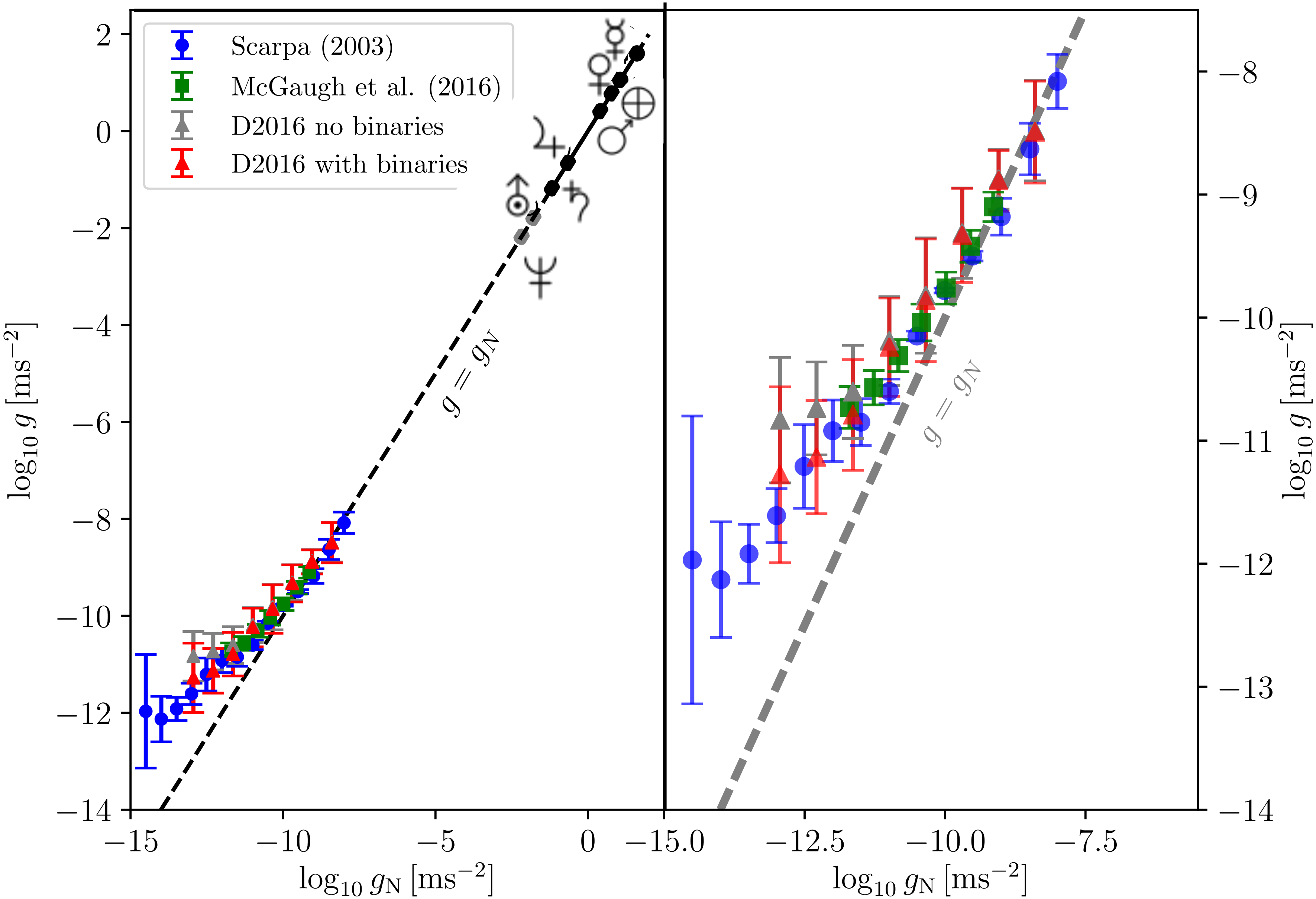

g = observed acceleration from rotation curve
g_N = expected acceleration from observed matter distribution

D2016 = Dabringhausen&Kroupa2023
see also
Lelli et al. (2017)

The standard Poisson equation : $\vec{\nabla} \cdot \vec{\nabla} \Phi = 4\pi G \rho$

The standard Poisson equation : $\vec{\nabla} \cdot \vec{\nabla} \Phi = 4\pi G \rho$

This can be re-written in terms of the *p-Laplace operator* , $\Delta_p u := \nabla \cdot (|\nabla u|^{p-2} \nabla u),$ as

The standard Poisson equation: $\vec{\nabla} \cdot \vec{\nabla} \Phi = 4\pi G \rho$

This can be re-written in terms of the *p-Laplace operator*, $\Delta_p u := \nabla \cdot (|\nabla u|^{p-2} \nabla u)$, as

$$\vec{\nabla} \cdot \left(\left(\, | \vec{\nabla} (\Phi / a_0) | \, \right)^{p-2} \vec{\nabla} (\Phi / a_0) \right) = 4\pi G \frac{\rho}{a_0}$$ (Kroupa, Gjergo+2023; Kroupa, Pflamm-Altenburg+2024)

The standard Poisson equation : $\vec{\nabla} \cdot \vec{\nabla} \Phi = 4\pi G \rho$

This can be re-written in terms of the *p-Laplace operator* , $\Delta_p u := \nabla \cdot (|\nabla u|^{p-2} \nabla u),$ as

$$\vec{\nabla} \cdot \left(\left(| \vec{\nabla} (\Phi/a_0) | \right)^{p-2} \vec{\nabla} (\Phi/a_0) \right) = 4\pi G \frac{\rho}{a_0}$$

(Kroupa, Gjergo+2023; Kroupa, Pflamm-Altenburg+2024)

p=2 standard Poisson equation above

→ Newtonian gravitation

The standard Poisson equation : $\vec{\nabla} \cdot \vec{\nabla} \Phi = 4\pi G \rho$

This can be re-written in terms of the *p-Laplace operator*, $\Delta_p u := \nabla \cdot (|\nabla u|^{p-2} \nabla u)$, as

$$\vec{\nabla} \cdot \left(\left(| \vec{\nabla} (\Phi/a_0) | \right)^{p-2} \vec{\nabla} (\Phi/a_0) \right) = 4\pi G \frac{\rho}{a_0}$$

(Kroupa, Gjergo+2023; Kroupa, Pflamm-Altenburg+2024)

p=2 standard Poisson equation above

Newtonian gravitation

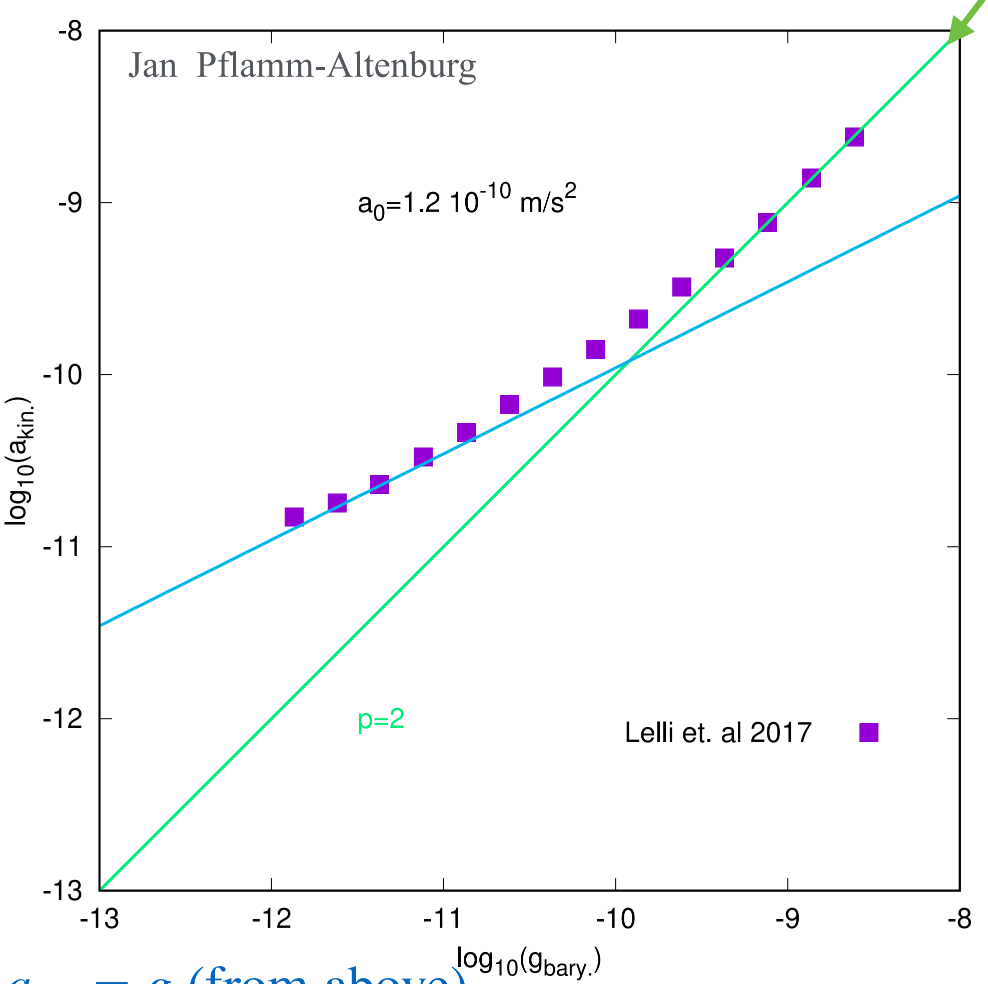

$a_{\mathrm{kin}} = g$ (from above)

$g_{\mathrm{bary}} = g_{\mathrm{N}} =$ from above

The standard Poisson equation : $\vec{\nabla} \cdot \vec{\nabla} \Phi = 4\pi G \rho$

This can be re-written in terms of the *p-Laplace operator* , $\Delta_p u := \nabla \cdot (|\nabla u|^{p-2} \nabla u)$, as

$$\vec{\nabla} \cdot \left(\left(|\vec{\nabla} (\Phi/a_0)| \right)^{p-2} \vec{\nabla} (\Phi/a_0) \right) = 4\pi G \frac{\rho}{a_0}$$

(Kroupa, Gjergo+2023; Kroupa, Pflamm-Altenburg+2024)

$p=2$ standard Poisson equation above → Newtonian gravitation

$p=3$ non-standard Poisson equation → which gravitational dynamics ?

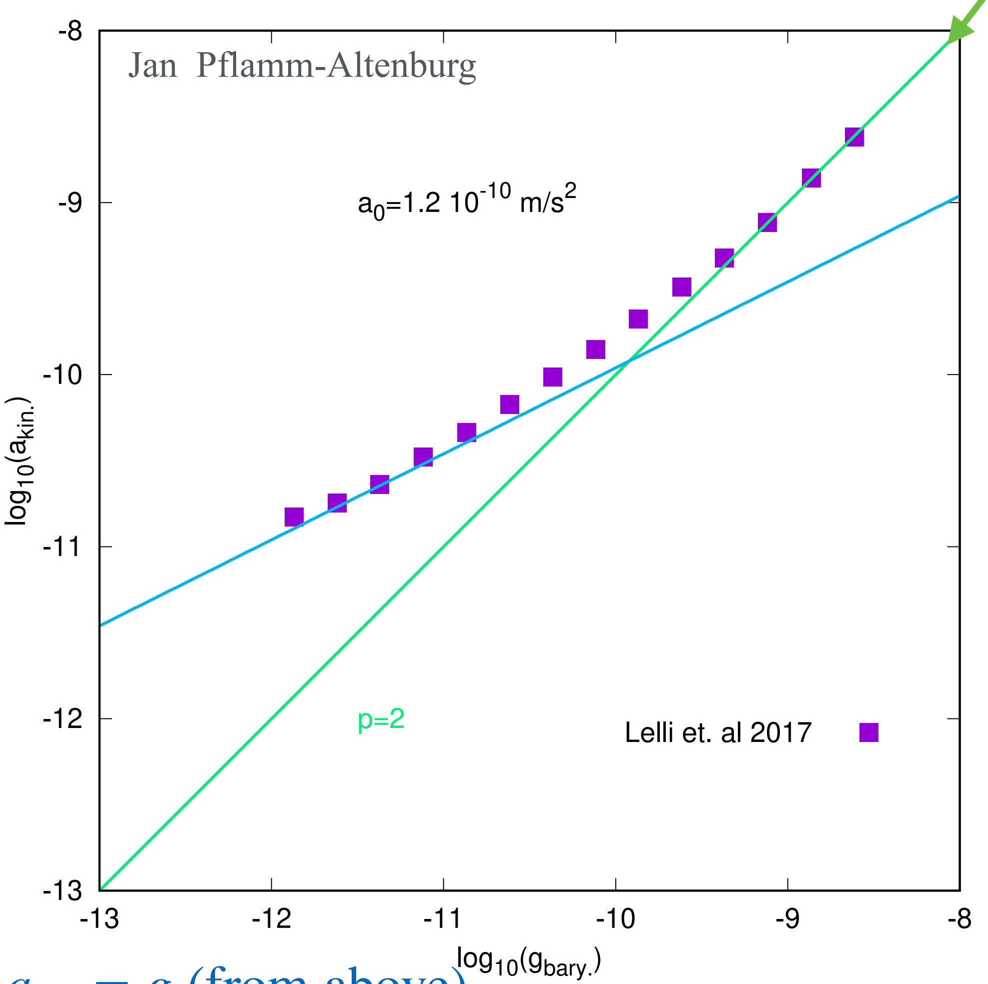

$a_{\rm kin} = g$ (from above)

$g_{\rm bary} = g_{\rm N}$ = from above

The standard Poisson equation : $\vec{\nabla} \cdot \vec{\nabla} \Phi = 4\pi G \rho$

This can be re-written in terms of the *p-Laplace operator*, $\Delta_p u := \nabla \cdot (|\nabla u|^{p-2} \nabla u)$, as

$$\vec{\nabla} \cdot \left(\left(| \vec{\nabla} (\Phi/a_0) | \right)^{p-2} \vec{\nabla} (\Phi/a_0) \right) = 4\pi G \frac{\rho}{a_0}$$

(Kroupa, Gjergo+2023; Kroupa, Pflamm-Altenburg+2024)

p=2 standard Poisson equation above

→ Newtonian gravitation

p=3 non-standard Poisson equation

→ which gravitational dynamics ?

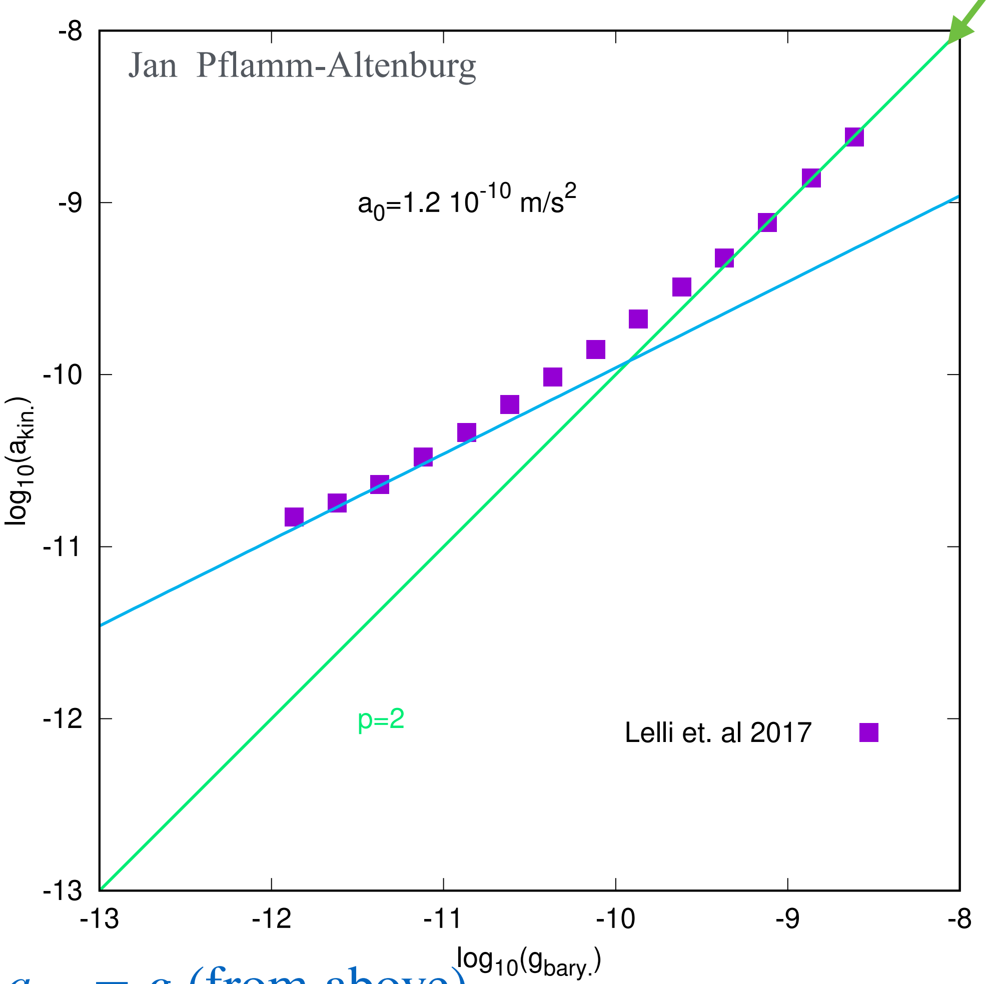

→

$$\vec{\nabla} \cdot \left(\left(| \vec{\nabla} (\Phi/a_0) | \right) \vec{\nabla} (\Phi/a_0) \right) = 4\pi G \frac{\rho}{a_0}$$

$a_{\rm kin} = g$ (from above)

$g_{\rm bary} = g_{\rm N}$ = from above

The standard Poisson equation : $\vec{\nabla} \cdot \vec{\nabla} \Phi = 4\pi G \rho$

This can be re-written in terms of the *p-Laplace operator* , $\Delta_p u := \nabla \cdot (|\nabla u|^{p-2} \nabla u)$, as

$$\vec{\nabla} \cdot \left(\left(|\vec{\nabla}(\Phi/a_0)| \right)^{p-2} \vec{\nabla}(\Phi/a_0) \right) = 4\pi G \frac{\rho}{a_0}$$

(Kroupa, Gjergo+2023; Kroupa, Pflamm-Altenburg+2024)

p=2 standard Poisson equation above → Newtonian gravitation

p=3 non-standard Poisson equation → which gravitational dynamics **?**

→

$$\vec{\nabla} \cdot \left(\left(|\vec{\nabla}(\Phi/a_0)| \right) \vec{\nabla}(\Phi/a_0) \right) = 4\pi G \frac{\rho}{a_0}$$

Sufficiently far from ρ can assume spherical symmetry - integrate using divergence theorem

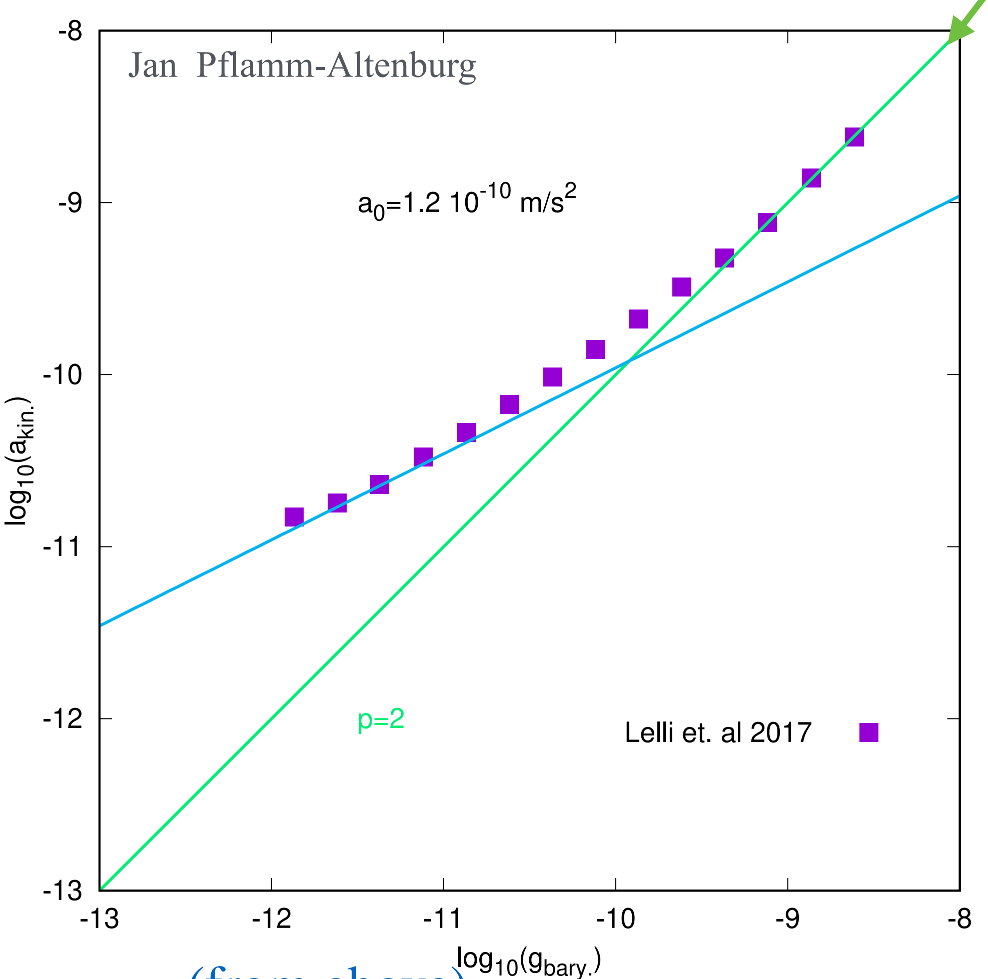

$a_{\rm kin} = g$ (from above)

$g_{\rm bary} = g_{\rm N}$ = from above

The standard Poisson equation : $\vec{\nabla} \cdot \vec{\nabla} \Phi = 4\pi G \rho$

This can be re-written in terms of the *p-Laplace operator*, $\Delta_p u := \nabla \cdot (|\nabla u|^{p-2} \nabla u)$, as

$$\vec{\nabla} \cdot \left(\left(| \vec{\nabla} (\Phi/a_0) | \right)^{p-2} \vec{\nabla} (\Phi/a_0) \right) = 4\pi G \frac{\rho}{a_0}$$

(Kroupa, Gjergo+2023; Kroupa, Pflamm-Altenburg+2024)

p=2 standard Poisson equation above → Newtonian gravitation

p=3 non-standard Poisson equation → which gravitational dynamics **?**

→

$$\vec{\nabla} \cdot \left(\left(| \vec{\nabla} (\Phi/a_0) | \right) \vec{\nabla} (\Phi/a_0) \right) = 4\pi G \frac{\rho}{a_0}$$

Sufficiently far from ρ can assume spherical symmetry - integrate using divergence theorem

→ $$\left(\frac{\partial \Phi}{\partial r} \right)^2 = \frac{a_0 \, G \, M(<r)}{r^2}$$

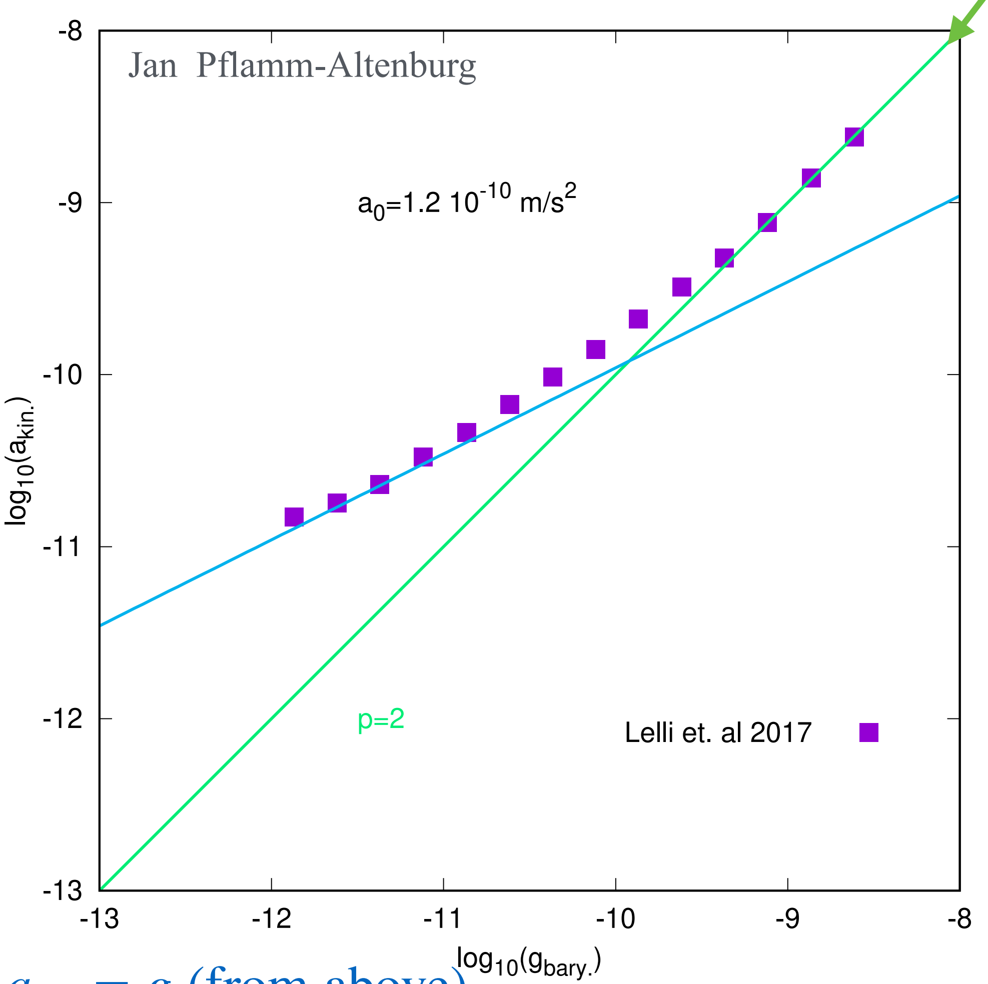

$a_{kin} = g$ (from above)
$g_{bary} = g_N =$ from above

The standard Poisson equation : $\vec{\nabla} \cdot \vec{\nabla} \Phi = 4\pi G \rho$

This can be re-written in terms of the *p-Laplace operator* , $\Delta_p u := \nabla \cdot (|\nabla u|^{p-2} \nabla u)$, as

$$\vec{\nabla} \cdot \left(\left(| \vec{\nabla} (\Phi / a_0) | \right)^{p-2} \vec{\nabla} (\Phi / a_0) \right) = 4\pi G \frac{\rho}{a_0}$$

(Kroupa, Gjergo+2023; Kroupa, Pflamm-Altenburg+2024)

p=2 standard Poisson equation above

→ Newtonian gravitation

p=3 non-standard Poisson equation

→ which gravitational dynamics ?

→

$$\vec{\nabla} \cdot \left(\left(| \vec{\nabla} (\Phi / a_0) | \right) \vec{\nabla} (\Phi / a_0) \right) = 4\pi G \frac{\rho}{a_0}$$

Sufficiently far from ρ can assume spherical symmetry - integrate using divergence theorem

→ $$\left(\frac{\partial \Phi}{\partial r} \right)^2 = \frac{a_0 \, G \, M(<r)}{r^2}$$

→ $$a_{p=3} = \sqrt{a_0 \, a_{p=2}}$$

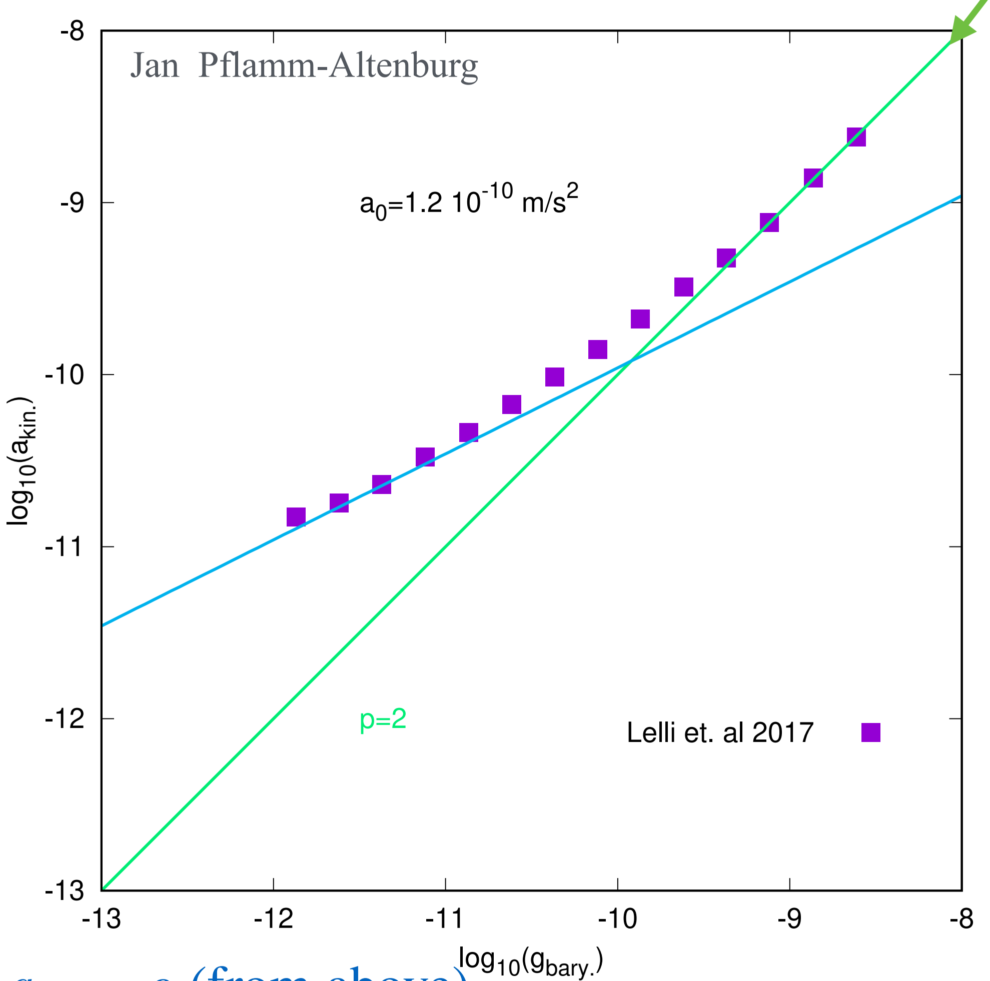

$a_{\rm kin} = g$ (from above)

$g_{\rm bary} = g_{\rm N}$ = from above

The standard Poisson equation : $\vec{\nabla} \cdot \vec{\nabla} \Phi = 4\pi G \rho$

This can be re-written in terms of the *p-Laplace operator*, $\Delta_p u := \nabla \cdot (|\nabla u|^{p-2} \nabla u)$, as

$$\vec{\nabla} \cdot \left(\left(|\vec{\nabla}(\Phi/a_0)| \right)^{p-2} \vec{\nabla}(\Phi/a_0) \right) = 4\pi G \frac{\rho}{a_0}$$

(Kroupa, Gjergo+2023; Kroupa, Pflamm-Altenburg+2024)

$p=2$ standard Poisson equation above → Newtonian gravitation

$p=3$ non-standard Poisson equation → which gravitational dynamics **?**

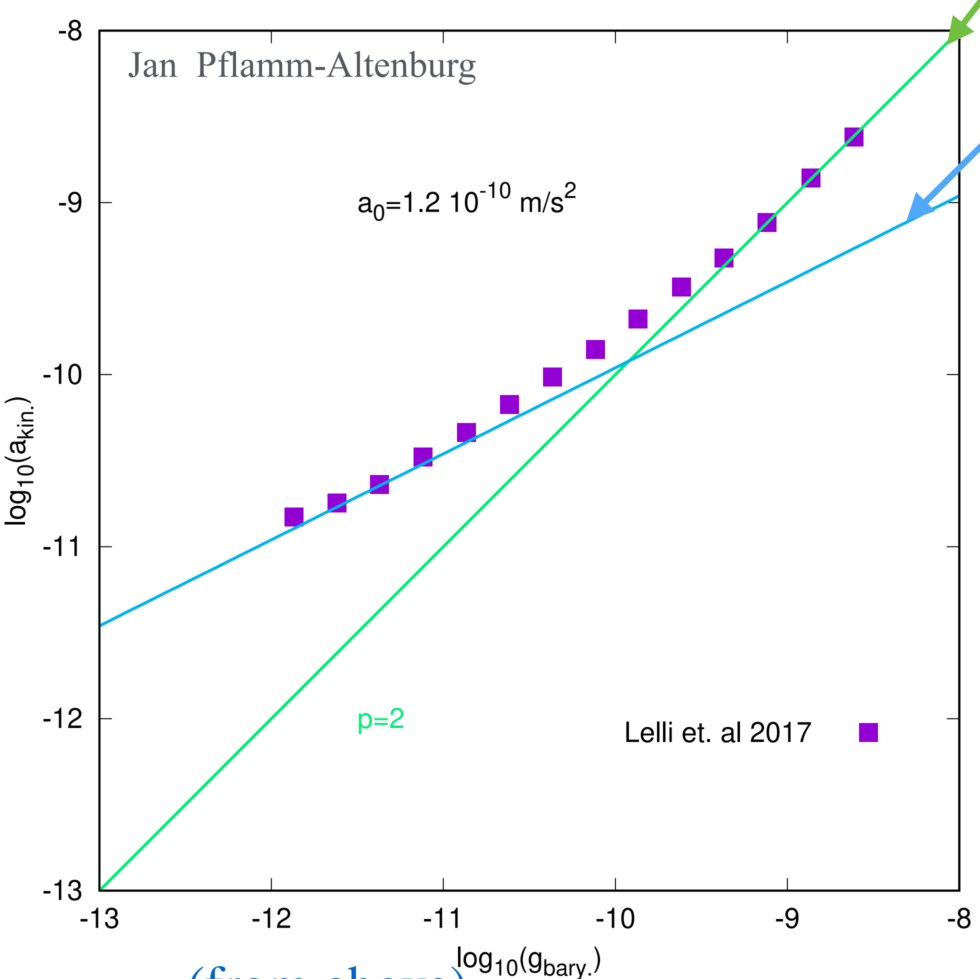

→

$$\vec{\nabla} \cdot \left(\left(|\vec{\nabla}(\Phi/a_0)| \right) \vec{\nabla}(\Phi/a_0) \right) = 4\pi G \frac{\rho}{a_0}$$

Sufficiently far from ρ can assume spherical symmetry - integrate using divergence theorem

→ $$\left(\frac{\partial \Phi}{\partial r}\right)^2 = \frac{a_0 \, G \, M(<r)}{r^2}$$

→ $$a_{p=3} = \sqrt{a_0 \, a_{p=2}}$$

$a_{\rm kin} = g$ (from above)
$g_{\rm bary} = g_{\rm N}$ = from above

This can be re-written in terms of the *p-Laplace operator*, $\Delta_p u := \nabla \cdot (|\nabla u|^{p-2} \nabla u)$, as

$$\vec{\nabla} \cdot \left(\left(\frac{|\vec{\nabla}\Phi|}{a_o} \right)^{p-2} \frac{\vec{\nabla}\Phi}{a_0} \right) = 4\pi G \frac{\rho}{a_0}$$

$p=2$ → standard Poisson equation above Newtonian gravitation

$p=3$ → non-standard Poisson equation → which gravitational dynamics **?**

→ $$\vec{\nabla} \cdot \left(\frac{|\vec{\nabla}\Phi|}{a_o} \vec{\nabla}\Phi \right) = 4\pi G \rho$$

Sufficiently far from ρ can assume spherical symmetry - integrate using divergence theorem

→ $$\left(\frac{\partial \Phi}{\partial r} \right)^2 = \frac{a_0 \, G \, M(<r)}{r^2}$$

→ $$a_{p=3} = \sqrt{a_0 \, a_{p=2}}$$

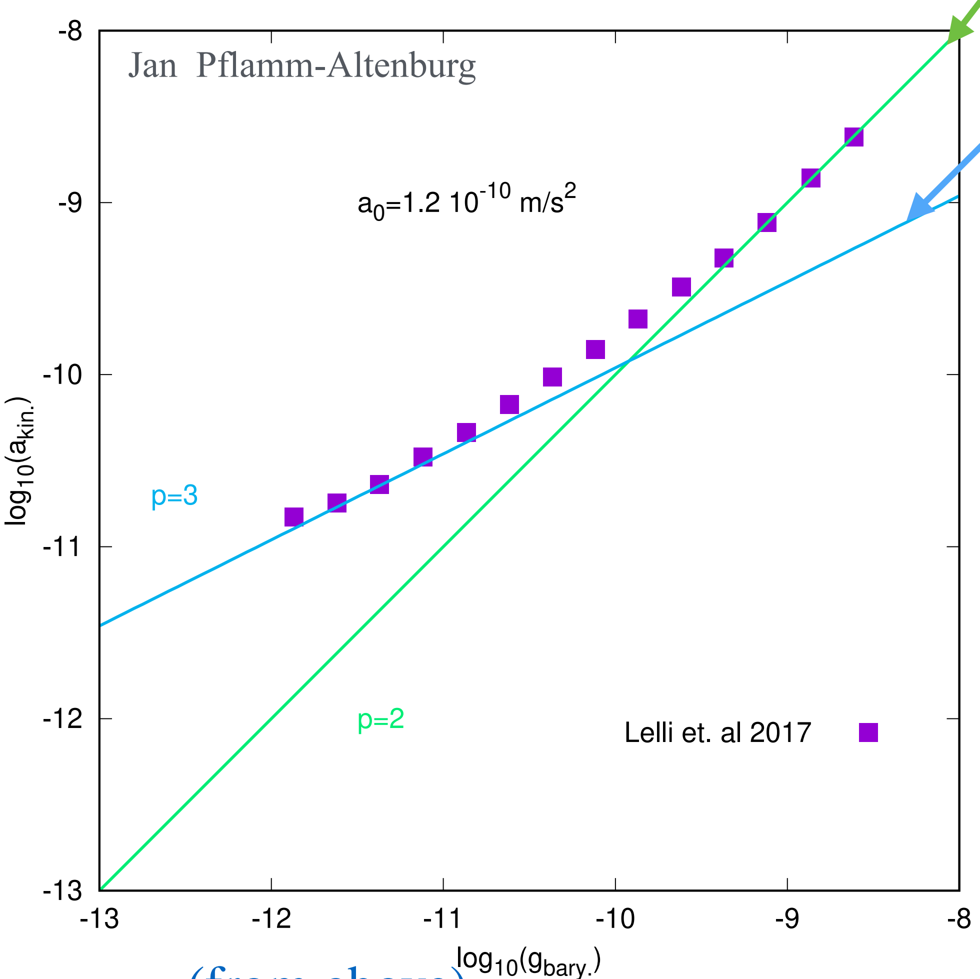

$a_{\rm kin} = g$ (from above)
$g_{\rm bary} = g_{\rm N}$ = from above

i.e., the *Milgromian acceleration* in terms of the *Newtonian acceleration* : $g_{\rm M} = \sqrt{a_0 \, g_{\rm N}}$

The standard Poisson equation : $\vec{\nabla} \cdot \vec{\nabla} \Phi = 4\pi G \rho$

This can be re-written in terms of the *p-Laplace operator* , $\Delta_p u := \nabla \cdot (|\nabla u|^{p-2} \nabla u)$, as

$$\vec{\nabla} \cdot \left(\left(\frac{|\vec{\nabla}\Phi|}{a_o} \right)^{p-2} \frac{\vec{\nabla}\Phi}{a_0} \right) = 4\pi G \frac{\rho}{a_0}$$

$p=2$ standard Poisson equation above → Newtonian gravitation

$p=3$ non-standard Poisson equation → which gravitational dynamics **?**

$$\rightarrow \quad \vec{\nabla} \cdot \left(\frac{|\vec{\nabla}\Phi|}{a_o} \vec{\nabla}\Phi \right) = 4\pi G \rho$$

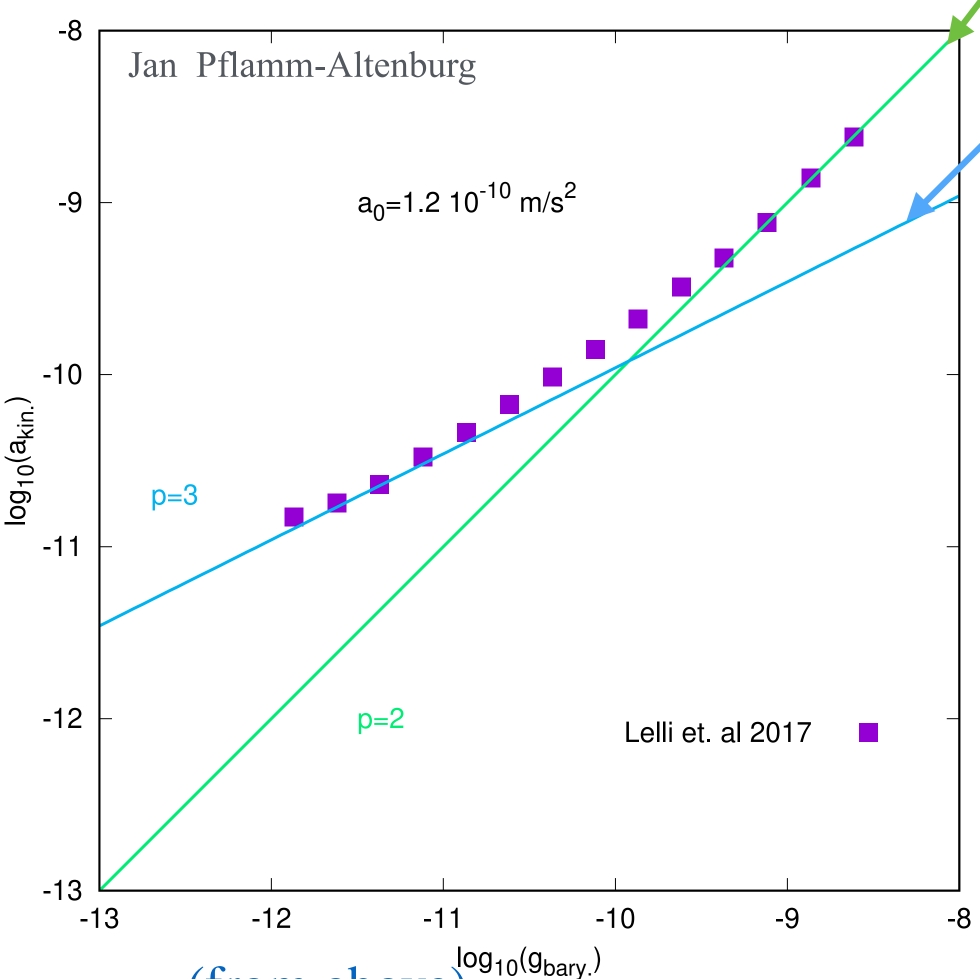

$a_{kin} = g$ (from above)
$g_{bary} = g_N$ = from above

Sufficiently far from ρ can assume spherical symmetry - integrate using divergence theorem

$$\rightarrow \quad \left(\frac{\partial \Phi}{\partial r} \right)^2 = \frac{a_0 \, G \, M(<r)}{r^2}$$

$$\rightarrow \quad a_{p=3} = \sqrt{a_0 \, a_{p=2}}$$

i.e., the *Milgromian acceleration* in terms of the *Newtonian acceleration* : $g_M = \sqrt{a_0 \, g_N}$

$$\left(\frac{\partial \Phi}{\partial r}\right)^2 = \frac{a_0\, G\, M(<r)}{r^2} \quad \Rightarrow \quad g_{\mathrm{M}} = \sqrt{a_0\, g_{\mathrm{N}}}$$

$$\left(\frac{\partial\Phi}{\partial r}\right)^2 = \frac{a_0\, G\, M(<r)}{r^2} \quad \Longrightarrow \quad g_{\rm M} = \sqrt{a_0\, g_{\rm N}}$$

Centripetal acceleration $g_{\rm M} = \frac{v_{\rm c}^2}{r} = \frac{\partial\Phi}{\partial r}$

$$\left(\frac{\partial \Phi}{\partial r}\right)^2 = \frac{a_0 \, G \, M(<r)}{r^2} \quad \Longrightarrow \quad g_{\mathrm{M}} = \sqrt{a_0 \, g_{\mathrm{N}}}$$

Centripetal acceleration $g_{\mathrm{M}} = \frac{v_{\mathrm{c}}^2}{r} = \frac{\partial \Phi}{\partial r} \quad \Longrightarrow \quad \frac{v_{\mathrm{c}}^2}{r} = \frac{\sqrt{a_0 \, G \, M(<r)}}{r}$

$$\left(\frac{\partial\Phi}{\partial r}\right)^2 = \frac{a_0\, G\, M(<r)}{r^2} \quad \Longrightarrow \quad g_{\rm M} = \sqrt{a_0\, g_{\rm N}}$$

Centripetal acceleration $g_{\rm M} = \frac{v_{\rm c}^2}{r} = \frac{\partial\Phi}{\partial r} \quad \Longrightarrow \quad \frac{v_{\rm c}^2}{r} = \frac{\sqrt{a_0\, G\, M(<r)}}{r}$

$\Longrightarrow$ $v_{\rm c} = \left(a_0\, G\, M_{\rm bar}\right)^{\frac{1}{4}}$

with $M_{\rm bar}$ being total baryonic mass (gas + stars + remnants) of the galaxy.

$$\left(\frac{\partial\Phi}{\partial r}\right)^2 = \frac{a_0\, G\, M(<r)}{r^2} \quad \Rightarrow \quad g_{\mathrm{M}} = \sqrt{a_0\, g_{\mathrm{N}}}$$

Centripetal acceleration $g_{\mathrm{M}} = \frac{v_{\mathrm{c}}^2}{r} = \frac{\partial\Phi}{\partial r}$ $\Rightarrow$ $\frac{v_{\mathrm{c}}^2}{r} = \frac{\sqrt{a_0\, G\, M(<r)}}{r}$

$\Rightarrow$ $$\boxed{v_{\mathrm{c}} = \left(a_0\, G\, M_{\mathrm{bar}}\right)^{\frac{1}{4}}}$$

with M_{bar} being total baryonic mass (gas + stars + remnants) of the galaxy.

Integrate $\frac{\partial\Phi}{\partial r} = \frac{\left(a_0\, G\, M(<r)\right)^{\frac{1}{2}}}{r}$ assuming r sufficiently large that $M(<r)$ invariant $= M_{\mathrm{bar}} = M_{\mathrm{tot}}$

$$\left(\frac{\partial \Phi}{\partial r}\right)^2 = \frac{a_0\, G\, M(<r)}{r^2} \quad \Rightarrow \quad g_{\mathrm{M}} = \sqrt{a_0\, g_{\mathrm{N}}}$$

Centripetal acceleration $g_{\mathrm{M}} = \frac{v_{\mathrm{c}}^2}{r} = \frac{\partial \Phi}{\partial r} \quad \Rightarrow \quad \frac{v_{\mathrm{c}}^2}{r} = \frac{\sqrt{a_0\, G\, M(<r)}}{r}$

$\Rightarrow$ $\boxed{v_{\mathrm{c}} = \left(a_0\, G\, M_{\mathrm{bar}}\right)^{\frac{1}{4}}}$

with M_{bar} being total baryonic mass (gas + stars + remnants) of the galaxy.

Integrate $\frac{\partial \Phi}{\partial r} = \frac{\left(a_0\, G\, M(<r)\right)^{\frac{1}{2}}}{r}$ assuming r sufficiently large that $M(<r)$ invariant $= M_{\mathrm{bar}} = M_{\mathrm{tot}}$

$$\Rightarrow \int_{\Phi_0}^{\Phi_b} \mathrm{d}\Phi = \left(a_0\, G\, M_{\mathrm{bar}}\right)^{\frac{1}{2}} \int_{r_0}^{r_b} \frac{1}{r}\, \mathrm{d}r$$

$$\left(\frac{\partial\Phi}{\partial r}\right)^2 = \frac{a_0\, G\, M(<r)}{r^2} \quad \Rightarrow \quad g_{\mathrm{M}} = \sqrt{a_0\, g_{\mathrm{N}}}$$

Centripetal acceleration $g_{\mathrm{M}} = \frac{v_{\mathrm{c}}^2}{r} = \frac{\partial\Phi}{\partial r} \quad \Rightarrow \quad \frac{v_{\mathrm{c}}^2}{r} = \frac{\sqrt{a_0\, G\, M(<r)}}{r}$

$\Rightarrow$ $v_{\mathrm{c}} = \left(a_0\, G\, M_{\mathrm{bar}}\right)^{\frac{1}{4}}$
with M_{bar} being total baryonic mass (gas + stars + remnants) of the galaxy.

Integrate $\frac{\partial\Phi}{\partial r} = \frac{\left(a_0\, G\, M(<r)\right)^{\frac{1}{2}}}{r}$ assuming r sufficiently large that $M(<r)$ invariant $= M_{\mathrm{bar}} = M_{\mathrm{tot}}$

$$\Rightarrow \int_{\Phi_0}^{\Phi_b} \mathrm{d}\Phi = \left(a_0\, G\, M_{\mathrm{bar}}\right)^{\frac{1}{2}} \int_{r_0}^{r_b} \frac{1}{r}\,\mathrm{d}r \quad \Rightarrow \quad \Phi(r_b) - \Phi(r_0) = \sqrt{a_0\, G\, M_{\mathrm{bar}}}\ \left(\ln r_b - \ln r_0\right)$$

$$\left(\frac{\partial\Phi}{\partial r}\right)^2 = \frac{a_0\, G\, M(<r)}{r^2} \quad \Longrightarrow \quad g_{\rm M} = \sqrt{a_0\, g_{\rm N}}$$

Centripetal acceleration $g_{\rm M} = \frac{v_{\rm c}^2}{r} = \frac{\partial\Phi}{\partial r} \quad \Longrightarrow \quad \frac{v_{\rm c}^2}{r} = \frac{\sqrt{a_0\, G\, M(<r)}}{r}$

$\Longrightarrow$

$$v_{\rm c} = \left(a_0\, G\, M_{\rm bar}\right)^{\frac{1}{4}}$$

with $M_{\rm bar}$ being total baryonic mass (gas + stars + remnants) of the galaxy.

Integrate $\frac{\partial\Phi}{\partial r} = \frac{\left(a_0\, G\, M(<r)\right)^{\frac{1}{2}}}{r}$ assuming r sufficiently large that $M(<r)$ invariant $= M_{\rm bar} = M_{\rm tot}$

$$\Longrightarrow \int_{\Phi_0}^{\Phi_b} {\rm d}\Phi = \left(a_0\, G\, M_{\rm bar}\right)^{\frac{1}{2}} \int_{r_0}^{r_b} \frac{1}{r}\, {\rm d}r \quad \Longrightarrow \quad \Phi(r_b) - \Phi(r_0) = \sqrt{a_0\, G\, M_{\rm bar}}\, \left(\ln r_b - \ln r_0\right)$$

$$\Longrightarrow \Phi(r) = v_{\rm c}^2 \ln\left(\frac{r}{r_0}\right) + \Phi(r_0)$$

$$\left(\frac{\partial\Phi}{\partial r}\right)^2 = \frac{a_0\, G\, M(<r)}{r^2} \quad \Rightarrow \quad g_M = \sqrt{a_0\, g_N}$$

Centripetal acceleration $g_M = \frac{v_c^2}{r} = \frac{\partial\Phi}{\partial r} \Rightarrow \frac{v_c^2}{r} = \frac{\sqrt{a_0\, G\, M(<r)}}{r}$

$\Rightarrow$ $\boxed{v_c = \left(a_0\, G\, M_{bar}\right)^{\frac{1}{4}}}$

with M_{bar} being total baryonic mass (gas + stars + remnants) of the galaxy.

Integrate $\frac{\partial\Phi}{\partial r} = \frac{\left(a_0\, G\, M(<r)\right)^{\frac{1}{2}}}{r}$ assuming r sufficiently large that $M(<r)$ invariant $= M_{bar} = M_{tot}$

$$\Rightarrow \int_{\Phi_0}^{\Phi_b} d\Phi = \left(a_0\, G\, M_{bar}\right)^{\frac{1}{2}} \int_{r_0}^{r_b} \frac{1}{r}\, dr \quad \Rightarrow \quad \Phi(r_b) - \Phi(r_0) = \sqrt{a_0\, G\, M_{bar}}\,\left(\ln r_b - \ln r_0\right)$$

$$\Rightarrow \Phi(r) = v_c^2 \ln\left(\frac{r}{r_0}\right) + \Phi(r_0)$$

i.e., the p=3 Laplacian generates a *logarithmic potential* around a point mass (remember: the p=2 Laplacian generates a *1/r (Kepler) potential*).

The observational Baryonic Tully-Fisher Relation (BTFR)

Famaey & McGaugh 2012

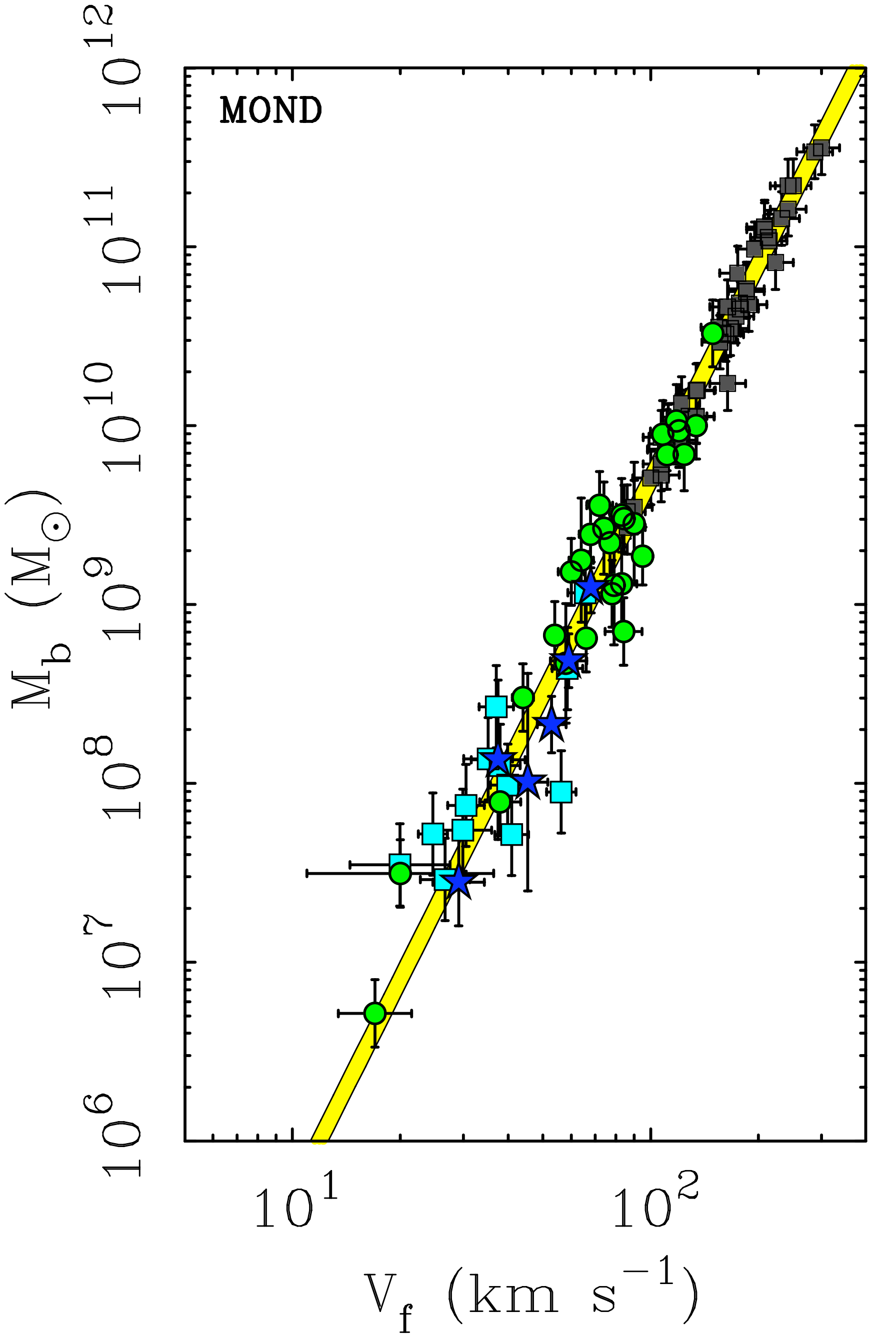

$$V_{\rm f} = (G\, a_0\, M_{\rm bar})^{\frac{1}{4}}$$

The observational Baryonic Tully-Fisher Relation (BTFR)

Famaey & McGaugh 2012

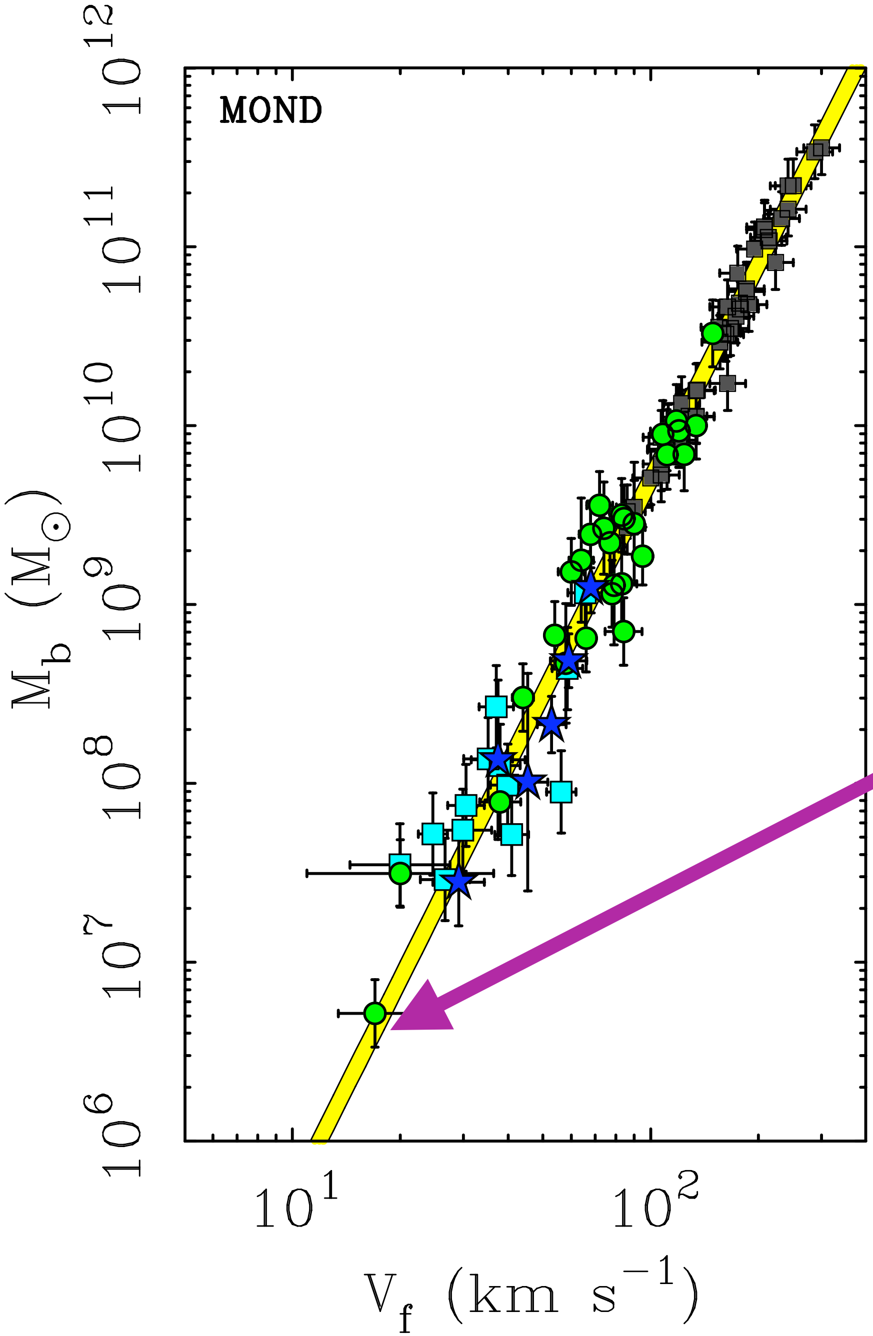

$$V_\mathrm{f} = (G\, a_0\, M_\mathrm{bar})^{\frac{1}{4}}$$

DDO 210

$15\,\mathrm{km/s}; \quad M_\mathrm{bar} = M_\mathrm{tot} \approx 5 \times 10^6\, M_\odot$

The observational Baryonic Tully-Fisher Relation (BTFR)

Famaey & McGaugh 2012

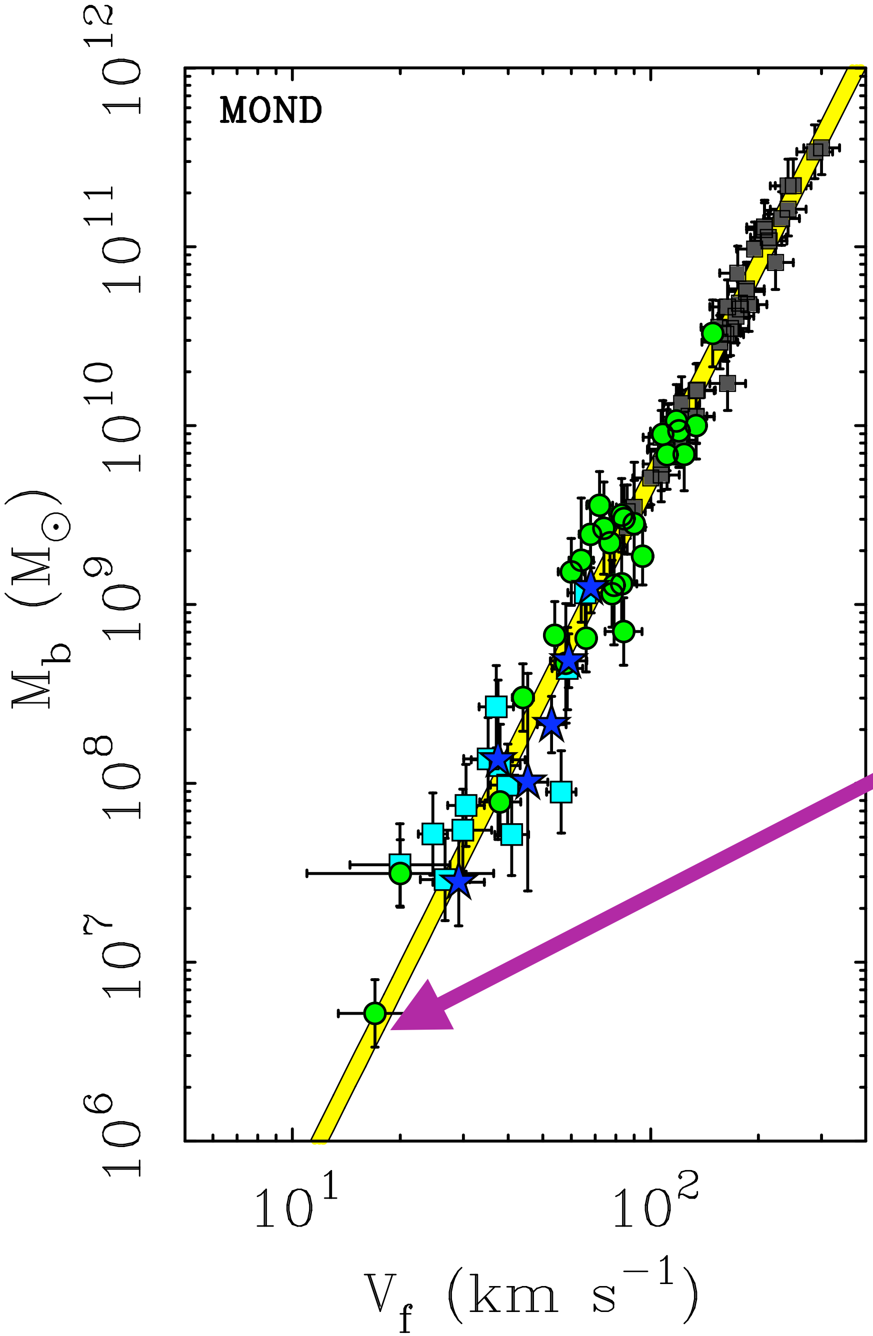

$$V_{\rm f} = (G\, a_0\, M_{\rm bar})^{\frac{1}{4}}$$

$$a_0 \approx 3.8\, \mathrm{pc/Myr^2}$$

DDO 210

$$15\, \mathrm{km/s}; \quad M_{\rm bar} = M_{\rm tot} \approx 5 \times 10^{6}\, M_\odot$$

The observational Baryonic Tully-Fisher Relation (BTFR)

Famaey & McGaugh 2012

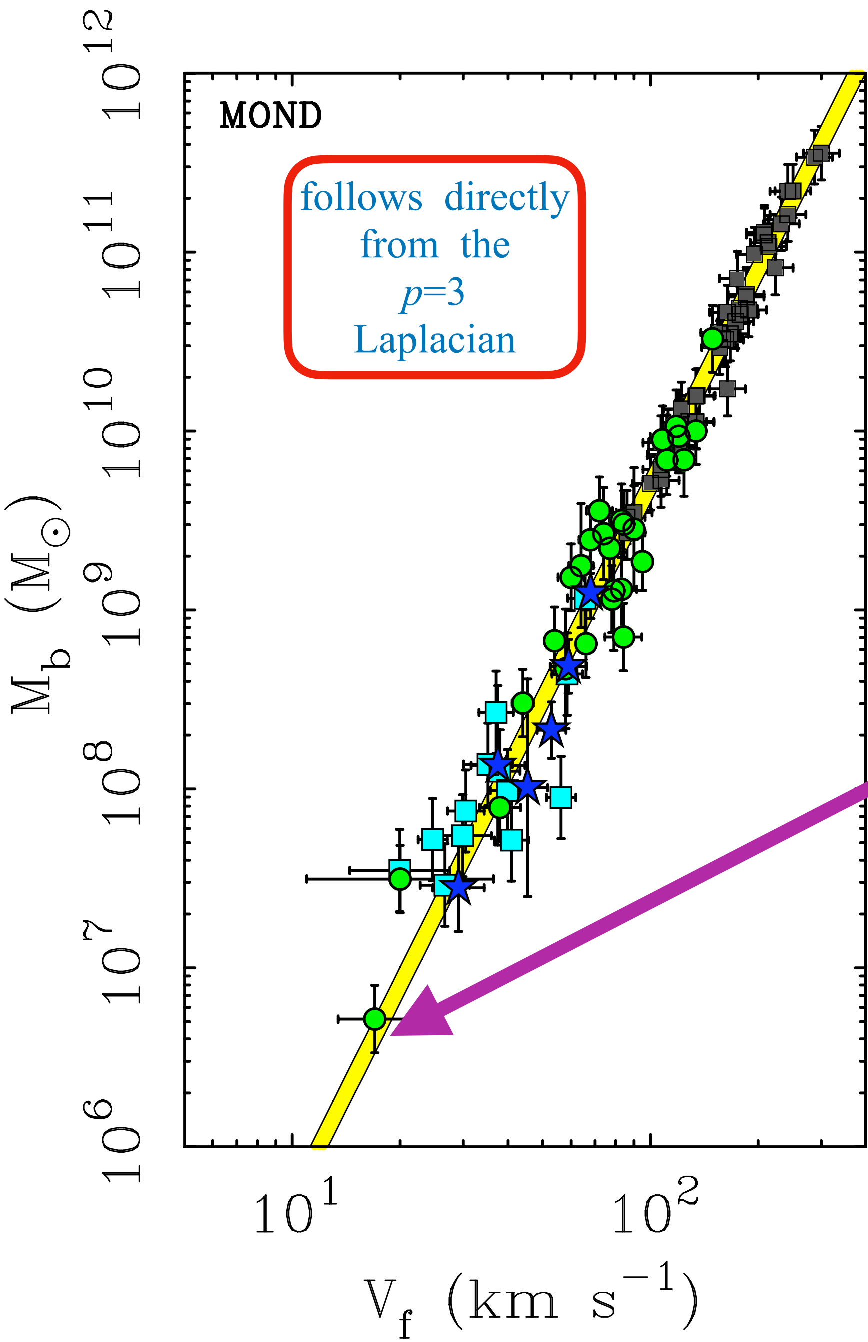

$V_f = (G\, a_0\, M_{bar})^{\frac{1}{4}}$

$a_0 \approx 3.8\,\mathrm{pc/Myr^2}$

DDO 210

15 km/s; $M_{bar} = M_{tot} \approx 5 \times 10^6\, M_\odot$

Galaxies follow the same law, independently how they formed.

Galaxies follow the same law,
independently how they formed.

Exactly like planetary systems :
all follow the Kepler's laws,
independently how they formed.

Galaxies follow the same law,
independently how they formed.

Exactly like planetary systems :
all follow the Kepler's laws,
independently how they formed.

This is a most remarkable observational fact.

Galaxies follow the same law,
independently how they formed.

Exactly like planetary systems :
all follow the Kepler's laws,
independently how they formed.

This is a most remarkable observational fact.

The
BTFR (the Baryonic-Tully-Fisher relation)
and the
RAR (radial-acceleration relation)
and the
MDR (mass-discrepancy relation)
are
fundamental relations
obeyed by galaxies.
These cannot be explained in the SMoC
(a few authors claim so, but these publications are flawed).

Galaxies follow the same law,
independently how they formed.

Exactly like planetary systems :
all follow the Kepler's laws,
independently how they formed.

This is a most remarkable observational fact.

The
BTFR (the Baryonic-Tully-Fisher relation)
and the
RAR (radial-acceleration relation)
and the
MDR (mass-discrepancy relation)
are
fundamental relations
obeyed by galaxies.
These cannot be explained in the SMoC
(a few authors claim so, but these publications are flawed).

follow directly from the p=3 Laplacian

Is there a Lagrangian formulation ?

Is there a Lagrangian formulation ?

Yes : Bekenstein & Milgrom 1984 = AQUAL (related to the p=Laplacian)

Milgrom 2010 = QUMOND (based on the concept of phantom dark matter)

Is there a Lagrangian formulation ?

Yes : Bekenstein & Milgrom 1984 = AQUAL (related to the p=Laplacian)

Milgrom 2010 = QUMOND (based on the concept of phantom dark matter)

Relativistic formulation : Skordis & Zlosnik (2021, 2020)

Reviews :

Sanders (2007, 2009a, 2009b, 2015)
Scarpa (2006)
Famaey & McGaugh (2012)
Trippe (2014, ZNatA)
Milgrom (2014, Scholarpedia)
Banik & Zhao (2022, Symmetry)

(see Kroupa et al. arXiv2309.11552 for these)